Design of Photoswitchable Catalyst Systems

Dissertation

zur Erlangung des akademischen Grades
doctor rerum naturalium
(Dr. rer. nat.)
im Fach Chemie
eingereicht an der

Mathematisch-Naturwissenschaftlichen Fakultät I
der Humboldt Universität zu Berlin
von

Ragnar Samson Stoll
geboren am 15.05.1979 in Bad Homburg vor der Höhe

Präsident der Humboldt Universität zu Berlin
Prof. Dr. Dr. h.c. Christoph Markschies

Dekan der Mathematisch-Naturwissenschaftlichen Fakultät I
Prof. Dr. Lutz-Helmut Schön

Gutachter: 1. Prof. Dr. Stefan Hecht
2. Prof. Dr. Jürgen Liebscher
3. Prof. Dr. Marcel Mayor

Tag der mündlichen Prüfung: 20.05.2009

Die vorliegende Arbeit wurde in der Zeit von Februar 2005 bis September 2006 am Max-Planck-Institut für Kohlenforschung in Mülheim an der Ruhr und von Oktober 2006 bis März 2009 am Institut für Chemie der Humboldt Universität zu Berlin unter Anleitung von Herrn Prof. Dr. Stefan Hecht durchgeführt.

Danksagung

Prof. Dr. Stefan Hecht danke ich für die Möglichkeit, ein interessantes Thema in einer optimalen Umgebung zu bearbeiten. Die hervorragenden Arbeitsbedingungen und die stets engagierte fachliche Betreuung haben wesentlich zum Gelingen der Arbeit beigetragen. Ohne die Vielzahl der fachlichen als auch privaten Gespräche wäre die Zeit der Promotion weit weniger lehrreich gewesen.

Ich möchte mich bei allen meinen Laborkollegen an den verschiedenen Instituten für die hervorragende Zusammenarbeit und die nette Atmosphäre bedanken. Besonders möchte ich den „Mülheimern“ Maike Peters, Marco Balbo-Block, Sebastian Hartwig und Robert Meudtner für den großartigen Zusammenhalt und die schönen Zeiten außerhalb des Labors danken. Ihr habt die Mülheimer Zeit zu einer besonderen gemacht!

Allen Mitarbeiterinnen und Mitarbeitern des Max-Planck-Institutes für Kohlenforschung in Mülheim/Ruhr möchte ich für die zuverlässig und stets höchst zufriedenstellend erbrachten Serviceleistungen danken. Mein spezieller Dank geht an Alfred Deege und sein Team für zahlreiche gemessene HPLCs und noch mehr Späße. Weiterhin möchte ich den Mitarbeiterinnen und Mitarbeitern des Instituts für Chemie der Humboldt Universität zu Berlin für die hervorragende Zusammenarbeit danken. Insbesondere bei Frau Thiesies von der NMR-Abteilung möchte ich mich für die stets unkomplizierte Zusammenarbeit bedanken. Dr. Goddard (MPI) und Dr. Ziemer (HUB) danke ich für die Aufklärung der Kristallstrukturen.

Bei Christina Thiele (TU Darmstadt, NMR-Messungen) und Michael Bühl (University of St. Andrews, DFT-Rechnungen) möchte ich mich für die hervorragende Kooperation bedanken, die erheblich zum Verständnis der photoschaltbaren Basen beigetragen hat.

Der Studienstiftung des deutschen Volkes möchte ich für die großzügige finanzielle und ideelle Förderung danken.

Mein besonderer Dank gilt natürlich meiner Familie, die mich während Studium und Doktorarbeit immer unterstützt hat und mir in schwierigen Situationen mit Rat und Tat zur Seite stand.

Meinen Freunden möchte ich für die gemeinsamen Erlebnisse in Berlin und Mülheim danken, die die Promotion zu einer schönen Zeit gemacht haben. Ganz besonderer Dank gilt hierbei Susanne Grützner, ohne die der Berliner Zeit etwas Wichtiges gefehlt hätte.

Abstract

Photocontrol over properties of single molecules and assemblies thereof is an appealing area of current chemical research. The mere potential to selectively address chemical reactivity as well as the possibility to transform an incoming light stimulus into an amplified chemical signal by exploiting the associated catalytic cycle renders photocontrol of catalytic activity a particularly attractive goal. In this dissertation, a general concept for the realization of photoswitchable catalysts was developed, based on reversible steric shielding of a catalyst's active site by a photochromic blocking group. Dictating the photochrome's switching state enables gated access to the active site, thereby photocontrolling the catalyst's chemical reactivity. The concept was realized by designing conformationally restricted, photoswitchable piperidine bases, which were easily synthesized exploiting a highly modular approach. Indeed, the developed piperidine bases allowed to photocontrol the catalysts' activities in the nitroaldol reaction (Henry reaction) and by tuning of the substituents significant catalytic ON/OFF-ratios were achieved. The reactivity differences could be correlated with changes of basicity depending on the photochrome's switching state. Systematic NMR-spectroscopic and computational studies of the catalysts' structural dynamics in solution enabled the formulation of detailed structure-reactivity relationships. Extension of the concept to intrinsically more reactive catalysts is expected to greatly enhance the utility of the concept. Therefore, strategies for the implementation of the concept of reversible steric shielding into the *N*-heterocyclic carbene motif (especially imidazolin-2-ylidenes and imidazolidin-2-ylidenes) were devised to exploit the high reactivity of *N*-heterocyclic carbenes in numerous catalytic processes. Efficient steric shielding of the active site to suppress unwanted OFF-state reactivity was anticipated to arise from bulky substituents on the carbene's nitrogen atoms. However, synthetic realization of the concept was hampered by the build-up of unfavorable steric interactions upon formation of the *N*-heterocyclic carbene from suitably substituted precursors.

Kurzzusammenfassung

Photokontrolle von Eigenschaften einzelner Moleküle und größerer Molekülvereinigungen ist ein faszinierendes Feld aktueller chemischer Forschung. Das schlichte Potential der genauen Adressierbarkeit von chemischer Reaktivität sowie die Möglichkeit durch Ausnutzen des katalytischen Zyklus einen Lichtstimulus in ein verstärktes chemisches Signal zu übersetzen, machen die Photokontrolle über katalytische Aktivität zu einem besonders attraktiven Ziel. Daher wurde im Rahmen dieser Dissertation ein allgemeines Konzept zur Realisierung von photoschaltbaren Katalysatoren entwickelt, das auf der reversiblen sterischen Abschirmung eines katalytisch aktiven Zentrums durch eine photochrome Abschirmungsgruppe beruht. Durch Vorgabe des Schaltzustandes des Photochromes kann die Aktivität des Katalysators bestimmt werden. Das Konzept wurde durch die Entwicklung von konformativ eingeschränkten, photoschaltbaren Piperidinbasen umgesetzt, die synthetisch leicht durch einen in hohem Maße modularen Zugang erhalten werden konnten. Die Piperidinbasen erlaubten die Photokontrolle der Katalysatoraktivität in der Nitroaldol-Reaktion (Henry-Reaktion). Durch die Optimierung der Substituenten konnten bemerkenswerte katalytische AN/AUS-Verhältnisse erreicht werden. Die Reaktivitätsunterschiede konnten mit Änderungen der Basizität in Abhängigkeit vom Schaltzustand korreliert werden. Systematische NMR-spektroskopische und theoretische Untersuchungen der strukturellen Dynamik des Katalysators in Lösung ermöglichten die Formulierung von detaillierten Struktur-Reaktivitäts-Beziehungen. Eine Erweiterung des Konzepts auf intrinsisch reaktivere Katalysatoren sollte zu einer verbesserten Anwendbarkeit beitragen. Daher wurde das Konzept der reversiblen sterischen Abschirmung auf katalytisch aktive *N*-heterozyklische Carbene (insbesondere Imidazolin-2-ylidene und Imidazolidin-2-ylidene) übertragen. Räumlich anspruchsvolle Substituenten an den Stickstoffatomen des Carbenes sollten ungewollte Restreaktivität unterdrücken, verhinderten aber durch ungünstige sterische Wechselwirkungen eine erfolgreiche Synthese des Carbengrundkörpers.

Table of Contents

1 Introduction 1

1.1 Literature 5

2 General Part 9

2.1 Photochromism 9
2.2 Azobenzenes 11
2.2.1 Introduction 11
2.2.2 Spectral Features 13
2.2.2.1 Azobenzene Type 13
2.2.2.2 Aminoazobenzene Type 14
2.2.2.3 Pseudostilbene Type 15
2.2.3 Isomerization 15
2.2.3.1 Azobenzene Type 15
2.2.3.2 Aminoazobenzene Type 20
2.2.3.3 Pseudostilbene Type 20
2.2.4 Synthesis 21
2.2.5 Applications of Azobenzenes 24
2.3 Diarylethenes 25
2.3.1 Introduction 25
2.3.2 Spectral Features 27
2.3.3 Isomerization 28
2.3.4 Synthesis 29
2.3.5 Applications of Diarylethenes 31
2.4 Other Photochromic Systems 32
2.4.1 Stilbene 32
2.4.2 Spiropyranes and Spirooxazines 33
2.4.3 Fulgides 34
2.5 Photocontrol of Catalytic Activity 35
2.5.1 General Considerations 35

2.5.2 Concepts 37
2.5.3 Photoswitchable Catalysts 43
2.5.3.1 Photochromic Additives 43
2.5.3.2 Photochromic Templates 47
2.5.3.3 Reversible Steric Shielding 51
2.5.3.4 Switching Electronic Situations 52
2.6 Literature 52

3 Photoswitchable Bases 61

3.1 Introduction 61
3.2 Synthesis of Photoswitchable Bases 63
3.3 Structure and Conformational Dynamics 68
3.3.1 Solid-State Structural Analysis 68
3.3.2 Structure and Dynamics in Solution 70
3.4 Photochromism 81
3.5 Reactivity 98
3.5.1 Basicity 98
3.5.2 General Base Catalysis 104
3.6 Immobilization 119
3.6.1 Motivation and Strategy 119
3.6.2 Synthesis 124
3.6.3 Photochromism in Solution 129
3.6.4 Photochromism on Solid-Support 133
3.6.5 Characterization of Monolayers 135
3.7 Conclusion and Outlook 137
3.8 Experimental 137
3.8.1 General Methods 137
3.8.2 Spectroscopy 138
3.8.3 pKa-Determination 139
3.8.4 Kinetic Experiments 140
3.8.5 NMR Spectroscopy 140
3.8.6 Computational Details 143

3.8.7 Synthetic Procedures 144
  3.8.7.1 Azobenzene Catalysts 144
  3.8.7.2 Stilbene Catalyst 151
  3.8.7.3 Bromo-Spiro Building Blocks 153
  3.8.7.4 BOC-Protected Hydrazines 155
  3.8.7.5 Styryl Boronic Ester 157
  3.8.7.6 *N*-tert-Butyl-4-piperidone 158
  3.8.7.7 Spiro-Hydrazo Compounds 159
  3.8.7.8 Blocking-Group Precursors 162
  3.8.7.9 Immobilization Precursor 167
  3.8.7.10 Supported Catalysts 175
3.9 Literature 177

4 Towards Photoswitchable *N*-Heterocyclic Carbenes 185

4.1 Introduction 185
  4.1.1 *N*-Heterocyclic Carbenes 185
  4.1.2 Synthesis of *N*-Heterocyclic Carbenes 193
  4.1.3 Application of the Concept of Reversible Steric Shielding 197
4.2 Pentiptycene-Based *N*-Heterocyclic Carbenes 200
  4.2.1 Shielding Concept 200
  4.2.2 Synthesis 201
4.3 Tetramethyl-Terphenyl-Based *N*-Heterocyclic Carbenes 204
  4.3.1 Shielding Concept 204
  4.3.2 Synthesis 206
4.4 Terphenyl-Based *N*-Heterocyclic Carbenes 214
  4.4.1 Shielding Concept 214
  4.4.2 Synthesis 215
4.5 Non-symmetrical Terphenyl-Based *N*-Heterocyclic Carbenes 219
  4.5.1 Shielding Concept 219
  4.5.2 Synthesis 221
    4.5.2.1 Synthesis of the Photochromic Terphenyl Aniline 224
    4.5.2.2 Synthesis of the Nonsymmetrical NHC-Framework 233

4.6 Concluding Remarks 239
4.7 Experimental 240
4.8 General Methods 240
4.9 Synthetic Procedures 241
4.10 Literature 270

5 Outlook 277

5.1 Photoswitchable Bases 277
5.2 Photoswitchable NHC-Ligands 280
5.3 Literature 282

6 Appendix 285

6.1 Abbreviations 285
6.2 Publications 287

1 Introduction

The potential of nanoscale devices and structures for innovative applications in all fields of science and technology was realized as early as 1959 by Richard Feynman, distilled in his famous quote "There is plenty of room at the bottom".[1] His ideas of obtaining nanoscale devices by continuous miniaturization of known structures inspired generations of scientists, leading to tremendous advances in the production of nanoscale objects and patterns by utilizing a variety of lithographic techniques (Figure 1).[2,3] The economical aspects of this development can not be underestimated, considering the outstanding importance of integrated circuits in modern semiconductor industries.[4] However, the trend of building nanostructures from top down is intrinsically limited, due to physical constraints of the methods applied.[5] Therefore, alternative pathways have started to emerge, trying to construct functional features on the nanoscale starting from the molecular level upwards (Figure 1).[3,6] These efforts led to the development of a variety of functional units, ranging from molecular shuttles[7] to nanoscale tools,[8] which allow for a controlled manipulation of molecular-scale work-pieces.

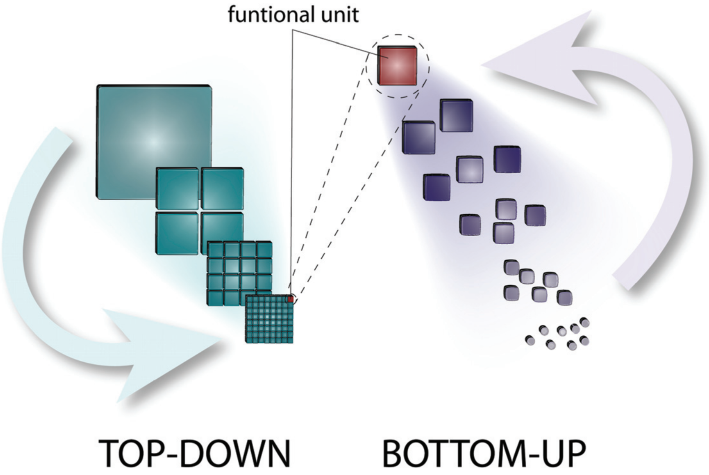

Figure 1: Schematic representation of two different approaches to nanoscale devices and functional units. The top-down approach (left part) is characterized by a repeated miniaturization of larger structures, whereas the bottom-up approach (right part) is characterized by the assembly of nanoscale structures from smaller precursors (atoms/molecules, nanoparticles, polymers, etc.).

One important requirement for successfully entering this field is precise control over the properties of single molecules and assemblies thereof. The development of stimuli-responsive, so-called “intelligent”, molecules with specific function is a major step in pioneering this field. Many functions have been successfully controlled by incorporation of suitable switches, which allow to drive the system between at least two or more resting states. Pronounced changes of the corresponding bulk material evolve from these changes at the molecular level, leading to new fields of applications that cannot be derived from the individual functional units. Functions that have been successfully controlled by application of external stimuli are for example electron- and energy transfer processes,[9] the aggregation behavior of small molecule gelators,[10] or the activity of enzymes.[11]

In analogy to the macroscopic world, nanoscopic functional units need some energy input in order to operate. Evolving from the chemist’s daily laboratory experience, chemical reactions were initially utilized as convenient sources of energy to fuel functional units. However, this kind of energy input demands for pronounced interactions between functional units and the environment, since mass transfer over the system’s borders is necessary to supply chemical energy in the form of suitable reactants. Undoubtedly, light and electrons constitute more elaborate energy inputs, as they are easily provided by a variety of suitable light sources or by electrochemical setups. The possibility to achieve high spatial as well as temporal control in combination with the availability of advanced optical systems, potentially allowing to set-up highly parallel processes, distinguishes light as a superior stimulus that is furthermore able to deliver its energy in a non-invasive fashion. A versatile interface for the interaction of the functional unit and the light stimulus is provided by photochromes, allowing to reversibly drive the system between two or more resting states.[12,13]

Light is a frequently encountered stimulus for various biological processes, ranging from the initiation of the photosynthetic water-splitting by photooxidation of chlorophyll[14] to the $Z \rightarrow E$ isomerization of retinal, triggering a cascade of events finally leading to vision by the human eye[15] or energy production by purple bacteria.[16] In these examples a relatively simple event, that is absorption of a photon, is translated to a much more complex outcome over numerous steps, demonstrating the efficiency of these cascades. Noteworthy, additional amplification of the incoming signal is encountered in many of these light-induced processes by a subsequent sequence of catalytic cycles.

Despite numerous examples of successful photoswitching of molecular functions, reports on photoswitchable catalysis are rather scarce.[17] From a chemist's view point, catalytic activity is one of the most intriguing functions to be rendered photoswitchable, due to the unique possibility to translate a light stimulus to a chemical signal, which is tremendously amplified by the catalytic cycle, thereby mimicking fundamental biological processes (Figure 2). To illustrate this point, consider an inactive catalyst (OFF-state) that can be activated by a light stimulus. As long as the catalyst rests in its inactive state, it co-exists with a stock of substrate molecules without detectable formation of products. An incoming light stimulus converts the inactive catalyst to an active form (ON-state), reactive enough to convert the substrate to product, thereby translating the light stimulus into a chemical signal. The chemical signal can easily be read out by standard analytic methods or exploited in some other way, e.g. for the control of biological functions provided the products are biologically active. Taking advantage of the reversibility of the activation process, the ON-state can be deactivated on demand, adding an additional temporal component to the control over the overall process.

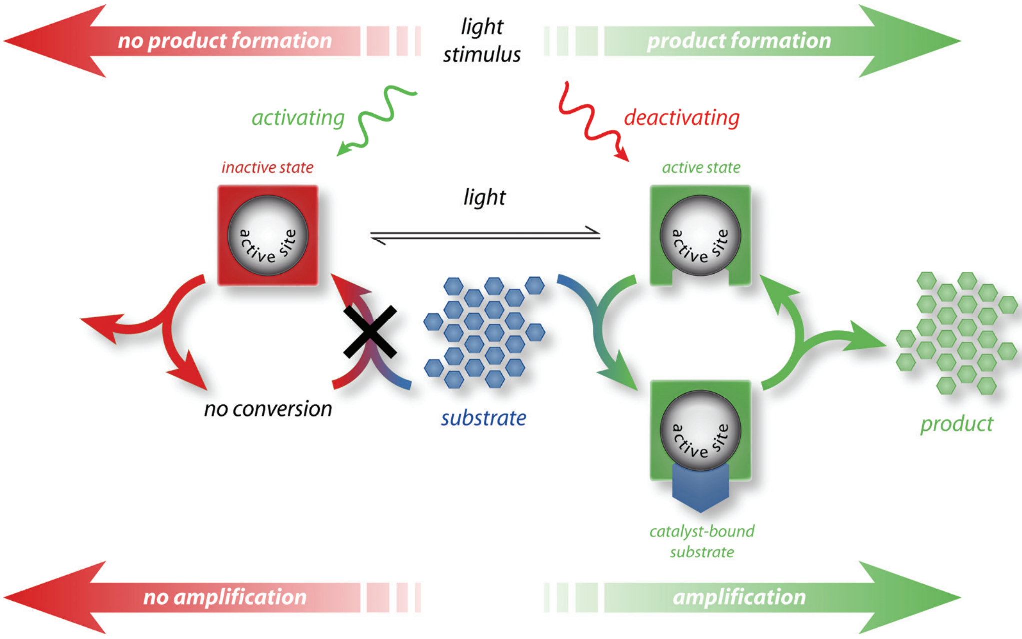
no product formation
light stimulus
product formation
activating
deactivating
inactive state
active state
active site
light
no conversion
substrate
product
catalyst-bound substrate
no amplification
amplification

Figure 2: Concept of a photoswitchable catalyst, which allows for the amplification of an incident light stimulus. The inactive catalyst (red, left part) shows no detectable reactivity towards substrate (blue hexagons, middle), whereas the active form (green, right part) exhibits a distinct reactivity, allowing to react the substrate to product (green hexagons, right).

Aim of this Work

The aim of the work presented in this thesis is the synthesis and characterization of photoswitchable catalyst-systems. A general concept for the design of photoswitchable catalysts is developed and applied to different catalytically active systems. Application of the concept to organic piperidine bases goes beyond the mere spatial and temporal control of chemical reactivity, since basicity as a very fundamental chemical property is rendered photoswitchable (Chapter 3). Photoswitching of basicity is expected to have tremendous impact on chemistry, biology, and related fields, since precise and reversible fine-tuning of pH-values in closed compartments by non-invasive stimuli is now within reach. In combination with the potential to amplify the incident light stimuli, novel innovative sensing techniques seem to be possible. Surface tethering of the photoswitchable base is expected to significantly expands the scope of the concept, potentially enabling new strategies for surface functionalization and patterning. With the aim of extending the concept to organocatalysts of high intrinsic reactivity, the general concept for the development of photoswitchable catalysts is applied to *N*-heterocyclic carbenes, which are known to efficiently catalyze numerous organic transformations (Chapter 4).[18]

1.1 Literature

(1) Feynman, R. *Eng. Sci.* **1960**, *23*, 22-36.

(2) Wallraff, G. M.; Hinsberg, W. D. *Chem. Rev.* **1999**, *99*, 1801-1821; Xia, Y. N.; Rogers, J. A.; Paul, K. E.; Whitesides, G. M. *Chem. Rev.* **1999**, *99*, 1823-1848; Gates, B. D.; Xu, Q. B.; Stewart, M.; Ryan, D.; Willson, C. G.; Whitesides, G. M. *Chem. Rev.* **2005**, *105*, 1171-1196; Xia, Y. N.; Whitesides, G. M. *Angew. Chem., Int. Ed. Engl.* **1998**, *37*, 551-575; Geissler, M.; Xia, Y. N. *Adv. Mater.* **2004**, *16*, 1249-1269; Ginger, D. S.; Zhang, H.; Mirkin, C. A. *Angew. Chem., Int. Ed. Engl.* **2004**, *43*, 30-45.

(3) Special Issue of *Scientific American* **2001**, *285*, Issue: 3.

(4) Heck, S.; Pinner, D. "Creating Value in the Semiconductor Industry," McKinsey & Company, 2007.

(5) Ito, T.; Okazaki, S. *Nature* **2000**, *406*, 1027-1031.

(6) Lehn, J.-M. *Angew. Chem., Int. Ed. Engl.* **1988**, *27*, 89-112; Lehn, J. M. *Angew. Chem., Int. Ed. Engl.* **1990**, *29*, 1304-1319; Ozin, G. A. *Adv. Mater.* **1992**, *4*, 612-649; Balzani, V.; Credi, A.; Raymo, F. M.; Stoddart, J. F. *Angew. Chem., Int. Ed. Engl.* **2000**, *39*, 3349-3391; Kay, E. R.; Leigh, D. A.; Zerbetto, F. *Angew. Chem., Int. Ed. Engl.* **2007**, *46*, 72-191.

(7) Bissell, R. A.; Cordova, E.; Kaifer, A. E.; Stoddart, J. F. *Nature* **1994**, *369*, 133-137.

(8) Muraoka, T.; Kinbara, K.; Kobayashi, Y.; Aida, T. *J. Am. Chem. Soc.* **2003**, *125*, 5612-5613; Muraoka, T.; Kinbara, K.; Aida, T. *Nature* **2006**, *440*, 512-515.

(9) Raymo, F. M.; Tomasulo, M. *Chem. Soc. Rev.* **2005**, *34*, 327-336.

(10) Hecht, S. *Small* **2005**, *1*, 26-29.

(11) Willner, I.; Rubin, S. *Angew. Chem., Int. Ed. Engl.* **1996**, *35*, 367-385; Willner, I. *Acc. Chem. Res.* **1997**, *30*, 347-356.

(12) El'tsov, A. V. *Organic Photochromes*; 1. ed.; Consultants Bureau: New York, 1990; Dürr, H.; Bouas-Laurent, H. *Photochromism: Molecules and Systems: Revised Edition*, 2003.

(13) Special Issue "Photochromism: Memories and Switches" edited by M. Irie: *Chem. Rev.* **2000**, *100*, 1683-1890.

(14) Kurreck, J.; Niethammer, D.; Kurreck, H. *Chemie in Unserer Zeit* **1999**, *33*, 72-83.

(15) Rando, R. R. *Angew. Chem., Int. Ed. Engl.* **1990**, *29*, 461-480.

(16) Deisenhofer, J.; Michel, H. *Angew. Chem., Int. Ed. Engl.* **1989**, *28*, 829-847; Gennis, R. B.; Ebrey, T. G. *Science* **1999**, *286*, 252-253; Haupts, U.; Tittor, J.; Oesterhelt, D. *Annu. Rev. Biophys. Biomol. Struc.* **1999**, *28*, 367-399; Lanyi, J. K. *FEBS Lett.* **1999**, *464*, 103-107; Heberle, J. *Biochimica Et Biophysica Acta-Bioenergetics* **2000**, *1458*, 135-147; Kuhlbrandt, W. *Nature* **2000**, *406*, 569-570; Lanyi, J. K.; Luecke, H. *Curr. Opin. Struct. Biol.* **2001**, *11*, 415-419.

(17) Ueno, A.; Takahashi, K.; Osa, T. *Chem. Commun.* **1980**, 837-838; Ueno, A.; Takahashi, K.; Osa, T. *Chem. Commun.* **1981**, 94-96; Würthner, F.; Rebek, J., Jr. *Angew. Chem., Int. Ed. Engl.* **1995**, *34*, 446-450; Würthner, F.; Rebek, J., Jr. *J. Chem. Soc.,*

Perkin Trans. 2 **1995**, 1727-1734; Sugimoto, H.; Kimura, T.; Inoue, S. *J. Am. Chem. Soc.* **1999**, *121*, 2325-2326; Cacciapaglia, R.; Di Stefano, S.; Mandolini, L. *J. Am. Chem. Soc.* **2003**, *125*, 2224-2227; Sud, D.; Norsten, T. B.; Branda, N. R. *Angew. Chem., Int. Ed. Engl.* **2005**, *44*, 2019-2021.

(18) Enders, D.; Balensiefer, T. *Acc. Chem. Res.* **2004**, *37*, 534-541; Enders, D.; Niemeier, O.; Henseler, *Chem. Rev.* **2007**, *107*, 5606-5655; Marion, N.; Diez-Gonzalez, S.; Nolan, I. P. *Angew. Chem., Int. Ed. Engl.* **2007**, *46*, 2988-3000; *N-Heterocyclic Carbenes in Synthesis*; Nolan, S. P., Ed.; Wiley-VCH: Weinheim, 2006.

2 General Part

2.1 Photochromism

Photochromism is defined as "a reversible transformation of a chemical species induced in one or both directions by absorption of electromagnetic radiation between two forms, **A** and **B**, having different absorption spectra" (Figure 1).[1] The difference in absorption properties, i.e. color, is accompanied by differences in other properties, such as refractive index, chemical reactivity, or solubility.

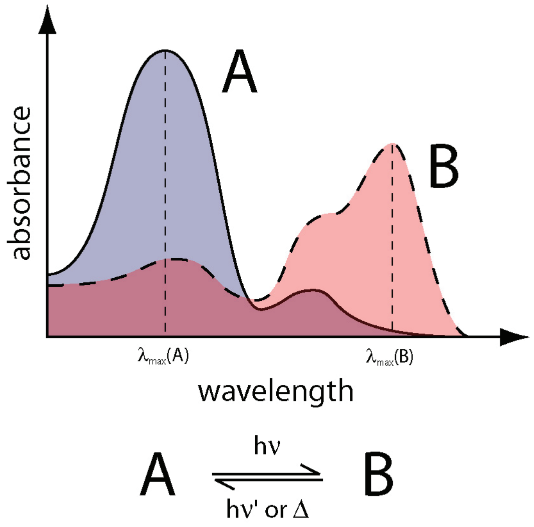

Figure 1: Schematic representation of the absorbance of a photochromic system. Species **A** absorbs more intensely in the blue region of the electromagnetic spectrum while species **B** absorbs more intensely in the red region.

The reversible transformation can be induced by either UV, vis, or IR radiation, however, irradiation with UV and vis light is most frequently encountered. Reversibility is an important criterion since it separates photochromism from the broad field of photochemistry leading to irreversible chemical transformations.

Typically, the energy barrier for the transformation **A** → **B** is too high for the reaction to occur under normal laboratory conditions (e.g. the reaction is thermally forbidden by orbital symmetry). Absorption of light by **A** yields an excited state **A***, which is able to overcome the energy barrier for the conversion of **A** to **B**. Since **A** and **B** are different chemical species, there is a change in enthalpy of formation of reactant and product associated with the photochemical reaction, which causes a thermodynamic driving force for the back-reaction.[a] Depending on the energy barrier for the transformation **B** → **A** the reaction occurs either solely via a photochemical pathway (high barrier, photochromism of the P-type) or via an additional thermal pathway, if the barrier can be overcome in the ground state (photochromism of the T-type).

Considering a photochromic system of the P-type, irradiation of a sample with light mainly absorbed by species **A** leads to an increase of concentration of species **B** due to the photochemical conversion **A** → **B**. However, a complete conversion of **A** to **B** is scarcely observed, since non-negligible absorption of **B** in the wavelength region used for irradiation causes a photochemical conversion of **B** → **A**. In the event of both conversions occurring to the same extent, an equilibrium situation, the photostationary state, is obtained, which does not change composition upon continued irradiation. The composition of the photostationary state is given by:[2,3]

$$\frac{[A]}{[B]} = \frac{\varepsilon_A \cdot \phi_{A\rightarrow B}}{\varepsilon_B \cdot \phi_{B\rightarrow A}} \tag{1}$$

where ε_A and ε_B are the extinction coefficients of **A** and **B**, respectively, and $\Phi_{A\rightarrow B}$ and $\Phi_{B\rightarrow A}$ are the quantum yields for the indicated photochemical reactions. Clearly, the difference in extinction coefficients of **A** and **B** is not solely responsible for the observed photostationary state mixture. The efficiencies of both photochemical reactions associated with the photochromic behavior influence the photostationary state as well, potentially leading to more efficient switching than expected from inspection of the absorption spectra in some cases. Nevertheless, to ensure efficient switching the irradiation wavelength should be chosen in a region, dominated by the absorption of one component of the photochromic system.

---

[a] The common case that $\lambda_{max}(A) < \lambda_{max}(B)$ and $\Delta H_f(A) > \Delta H_f(B)$ is referred to as positive photochromism. The rare case $\lambda_{max}(A) > \lambda_{max}(B)$ and $\Delta H_f(A) > \Delta H_f(B)$ is referred to as negative or inverse photochromism.

A number of photochromic systems were investigated in detail.[3-6] Four major families can be identified based on the mechanism of the molecular transformation leading to photochromic behavior: (a) photochromism based on the *E*/*Z* isomerization of double bonds, (b) photochromism based on electrocyclization reactions, (c) photochromism based on cycloaddition reactions, and (d) photochromism based on tautomerism (proton transfer processes).[4] Among the variety of systems studied so far, a number of photochromes reached outstanding importance. These are photochromes based on the isomerization of N=N- and C=C-bonds in azobenzenes and stilbenes, respectively, photochromes based on the reversible ring closure and opening of diarylethenes, photochromic spiropyranes, and photochromic fulgides. The other families of photochromes received much less attention in chemical research and applications despite the – in parts – detailed knowledge of the photophysical properties. In the following, the isomerization of azobenzenes and of diarylethenes will be discussed in more detail.

2.2 Azobenzenes

2.2.1 Introduction

Azobenzenes belong to the large group of azo-compounds carrying the characteristic N=N-moiety. Organic,[7,8] inorganic,[9], and organometallic[10] azo compounds have been investigated. Only organic azo compounds shall be described in the following section and the discussion will be limited to purely aromatic azo compounds. For the discussion of aliphatic and mixed aliphatic/aromatic azo compound the reader is referred to the literature.[7,8]

The photochromism of azobenzene was first recognized by Hartley in 1937.[11,12] The existence of two isomeric forms of azobenzene is in accordance to the isosteric relation of the azo group and the vinylene group. The *Z*-isomer reverts to the thermodynamically more stable *E*-isomer with an half-life depending on the substitution pattern of both aryl rings (T-type photochromism, Figure 2). Besides the *E*/*Z*-isomerization, azobenzenes carrying hydroxyl- or amino-groups in the *ortho*- or *para*-position may exhibit photochromism based on intramolecular proton transfer (azo-hydrazone tautomerism).

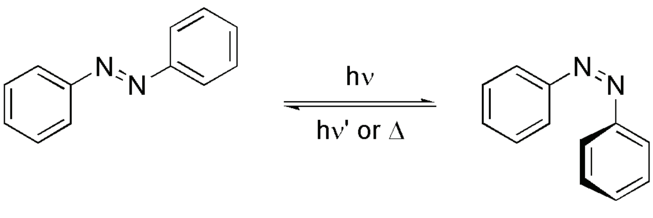

Figure 2: *E*/*Z*-Isomerization of azobenzene.

Three different types of azobenzenes can be distinguished on the basis of the relative energetic order of (n,π*)- and (π,π*)-states: (a) azobenzene type, (b) amino-azobenzene type, and (c) pseudo stilbene type. The differences in relative energetic order go along with pronounced differences in properties other than photophysical, e.g. thermal half-lifes of the respective *Z*-isomers. In the following sections, an introduction into the spectral features of azobenzenes of the three different types will be given, followed by an overview over the mechanisms of $E \rightarrow Z$ isomerization. Finally, a brief overview over synthesis and applications of azobenzene chromophores will be given.

2.2.2 Spectral Features

2.2.2.1 Azobenzene Type

Azo compounds of the azobenzene type are characterized by a broad, long wavelength absorption, which is attributed to the n → π* absorption and a well-separated π → π* absorption at shorter wavelengths giving this class a yellow to red appearance. These spectral features are characteristic for a relatively low lying ^{1}(n,π*)-state and a substantial energy gab to the next higher ^{1}(π,π*)-state. Typical spectra are shown in Figure 3.

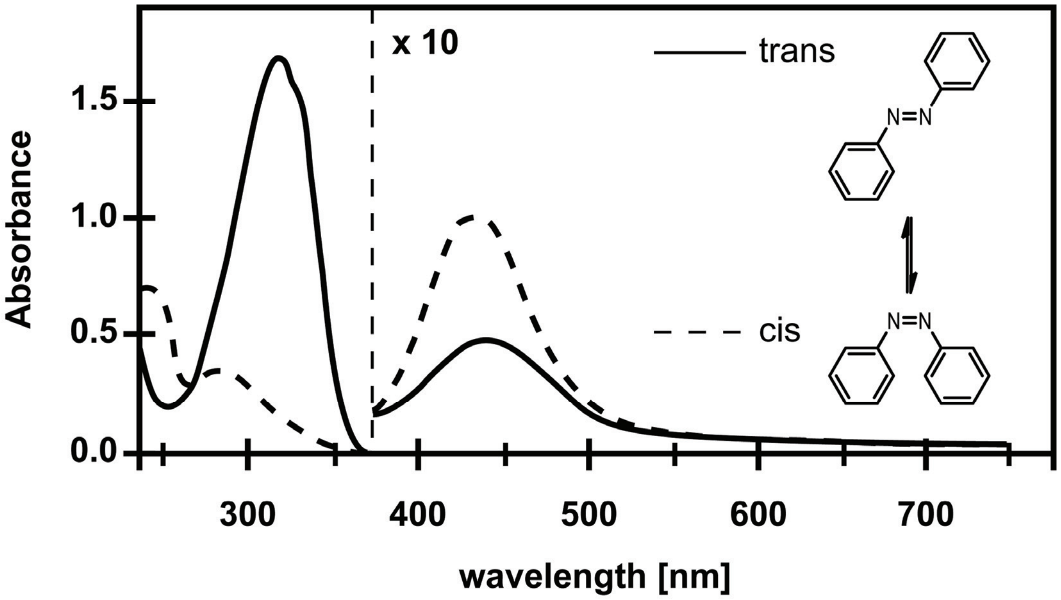

Figure 3: Typical absorption spectra of neat azobenzene. The n → π* absorption is magnified by a factor of 10. Taken from reference[13].

The band attributed to the n → π* absorption around 440 nm is relatively strong compared to carbonyl compounds: $\varepsilon_{449} = 405\ M^{-1}\ cm^{-1}$ for *E*-azobenzene and $\varepsilon_{405} = 1250\ M^{-1}\ cm^{-1}$ for *Z*-azobenzene clearly exceed the values around $20\ M^{-1}\ cm^{-1}$ typically found for carbonyl compounds.[14] The higher extinction coefficient of the *Z*-isomer has been attributed to the distortion of the chromophore due to steric interactions of 2- and 2'-substituents. Indeed, *Z*-azobenzene exhibits a parallel alignment of both phenyl rings in the crystal with a twist of 53° out of the plane of the azo group.[15] Nevertheless, the *E*-isomer's extinction coefficient is remarkably high, which has been attributed to non-planar distortions of the molecule and to a coupling of the $^1(n,\pi^*)$-state to the $^1(\pi,\pi^*)$-state. As for carbonyl compounds, the pure $n \rightarrow \pi^*$ transition is symmetry forbidden, but mixing in the character of the symmetry allowed $\pi \rightarrow \pi^*$ absorption makes the $n \rightarrow \pi^*$ transition partially allowed. The absorption around 320 nm is attributed to the $\pi \rightarrow \pi^*$ absorption.

These spectral features are typically found for azobenzenes carrying electronically "innocent" substituents, which are not in conjugation with the chromophore and which are not carrying acidic protons (e.g. $-NH_2$ and -OH). The spectra of azo compounds of the azobenzene type are remarkably insensitive to variations of the solvent polarity.[16] Variations of the substitution pattern using halogen, alkyl, or similar substituents cause some shifts in the spectra. However, the influence of other substituents is far more pronounced and is discussed below. Generally, azobenzene type molecules are non-emitting, apart from rare, special cases.

2.2.2.2 Aminoazobenzene Type

The spectral features of azobenzenes carrying amino or hydroxy groups in *ortho*- or *para*-position differ markedly from those of the azobenzene type. The $\pi \rightarrow \pi^*$ absorption is bathochromically shifted by ~70 nm, whereas the $n \rightarrow \pi^*$ absorption remains essentially unchanged. Therefore, the spectral separation of both absorption bands becomes smaller and a partial overlap of both absorption bands is observed. The spectral features are relatively sensitive to variations of the solvent polarity.[16] Furthermore, the presence of acidic protons ($-NH_2$ and -OH) further complicates the situation since competing photochromism based on azo hydrazo tautomerism can occur. Fluorescence might be observed for azo compounds of the aminoazobenzene type.

2.2.2.3 Pseudostilbene Type

Azobenzene molecules carrying strong donor and acceptor substituents in *ortho*- or *para*-position are characterized by a relatively low-lying $^1(\pi,\pi^*)$-state, usually leading to a complete spectral overlap of the $\pi \rightarrow \pi^*$ and $n \rightarrow \pi^*$ absorption. The energetic order can even be reverted, that is the energy of the $^1(\pi,\pi^*)$-state becomes lower than the energy of the $^1(n,\pi^*)$-state. Solvent polarity has a marked effect on the position of the absorption bands. Most commercial azo dyes belong to the pseudostilbene type with tremendous impact on their properties (*vide infra*). Some azo compounds of the pseudostilbene type might exhibit fluorescence.

A low-lying $^1(\pi,\pi^*)$-state can also be caused by protonation of the azo group, leading to a disappearance of the $n \rightarrow \pi^*$ absorption and a bathochromic shift of the $\pi \rightarrow \pi^*$ absorption.[17] Protonation of the azo group occurs nonsymmetrically on one N-atom.[18] A similar effect is observed upon complexation of one N=N lone pair by Lewis acids.[19]

2.2.3 Isomerization

2.2.3.1 Azobenzene Type

Irradiation of thermally equilibrated samples of azobenzene with light predominantly absorbed by the *E*-isomer leads to a deepening of the sample's color, due to formation of the *Z*-isomer. The reveres reaction can be affected by irradiation with light mainly absorbed by the *Z*-isomer. The *Z*-isomer is thermodynamically less stable than the *E*-isomer, the energy difference for neat azobenzene being 56 kJ mol^{-1}. The kinetic stabilization of the *Z*-isomer is not sufficient to prevent thermal reversion, therefore photochromism of the T-type is observed. Activation energies in the range of 85 - 100 kJ mol^{-1} and pre-exponential factor between 10^{12} and 3×10^{12} s^{-1} have been reported.[20] The rate for the thermal reversion is strongly depended on the substitution pattern (*vide infra*). Almost no side-reactions are observed when irradiating azobenzene samples for days, rendering the isomerization of azobenzenes one of the cleanest photoreactions known. Only in the presence of oxygen a slow photooxidation is observed. Extrusion of nitrogen, commonly encountered upon irradiation of (strained) alkyl-diazocompounds is not observed for aromatic azobenzenes when the isomerization pathway is accessible.

The mechanism of isomerization of azobenzenes has been extensively studied. Two major pathways have been discussed: (a) isomerization by rotation of one aryl ring and (b) isomerization by inversion of the azo-group (Figure 4). Rotational isomerization involves a non-planar transition state, with one aryl ring being moved out of the plane of the remaining planar C-C-N-N-fragment and its ring-plane being oriented perpendicular to the plane of the C-C-N-N-fragment. The π-bond of the azo-fragment is either homolytically or heterolytically broken, that is either diradical or zwitterionic intermediates are encountered during isomerization. On the other hand, the π-bond remains intact upon inversion since the transition state is planar and corresponds to a linear alignment of the moving C-atom connected to the azo-fragment and the N=N-double bond.

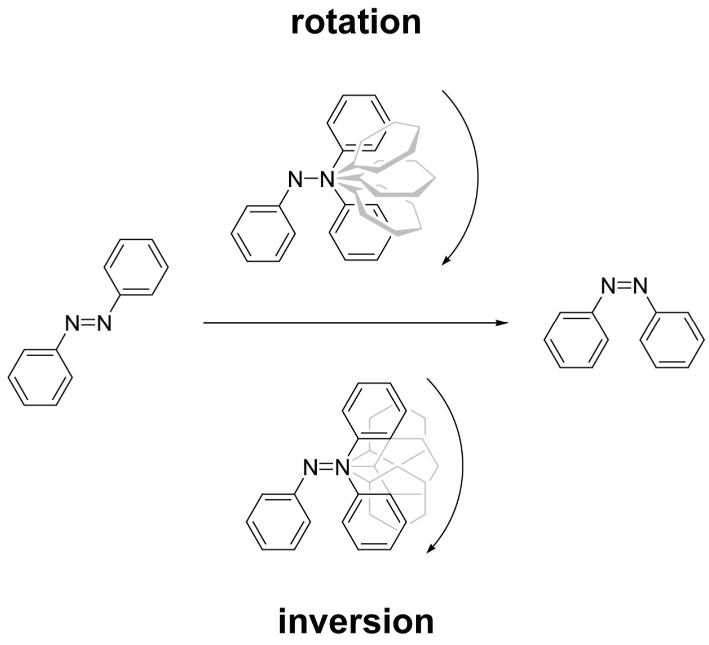

Figure 4: Schematic representation of the two major isomerization pathways discussed for azobenzenes.

The quantum yields for the isomerization of azobenzenes depend on the excitation wavelength, therefore Kasha's rule is violated. Quantum yields for excitation of the π → π* transition are generally smaller than quantum yields for the excitation of the n → π* transition. This caused a debate on which mechanism is operating during isomerization. Initially, it was assumed that two different mechanisms for the $E \rightarrow Z$ isomerization are operating depending on the excitation wavelength. Excitation of the π → π* transition was thought to lead to isomerization by rotation, whereas excitation of the n → π* transition was thought to lead to isomerization by inversion. This was concluded on the basis of quantum yield measurements for isomerization of azobenzenes lacking the possibility to rotate their aryl rings due to incorporation of the chromophore in cyclophane-like structures. However, on the basis of experimental and theoretical findings Orlandi and co-workers developed a different scheme (Figure 5).[21] Again, excitation of the n → π* transition causes isomerization by inversion. However, excitation of the π → π* transition leads to an energy minimum on the excited energy surface by rotational motion, which is coupled to the ^{1}(n,π) state and the ground state. The bifurcation to the ^{1}(n,π*) and the ground state accounts for the reduced isomerization quantum yields observed for π → π* excitation. Molecules passing to the ^{1}(n,π*) surface are expected to go back to the Franck-Condon geometry by rotation and to proceed further to *Z*-azobenzene following an inversion coordinate.

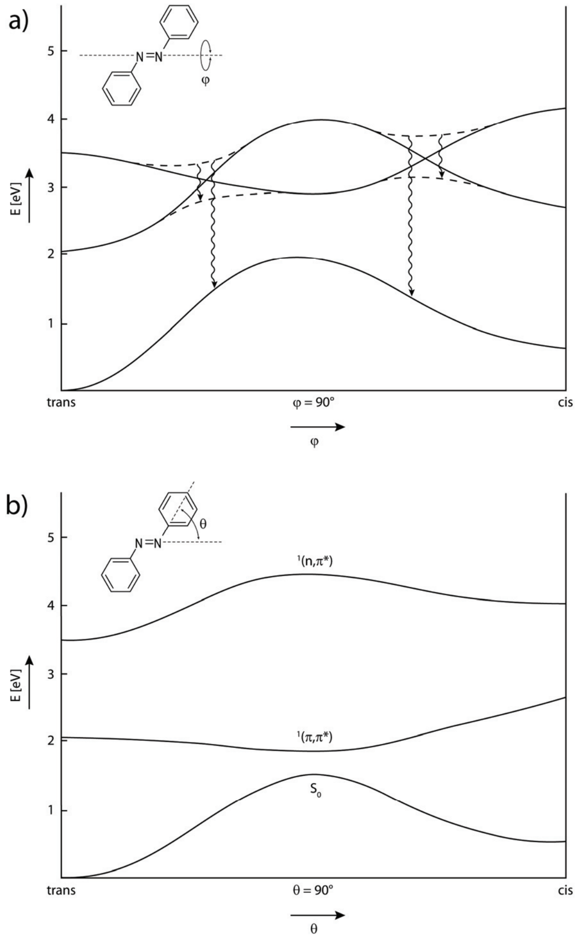

Figure 5: Energy state diagram for azobenzene considering only singly excited states for different coordinates: a) rotational coordinate and b) inversion coordinate. Wavy lines indicate internal conversion pathways, dotted lines indicate avoided crossings. Adapted from reference[21].

Recent high-level ab-initio calculations taking configuration interactions into account led to a reformulation of the above mechanism (Figure 6).[22,23] A rotational reaction path is found upon excitation of the n → π* transition, which is in contradiction to earlier findings. Isomerization starting from the $^1(\pi,\pi^*)$-state is influenced by a doubly excited state, arising from π,π → π*,π* excitation of the azo fragment. This state is intermediate between $^1(\pi,\pi^*)$ and $^1(n,\pi^*)$ and leads to fast internal conversion of $^1(\pi,\pi^*)$ to $^1(n,\pi^*)$. The difference of quantum yields for both types of excitation is explained by the high vibronic excitation of the $^1(n,\pi^*)$, obtained via this internal conversion pathway from former π → π* excitation, leading to substantial leakage to the starting ground state of *E*-azobenzene. These results do not completely exclude the presence of an inversion pathway. Depending on the extent of vibrational energy accumulated in the molecule by excitation, the rotational pathway might have certain characteristics of an inversion pathway. Equal quantum yields found for azo-phanes are explained by an unexpectedly high flexibility of these systems in the excited states.

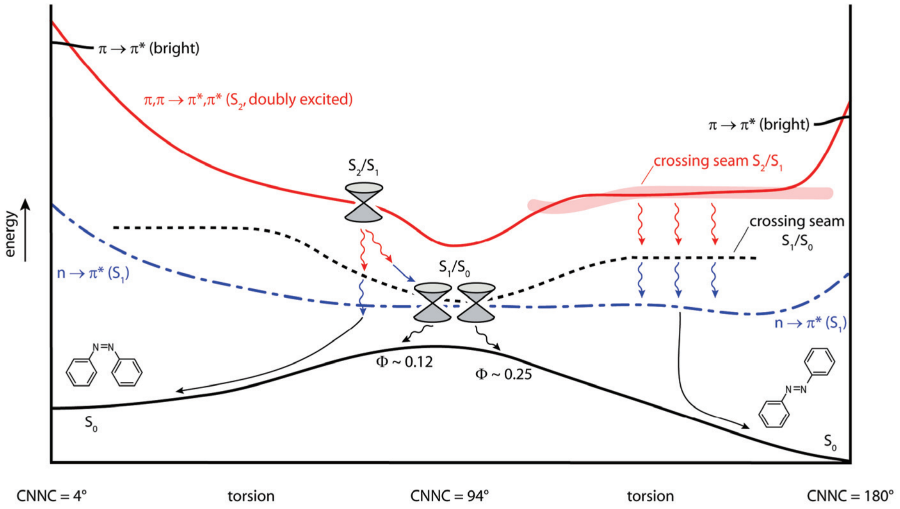

Figure 6: Summary of photoisomerization pathways for azobenzene. Excitation of *E*-azobenzene to the bright $^1(\pi,\pi^*)$ state is followed by very fast internal conversion to a state based on a doubly excited configuration π,π → π*,π*. This state is strongly coupled to the $^1(n,\pi^*)$ state facilitating internal conversion followed by isomerization on the $^1(n,\pi^*)$ surface on a rotational coordinate. Adapted from reference[23].

The mechanism of *Z* → *E* isomerization was studied to a smaller extent, most likely due to the less accurate data of quantum yields obtained experimentally. The data and computational investigations are in accordance with the mechanistic picture proposed above. The thermal *Z* → *E* isomerization most likely proceed via an inversion pathway, however, some experimental results are in good accordance with a rotational pathway. The *Z* → *E* isomerization of azobenzenes can also be photocatalyzed by iodine or bromine and by electron transfer employing electron donors and acceptors. The photocatalyzed isomerization most likely proceeds by temporal addition of the catalyst to the N=N-double bond, thereby breaking the π-bond and enabling rotation around the single bond formed.

Beside direct excitation, triplet sensitization can also lead to the isomerization of azobenzenes.

2.2.3.2 Aminoazobenzene Type

Azobenzenes carrying amino- or hydroxyl-groups isomerize upon exposure to light. However, the *Z*-isomer quickly reverts to the more stable *E*-isomer. Half-lifes between a few hours and several minutes have been reported for 4-dimethylaminoazobenzene depending on the solvent. Activation energies of this group are somewhat lower than those reported for azobenzene. As for the azobenzene type, quantum yields of $E \rightarrow Z$ isomerization are wavelength-dependent for the aminoazobenzene type: usually larger quantum yields are found for long-wavelength excitation leading to preferential $n \rightarrow \pi^*$ excitation.[24] The fast thermal reversion of the *Z*-isomer prevents an accurate determination of quantum yields of $Z \rightarrow E$ isomerization at room temperature. Aminoazobenzenes are prone to irreversible photoreduction when excited to higher states.

2.2.3.3 Pseudostilbene Type

The thermal half lifes of *Z*-isomers of azobenzenes of the pseudostilbene type are very short, namely in the range of ms.[25] The photophysical properties greatly depend on the nature of the solvent, as is expected for highly polarized compounds. Quantum yields for $E \rightarrow Z$ isomerization are low, but they are comparable for both types of excitation, as expected for pseudo stilbenes due to the close proximity of the $^1(n,\pi^*)$- and $^1(\pi,\pi^*)$-states. Possible side-reactions upon exposure to light are photooxidation and photoreduction, however, quantum yields for these processes are exceptionally small.

As already mentioned, most commercial azo dyes belong to the pseudostilbene type. The combination of photochemical $E \rightarrow Z$ isomerization with a fast thermal $Z \rightarrow E$ reaction along with azo-hydrazone tautomerism is a formidable prerequisite for an efficient conversion of light into heat, thereby accounting for the fastness to light found for these azo dyes.

2.2.4 Synthesis

A variety of synthetic pathways leading to azobenzenes of varying substitution patterns have been developed (Figure 7). Most of the commercially available azo dyes are produced by classical azo coupling of a diazonium salt with an activated aromatic system, usually donor substituted benzene or naphthalene derivatives.[26] The electrophilicity of the diazonium salt can be further increased by introduction of electron-withdrawing substituents. Access to the diazonium salt is conveniently provided by simple diazotation of anilines and similar substrates. Non-symmetrical azobenzenes carrying donor- or donor- as well as acceptor-substituents are easily available by the azo coupling protocol, however, the reaction is limited by the choice of suitable substrates and by the relatively harsh reaction conditions.

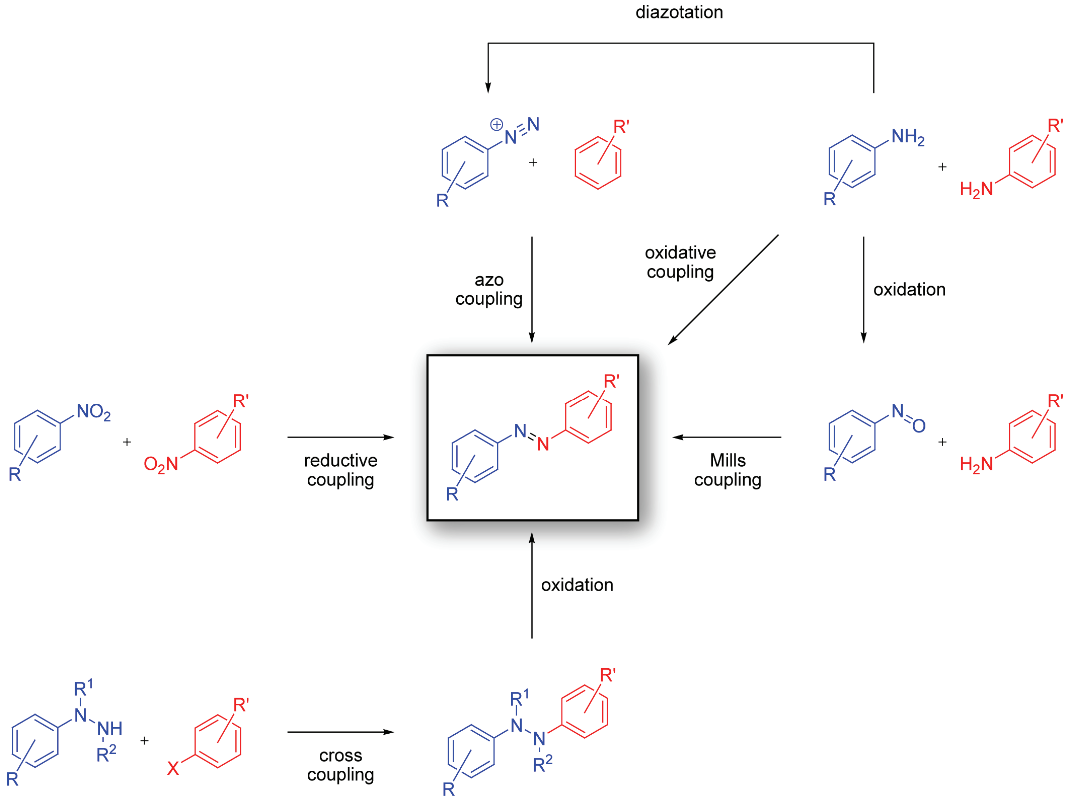
diazotation
azo coupling
oxidative coupling
oxidation
reductive coupling
Mills coupling
oxidation
cross coupling
R
R'
NH2
H2N
NO2
O2N
R1
R2
NH
X

Figure 7: Overview of different synthetic pathways leading to azobenzenes with varying substitution patterns.

Symmetrical and non-symmetrical azobenzenes carrying functional groups not compatible with the azo coupling conditions can be accessed by the reaction of an aromatic nitroso compound with an aniline in glacial acetic acid, the so-called Mills reaction.[27] A wide variety of functional groups is tolerated by this methodology. The nitroso compound can be accessed by selective oxidation of anilines with suitable oxidizing agents, e.g. oxone.[28] Furthermore, it is possible to generate the nitroso compound and react it *in situ* with an amine. Depending on the course of the reaction, it is possible to synthesize symmetrically but also nonsymmetrically substituted azobenzenes. A number of suitable oxidizing reagents have been reported, among which manganese dioxide seems to be compatible with a number of functional groups.[29]

Reductive coupling of nitro compounds to yield azo benzenes has been reported. Reduction can be accomplished by a variety of reducing agents. For example, nitrobenzene has been reductively coupled to yield neat azobenzene by treatment with zinc in basic aqueous methanol.[30] As for the oxidative procedures, the intermediacy of a nitroso benzene derivative is assumed. The aniline coupling partner is most likely accessed by over-reduction of the nitro compound.

Recently, a new synthetic route based on modern metal-catalyzed cross-coupling techniques was developed.[31] Palladium-catalyzed cross coupling of *N*-BOC protected *N*-phenyl hydrazines with aryl bromides or iodides yields *N*-BOC-*N*,*N*'-diphenyl hydrazines (R^2 = H, lower part of Figure 7), which can be further oxidized to yield azobenzenes by employing either NBS/pyridine in methylene chloride at room temperature or CuI/Cs_2CO_3 in DMF at 140 °C.[32] The BOC-protected hydrazines are easily synthesized by copper-catalyzed cross-coupling of aryl iodides with mono-BOC-protected hydrazine.[33] Alternatively, *N*,*N'*-bis-BOC-protected hydrazine can be employed to give *N*,*N'*-bis-BOC-*N*,*N*'-diphenyl hydrazines, which can be oxidized to the corresponding azobenzenes employing CuI/Cs_2CO_3 after copper-mediated coupling with suitable aryl iodides (R^2 = BOC, lower part of Figure 7).[34] The authors extended this methodology to a one-pot procedure directly yielding the corresponding azobenzenes. The transformation was achieved by reacting the *N*,*N'*-bis-BOC-*N*-phenyl hydrazines with an aryl iodide in DMF at elevated temperatures in the presence of CuI, phenanthrene, and Cs_2CO_3.

2.2.5 Applications of Azobenzenes

Despite the early first mentioning of azobenzene in the chemical literature in 1880 by Frankland and co-workers[35] and the discovery of the photochromic properties in 1937,[11] azobenzene and its derivatives attracted increasing interest in the chemical community starting in the early 1990s, indicated by a sharp rise in the number of publications.[b] Most of the applications utilized the photochromic properties of azobenzene. The following short overview shall mostly limit on applications concerned with the switching properties of azobenzene. The overview is necessarily limited in scope and focuses on the most prominent fields, since over 6000 publications deal with azobenzenes.

The most prominent application of azobenzenes is as colorful dyes of yellowish to red color. Most of these dyes belong to the pseudostilbene type and therefore exhibit limited photochromic applicability (*vide supra*).[8] The application of azo-dyes in recordable compact discs constitutes another commercially important application. However, this application is not based on their photochromic behavior.[36]

Besides these truly commercial applications, azobenzenes have extensively been used to control molecular or supramolecular properties by light.[4,6] Azobenzenes were incorporated into polymeric[37] and liquid crystalline materials.[38] Applications of these photochromic systems are various, ranging from modern techniques of (holographic) data storage over micro-lithography to surface relief gratings (SRGs) generated by irradiation of polymeric films, which have been used for the construction of photonic devices, optical fibers, and displays. Azobenzene-functionalized surfaces have been used to control the wetting and dewetting behavior.[39] Possible applications include the photocontrol of microfluidic devices, smart “windows” and related surfaces, as well as use of these surfaces in bioapplications, e.g. to control cell adhesion.

---

[b] Based on a query of the word „azobenzene“ in the ISI Web of Knowledge.

Azobenzenes have been utilized to control various biological and bio-related structures.[40-42] The conformational behavior of polypeptide strands[42] and α-helices[40] was successfully controlled by incorporation of azobenzene moieties. Attachment of azobenzenes to larger biological structures allowed for photocontrol of enzyme activity[41] and for the control of neuronal firing by triggering the opening/closing of a potassium channel with an attached azobenzene. [43]

Two examples shall help to cover the range of implementations of azobenzenes in functional organic materials. It was shown, for instance, that azobenzenes carrying dendritic polyether moieties act as efficient antennas for IR-photons.[44] The *E*/*Z*-isomerization can be triggered by multi-photonabsorption. The polyether dendrons transfer the energy to the vibrationally isolated azobenzene-core, thereby providing enough energy for isomerization. Here, the switching event is exploited for the detection of a molecular property. On the other hand, the azobenzene has also been used to directly influence structural properties as a result of isomerization. A azobenzene-functionalized ferrocene carrying porphyrin-based coordination sites was successfully used to control the conformational behavior of a guest molecule.[45] This represents the first successful operation of a nanoscale tool acting on a molecular workpiece.

2.3 Diarylethenes

2.3.1 Introduction

Stilbene is well-known to undergo reversible *E*/*Z*-isomerization upon exposure to UV light. In contrast to azobenzenes, the thermal $Z \rightarrow E$ is not feasible under ambient conditions. In addition, *Z*-stilbene undergoes an electrocyclization to produce dihydrophenanthrene – a reaction not possible for *E*-stilbene. In the presence of oxygen or other oxidizing agents, dihydrophenanthrene is irreversibly oxidized to yield phenanthrene.[5,46]

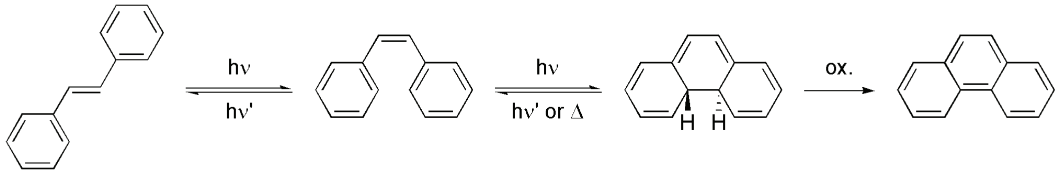

Figure 8: Photochromic behavior of stilbene: Reversible *E*/*Z* isomerization of the double bond and reversible electrocyclization to yield dihydrophenanthrene. The dihydrophenanthrene can be irreversibly oxidized to give phenanthrene.

The oxidation of dihydrophenanthrene can be prevented by introduction of methyl groups in the 2- and 6-positions of the phenyl rings. However, the lifetime of the yellow ring-closed isomer is limited by fast thermal ring-opening to colorless *Z*-stilbene. Replacement of the phenyl ring by heterocyclic five-membered rings, e.g. thiophene or furane, drastically increases the lifetime of the ring-closed isomer, that is P-type photochromism is observed.[47] The switching performance is further enhanced by fixing the two aryl moieties in a *Z*-geometry, also preventing competing *Z* → *E* isomerization. Geometrical fixation is usually achieved by incorporation of the double bond into suitable cyclic structures. Some representative examples are given in Figure 9. Most commonly encountered are structures with perfluorocyclopentenes,[48] perhydrocyclopentenes,[49] and maleic anhydrides[47] or maleiimides.[50]

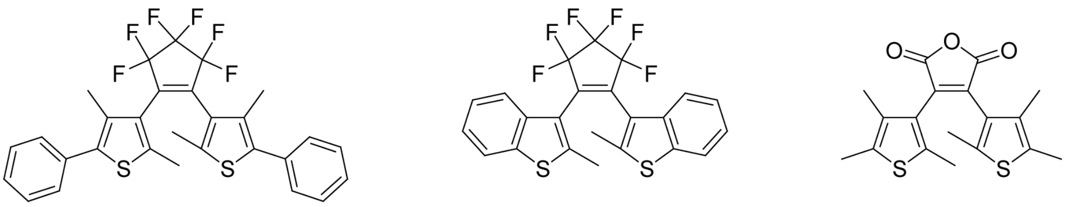

Figure 9: Some representative examples of diarylethenes.

2.3.2 Spectral Features

The absorption spectra of diarylethene photochromes are characterized by short-wavelength absorptions of the ring-opened isomers. Upon irradiation, a new absorption band at longer wavelengths evolves accompanied by the build-up of a pronounced absorption at shorter wavelengths. In contrast to azobenzenes, the thermal stability of diarylethenes allows to isolate the ring-closed isomer. Typical absorption spectra of prototype diarylethene derivatives are shown in Figure 10.

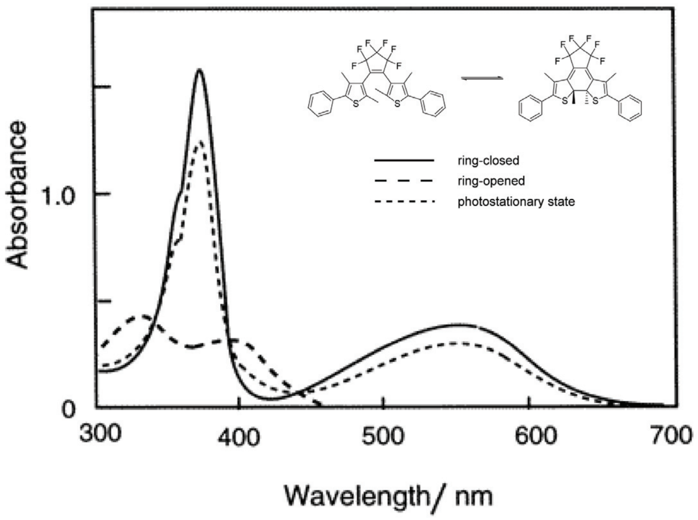

Figure 10: Typical absorption spectra of a dithienylethene in its ring-opened and ring-closed form. The spectra of the photostationary state obtained by irradiation at 405 nm is shown as well. Taken from reference[46].

The spectral features are relatively sensitive to variations of the molecular structure. In general, incorporation of a maleic anhydride or maleiimide bridge shifts the absorption maxima to the red. Incorporation of donor-acceptor moieties on the aryl rings has a similar yet larger effect.

Extinction coefficients of diarylethenes are rather low for simple systems carrying just methyl groups on the aryl rings (see Figure 11a). Exchange of methyl groups for a phenyl group (see Figure 10) increases the extinction coefficients, an effect that is even more pronounced, if the phenyl rings carry electron-donating or electron-withdrawing substituents. The incorporation of donor-acceptor moieties on the aryl rings not only causes a bathochromic shift of the entire absorption spectra, but also leads to an increase of the extinction coefficients.

The connection-mode of the thiophene to the bridging ring has drastic influence on the absorption spectra (Figure 11). Change from the usual 3-substitution pattern on the thiophene ring to a 2-substitution pattern causes a blue-shift of the absorption of the ring-closed isomer, presumably due to the lower extent of conjugation in the ring-closed form.

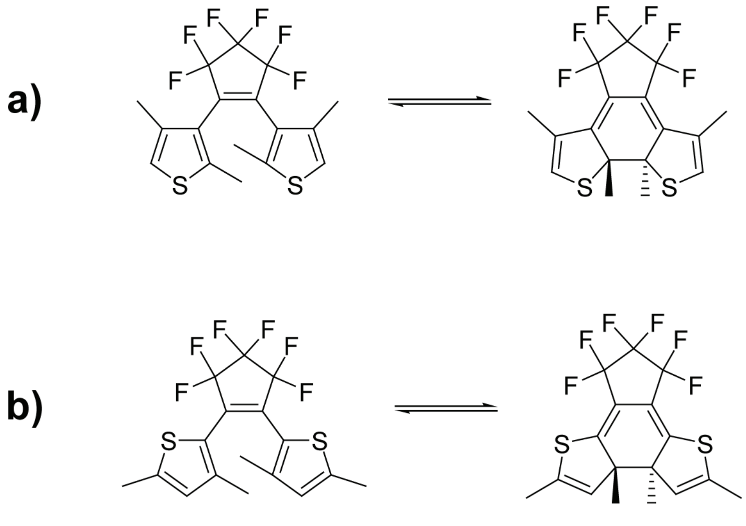

Figure 11: Two dithienylethenes with varying connectivity of the thiophene rings: a) connection via the 3-position b) connection via the 2-position.

2.3.3 Isomerization

According to the rules of the conservation of orbital symmetry,[51] the light-induced ring-opening/ring-closing proceeds conrotatory, whereas the thermal ring-opening follows a disrotatory pathway. Thermal ring-closure is not observed, due to the increased energy of the ring-closed structure.

Isomerization of diarylethenes is a rather clean photochemical reaction, if positions prone to oxidation are blocked by methyl groups. Stilbene and its derivatives have only limited applicability due to the fast thermal ring-opening of the closed form. Replacing the phenyl ring by heteroaromatic rings such as thiophene, furane or thiazole greatly increases the thermal stability. The effect has been attributed to the decreased aromatic stabilization energy of these heteroaromatic rings.[52] Indeed, a correlation of aromatic stabilization energy and thermal stability of the ring-closed isomer has been established. Nonsymmetric diarylethenes have been prepared in the search for systems with higher extinction coefficients and led to the conclusion that the presence of one thiophene ring is sufficient to ensure thermal stability of the ring-closed isomer.

One of the prime advantages of diarylethenes is their excellent fatigue resistance. Some systems can be switched for at least 30.000 times in solution without the observation of any detectable degradation. In general, diarylethenes of the maleic anhydride type have a limited switchability, whereas systems constructed from benzothiophenes are extremely robust. The kinetics of the switching process reveal fast ring-closure and ring-opening in the range of few picoseconds.

2.3.4 Synthesis

A number of synthetic routes towards diarylethenes have been described in the literature.[5,46] The four most prominent pathways are summarized in Figure 12. Perfluorocyclopentene-based systems are accessed by reaction of metalated heteroaromatic rings with octafluorocyclopentene (Figure 12a).[48] Consecutive addition of two different metalated heteroaromatics allows to synthesize nonsymmetrical diarylethenes. A drawback commonly encountered during preparation is the volatility of octafluorocyclopentene and the low yield of the addition-elimination cascade.

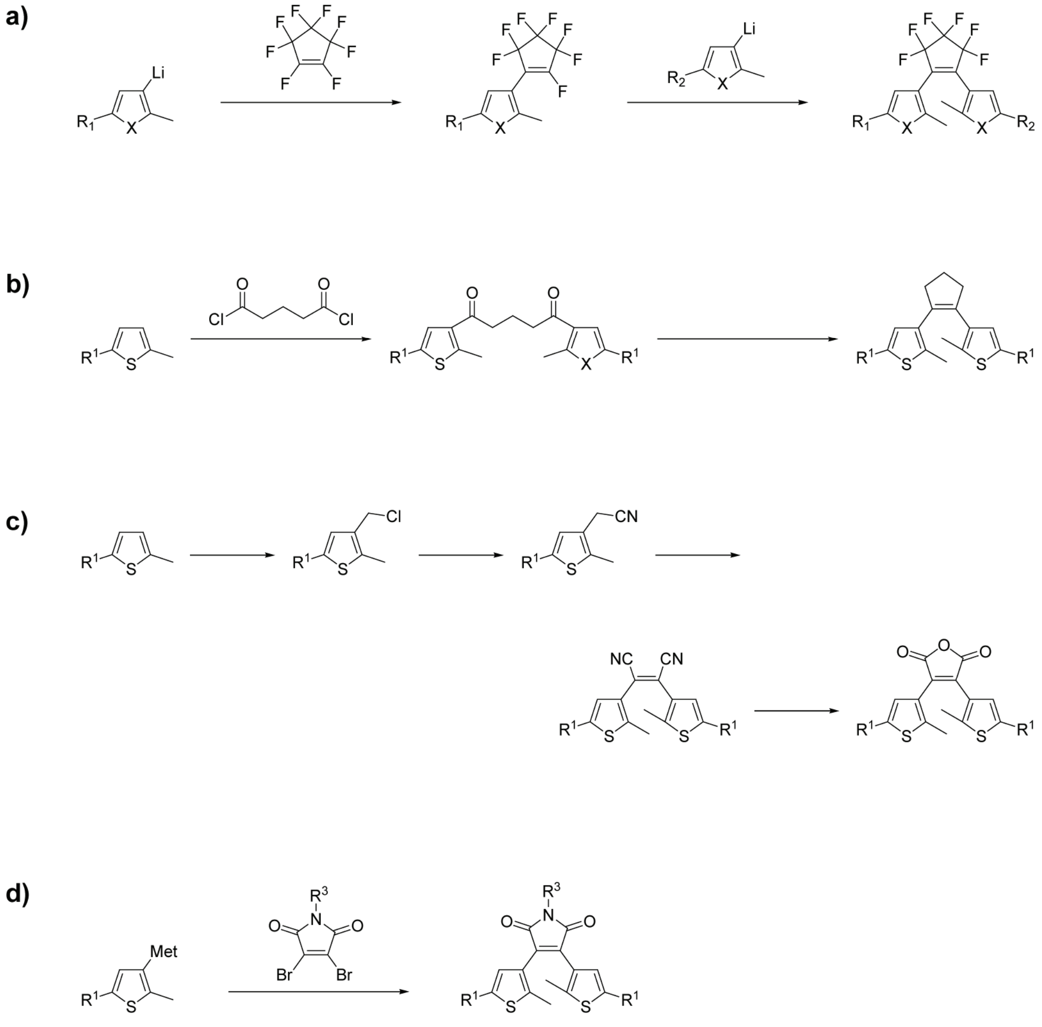

Figure 12: Summary of four main synthetic routes towards diarylethenes.

Therefore, alternative pathways have been devised. Feringa and co-workers developed a synthetic protocol granting access to perhydrocyclopentene-based diarylethenes (Figure 12b).[49] Reactions of suitable thiophenes with glutaryl dichloride in the presence of $AlCl_3$ as Lewis-acid affords a 1,5-dithiophenyl-1,5-diketone as a key intermediate. Cyclization of the diketone using McMurry-conditions gives the desired diarylethene in moderate to good yields.

Diarylethenes carrying a maleic anhydride or maleiimide bridge are more difficult to synthesize. Initially, maleic anhydride-based diarylethenes were accessed by a low-yielding multistep procedure (Figure 12c).[47] Maleiimide-bridged systems were even more difficult to synthesize.[50] Recently, an easy access to maleiimide-based systems was developed, based on Suzuki-type cross-coupling of a thiophene-based boronic acid and 3,4-dibromomaleiimide derivatives (Figure 12d).[53]

2.3.5 Applications of Diarylethenes

Similar to azobenzenes, diarylethenes found multiple applications in a variety of fields. These include photoregulation of electron and energy transfer processes,[54] host-guest-chemistry,[55], and magnetic properties.[56] Diarylethenes have been extensively used for switching supramolecular structures and function. For instance, the phases transition behavior of liquid crystals has been successfully photoregulated[57] as well as the gelation behavior of small molecules.[58]

Successful switching of diarylethenes is not limited to solution phase or similar “soft” environments, e.g. gels or liquid crystals, but can also be affected in bulk single crystals, as demonstrated by Irie and co-workers.[59,60] The close structural relation between both isomers prevents substantial reorganization of the crystalline lattice, thereby rendering the switching process feasible also in the rigid environment of a crystal. However, the small geometrical changes associated with isomerization lead to a modest reorganization of the molecular packing, causing either changes of the crystals’ surface morphologies[59] or shapes.[60] Potential applications as photodriven, molecular actuators can be envisioned for these systems, as exemplarily demonstrated by the movement of gold micro-particles utilizing rod-like crystals, which bend upon irradiation with UV-light.

2.4 Other Photochromic Systems

2.4.1 Stilbene

The photochromic behavior of stilbene is based on the *E*/*Z* isomerization of the C=C-double bond making the process geometrically analogous to the isomerization of azobenzenes (*vide supra*).[4] However, the absence of non-bonding electron pairs causes some distinct difference in the isomerization behavior. The photoisomerization of stilbene is one of the best understood photochemical reactions.

E-Stilbene is almost perfectly planar allowing for efficient packing in the crystalline solid, whereas *Z*-stilbene is significantly distorted from planarity due to steric interactions of both phenyl rings, reflected in its liquid nature at room temperature. The thermal $Z \rightarrow E$ process is associated with a significant barrier, though P-type photochromism is observed (Figure 13a). Photochemical excitation of *E*-stilbene significantly reduces the C,C-bond order, allowing the molecule to relax to a so-called phantom state $^1p^*$ with a perpendicular orientation of the formerly co-planar halves of the molecule (Figure 13b). The geometry of the phantom state closely resembles that of the transition state of thermal isomerization. Relaxation of the phantom state gives ground state stilbene in either *E*- or *Z*-configuration, depending on the conditions and on the substitution pattern. The efficiency of conversion to ground-state *E*-stilbene is described by the factor α_s and conversely conversion to *Z*-stilbene is described by 1-α_s. A schematic representation of the processes involved in the photochemical isomerization of stilbene is given in Figure 13c. Isomerization can also be effected by triplet sensitization.

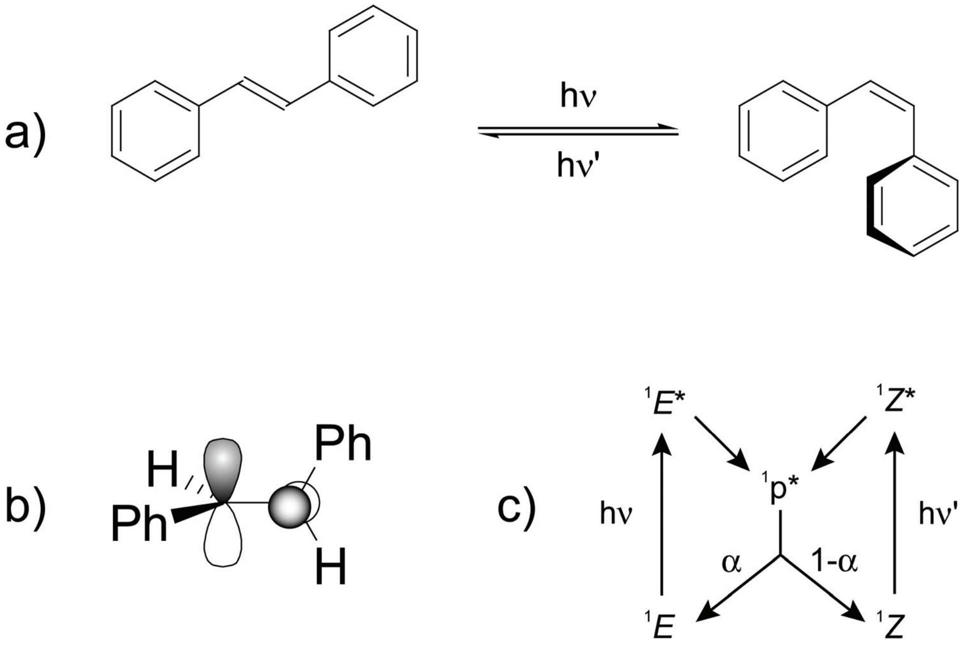

Figure 13: a) Isomerization of stilbene. b) Perpendicular geometry of the phantom state p*. c) Schematic representation of the singlet mechanism of isomerization (α_s denotes the fraction the fraction of ^{1}p*, which decays to ^{1}*E*).

2.4.2 Spiropyranes and Spirooxazines

Spiropyranes and spirooxazines are well-known photochromes based on reversible ring-opening/ring-closing at a spirojunction between a benzopyrane or benzoxazine moiety, respectively, and an structurally variable heterocyclic part.[4,61] A common class of spiropyranes carries an indole-residue as the heterocyclic moiety (Figure 14 for X = CH).

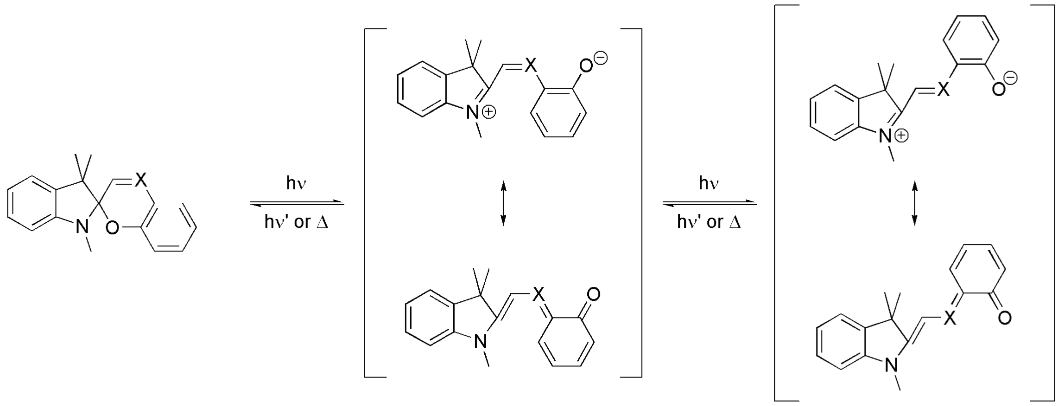

Figure 14: Schematic representation of the photochromic behavior of spiropyranes (X = CH) and spirooxazines (X = N).

The photochromic behavior is complex, due to the simultaneous occurrence of ring-opening/ring-closing and *E*/*Z*-isomerization of the double-bond. Furthermore, analysis of the photochromic behavior is complicated by fast thermal ring-closure and complex equilibria between ring-opened forms as can be concluded from the complex temperature dependence of the absorption spectra. Beside T-type photochromism, spiropyranes exhibit thermochromism, indicated by a color-deepening of solutions upon heating. Spiropyranes found multiple applications ranging from self-coloring sun-glasses to plastic photochromic lenses. However, applicability of spiropyranes is sometimes limited by their relatively low fatigue resistance.

Spirooxazines are very similar to spiropyranes in the photochromic properties, as can be expected from their close structural relation (Figure 14 for X = N). Their major advantage is a significantly increased fatigue resistance, qualifying them as ideal materials for commercial applications.

2.4.3 Fulgides

Derivatives of dimethylene succinic anhydride are named fulgides and exhibit photochromic behavior due to reversible ring-closure/ring-opening (see Figure 15).[4,62] Depending on the substitution pattern, the closed ring isomer is thermally stable or not, i.e. T-type or P-type photochromism can be found. The ring-closing and ring-opening reaction follows the rules of Woodward and Hoffmann.[51] Investigation of the photochromic behavior is complicated by concomitant *E*/*Z*-isomerization of both double bonds. Fulgides are prone to undergo irreversible side-reactions under irradiation. Rearrangements, i.e. proton- and methyl-group shifts, and photo-oxidation a commonly encountered with simple derivatives, thereby narrowing the scope for applications.

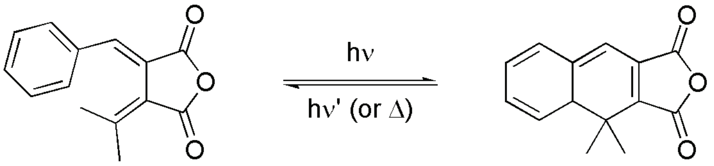

Figure 15: Prototypical example of a fulgide and its photochromic ring-closure. Competing pathways of *E*/*Z*-isomerization are not shown.

It should be emphasized, that the listing of photochromes given above is far from being complete. For example, the large field of bimolecular photochromism based on reversible dimerization, e.g. of anthracenes, is not covered as well as photochromism based on photoinduced proton transfer reactions (tautomerism). Photochromism has been extensively reviewed and the interested reader is referred to the literature.[3-6,63]

2.5 Photocontrol of Catalytic Activity

2.5.1 General Considerations

Photocontrol of catalytic activity can be achieved by several conceptually different approaches, depending on the electronic state of the active catalyst and the reversibility of the overall process (Figure 16). Catalysis brought about by an electronically excited state of the catalyst is commonly referred to as “photocatalysis” (Figure 16a).[64] A basic requirement for successful photocatalysis is an energy or electron transfer process between the catalyst and the substrate. This, in combination with the inherently short half-lifes of electronically excited states, requires continuous irradiation of the reaction mixture. Unwanted side reactions are frequently encountered in photocatalysis, partially due to photoreactions of the substrate or product molecules and partially due to the unselective nature of chemical reactions involving species in high energy excited states.

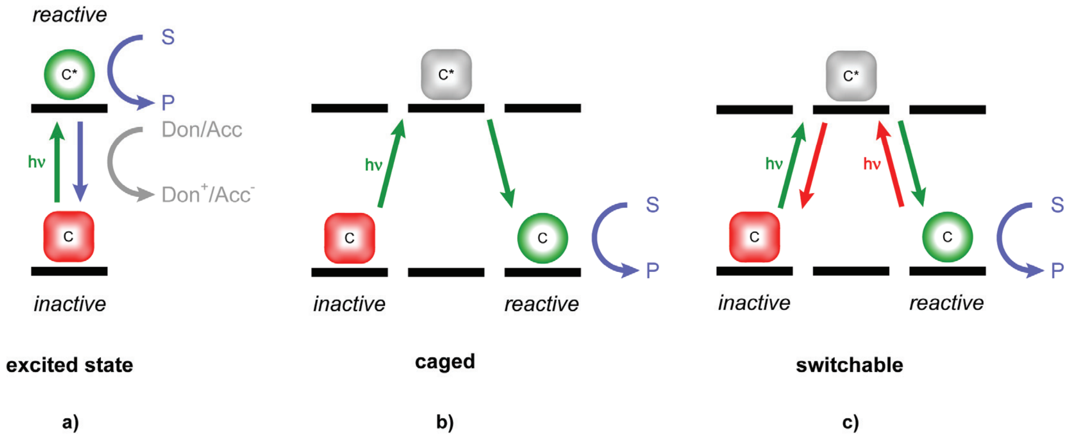

Figure 16: General approaches towards photocontrol of catalytic activity: a) true photocatalysis, that is catalytic activity is brought about by the catalyst's excited state. b) Photocaged catalysts lacking the possibility of reversible activation and deactivation. The catalytic activity originates from a ground state species. c) Photoswitchable catalysts allowing to reversibly switch the catalyst between its inactive and reactive form. The catalytic activity originates from a ground state species (red: inactive species, OFF-state; green: reactive species, ON-state).

In view of the superior scope of "thermal" catalysis, i.e. catalysis taking place on the ground state potential energy surface, it seems desirable to use light to gate a given "thermal" catalyst's activity. If catalysis is brought about by the catalyst's ground state, it is necessary to shuffle the catalyst from an inactive form into a reactive form by light (Figure 16b,c). It is important to note that energy supplied by light is not used to overcome the barrier from substrate to product, but to overcome the barrier between the catalyst's inactive and reactive states. The catalyst can either be irreversibly activated, a process commonly referred to as "photocaging" (Figure 16b),[65] or the overall process can be reversible, which requires implementation of a photoswitchable, i.e. photochromic, unit into the catalyst (Figure 16c).

Photocaging is strongly related to the development of photoremovable protecting groups[66] and found wide-spread use in bio-related applications,[67] allowing to suppress the activity of a biological species, e.g. an enzyme, and to "unleash" its activity by the use of light. However, the stoichometric liberation of by-products constitutes a major draw-back of this approach. Besides biological applications, the concept of photocaging was extensively exploited in the development of chemically amplified resists for the production of integrated circuits.[68] The most common system nowadays use the "uncaging" of protons, which catalyze the deprotection of polymeric resists causing solubility differences between exposed and unexposed regions.

2.5.2 Concepts

Despite the wide use of photochromes to photoregulate chemical function (*vide supra*), their utilization to reversibly control the outcome of a catalyzed reaction is rarely described. In this section, general concepts for the implementation of photoswitchable elements capable to drive a catalyst system between two states of different reactivity are discussed and reported examples are categorized along these lines.

In general, the reactivity state of a photoswitchable catalyst is gated by light of different wavelengths and the interface between system and stimulus is provided by a suitable photochrome. The state of higher reactivity is commonly referred to as the ON-state, whereas the state of lower reactivity is referred to as the OFF-state. A switchable catalyst system is best characterized by the ON/OFF-ratio k_{rel}, which is given by the ratio of rate constants for substrate conversion by the ON- and OFF-states, i.e. $k_{rel} = k_{ON} / k_{OFF}$. Several prerequisites can be viewed as mandatory for obtaining high ON/OFF-ratios to efficiently modulate, i.e. switch, catalytic activity. Significant population of a desired reactivity state, manifested in high attainable photostationary states for the forward and backward photochemical reactions, ensures maximum efficiency in catalyst activation and deactivation, i.e. high ON/OFF-ratios. In general, this puts certain geometrical requirements to the catalyst, which depend on the photochrome in use, and emphasizes the importance of a careful choice of chromophores present in the system. Moieties strongly absorbing in the wavelength range of the photochrome or capable to undergo detrimental energy or electron transfer processes with the photochrome should be excluded.[69] Furthermore, a high activity ratio not only implies a high reactivity of the ON-state, but also a low OFF-state reactivity to avoid undesirable substrate conversion by the OFF-state on long time scales.

Implementation of the photochromic elements necessary to gate the catalyst system’s reactivity state is possible by the addition of suitable additives to a given catalyst system, by direct incorporation of photochromic units into the catalyst’s framework, or by modulation of the electronic situation of the catalyst’s active site. Considering photochromic additives, one switching state of the additive suppresses catalytic activity, whereas the other switching state “unleashes” a catalytically active species. Therefore, two closely related classes of additives can be identified: a) inhibitors, forming an inactive complex with an inherently active catalyst, and b) activators, constituting a mandatory part of an active catalyst system (Figure 17). Switching of the photochromic inhibitor prevents further binding to the catalyst and releases a catalytically active species. Similarly, switching of the photochromic activator leads to a fragmentation of the reactive catalyst-activator complex, yet releasing an inactive species.

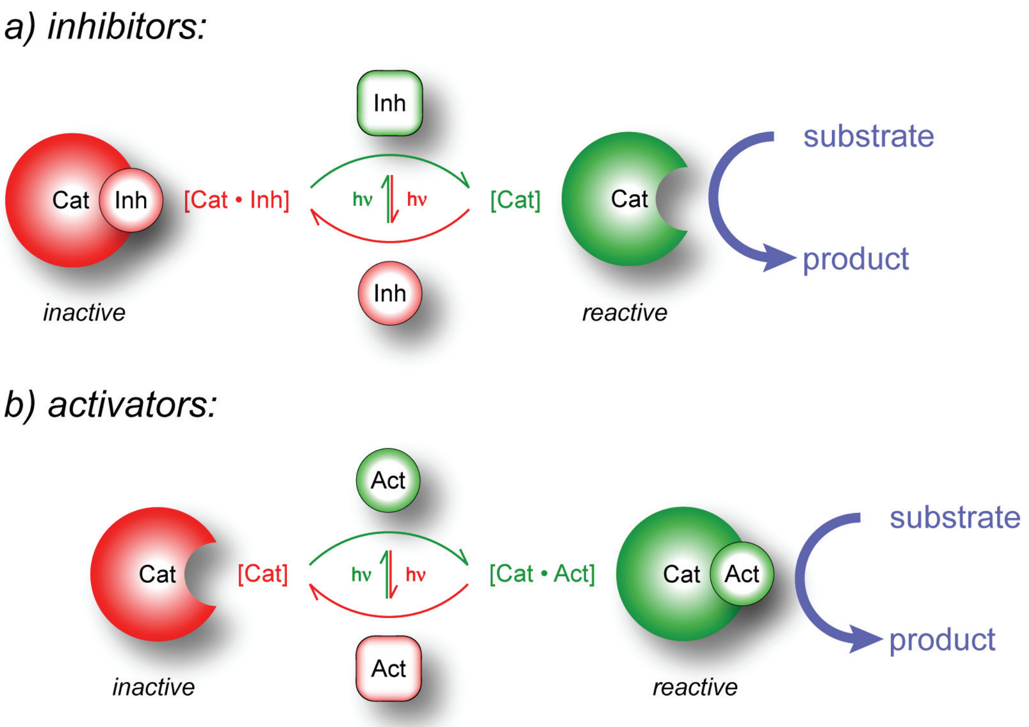
a) inhibitors:
Cat
Inh
[Cat • Inh]
Inh
hν
hν
Inh
[Cat]
Cat
substrate
product
inactive
reactive
b) activators:
Act
Cat
[Cat]
hν
hν
Act
[Cat • Act]
Cat
Act
substrate
product
inactive
reactive

Figure 17: Schematic representation of the control of catalytic activity utilizing photochromic additives: a) inhibitors and b) activators (Cat: catalyst; Inh: inhibitor; Act: activator; red: inactive species, OFF-state; green: reactive species, ON-state).

Preorganization of reactants is a commonly encountered motif in enzymatic reactions[70] and bifunctional catalysis[71] requiring suitable binding sites for the recognition and orientation of the substrate(s). Photocontrol over catalysis can be achieved by photochromic templates with marked geometrical differences associated with both switching states (Figure 18). The more contracted form of the template corresponding to the catalyst's ON-state is able to bind substrate molecules, thereby increasing the effective concentration and accelerating the reaction. Furthermore, the substrates' reactive sites are arranged in a favorable geometry to further facilitate the reaction and/or are activated by other mechanisms. In contrast, the more extend template corresponding to the catalyst's OFF-state is not able to arrange the substrate molecules in a favorable manner due to geometrical constraints associated with the remote orientation of the binding sites, although individual yet unproductive binding events may occur. It is expected that product inhibition is a serious problem of this approach towards photoswitchable catalysts, unless the binding affinities for the products are sufficiently diminished during the reaction of the substrates.

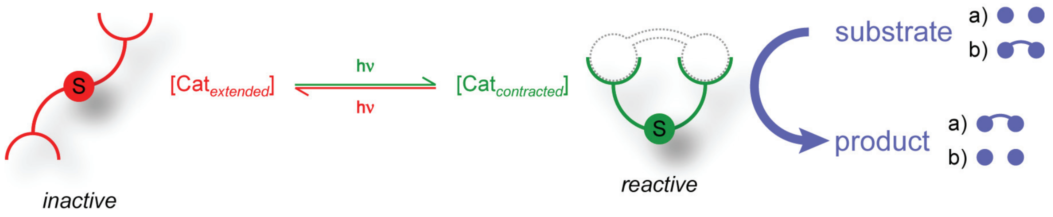

Figure 18: Schematic representation of the control of catalytic activity utilizing photochromic templates. Two possible modes of reaction are shown: a) merging of two substrate molecules and b) splitting of one substrate molecule (Cat: catalyst; S: photochromic switch; red: inactive species, OFF-state; green: reactive species, ON-state).

The catalytically active site constitutes the key component of any catalyst, as it is the center of substrate conversion. No catalytic activity is observed, if the substrate molecules are not able to access the active site for steric reasons. Reversible steric blocking of the catalytically active site therefore provides a general pathway towards photoswitchable catalysts (Figure 19). Access to the active site is controlled by an ensemble comprised of a blocking group, intercepting trajectories directed towards the active site, and a photochromic unit, which in the OFF-state holds the blocking group in the correct orientation to prevent substrate approaches to the active site and moves the blocking group away from the active site in the ON-state, thereby providing free access to the active site.

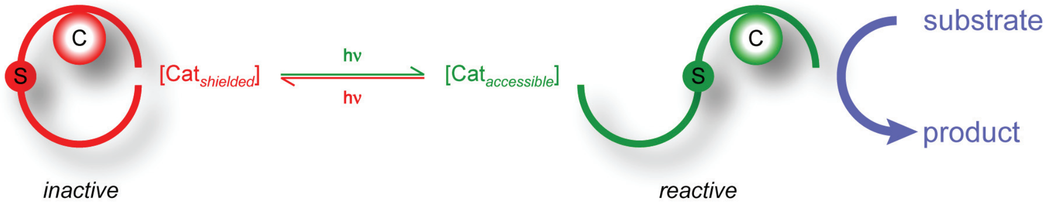

Figure 19: Schematic representation of the control of catalytic activity by reversible steric shielding. A photochromic switch S is used to gate access to the catalytically active site (Cat: catalyst; S: photochromic switch; C: catalytically active site; red: inactive species, OFF-state; green: reactive species, ON-state).

Besides the accessibility of the catalytically active site, its electronic situation is of outmost importance for the performance of a catalyst system. Therefore, manipulating the electronic situation of a catalytically active site provides a very fundamental way to control catalytic activity (Figure 20). Photochromes provide a suitable interface to gate the interaction between groups able to influence a given electronic situation, e.g. electron donating and withdrawing groups, and the active site, allowing to photomodulate catalytic activity. However, it is important to note that photocontrol of catalytic activity by influencing the electronic properties of a catalyst's active site constitutes an inherently difficult task since it requires a detailed knowledge of the interplay of electronic factors and catalytic activity.

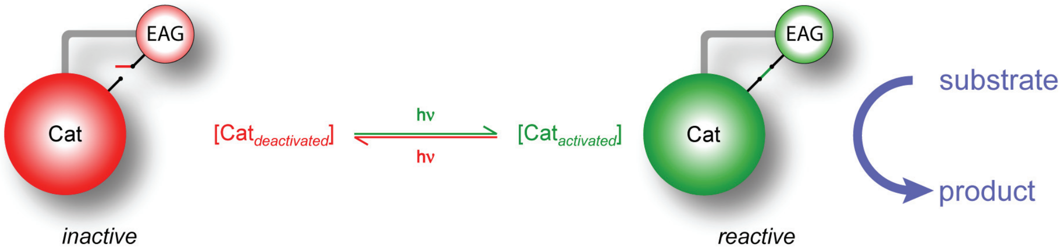

Figure 20: Schematic representation of the control of catalytic activity by switching the electronic situation of the catalyst. A photochromic element gates the electronic communication between an electronically active group EAG and the catalyst Cat. Only the activation of the catalyst by the EAG moiety is shown. Conversely, a deactivation of the catalyst by the EAG moiety is possible as well (Cat: catalyst; EAG: electronically active group (i.e. an electron donating or withdrawing group); red: inactive species, OFF-state; green: reactive species, ON-state).

Each concept described above demands for special requirements concerning the photochrome in order to successfully implement the switching unit into the catalyst system and to achieve optimal performance in catalyst activation and deactivation. Clearly, the template and the shielding approach demand for large geometrical changes associated with the switching of the photochrome, because these concepts rely on substantial displacements of large parts of the catalyst's framework. Therefore, azobenzenes, stilbenes, and related photochromes are of outstanding importance for the realization of these concepts due to the large geometrical changes accompanying the switching process. Requirements are less strict for approaches involving additives since the possibility of inhibition or activation based on steric grounds is complemented by the possibility to control the electronic situation of the inhibitor or activator, thereby controlling the overall catalyst system's activity. Finally, photoswitching of a catalyst's electronic properties solely demands for successful switching of electronic interactions, which are largely independent from geometrical requirements. Therefore, the range of suitable photochromes is significantly extended when considering switching of electronic properties.

2.5.3 Photoswitchable Catalysts

2.5.3.1 Photochromic Additives

The first example of a photoswitchable catalyst system was described by Ueno and co-workers in 1980 (Figure 21).[72] β-Cyclodextrin is known to aid the hydrolysis of benzoic ester derivatives by providing a host for the hydrophobic aryl residue of the ester, while the hydrophilic periphery of the cyclodextrin aids hydrolysis. The system was rendered photoswitchable by introduction of 4-carboxyazobenzene as a photochromic inhibitor. Cyclodextrin is only able to bind the extended *E*-isomer of the inhibitor, whereas the kinked *Z*-isomer does not fit into the cyclodextrin's cavity. Systems comprised of inhibitor, cyclodextrin, and substrate showed a lower hydrolysis activity before irradiation compared to irradiated samples, because the excess *E*-azobenzene efficiently competes with the benzoic ester for the cyclodextrin's binding pocket, whereas the *Z*-isomer is not able to compete due to steric reasons. However, the system is not truly catalytic, since the catalyst concentration exceeds the substrate concentration by roughly two orders of magnitude, and the overall effect is rather small.

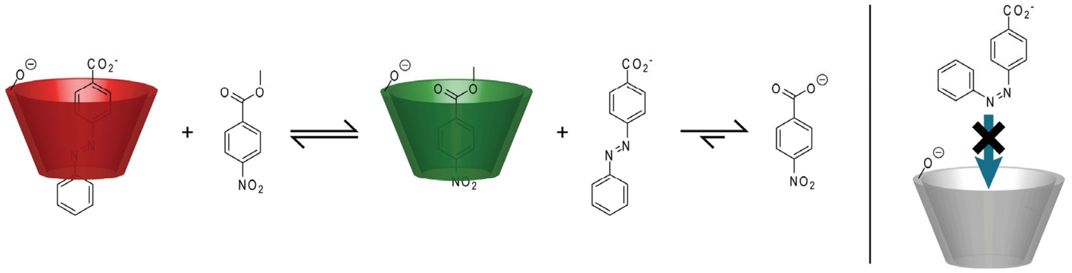

Figure 21: Photoswitchable catalyst system based on a β-cyclodextrin macrocycle and a photochromic azobenzene inhibitor. Switching the azobenzene to the *Z*-isomer prevents binding of the inhibitor, thereby accelerating the rate of hydrolysis (red: OFF-state with low activity; green: ON-state with high activity).

Photocontrol of catalysis utilizing a photochromic activator was described by Inoue and co-workers.[73] Aluminum porphyrins are known to catalyze the reaction of carbon dioxide and propylene oxide to yield cyclic propylene carbonate.[74] However, conversion is only observed in the presence of axial nitrogen based ligands, e.g. pyridine.

Photocontrol over the rate of conversion was achieved by replacing the pyridine moiety with a photochromic stilbazole acting as a photoswitchable activator (Figure 22). Steric interactions between the *E*-stilbazole's 3,5-di-*tert*-butylphenyl moiety and the porphyrin macrocycle presumably prevent efficient coordination of the stilbazole's pyridine to the aluminum center, thereby inhibiting conversion in the OFF-state. Switching the stilbazole to the sterically less demanding *Z*-isomer enables its coordination to the aluminum center of the porphyrin framework rendering the overall catalyst system active. A ten-fold rate acceleration was observed under catalytic conditions using 20 equivalents of propylene oxide under an atmosphere of carbon dioxide. However, the switching response was slow and the overall performance of the catalytic system was low, that is substantial conversion was only observed over the course of days.

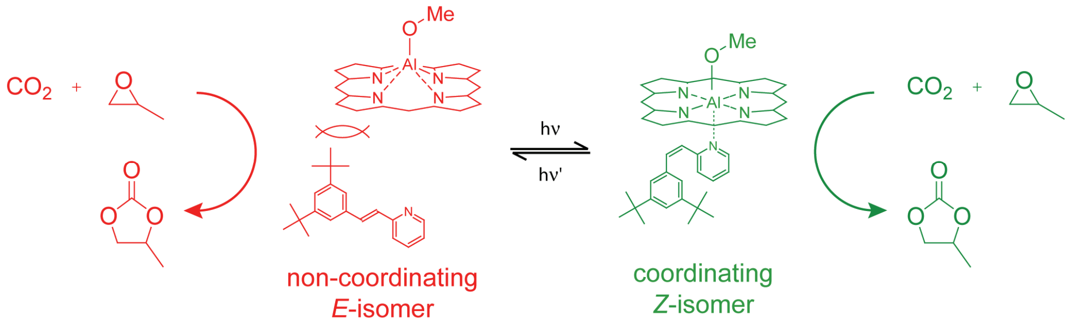

Figure 22: Photocontrolling the chemical fixation of carbon dioxide by modulation of an aluminum porphyrin's activity. The coordination behavior of an ancillary stilbazole ligand, which is needed as an activator if catalysis is to be observed, is controlled by dictating its switching state (red: OFF-state with low activity; green: ON-state with high activity; porphyrin: methoxyaluminum *meso*-tetraphenylporphyrin).

Successful photocontrol of the stereochemical outcome of a cyclopropanation reaction was demonstrated by Branda and co-workers utilizing chiral dithienylethene ligands.[75] It should be emphasized that no switching of reactivity is described, but switching of selectivity, clearly separating the system from other examples described in the literature. Furthermore, a classification according to the concepts given in section 2.5.2 is not straight forward. Considering the assembly of the catalyst from a Cu(I)-source and the chiral dithienylethene (*vide infra*), the ligand is viewed as a photochromic additive, which influences the stereochemical outcome of the cyclopropanation reaction. However, a classification of the ligand as a photochromic template inducing either a chiral or achiral environment seems appropriate as well. In the light of possible applications, switching of selectivity offers completely different opportunities than switching of reactivity, since the latter allows to change the connectivity of atoms whereas selectivity switching allows to control the relative orientation of atoms within otherwise identical entities.

Structural changes associated with the ring-closure/ring-opening of dithienylethenes are small, when considering substitution in 5- and 5'-positions, which are easily substituted without far-reaching influence on the switching behavior. A substantial structural difference is observed for substituents in the 2- and 2'-position: close proximity in both conformations of the ring-opened isomer is changed into an anti-parallel arrangement upon ring-closure (top of Figure 23). However, substituents in 2-position may have a marked effect on the switching behavior (*vide infra*). Exploiting the structural differences of ring-closed and ring-opened 2-substituted dithienylethenes, it was possible to photocontrol the stereoselectivity in the cyclopropanation of styrene catalyzed by copper(I) complexes derived from chiral, 2-bisoxazoline-substituted dithienylethene ligands and a Cu(I)-source (Figure 23).

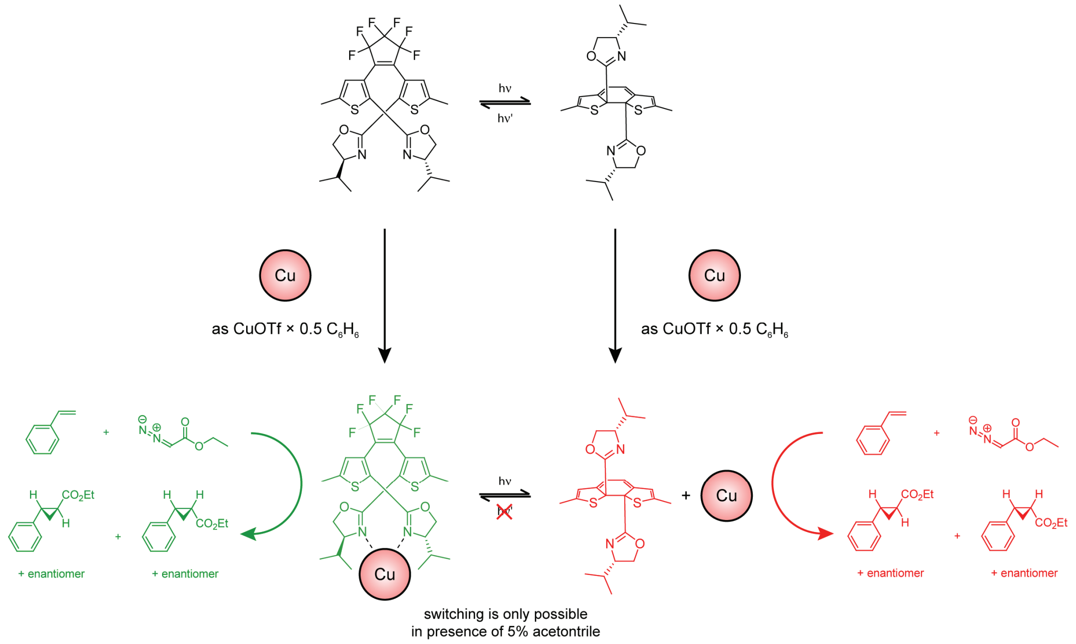
hν
hν'
Cu
as CuOTf × 0.5 C_6H_6
Cu
as CuOTf × 0.5 C_6H_6
+ enantiomer
+ enantiomer
Cu
hν
hν'
+
Cu
+ enantiomer
+ enantiomer
switching is only possible
in presence of 5% acetontrile

Figure 23: Photoswitching of stereoselectivity in Cu(I)-catalyzed cyclopropanations by controlling the geometry of a chiral dithienylethene ligand (green: ON-state with high stereoselectivity; red: OFF-state with low stereoselectivity).

Complexes generated from the ring-opened ligand and a copper(I) source are able to transfer the chiral information of the ligand to the substrate, leading to modest stereoselectivity in the copper(I)-catalyzed cyclopropanation of styrene employing a diazoester (*trans*: 30% *ee*, *cis*: 50% *ee*). On the other hand, complexes derived from the ring-closed ligand are structurally less defined, leading to a drop in stereoselectivity (*trans*: 5% *ee*, *cis*: 5% *ee*; for a sample containing 97% ring-closed ligand).[c] Upon photochemical ring-opening, the modest stereoselectivity of the complex derived from the ring-opened ligand is completely restored. The reverse process, i.e. ring-closure in the presence of copper(I), is not possible, presumably because the ring-opened ligand binds to tightly to the copper center. Addition of 5% of strongly coordinating acetonitrile to the initial methylene chloride solution enables switching by providing an alternative ligand for the metal. However, ring-closure of the ligand in presence of copper(I) leads only to a weak drop in stereoselectivity (*trans*: 11% *ee*, *cis*: 37% *ee*), because the photostationary state is comprised of only 23% of the ring-closed isomer. The result could be reproduced by assembly of the catalyst from a photostationary state mixture of the ligand and a Cu(I)-source.

---

[c] Chromatographic separation of the ring-closed isomer from a photostationary state mixture was carried out and the purified ligand was subsequently used for catalyst preparation.

The unfavorable photostationary state for the *open* → *closed* isomerization can be attributed to steric interactions of the substituents in the thiophenes' 2-positions upon ring-closure. The rather low stereoselectivity observed for the ring-opened isomer is presumably due to the larger number of accessible conformations as compared to the ring-closed isomer arising form the increased flexibility of the ring-opened form, which leads to a poor transfer of stereochemical information from the ligand to the substrate.

2.5.3.2 Photochromic Templates

Carbazole-based receptors derived from derivatives of Kemp's triacid are known to efficiently bind adenine moieties. Connection of two receptor units by a photochromic azobenzene enabled successful photocontrol of amide bond formation between substrates carrying adenine residues (Figure 24).[76] A significant increase of the effective concentration of substrate can be affected by the *Z*-template. Arranging the substrates' reacting sites in a favorable geometry leads to an about ten-fold acceleration of amide bond formation. The more extended *E*-isomer does not allow for such favorable orientation of the reactants, thereby causing only a modest rate acceleration compared to the noncatalyzed reaction. The relatively high flexibility of the template accounts for the small residual activity of the *E*-isomer. However, the rate of the noncatalyzed reaction has to be taken into account when evaluating the catalyst's performance. Essentially, an acceleration of a reaction is observed, which is relatively fast even without catalyst. This significantly lowers the performance of the catalytic system.

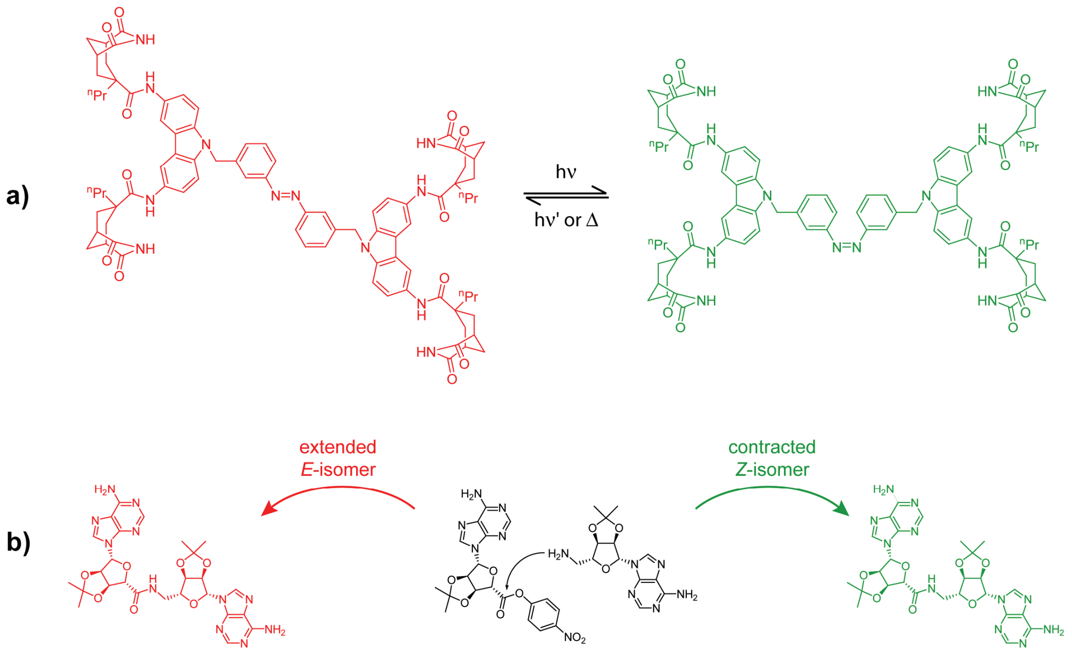

Figure 24: Photoregulation of amide-bond formation: a) switching of the catalytic template carrying adenine receptors (some ^{n}Pr-groups are omitted for clarity; red: OFF-state; green: ON-state). b) Amide bond formation between adenine-functionalized active ester and amine (red: low activity; green: high activity).

Product-inhibition is a severe draw-back for this system due to the close structural relation between substrates and product. Equimolar amounts of template are therefore required to ensure efficient substrate conversion. However, due to the unfavorable photostationary state composition comprised of only 50% of reactive *Z*-isomer after irradiation at 366 nm, the effective loading of ON-state catalyst is only 50%, therefore neglecting one half of the catalyst reactivity possible. The low photostationary state is attributed to the marked carbazole absorption in the wavelength region of azobenzene absorption and underlines the importance of proper catalyst design, not only taking geometrical considerations into account, but also the photophysical characteristics of all catalyst components (*vide supra*).

A similar template approach was devised to photocontrol the rate for ethanolysis of 4-carboxy acetanilides in basic solution (Figure 25). Dinuclear alkaline-earth metal ion complexes of bis-crown ethers connected by a suitable bridging unit are known to catalyze the ethanolysis of acetanilides carrying distal carboxy groups for binding to both metal ions. A close proximity of the metal centers is necessary to ensure a bridging binding mode of the anilide. Mandolini and co-workers realized that an *E*-azobenzene-bridged bis-crown ether would be too extended for efficient bridging to occur, but that the more contracted *Z*-isomer should favor binding.[77] Indeed, activity ratios for the ethanolysis of the acetanilide shown in Figure 25b of around 5.5 were observed, comparing a thermally equilibrated sample with an irradiated sample. Noteworthy, the photostationary state for *E* → *Z* switching is comprised of 95% *Z*-isomer, ensuring an efficient generation of ON-state catalyst. Back-switching from the *Z*- to the *E*-isomer is a bit less efficient, leading to photostationary state mixtures composed of 81% *E*-isomer and 19% *Z*-isomer. Taking these numbers into account, the activity ratio is lowered to around 3, when comparing the two photostationary state mixtures. Molecular models confirmed the intended close proximity of both metal centers in the ON-state catalyst, ideal for a dual-mode binding of the acetanilide substrate (Figure 25c).

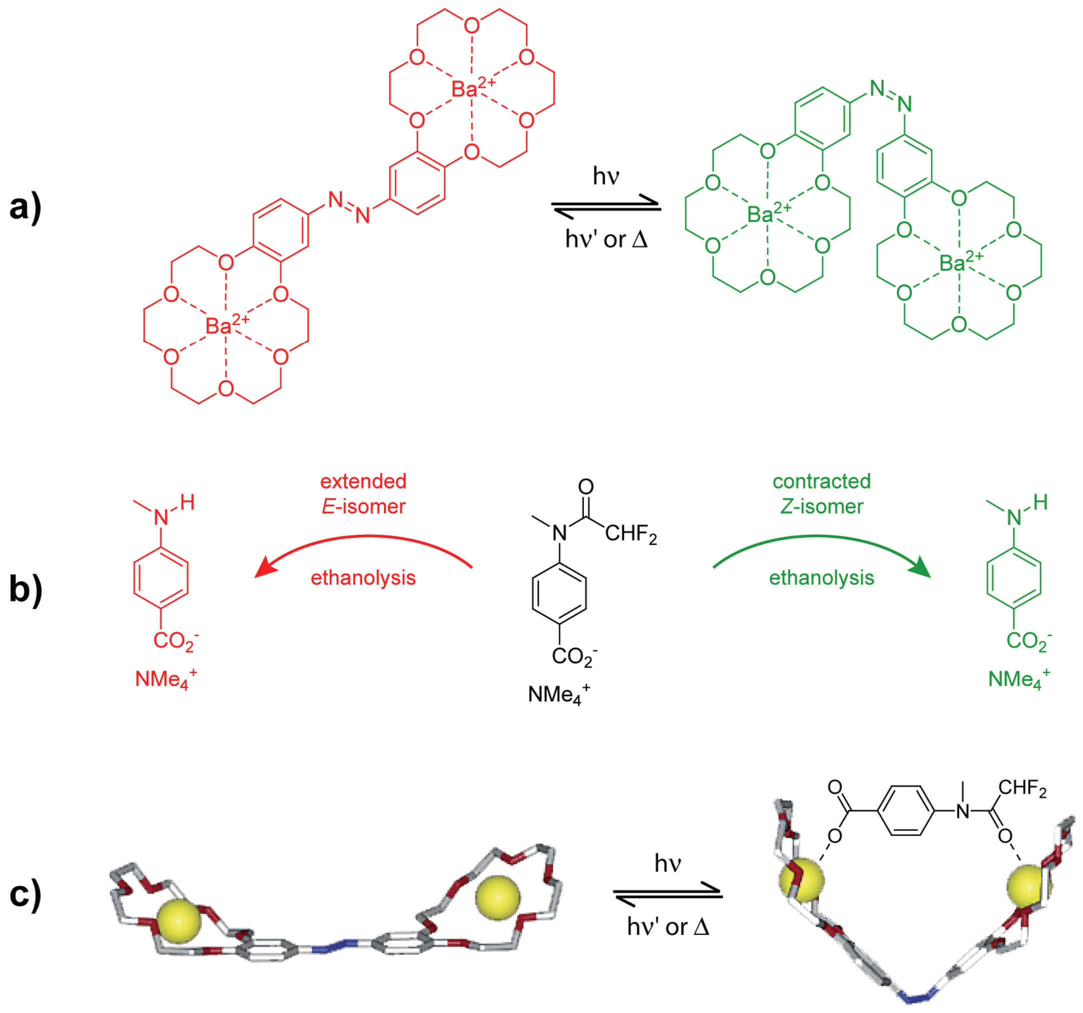

Figure 25: Photoswitchable crown ethers for controlling the ethanolysis of acetanilides: a) switching of Ba^{2+} crown ethers (red: OFF-state; green: ON-state). b) Effect of the template's geometry on the ethanolysis of acetanilide (red: low reactivity; green: high reactivity). c) Model of the bis-crown ether in both switching states with a tentative representation of activating acetanilide binding.

The catalyst's performance is lowered by a substantial OFF-state reactivity, which can be attributed to the high flexibility of the crown-ether moieties allowing activating binding events to occur even in the extended *E*-isomer. As can be expected from the close structural relation of substrate and product, product inhibition comes into play at higher conversions. Therefore, equimolar amounts of catalyst had to be employed for efficient catalysis, rendering the system not truly catalytic. The strict structural requirements needed for fitting the substrate into the activating binding pocket significantly narrows the scope of the system.

2.5.3.3 Reversible Steric Shielding

The development of photoswitchable catalysts based on cyclodextrins (cf. Figure 21) was complemented by covalently linking the photochromic azobenzene with the catalytically active macrocycle.[78] Capping of the cyclodextrin's shallow end with a 4,4'-carboxy azobenzene gave a molecularly defined catalyst, which allowed to photomodulate the binding behavior of the hydrophobic pocket by dictating its size via the photochrome (Figure 26). The more extended *E*-isomer leaves less free space below the cavity as compared to the bent *Z*-isomer, thereby decreasing the cyclodextrin's affinity for binding benzoic esters. The binding behavior is modulated on steric grounds and the system is therefore classified as a reversible steric shielding approach, despite opposing steric requirements for efficient catalysis and binding (*vide supra*).

Kinetic analysis of the hydrolysis of methyl 4-nitrobenzoate in buffered solution revealed a maximum 5.5-fold rate-acceleration for an irradiated sample of the catalyst compared to a sample in thermal equilibrium under otherwise identical conditions. Two effects operating in different direction could be identified: (a) better binding of the substrate by the *Z*-isomer, due to the larger cavity and (b) slowed hydrolysis rates for the *Z*-isomer, due to geometrically unfavorable placement of the substrate deep inside the cavity. The latter effect is overweight by the enhanced binding, leading to the overall rate acceleration observed for irradiated samples. However, kinetics are complicated by the presence of both isomers in solution and the different extent of switching possible at varying concentrations of catalyst. Furthermore, the system is not truly catalytic, since an excess of catalyst over substrate was necessary to compensate for unfavorable product inhibition.

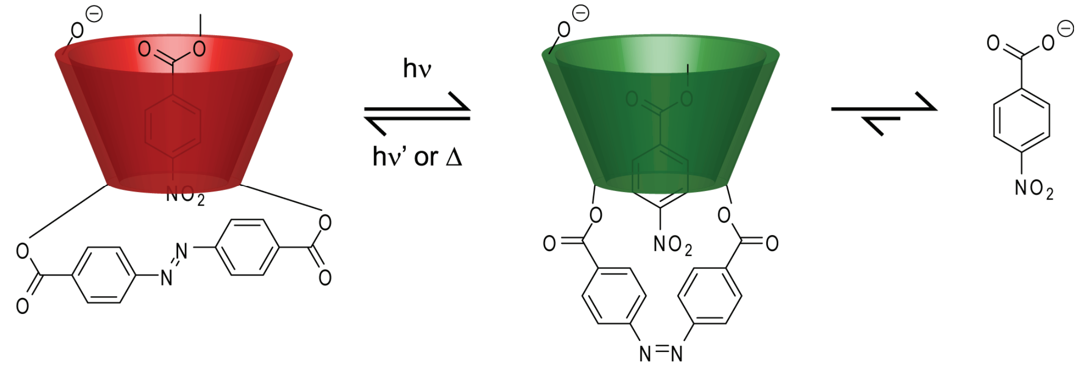

Figure 26: Photoswitchable catalyst based on an azobenzene capped β-cyclodextrin macrocycle. The size of the binding pocket is dictated by the switching state of the azobenzene (red: OFF-state with low activity; green: ON-state with high activity).

2.5.3.4 Switching Electronic Situations

So far, no example of successful reactivity switching via a photochrome-mediated electronic modulation of a catalyst's active site has been described. However, the differentiation to other approaches described in section 2.5.2 is somewhat ambiguous, since for example the photocontrol of CO_2-fixation utilizing an aluminum-porphyrin in combination with a photochromic activator clearly involves switching of the electronic situation of the active site.

2.6 Literature

(1) Bouas-Laurent, H.; Dürr, H. *Pure Appl. Chem.* **2001**, *73*, 639-665.

(2) Nishino, H.; Nakamura, A.; Shitomi, H.; Onuki, H.; Inoue, Y. *J. Chem. Soc., Perkin Trans. 2* **2001**, 1706-1713.

(3) *Organic Photochromic and Thermochromic Compounds, Volume 2: Physicochemical Studies, Biological Applications, and Thermochromism*; Crano, J. C.; Guglielmetti, R. J., Eds.; Plenum Press: New York, 1999.

(4) Dürr, H.; Bouas-Laurent, H. *Photochromism: Molecules and Systems: Revised Edition*, 2003.

(5) *Organic Photochromic and Thermochromic Compounds, Volume 1: Main Photochromic Families*; Crano, J. C.; Guglielmetti, R. J., Eds.; Plenum Press: New York, 1999.

(6) El'tsov, A. V. *Organic Photochromes*; 1. ed.; Consultants Bureau: New York, 1990.

(7) Zollinger, H. *Diazo Chemistry II: Aliphatic, Inorganic and Organometallic Compounds*, 1995; Zollinger, H. *Diazo Chemistry I: Aromatic and Heteroaromatic Compounds*, 1994.

(8) Zollinger, H. *Color Chemistry: Syntheses, Properties and Applications of Organic Dyes and Pigments*, 1987.

(9) Bock, H. *Angew. Chem., Int. Ed. Engl.* **1965**, *4*, 457-471.

(10) Bruce, M. I. *Angew. Chem., Int. Ed. Engl.* **1977**, *16*, 73-86.

(11) Hartley, G. S. *Nature* **1937**, *140*, 281.

(12) The existence of *Z*-azobenzene was recognized earlier, but could not be attributed to a photochromic behavior: Gortner, C. V.; Gortner, R. A. *J. Am. Chem. Soc.* **1910**, *32*, 1294-1296.

(13) Nägele, T.; Hoche, R.; Zinth, W.; Wachtveitl, J. *Chem. Phys. Lett.* **1997**, *272*, 489-495.

(14) Turro, N. J. *Modern Molecular Photochemistry*; University Science Books: Sausalito, CA, 1991.

(15) Hampson, G. C.; Robertson, J. M. *J. Chem. Soc.* **1941**, 409-413; Mostad, A.; Romming, C. *Acta Chem. Scand.* **1971**, *25*, 3561.

(16) Bisle, H.; Romer, M.; Rau, H. *Berichte Der Bunsen-Gesellschaft-Physical Chemistry Chemical Physics* **1976**, *80*, 301-305.

(17) Rau, H. *Angew. Chem., Int. Ed. Engl.* **1973**, *12*, 224-235.

(18) Haselbach, E. *Helv. Chim. Acta* **1970**, *53*, 1526-1543; Haselbach, E.; Heilbronner, E. *Tetrahedron Lett.* **1967**, 4531-4535.

(19) Lewis, G. E.; Mayfield, R. J. *Aust. J. Chem.* **1966**, *19*, 1445.

(20) Talaty, E. R.; Fargo, J. C. *Chem. Comm.* **1967**, 65-66.

(21) Monti, S.; Orlandi, G.; Palmieri, P. *Chem. Phys.* **1982**, *71*, 87-99.

(22) Cembran, A.; Bernardi, F.; Garavelli, M.; Gagliardi, L.; Orlandi, G. *J. Am. Chem. Soc.* **2004**, *126*, 3234-3243.

(23) Conti, I.; Garavelli, M.; Orlandi, G. *J. Am. Chem. Soc.* **2008**, *130*, 5216-5230.

(24) Albini, A.; Fasani, E.; Pietra, S. *J. Chem. Soc., Perkin Trans. 2* **1983**, 1021-1024.

(25) Wildes, P. D.; Pacifici, J. G.; Irick, G.; Whitten, D. G. *J. Am. Chem. Soc.* **1971**, *93*, 2004-2008.

(26) Szele, I.; Zollinger, H. *Top. Curr. Chem.* **1983**, *112*, 1-66.

(27) Boyer, J. H. *Chemistry of Nitro and Nitroso Groups* **1969**, 215-299.

(28) Priewisch, B.; Rück-Braun, K. *J. Org. Chem.* **2005**, *70*, 2350-2352.

(29) Firouzabadi, H.; Mostafavipoor, Z. *Bull. Chem. Soc. Jpn.* **1983**, *56*, 914-917.

(30) Bigelow, H. E.; Robinson, D. B. *Org. Synth.* **1942**, *22*, 28-29.

(31) Hartwig, J. F. In *Handbook of Organopalladium Chemistry for Organic Synthesis*; Negishi, E.-i., Ed.; Wiley: New York, 2002; Vol. 1, p 1051-1096; Hartwig, J. F. In *Handbook of Organopalladium Chemistry for Organic Synthesis*; Negishi, E.-i., Ed.; Wiley: New York, 2002; Vol. 1, p 1097-1106; Muci, A. R.; Buchwald, S. L. *Cross-Coupling Reactions* **2002**, *219*, 131-209.

(32) Lim, Y.-K.; Choi, S.; Park, K. B.; Cho, C.-G. *J. Org. Chem.* **2004**, *69*, 2603-2606; Lim, Y.-K.; Lee, K.-S.; Cho, C.-G. *Org. Lett.* **2003**, *5*, 979-982.

(33) Wolter, M.; Klapars, A.; Buchwald, S. L. *Org. Lett.* **2001**, *3*, 3803-3805.

(34) Kim, K.-Y.; Shin, J.-T.; Lee, K.-S.; Cho, C.-G. *Tetrahedron Lett.* **2004**, *45*, 117-120.

(35) Frankland, E.; Louis, D. A.; Evans, J. C.; Tompkins, H. K. *J. Chem. Soc., Trans.* **1880**, *37*, 560-570.

(36) Mustroph, H.; Stollenwerk, M.; Bressau, V. *Angew. Chem., Int. Ed. Engl.* **2006**, *45*, 2016-2035.

(37) Yager, K. G.; Barrett, C. J. *J. Photochem. Photobiol., A* **2006**, *182*, 250-261; Natansohn, A.; Rochon, P. *Chem. Rev.* **2002**, *102*, 4139-4175.

(38) Ichimura, K. *Chem. Rev.* **2000**, *100*, 1847-1873; Matharu, A. S.; Jeeva, S.; Ramanujam, P. S. *Chem. Soc. Rev.* **2007**, *36*, 1868-1880.

(39) Wang, S.; Song, Y.; Jiang, L. *J. Photochem. Photobiol., C* **2007**, *8*, 18-29.

(40) Woolley, G. A. *Acc. Chem. Res.* **2005**, *38*, 486-493.

(41) Willner, I. *Acc. Chem. Res.* **1997**, *30*, 347-356; Willner, I.; Rubin, S. *Angew. Chem., Int. Ed. Engl.* **1996**, *35*, 367-385.

(42) Pieroni, O.; Fissi, A.; Angelini, N.; Lenci, F. *Acc. Chem. Res.* **2001**, *34*, 9-17.

(43) Banghart, M.; Borges, K.; Isacoff, E.; Trauner, D.; Kramer, R. H. *Nature neurosci.* **2004**, *7*, 1381-1386; Volgraf, M.; Gorostiza, P.; Numano, R.; Kramer, R. H.; Isacoff, E. Y.; Trauner, D. *Nature Chem. Bio.* **2006**, *2*, 47-52.

(44) Jiang, D. L.; Aida, T. *Nature* **1997**, *388*, 454-456.

(45) Muraoka, T.; Kinbara, K.; Kobayashi, Y.; Aida, T. *J. Am. Chem. Soc.* **2003**, *125*, 5612-5613; Muraoka, T.; Kinbara, K.; Aida, T. *Nature* **2006**, *440*, 512-515; Raymo, F. M. *Angew. Chem., Int. Ed. Engl.* **2006**, *45*, 5249-5251.

(46) Irie, M. *Chem. Rev.* **2000**, *100*, 1685-1716.

(47) Irie, M.; Mohri, M. *J. Org. Chem.* **1988**, *53*, 803-808.

(48) Hanazawa, M.; Sumiya, R.; Horikawa, Y.; Irie, M. *Chem. Comm.* **1992**, 206-207.

(49) Lucas, L. N.; De Jong, J. J. D.; Van Esch, J. H.; Kellogg, R. M.; Feringa, B. L. *Eur. J. Org. Chem.* **2003**, 155-166; Lucas, L. N.; van Esch, J.; Kellogg, R. M.; Feringa, B. L. *Chem. Comm.* **1998**, 2313-2314.

(50) Yamaguchi, T.; Uchida, K.; Irie, M. *J. Am. Chem. Soc.* **1997**, *119*, 6066-6071.

(51) Woodward, R. B.; Hoffmann, R. *Angew. Chem., Int. Ed. Engl.* **1969**, *8*, 781-853.

(52) Nakamura, S.; Irie, M. *J. Org. Chem.* **1988**, *53*, 6136-6138.

(53) El Yahyaoui, A.; Felix, G.; Heynderickx, A.; Moustrou, C.; Samat, A. *Tetrahedron* **2007**, *63*, 9482-9487.

(54) Raymo, F. M.; Tomasulo, M. *Chem. Soc. Rev.* **2005**, *34*, 327-336.

(55) Takeshita, M.; Irie, M. *J. Org. Chem.* **1998**, *63*, 6643-6649; Takeshita, M.; Irie, M. *Tetrahedron Lett.* **1998**, *39*, 613-616.

(56) Matsuda, K.; Irie, M. *J. Photochem. and Photobiol. C: Photochem. Rev.* **2004**, *5*, 169-182.

(57) Huck, N. P. M.; Jager, W. F.; deLange, B.; Feringa, B. L. *Science* **1996**, *273*, 1686-1688; Denekamp, C.; Feringa, B. L. *Adv. Mater.* **1998**, *10*, 1080-1082.

(58) Jong, J. J. D. d.; Lucas, L. N.; Kellogg, R. M.; Esch, J. H. v.; Feringa, B. L. *Science* **2004**, *304*, 278-281; Hecht, S. *Small* **2005**, *1*, 26-29.

(59) Irie, M.; Kobatake, S.; Horichi, M. *Science* **2001**, *291*, 1769-1772.

(60) Kobatake, S.; Takami, S.; Muto, H.; Ishikawa, T.; Irie, M. *Nature* **2007**, *446*, 778-781.

(61) Berkovic, G.; Krongauz, V.; Weiss, V. *Chem. Rev.* **2000**, *100*, 1741-1753.

(62) Yokoyama, Y. *Chem. Rev.* **2000**, *100*, 1717-1739.

(63) Feringa, B. L.; Editor *Molecular Switches*, 2001.

(64) Palmisano, G.; Augugliaro, V.; Pagliaro, M.; Palmisano, L. *Chem. Comm.* **2007**, 3425-3437; Parmon, V. N. *Catal. Today* **1997**, *39*, 137-144; Hoffmann, M. R.; Martin, S. T.; Choi, W. Y.; Bahnemann, D. W. *Chem. Rev.* **1995**, *95*, 69-96; Esswein, M. J.; Nocera, D. G. *Chem. Rev.* **2007**, *107*, 4022-4047; Linsebigler, A. L.; Lu, G. Q.; Yates, J. T. *Chem. Rev.* **1995**, *95*, 735-758.

(65) Kaplan, J. H.; Forbush, B.; Hoffman, J. F. *Biochemistry* **1978**, *17*, 1929-1935.

(66) Adams, S. R.; Tsien, R. Y. *Ann. Rev. Physiol.* **1993**, *55*, 755-784; Pelliccioli, A. P.; Wirz, J. *Photochem. Photobiol. Sci.* **2002**, *1*, 441-458; Pillai, V. N. R. *Synthesis* **1980**, 1-26.

(67) Mayer, G.; Heckel, A. *Angew. Chem., Int. Ed. Engl.* **2006**, *45*, 4900-4921; Goeldner, M.; Givens, R. *Dynamic Studies in Biology*; 1. ed.; Wiley-VCH: Weinheim, 2005.

(68) Ito, H. *Adv. Polym. Sci.* **2005**, *172*, 37-245; Macdonald, S. A.; Willson, C. G.; Fréchet, J. M. J. *Acc. Chem. Res.* **1994**, *27*, 151-158; Medeiros, D. R. *J. Photopolym. Sci. Tech.* **2002**, *15*, 411-416; Lee, D. K.; Pawlowski, G. *J. Photopolym. Sci. Tech.* **2002**, *15*, 427-434; Wallraff, G. M.; Hinsberg, W. D. *Chem. Rev.* **1999**, *99*, 1801-1821.

(69) Peters, M. V.; Goddard, R.; Hecht, S. *J. Org. Chem.* **2006**, *71*, 7846-7849.

(70) Pauling, L. *Nature* **1948**, *161*, 707-709; Lolis, E.; Petsko, G. A. *Annu. Rev. Biochem.* **1990**, *59*, 597-630; Schramm, V. L. *Annu. Rev. Biochem.* **1998**, *67*, 693-720.

(71) Kanai, M.; Kato, N.; Ichikawa, E.; Shibasaki, M. *Synlett* **2005**, 1491-1508; Paull, D. H.; Abraham, C. J.; Scerba, M. T.; Alden-Danforth, E.; Lectka, T. *Acc. Chem. Res.* **2008**, *41*, 655-663.

(72) Ueno, A.; Takahashi, K.; Osa, T. *Chem. Commun.* **1980**, 837-838.

(73) Sugimoto, H.; Kimura, T.; Inoue, S. *J. Am. Chem. Soc.* **1999**, *121*, 2325-2326.

(74) Aida, T.; Inoue, S. *J. Am. Chem. Soc.* **1983**, *105*, 1304-1309.

(75) Sud, D.; Norsten, T. B.; Branda, N. R. *Angew. Chem., Int. Ed. Engl.* **2005**, *44*, 2019-2021.

(76) Würthner, F.; Rebek, J., Jr. *Angew. Chem., Int. Ed. Engl.* **1995**, *34*, 446-450; Würthner, F.; Rebek, J., Jr. *J. Chem. Soc., Perkin Trans. 2* **1995**, 1727-1734.

(77) Cacciapaglia, R.; Di Stefano, S.; Mandolini, L. *J. Am. Chem. Soc.* **2003**, *125*, 2224-2227.

(78) Ueno, A.; Takahashi, K.; Osa, T. *Chem. Commun.* **1981**, 94-96.

3 Photoswitchable Bases

3.1 Introduction

Almost all examples describing the photocontrol of catalytic processes rely on geometrical changes of the catalyst's backbone, altering its interaction with the substrate (*vide supra*).[1] Although some photoswitchable catalyst systems have been described, no general and broadly applicable systems have been reported yet. Therefore, a conceptually new approach towards photoswitchable catalysts was developed (Figure 1a).[2] The concept is based on the reversible steric shielding of the catalyst's active site by a suitable blocking group, which can be moved away from the reactive center using a photochromic linker. A two-state catalyst system is obtained that can be driven between the ON-state, having an active site freely accessible for substrate molecules, and the OFF-state, which is sterically blocked and therefore inactive. To maintain the desired photochromic reactivity, other chromophores, potentially leading to detrimental energy transfer processes, should be excluded.[3]

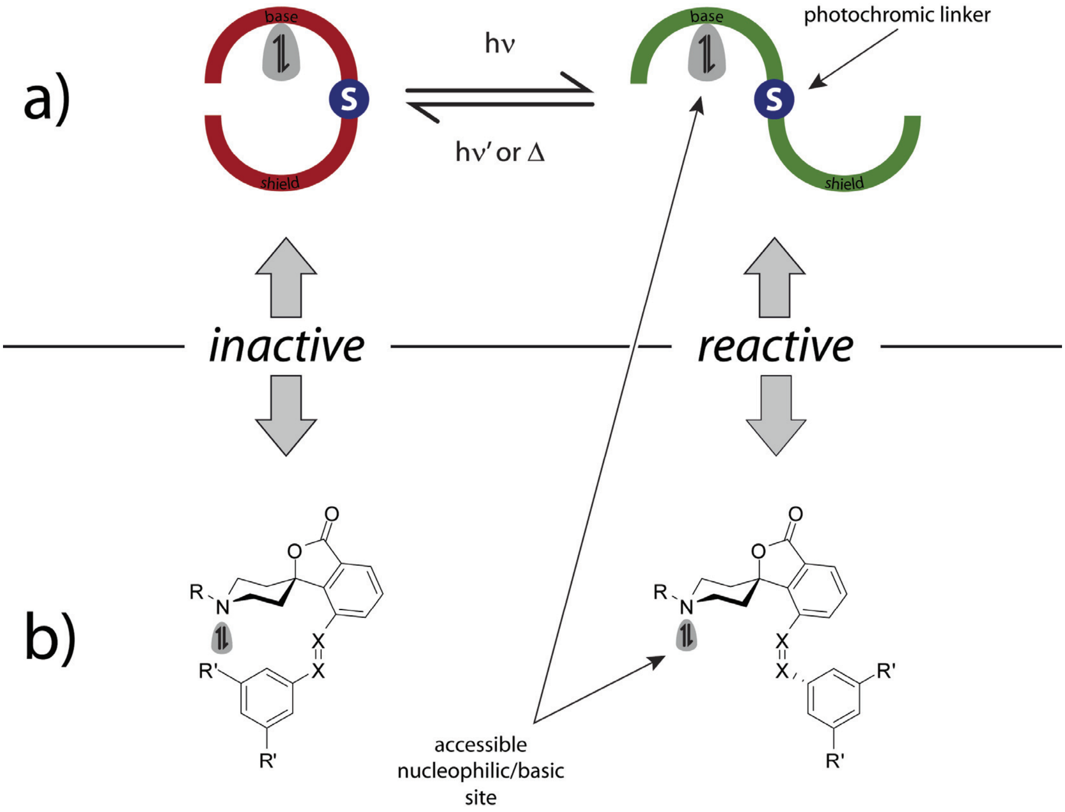
a)
base
S
shield
hν
hν' or Δ
base
photochromic linker
S
shield
inactive
reactive
b)
O
O
R
N
X
X
R'
R'
accessible
nucleophilic/basic
site
O
O
R
N
X
X
R'
R'

1a: R = Me, R' = *t*Bu, X = N
1b: R = *t*Bu, R' = *t*Bu, X = N
1c: R = *t*Bu, R' = 2,6Me$_2$Ph, X=N
2: R = Me, R' = *t*Bu, X=CH

Figure 1: a) Concept of reversible steric shielding of a catalyst's active site; b) schematic representation of a photoswitchable piperidine base.

Basicity constitutes an interesting functionality to be rendered photoswitchable, due to the overwhelming number of chemical transformations demanding for the presence of a base. Common organic Brønsted bases, e.g. amines, are frequently encountered in many reactions ranging from simple transformations, e.g. Henry reactions (*vide infra*), to sophisticated asymmetric transformations[4] and polymerizations.[5] Key structural element of amines is a basic trivalent nitrogen atom surrounded by a variable number of structurally diverse alkyl substituents, potentially carrying additional functionality. The basic reactivity is located on a non-bonding lone-pair, implying a directional character of the active site, which should facilitate shielding by suitable blocking groups when incorporated into a rigid framework. Shielding of the active site is expected to lead to a significant drop of basicity. Furthermore, an amine's basic lone-pair is expected to be optically silent, thereby avoiding unfavorable interactions with the photochrome.

The photoswitchable base is derived from a rigidified *N*-alkylated piperidine base, in which an attached bulky photochromic azobenzene moiety is used to reversibly shield the catalytically active site, i.e. the piperidine N-atom's lone pair (Figure 1b). Efficient shielding in *E*-**1a-c** was achieved by taking advantage of several conformationally restricting features: (i) the pronounced preference of the piperidine ring to adopt a chair conformation with the *N*-alkyl substituent occupying the equatorial position,[6] (ii) the spiro junction enabling rigid and orthogonal positioning of the photochromic azobenzene moiety, and (iii) the steric bulk of the symmetrical 3,5-disubstituted phenylazo substituent and its *ortho*-attachment adjacent to the spiro center. Irradiation of the shielded, inactive *E*-isomer, corresponding to the "resting state", is expected to trigger photochemical $E \rightarrow Z$ isomerization, accompanied by a large structural change and thereby revealing the active *Z*-isomer, in which the N-atom's lone pair becomes sterically accessible.

3.2 Synthesis of Photoswitchable Bases[a]

A modular synthesis of photoswitchable bases **1a-c** and **2** was developed to facilitate variation of key substituents at both, the piperidine's N-atom as well as the terminal phenyl moiety of the azobenzene, in order to tune the properties of the catalyst. By inspection of the synthetic route presented in Scheme 1, spiroannulated piperidines **3a,b** and BOC-protected hydrazines **4a,b** can be identified as key building blocks of azobenzene catalysts **1a-c**. Likewise, styryl boronic ester **5** was recognized to be a key building block for synthesis of stilbene catalyst **2**.

---

[a] Photoswitchable bases **1a** and **2** were prepared by Maike Peters, while **1b** was synthesized by Andreas Kühn.[7]

Scheme 1: Synthesis of azobenzene-derived catalysts **1a-c** and stilbene-derived catalyst **2**.

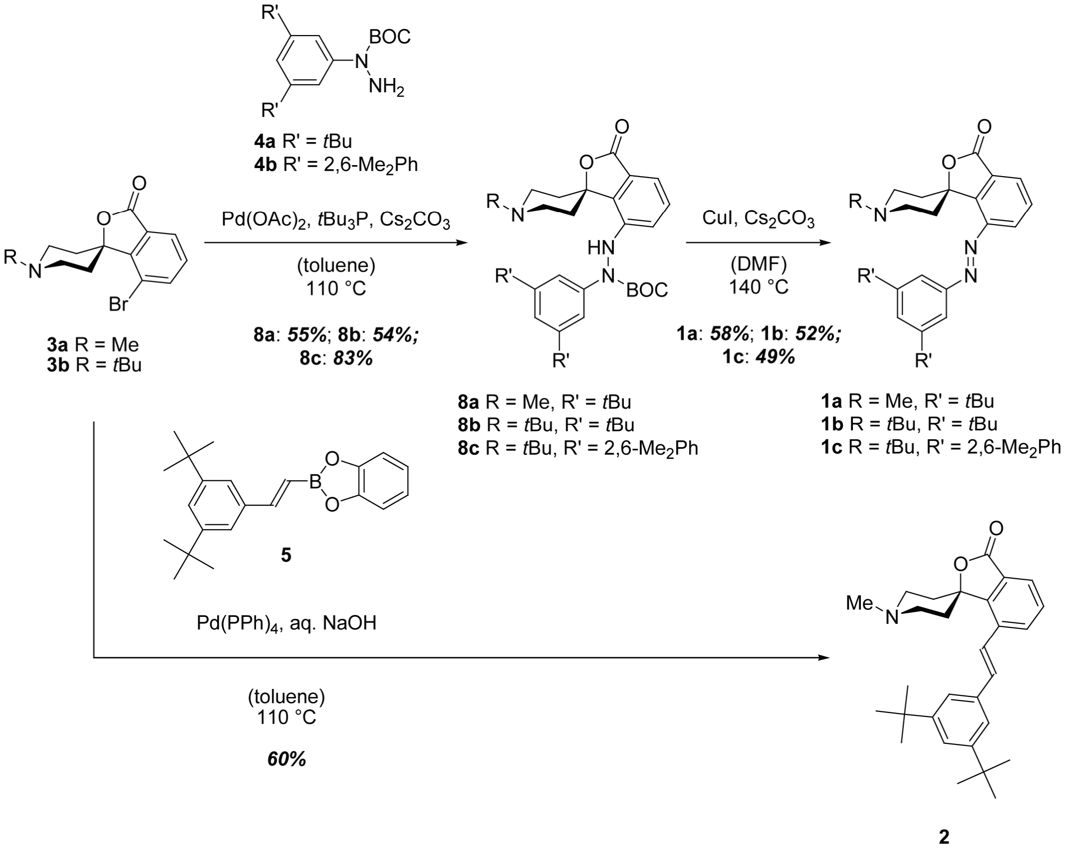
R'
BOC
N
NH2
R'
4a R' = tBu
4b R' = 2,6-Me2Ph
Pd(OAc)2, tBu3P, Cs2CO3
(toluene)
110 °C
8a: 55%; 8b: 54%;
8c: 83%
3a R = Me
3b R = tBu
Br
8a R = Me, R' = tBu
8b R = tBu, R' = tBu
8c R = tBu, R' = 2,6-Me2Ph
CuI, Cs2CO3
(DMF)
140 °C
1a: 58%; 1b: 52%;
1c: 49%
1a R = Me, R' = tBu
1b R = tBu, R' = tBu
1c R = tBu, R' = 2,6-Me2Ph
5
Pd(PPh)4, aq. NaOH
(toluene)
110 °C
60%
Me
2

Spiroannulated Piperidines

Spiroannulated piperidines were readily obtained from 3-bromobenzoic acid **6** and N-alkyl piperidones **7a,b** (Scheme 2).[8,9] Deprotonation of 3-bromobenzoic acid **6** by a bulky lithiumamide base occurs selectively at the 2-position, taking advantage of the metal-directing qualities of the carboxy functionality and the electron withdrawing, therefore activating, character of the bromo substituent.[8] Quenching the unstable lithiated species with piperidones **7a,b** gave a tertiary alcohol intermediate, which lactonized upon acidic work-up to give piperidines **3a,b**.[9] The lithiated species is prone to undergo irreversible elimination of lithium bromide to give an unstable aryne intermediate, which subsequently reacts with the conjugate amine of the amide base. Substitution products derived from 2,2,6,6-tetramethyl piperidine and benzoic acid are therefore frequently encountered by-products, significantly reducing the yield of the reaction. Minimization of the effect is possible by accurately controlling the temperature of the reaction mixture, an optimal value being -50 °C.

Scheme 2: Synthesis of spiroannulated piperidines **3a,b** from 3-bromobenzoic acid **6** and *N*-alkyl piperidones **7a,b**.

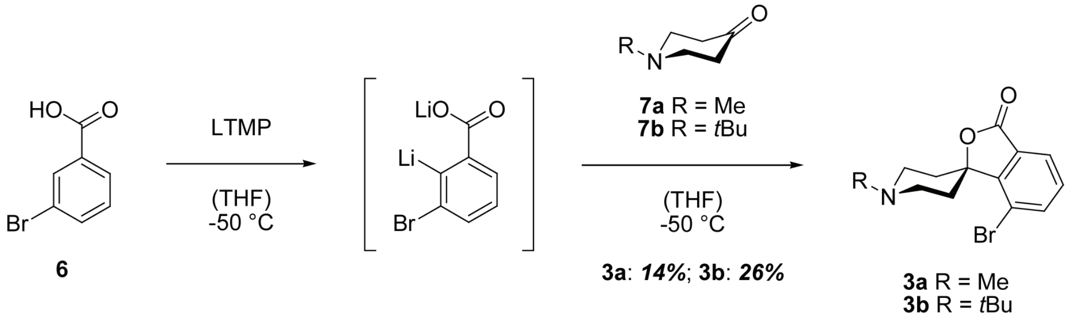
HO
O
Br
6
LTMP
(THF)
-50 °C
LiO
O
Li
Br
R
N
O
7a R = Me
7b R = tBu
(THF)
-50 °C
3a: 14%; 3b: 26%
O
O
R
N
Br
3a R = Me
3b R = tBu

Straight forward preparation of piperidone **7b** was accomplished by exhaustive methylation of piperidone **7a** with methyl iodide followed by exchange of the nitrogen atom's substituent by an elimination-addition sequence employing *tert*-butyl amine (Scheme 3).[10,11]

Scheme 3: Preparation of piperidone **7b** from piperidone **7a**.

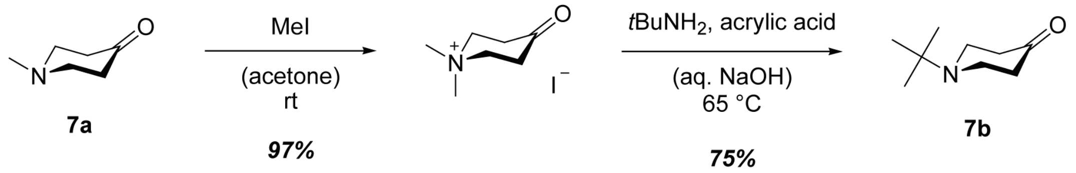
O
N
7a
MeI
(acetone)
rt
97%
O
N
+
I
I⁻
tBuNH2, acrylic acid
(aq. NaOH)
65 °C
75%
O
N
7b

BOC-Protected Hydrazines

BOC-Protected hydrazines **4a,b** constitute important intermediates for the synthesis of hydrazines **8a-c**, which are direct precursors of azobenzene catalysts **1a-c**. Direct synthesis of hydrazine **4a** by N-arylation of 3,5-di-*tert*-butylbromo benzene **9** is not possible, due to the inherently low reactivity of brominated aromatic compounds towards copper(I) catalyzed cross coupling reactions. Therefore, 3,5-di-*tert*-butylbromo benzene **9** was converted into the corresponding iodide **10** by halogen-metal exchange with *n*-butyl lithium and subsequent quench with iodine (Scheme 4). 3,5-Di-*tert*-butyliodo benzene **10** was reactive enough to undergo copper(I) catalyzed cross-coupling with BOC-hydrazine to give aryl hydrazine **4a** in good yields.[12]

Scheme 4: Synthesis of aryl hydrazine **4a**.

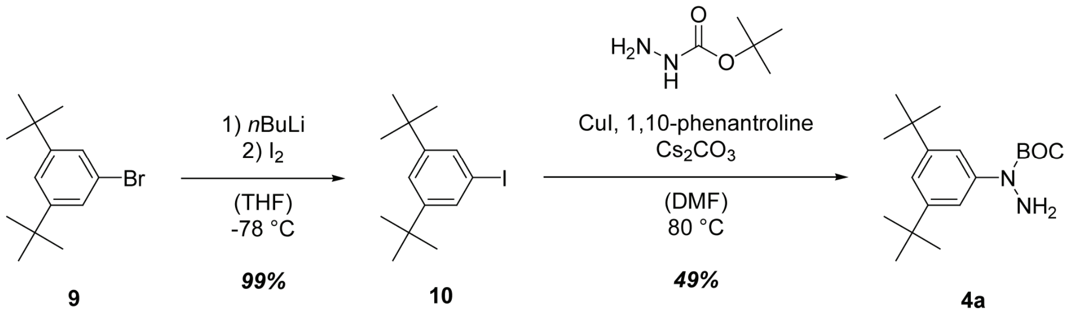

Synthesis of the more bulky terphenyl-based hydrazine **4b** followed the synthetic protocol, which enabled successful synthesis of hydrazine **4a**. Starting from terphenylbromide **11**, exchange of bromine for iodine gave terphenyliodide **12** in very good yields. Copper-mediate reaction of terphenyliodide **12** with BOC-protected hydrazine gave the blocking-group precursor **4b** (Scheme 5). Terphenyl bromide **11** was easily accessed starting from 2,4,6-tribromo aniline **13**, which was converted to 2,4,6-tribromoiodo benzene **14** by Sandmeyer reaction. Reaction of bromo-iodo compound **14** with three equivalents of a Grignard-reagent prepared from 2,6-dimethylbromo benzene afforded terphenylbromide **11**.[13,14] The reaction proceeds via an elimination-addition sequence involving initial transmetallation of one equivalent of Grignard-reagent with the iodine functionality and consecutive additions of the remaining two equivalents of Grignard-reagent to the aryne elimination products of the tribromo-magnesium intermediate.

Scheme 5: Synthesis of terphenyl-based hydrazine **4b**.

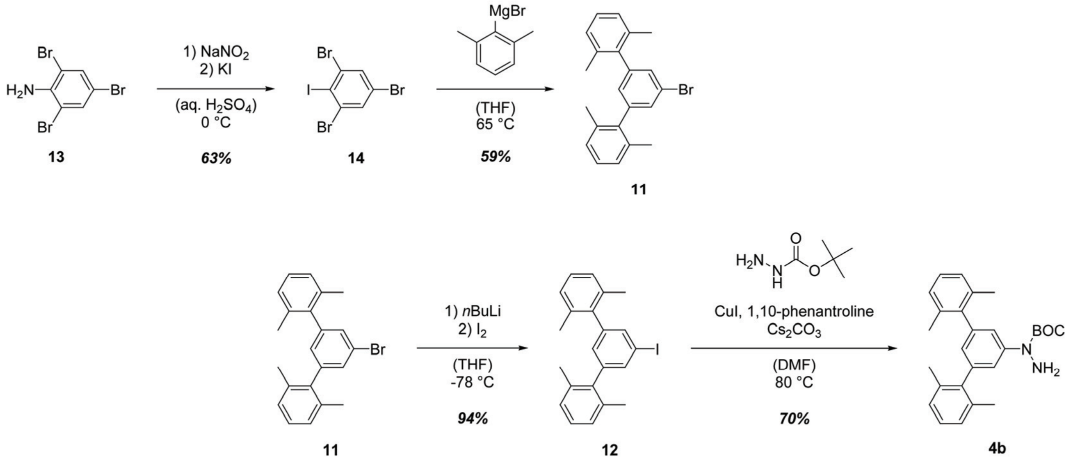

Azobenzene Catalysts

Precursors **8a-c** of azobenzene catalysts **1a-c** were readily assembled from the key intermediates **3a,b** and **4a,b** by palladium-catalyzed cross-coupling (Scheme 1).[15] Final oxidation of spiro hydrazines **8a-c** was achieved with copper(I) iodide and caesium carbonate in DMF to give catalysts **1a-c**.[16]

Stilbene Catalyst

Stilbene catalyst **2** was successfully synthesized by adapting the synthetic strategy leading to azobenzene catalysts **1a-c**. Key intermediates in the synthesis are the boronic ester **5** and the spiroannulated piperidine **3a**, which was synthesized according to Scheme 2. Styryl boronic ester **5** was obtained from 3,5-di-*tert*-butylbromo benzene **9** in three steps (Scheme 6). Sonogashira cross coupling with TMS-protected acetylene followed by basic deprotection using K_2CO_3 yielded the free acetylene **15**, which could be further reacted to give the catechol boronic ester **5** with perfect regiocontrol by hydroboration with catechol borane.[17] Suzuki cross coupling of spiroannulated piperidine **3a** and styryl boronic acid **5** enabled easy access to catalyst **2** carrying a photochromic stilbene moiety.

Scheme 6: Synthesis of styryl boronic ester **5**.

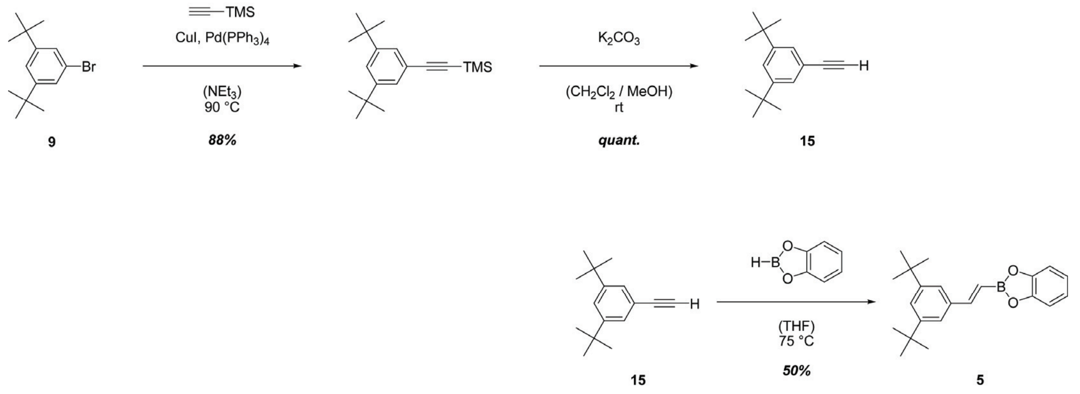

3.3 Structure and Conformational Dynamics

3.3.1 Solid-State Structural Analysis

If the concept of reversible steric shielding is to be applicable to the photocontrol of the activity of a catalyst, then a large structural change between ON- and OFF-states is required. Single crystals suitable for x-ray structural analysis of *E*-**1**, representing the OFF-states, and *Z*-**1b**, representing the ON-state were obtained, and their structures were determined. Figure 2 shows a superposition of the benzofuranone moieties of *E*-**1a**-**c** as well as *Z*-**1b**. Remarkable is the similarity of the structures *E*-**1a**-**c**, despite completely different crystal environments (root-mean-square deviation of the diazo-piperidyl-phthalide units: 0.1 Å). In the case of the crystal structure of *E*-**1b** there are three independent molecules in the asymmetric unit which differ only in the conformation of the methyl groups (root-mean-square deviation of non-methyl atoms: 0.2 Å). The common structural features of all structures *E*-**1** are (1) the placement of the blocking group directly in front of the lone pair of the nitrogen atom, with shortest intramolecular N-C distances 4.1-4.5 Å in the three structures, (2) the chair conformation of the piperidine ring, to within 0.02 Å, and (3) the perpendicular relationship between the benzofuranone unit and the piperidine mean ring plane (mean angle: 89º). Clearly, the blocking group takes up a position, which efficiently shields the lone pair of the piperidine N-atom.

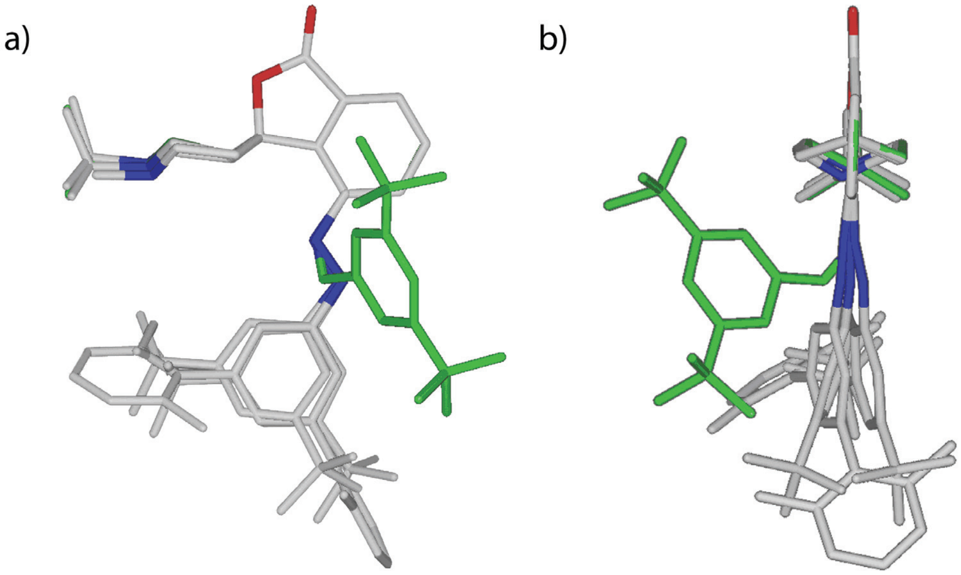

Figure 2: Overlay of x-ray crystal structures of catalysts *E*-**1a-c** and *Z*-**1b** (green): a) side view (projection onto the plane of the benzofuranone moiety); b) rear view.

In the case of the *Z* isomer (green in Figure 2), the azobenzene moiety has a torsion angle 7.1°, and the blocking group is moved away from the active site of the catalyst, leaving the active site freely accessible for reaction, as intended in the design, cf. Figure 1. The intramolecular N-C distance of the lone pair of the piperidine to the nearest *tert*-butyl group of the phenyl moiety is 7.1 Å, and therefore the substituents on the phenyl ring no longer provide a barrier. Otherwise, the conformation of the piperidine-benzofuranone moiety is essentially similar to those seen in *E*-**1a-c**. The conformation of the piperidine in all four crystal structures is such that the N-lone pair points away from the lone pairs on the furanone ring O-atom, in line with the less destabilizing 1,3-diaxial interactions of the two piperidine 2,6-H-atoms with the 4-carbonyloxy substituent of the lactone as compared to the alternative larger phenyl substituent of the benzofuranone. X-ray analysis, however, only provides a static picture of the structural situation in the solid state, so for a thorough understanding of the reactivity of catalysts *E*-**1a-c** and *Z*-**1** it is necessary to investigate their structure and conformational behavior in solution, and hence gain detailed insights into the dynamics of the systems.

3.3.2 Structure and Dynamics in Solution

To achieve the desired control over the accessibility of the basic/nucleophilic piperidine N-atom's lone pair, it is necessary to dictate both configuration (path a in Scheme 7) as well as conformation (paths b-d in Scheme 7) of the interconvertible *E* and *Z* isomers. Control of the latter one is a much more difficult task due to the complex dynamics under the reaction conditions. Therefore, a thorough investigation of the solution phase dynamics of **1** was carried out by NMR spectroscopic methods,[b] in particular variable temperature NMR,[18] EXSY,[19] and the recently introduced residual dipolar couplings (RDCs),[20,21] in combination with computational studies (Table 1).[c]

---

[b] In collaboration with Christina M. Thile, Clemens Schöpf Institut für organische Chemie und Biochemie, Technische Universität Darmstadt, Petersenstr. 22, 64287 Darmstadt, Germany.

[c] In collaboration with Michael Bühl, School of Chemistry, North Haugh, University of St. Andrews, St. Andrews, Fife KY16 9ST, UK.

Scheme 7: Schematic representation of selected local minima and transition states investigated by DFT calculations.

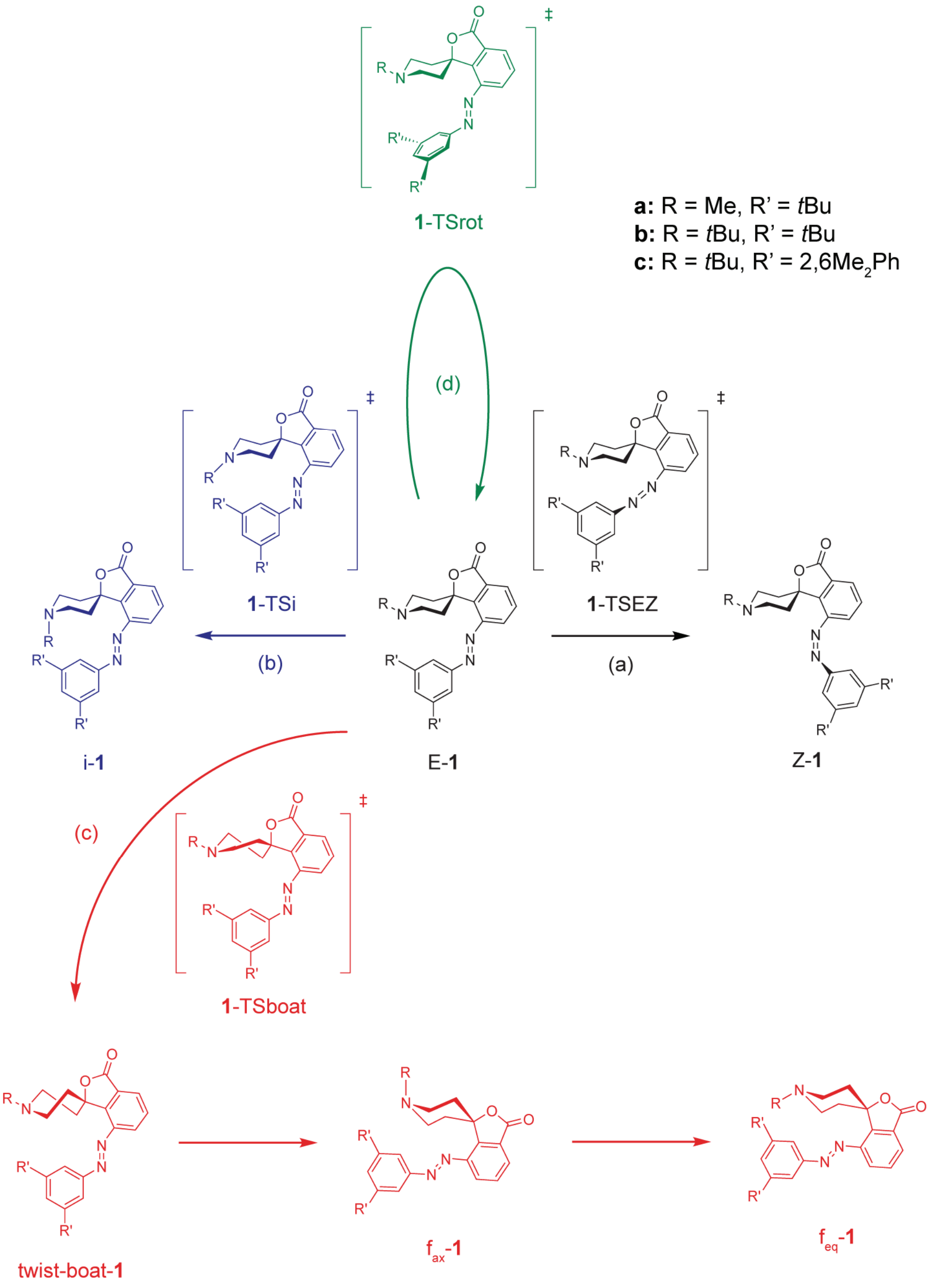
1-TSrot
a: R = Me, R' = tBu
b: R = tBu, R' = tBu
c: R = tBu, R' = 2,6Me2Ph
(d)
1-TSi
1-TSEZ
(b)
(a)
i-1
E-1
Z-1
(c)
1-TSboat
twist-boat-1
fax-1
feq-1

Table 1: Potential energies Δ*E* (in parentheses: free energies Δ*G*)[a] of selected isomers and transition states of **1a-c**.

	a	**b**	**c**
E-**1**	0.0 (0.0)	0.0 (0.0)	0.0 (0.0)
1-TSEZ	39.8 (37.6)	39.6 (37.6)	40.1 (38.0)
Z-**1**	15.8 (14.8)	15.4 (15.8)	15.3 (15.0)
1-TSi	8.5 (7.4)	7.0 (8.2)	5.8 (7.2)
i-**1**	3.8 (4.0)	6.0 (7.1)	5.5 (5.4)
1-TSboat	11.6 (12.0)	11.5 (12.7)	n.a.
f_{ax}-**1**	7.2 (7.8)	9.0 (10.9)	n.a.
f_{eq}-**1**	7.0 (7.6)	7.4 (8.7)	n.a.
1-TSrot	7.7 (7.0)	7.5 (6.9)	6.9 (5.6)

[a] In kcal/mol relative to *E*-**1** isomer, B3LYP/6-31G* level.

Inversion

Inversion at the piperidine's N-atom (blue path b in Scheme 7; exemplarily shown for **1b** in Figure 3) is of particular interest, because the concomitant exchange of equatorial alkyl group and axial lone pair in *E*-**1** exposes the latter to the environment, potentially bestowing residual catalytic activity on the formal OFF-state. The computed *N*-inversion barrier via **1**-TSi is rather similar for all bases, amounting to approximately 7-8 kcal/mol (Table 1). As expected, the N-inverted isomers i-**1** carrying an axial substituent R are significantly higher in energy than the equatorial ground state. The species with the smallest R, i-**1a**, is least disfavored by ca. 4 kcal/mol, according to

DFT,[d] whereas the increased bulk of that group in i-**1b** and i-**1c** results in further destabilization by approximately 1-3 kcal/mol (Table 1).

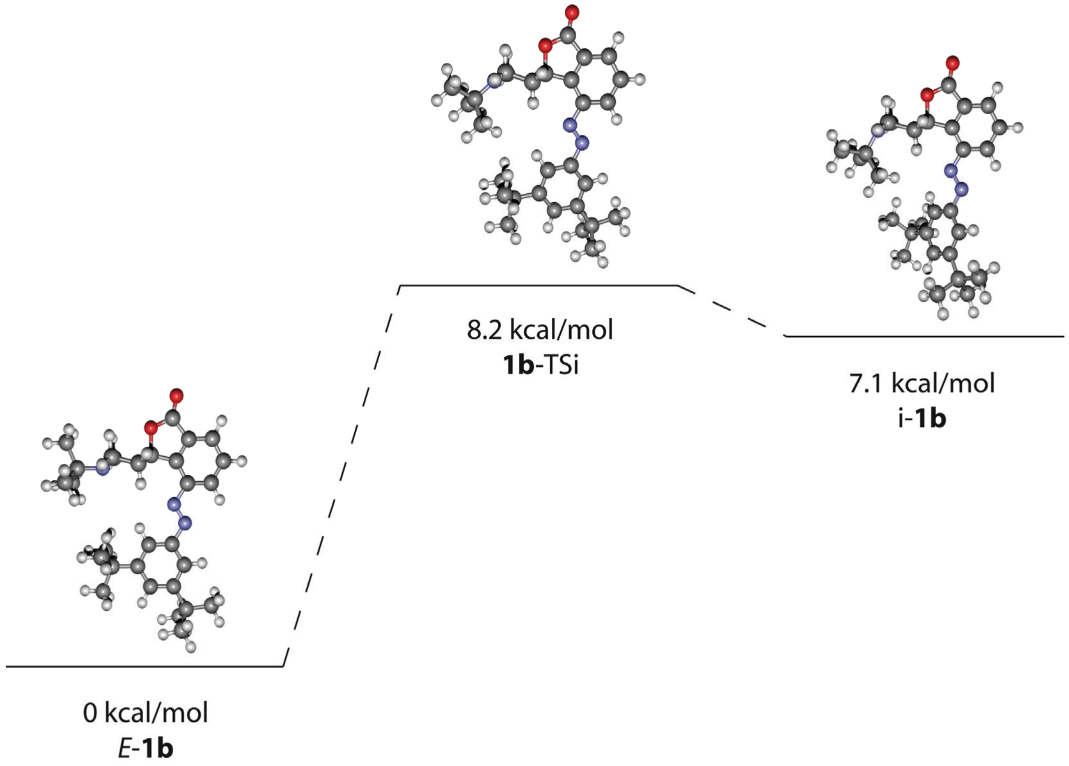

Figure 3: Energy level diagram of the calculated energies for N-inversion of **1b**. Free energies ΔG are given with respect to the energy of *E*-**1b** (see also Table 1; energies calculated on the B3LYP/6-31G* level of theory). Structures of stationary points along the reaction coordinate are shown as ball-stick models.

It is not straightforward to investigate N-inversion experimentally. For *N*-methyl substituted piperidines, ^{13}C chemical shifts for the *N*-methyl carbon for axial and equatorial methyl group have been reported.[23] However, the chemical shift of the one *N*-

---

[d] A similar energy difference has been obtained between equatorial and axial *N*-methyl piperidine, 3.9 kcal/mol at the MP2/cc-pVTZ level.[22]

methyl signal observed for *E*-**1a**, $\delta(^{13}C) = 45.6$ ppm, lies exactly in between those two values and does not change position or line shape even when lowering the temperature to 178 K. This observation can have two possible explanations: either only one conformer is mainly populated (no change in signal position and line shape) or N-inversion is fast on the NMR timescale even at low temperatures (chemical shift in between those reported for axial and equatorial *N*-methyl groups). As no conclusive experimental results for **1a** could be obtained by conventional NMR methods, the catalytically more active system **1b** was subjected to a detailed structural and dynamical NMR investigation of its solution phase dynamics in the thermally stable *E* isomer.

Residual dipolar couplings (RDCs) were used for this purpose, as the other conformationally relevant NMR-parameters (NOE, *J* couplings) are not expected to lead to unequivocal results. If only dipolar couplings of directly bonded nuclei (^{1}D) are used for the determination of the spatial structure of rigid compounds, RDCs can be used as angular restraints.[20,21] In this case, $^{1}D_{C\text{-}N}$, that is coupling between the quaternary carbon of the *N*-*tert*-butyl group and the piperidine N-atom, was employed to determine the orientation of the *N*-*tert*-butyl group with respect to the piperidine ring thus yielding information on N-inversion. Usually $^{1}D_{C\text{-}N}$ cannot be measured easily, yet in the case of **1b**, it can be determined indirectly from the $^{1}D_{C\text{-}H}$ coupling of the rotatable *tert*-butyl groups (attached to the piperidine N-atom and the steric blocker; see also Section 3.8.5). The structural proposal, fitting the experimentally derived RDCs best, can be considered as accurate representation of the spatial structure in solution.[21]

Compound *E*-**1b** was oriented in a lyotropic liquid crystalline matrix comprised of high molecular weight PBLG[24] with $CDCl_3$ as organic co-solvent and variable angle sample spinning (VASS)[25] was used to reduce RDCs to a suitable range, as strong coupling was observed between the diastereotopic protons of the piperidine methylene groups. This enabled the measurement of all $^{1}D_{C\text{-}H}$ and even some long-range $D_{\text{H-H}}$. The geometry optimized DFT structures of *E*-**1b** and i-**1b** were subsequently used to probe N-inversion. In order to distinguish between the two conformers, a scaling procedure had to be used such that $^{1}D_{C\text{-}N}$ gets approximately the same weight as $^{1}D_{C\text{-}H}$.[e] Two approaches of RDC data analysis were applied. First the respective coupling $^{1}D_{C\text{-}N}$, describing the orientation of the *tert*-butyl group with respect to the piperidine ring, was included in the fitting step using the DFT geometries of *E*-**1b** and i-**1b** and all RDCs except those of the steric blocker (*vide infra*). Using this procedure, a significantly better fit was obtained for *E*-**1b** (quality factor q = 0.131) than for i-**1b** (q = 2.046). This already suggests that the N-inverted isomer i-**1b** is not significantly populated while the proposed structure *E*-**1b** is matched extremely well by the experimental RDCs (Figure 4b). To independently confirm these findings, a second kind of analysis was performed by excluding $^{1}D_{C\text{-}N}$ from the fitting procedure and predicting its value from the orienting tensor of the rest of the compound (again without using the data of the steric blocker).[27] The predicted $^{1}D_{C\text{-}N}$ value of -24.1 Hz for *E*-**1b** is in good agreement with the measured coupling of -36±18 Hz as compared to the value of -248.8 Hz predicted for i-**1b**.[e] Therefore, from analysis of the RDC data it can be unequivocally concluded that no significant population of the N-inverted conformer i-**1b** could be detected by NMR spectroscopy.

---

[e] The two conformers could initially not be distinguished because of a fitting problem as $^{1}D_{C\text{-}N}$ becomes very small (because of the small gyromagnetic ratios) and the PALES program [26] used for fitting the data does not allow for weighing of couplings within the fitting procedure, resulting in equally good fits for *E*-**1b** and i-**1b**. To obtain conclusive results, the corresponding coupling was scaled by a factor of 1000 while the bond length was reduced in the coordinate file to 10 % of its original value using the program MolArch+ (Immel, molecular architecture modelling program, MolArch+, Universität Leipzig, 2008.). As ^{1}D is proportional to $1/r^{3}$ the physical information of $^{1}D_{C\text{-}N}$ is unchanged by this procedure.

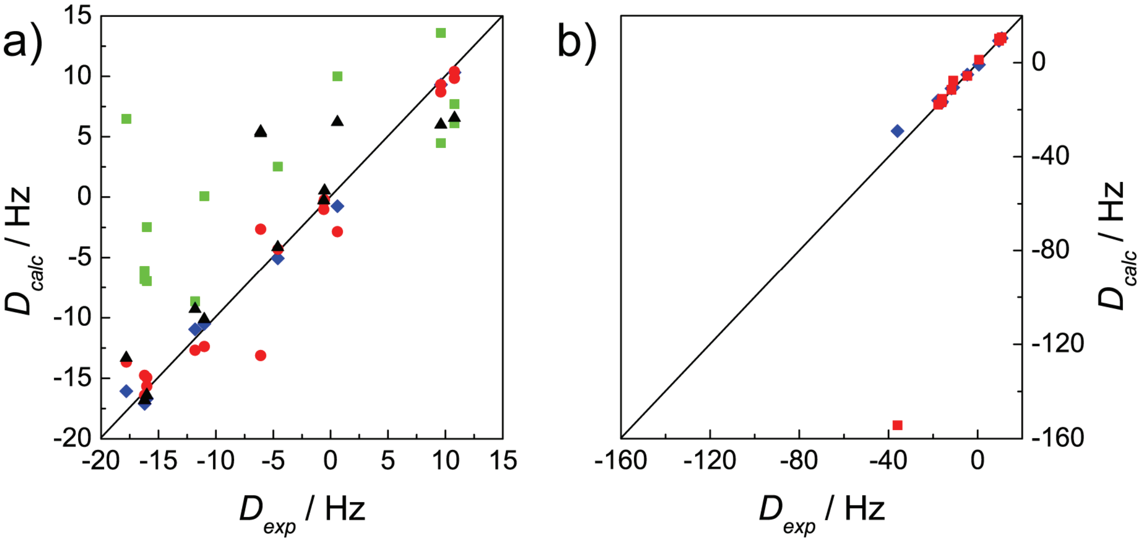

Figure 4: Comparison of RDCs calculated (D_{calc}) for the different possible conformational states of *E*-**1b** with the ones observed experimentally (D_{exp}). In a) the fit for the equilibrium structure *E*-**1b** (blue diamonds, without using the data from the steric blocker) is depicted together with the ring-flipped f_{eq}-**1b** (green squares). The red dots show the fit for all data (including the RDCs of the steric blocker) to *E*-**1b**, the black triangles to the transition structure for the rotation of the steric blocker **1b**-TSrot. In b) the fit for the equilibrium structure *E*-**1b** (blue diamonds, without using the data from the steric blocker, C-N bond length reduced to 10 % of its original length, see text) is compared to the N-inverted i-**1b** (red squares).

Chair Flip

Inversion of the six-membered piperidine chair, i.e. ring “flip” (red path c in Scheme 7, exemplarily shown for **1b** in Figure 5), represents another possible mechanism to render the axial lone pair in *E*-**1** accessible to the environment, thereby constituting a potential source of residual catalytic activity of the formal OFF-state. This ring flip is expected to proceed via one or more twist-boat intermediates to the ring-inverted form f_{ax}-**1**, which via N-inversion can subsequently rearrange to isomer f_{eq}-**1** with equatorial R and an exposed N-lone pair. After conformational analysis of the parent *N*-methyl piperidine at the B3LYP/6-31G* level, selected stationary points along this path were located for **1a** and **1b**, focusing on the final product and a representative transition state leading to a twist-boat (or twist) isomer. As expected, the ring-flipped isomers f_{eq}-**1a,b** are strongly disfavored, by ca. 7-9 kcal/mol, and are accessible only via significant barriers, up to ca.

12-13 kcal/mol (Table 1).[f] Incidentally, these numbers are close to the corresponding barrier for cyclohexane.[g] Overall, there is no indication from the computations that ring-flipped isomers could be populated to any significant extent. Very similar results are to be expected for the bulky derivative **1c**, which was not further studied computationally.

---

[f] There are many more possible twist or twist-boat intermediates and transition states, depending on which C-C or C-N bond in the ring is rotated relative to its opposite counterpart and in what direction. We have refrained from locating all of them, but from the present results it is already clear that the overall barrier must be in the range of ca. 7-13 kcal/mol, implying notable activation for this process.

[g] (18) E.g. ΔE = 11.4 kcal/mol at B3LYP/6-31G* for the C_2-symmetric twist-chair transition state (or half-chair), cf. structure 10 in the following reference, where a value of 11.9 kcal/mol has been obtained at MP2/6-31G*.[28]

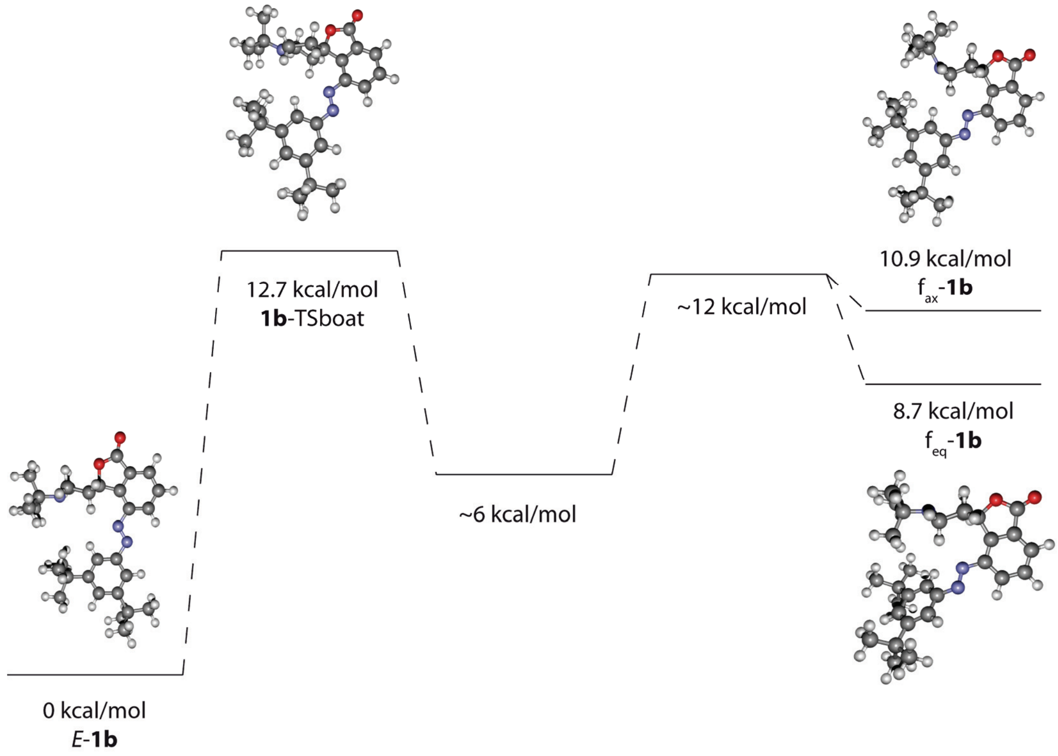

Figure 5: Energy level diagram of the calculated energies for chair flipping of **1b**. Free energies ΔG are given with respect to the energy of *E*-**1b** (see also Table 1; energies calculated on the B3LYP/6-31G* level of theory). Selected structures of stationary points along the reaction coordinate are shown as ball-stick models.

Compounds *E*-**1a** and *E*-**1b** were investigated experimentally and inspection of their ^{1}H NMR spectra shows that both pairs of diastereotopic protons of the piperidine methylene groups are anisochronous, indicative for locked chair conformations. These observations were further supported by EXSY experiments, revealing no exchange between these diastereotopic protons and thus excluding any significant population of ring flipped isomers f$_{eq}$-**1a,b**. Final confirmation of the absence of chair inversion was obtained by fitting the RDC data for *E*-**1b** to the DFT geometries of *E*-**1b** and its corresponding ring-flipped conformer f$_{eq}$-**1b**. As expected, the computed structure *E*-**1b** is in excellent agreement with the RDC data ($q = 0.067$, see Figure 4a, blue diamonds), whereas alternative structure f$_{eq}$-**1b** results in a poor fit ($q = 0.823$, see Figure 4a, green squares).

Rotation of the Blocking Group

Finally, rotation of the aromatic blocking group $C_6H_3R'_2$, about the N-C axis (green path d in Scheme 2) represents a fluxional process that could potentially affect the accessibility of the piperidine lone pair in *E*-**1**. The fact that this process is rapid at ambient temperature, at least on the NMR time scale, is already suggested by the equivalence of the two R' moieties in the NMR spectra. As the signals could be isochronous by coincidence,[29] detailed analysis of the collected RDC data for *E*-**1b** was carried out and conformational flexibility became apparent. Observed RDC values are usually smaller for flexible parts of the compound (due to averaging) and RDCs do not fit any of the structural proposals,[h] as observed when fitting the complete set of RDCs to the DFT-structure of *E*-**1b** ($q = 0.215$, see Figure 4a, red dots). Furthermore, the calculated $^1D_{C\text{-}H}$s for the two *ortho*-protons of the steric blocker in the case of a rigid structure (-13.1 Hz and -2.6 Hz) deviate largely from the measured averaged $^1D_{C\text{-}H}$ value (-6.1 Hz), confirming fast rotation on the NMR time scale.[i]

---

[h] Another indication is given by the fact that no differentiation of enantiotopic faces was observable, which is to be expected in a chiral orienting medium if no rotation of the steric blocker (converting one enantiotopic face into the other) is occurring.

[i] If the transition state structure of this rotation, **1**-TSrot, is used, the quality of the fit is further reduced ($q = 0.426$, Figure 4a, black triangles).

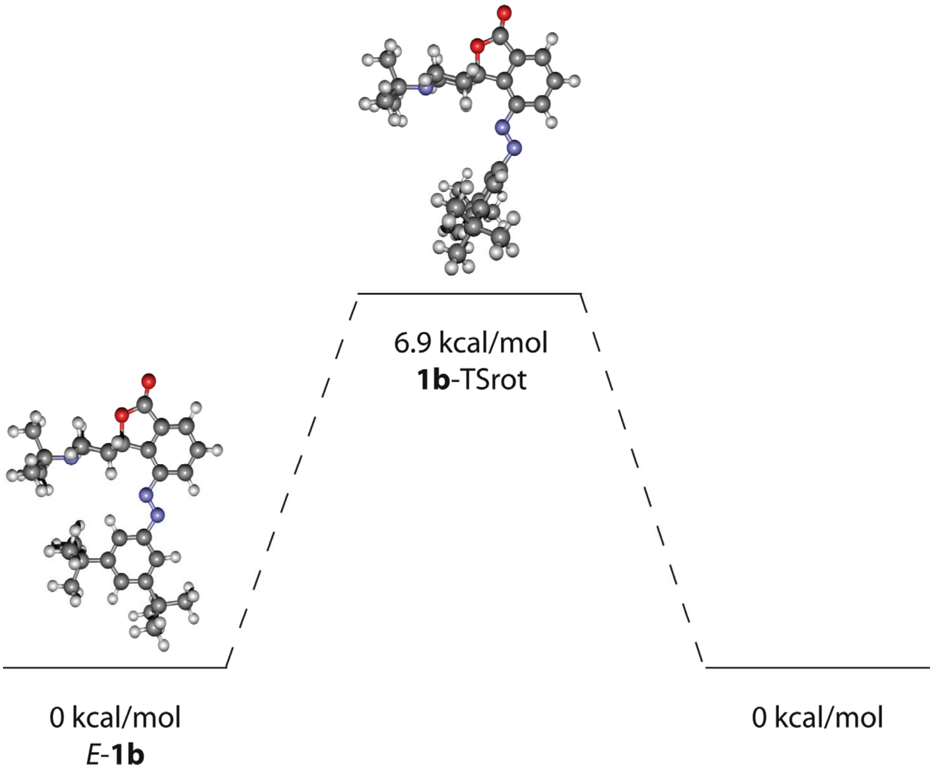

Figure 6: Energy level diagram of the calculated energies for blocker group rotation in **1b**. Free energies ΔG are given with respect to the energy of *E*-**1b** (see also Table 1; energies calculated on the B3LYP/6-31G* level of theory). Structures of stationary points along the reaction coordinate are shown as ball-stick models.

In accordance with these observations, only modest barriers ranging between 6-8 kcal/mol (Table 1) were computed for this rotation involving **1**-TSrot (green path d in Scheme 7). Interestingly, the lowest barrier was computed for the largest substituent. Indeed, visual inspection of the *E*-**1c** ground state shows that no serious clash between the R and R' groups is to be expected upon rigid rotation of the blocking group (Figure 7). Despite the comparably low hindrance toward blocking-group rotation in *E*-**1a**, *E*-**1b,** and *E*-**1c**, the bulky R' groups in the latter appear to be more effective in shielding the lone pair than those in the former (see discussion of reactivities below).

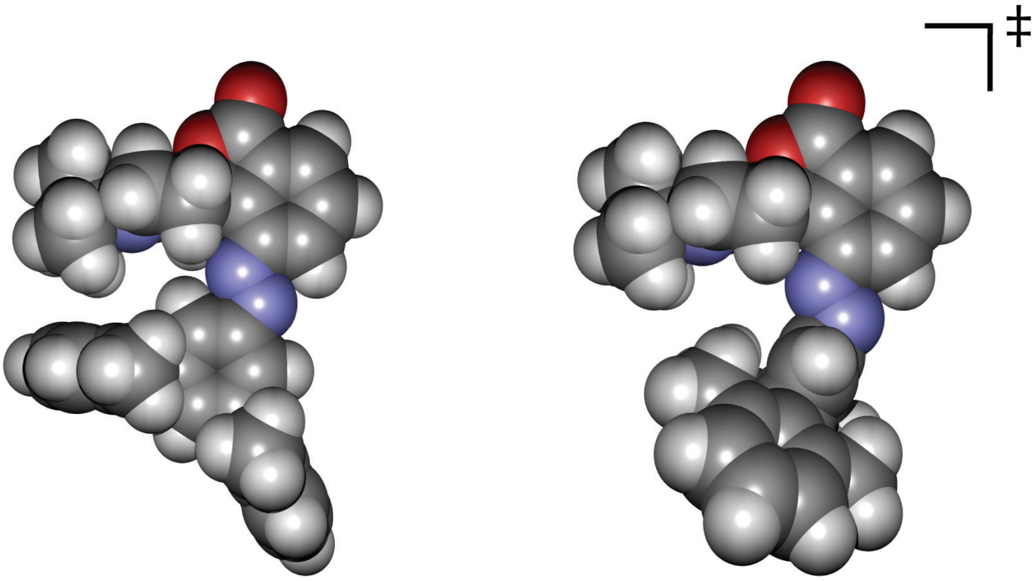

E-**1c** **1c**-TSrot

Figure 7: Calculated structures of *E*-**1c** and **1c**-TSrot (B3LYP/6-31G* optimized). The spacefill models show that no serious clash is expected upon rigid rotation of the blocking group.

3.4 Photochromism[j]

The photochromic behavior of photoswitchable piperidine bases **1a-c** and **2** was investigated in detail (Table 2). Azobenzene based catalysts **1a-c** showed the expected isomerization behavior upon irradiation of the thermally stable *E* isomers. As evident from UV/vis spectra, irradiation with light of 365 nm wavelength leads to a decrease in intensity of the absorption band at about 330 nm, which is attributed to the π,π*-transition of the azobenzene chromophore, along with an increase of the band around 450 nm, which is attributed to the n,π*-absorption (Figure 8).[30] Irradiation of larger quantities of catalysts **1a-c** in acetonitrile solution allowed for isolation of samples containing mainly the *Z* isomers. X-ray crystal structure analysis of *Z*-**1b** shows a pronounced deviation from planarity of the azobenzene core, leading to significant electronic decoupling of both phenyl rings in the *Z* isomer (Figure 2) and the resulting hypsochromic shift of the π,π^*-absorption constitutes the basis of photochromism in azobenzenes. Photostationary states obtained by irradiation of analytical samples of **1a-c** show a remarkably high content of *Z* isomer, amounting to at least 90% according to UPLC analysis. The *Z* isomer can be converted to the *E* isomer photochemically by irradiation with visible light ($\lambda \geq 400$ nm, Figure 8). However, the extent of switching is smaller due to the non-negligible absorption of the *E* isomer above 400 nm and yields photostationary state mixtures containing up to 90% *E* isomer in case of **1c** and around 85% for **1a** and **1b**.

---

[j] Photophysical data of piperidine bases **1a,b** and **2** were acquired by Maike Peters.[7]

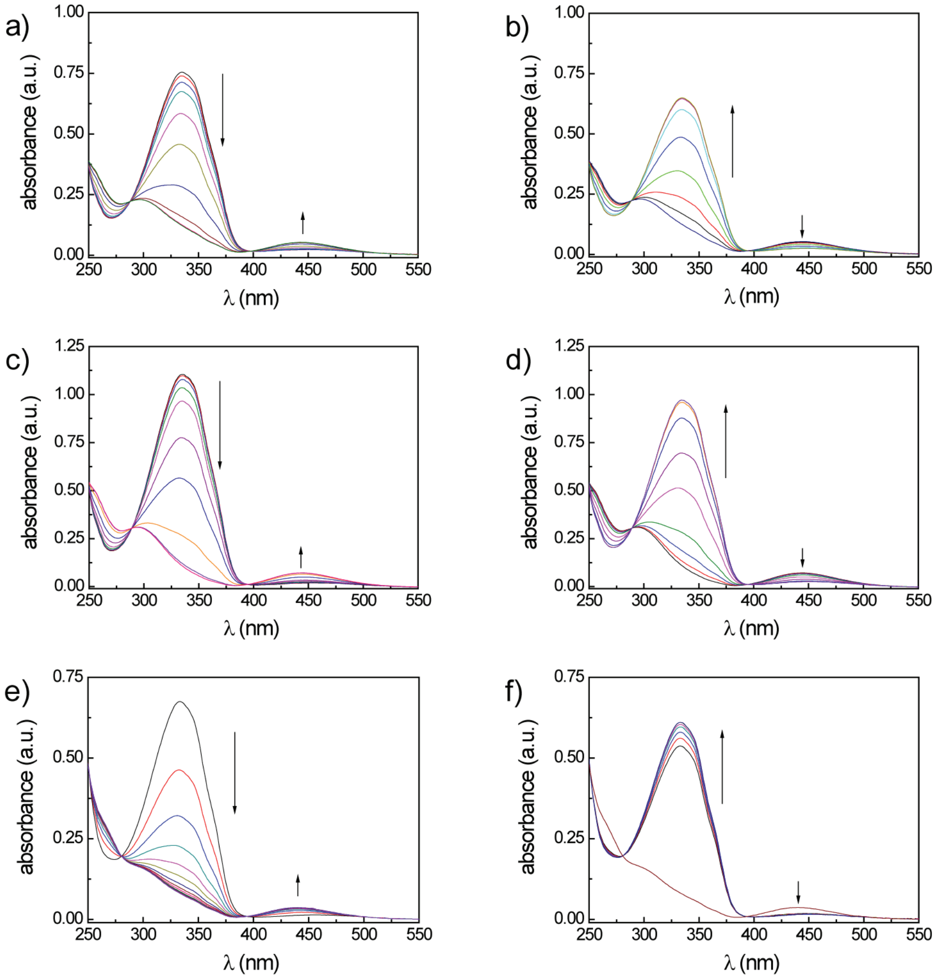

Figure 8: Irradiation of azobenzene catalysts **1a-c**: a) isomerization *E*-**1a** → *Z*-**1a** (365 nm interference filter, 12 min 48 s irradiation time, $2.8 \cdot 10^{-5}$ M in CH_3CN); b) isomerization *Z*-**1a** → *E*-**1a** (400 nm cut-off filter, 4 min 15 s irradiation time, $2.8 \cdot 10^{-5}$ M in CH_3CN); c) isomerization *E*-**1b** → *Z*-**1b**, (λ_{irr} = 365 nm, 12 min 46 s irradiation time, $3.1 \cdot 10^{-5}$ M in CH_3CN); d) isomerization *Z*-**1b** → *E*-**1b** ($\lambda_{irr} > 400$ nm, 6 min 22 s irradiation time, $3.1 \cdot 10^{-5}$ M in CH_3CN); e) isomerization *E*-**1c** → *Z*-**1c**, (λ_{irr}= 365 nm, 14 min irradiation time, $3.0 \cdot 10^{-5}$ M in CH_3CN); f) isomerization *Z*-**1c** → *E*-**1c** ($\lambda_{irr} > 400$ nm, 4 min irradiation time, $3.0 \cdot 10^{-5}$ M in CH_3CN).

Table 2: Photochromic properties and activation parameters for thermal *Z* → *E* isomerization of **1a-c** and **2**.

	absorption		**PSS composition**	
	$\lambda_{\mathrm{max}}(E)^{a}$ [nm]	$\lambda_{\mathrm{max}}(Z)^{b}$ [nm]	***E* → *Z*** (*Z*/*E*)	***Z* → *E*** (*Z*/*E*)
1a	335	444	90:10	15:85
1b	335	444	90:10	15:85
1c	333	440	>99:1[e]	10:90
2	298	279	93:7	78:22

	thermal *Z* → *E* isomerization			
	$\tau_{1/2}{}^{c}$ [h]	$\Delta G^{\ddagger}{}_{298\,\mathrm{K}}{}^{d}$ [kcal mol^{-1}]	$\Delta H^{\ddagger d}$ [kcal mol^{-1}]	$\Delta S^{\ddagger d}$ [cal mol^{-1} K^{-1}]
1a	268	26	23	-9
1b	286	25	22	-11
1c	466	25	23	-8
2	-	-	-	-

[a] π,π*-Absorption. [b] n,π*-Absorption. [c] At 20 °C (293.15 K). [d] Obtained from kinetic data of the thermal *Z* → *E* isomerization at various temperatures and Eyring analysis of the data. [e] No *E* isomer was detected by UPLC analysis.

The spectra of pure *E*-**1a-c** were readily obtained from thermally equilibrated samples, whereas spectra of *Z*-**1a-c** were either obtained by HPLC using a diode-array detector in the case of **1a** (Figure 9) or were calculated form the UV/vis spectra of pure *E*-**1b** and the *E* : *Z* mixture at the photostationary state, for which the *E* : *Z* ratio was determined by HPLC separation (Figure 10). Analytical irradiation of *E*-**1c** led to samples containing solely *Z*-**1c**, as indicated by UPLC analysis of the photostationary state mixture (Figure 11).

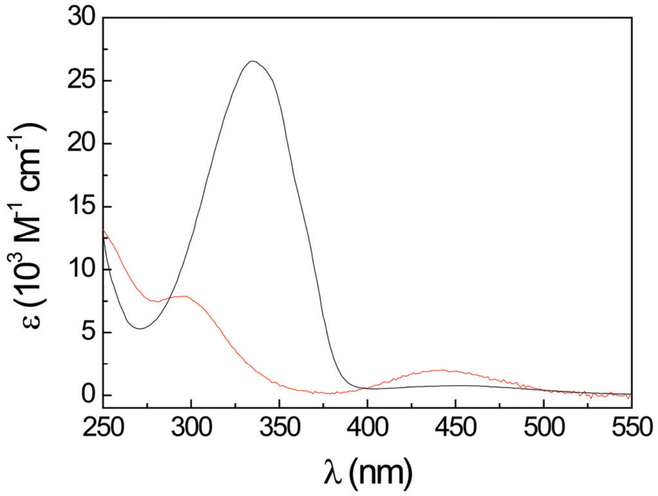

Figure 9: UV/vis-spectra of *E*-**1a** (black, c = 2.8 · 10^{-5} M, ε_{335nm} = 26600 M^{-1} cm^{-1}) and *Z*-**1a** (red, c = 2.8 · 10^{-5} M, ε_{296nm} = 7900 M^{-1} cm^{-1}) in CH_3CN. The spectrum of *Z*-**1a** was acquired using HPLC separation (125 mm Nucleodur, 2.0 mm i.d. in CH_3CN/10 mmol TEAA, pH 6.8, 0 85/15, 0.8 mL/min) coupled to a diode array detector and normalized at the isosbestic point (λ_{iso} = 288 nm).

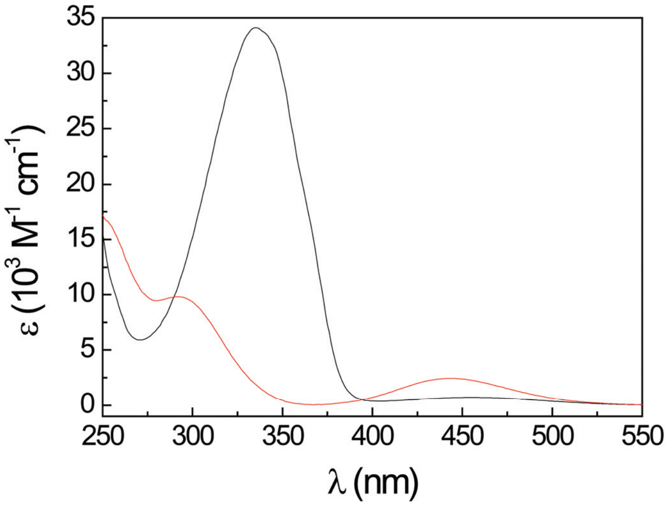

Figure 10: UV/vis-spectra of *E*-**1b** (black, c = 3.1 · 10^{-5} M, ε_{335nm} = 34100 M^{-1} cm^{-1}) and *Z*-**1b** (red, c = 3.1 · 10^{-5} M, $\varepsilon_{292\,nm}$ = 9800 M^{-1} cm^{-1}) in CH_3CN. The spectrum of *Z*-**1b** was calculated from the UV/vis spectra of pure *E*-**1b** and the *E* : *Z* mixture at the photostationary state, for which the *E* : *Z* ratio was determined by HPLC separation.

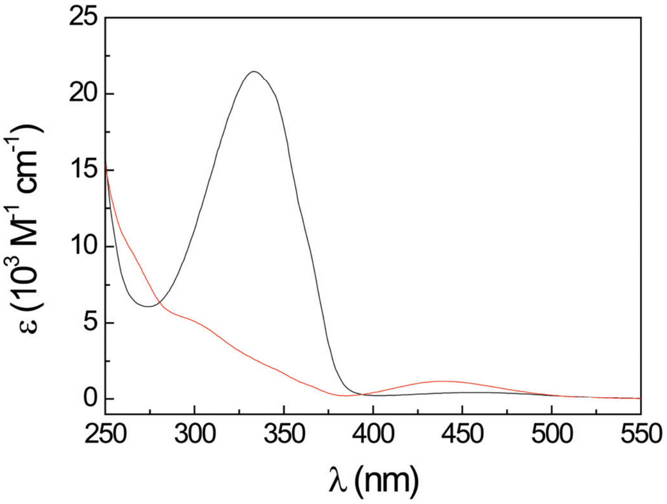

Figure 11: UV/vis-spectra of *E*-**1c** (black, c = 3.0 · 10^{-5} M, $\varepsilon_{333\,\mathrm{nm}} = 21484\ \mathrm{M^{-1}\,cm^{-1}}$) and *Z*-**1c** (red, c = 3.0 · 10^{-5} M, $\varepsilon_{440\,\mathrm{nm}} = 1181\ \mathrm{M^{-1}\,cm^{-1}}$) in CH_3CN. Spectra of *Z*-**1c** was obtained after analytical irradiation of a *E*-**1c** leading to quantitative conversion as indicated by UPLC analysis of the irradiated mixture showing no residual *E* isomer.

As expected for azobenzenes, catalysts **1a-c** thermally revert from the *Z* to the *E* isomer. Thermal half lifes $\tau_{1/2}$ observed for *Z*-**1a-c** were found to be extraordinarily extended as compared to the parent azobenzene ($\tau_{1/2}$ = 16 h in benzene).[31] Thermal isomerization of *Z*-**1a** and *Z*-**1b** was observed to occur with half lifes of 268 h and 286 h at 20 °C, respectively. Change of the steric demand of the blocking group by replacing the 3,5-di-*tert*-butylphenyl fragment with the 3,5-bis(2,6-dimethylphenyl)phenyl fragment further prolonged half life to 466 h at 20 °C for *Z*-**1c**.

Activation parameters for the thermal isomerization of *Z*-**1a-c** were determined by measuring the rate constants of thermal *Z* → *E* isomerization at different temperatures

(Figure 12, Figure 13, Figure 14 for **1a**, **1b**, **1c**, respectively).[k] The course of the reaction was followed by UV/vis spectroscopy, allowing to determine the concentrations of *E* and *Z* isomers at given time intervals. Plotting -ln([*Z*]) versus the time reveals a linear dependency of ln([*Z*]) on time, as expected for a unimolecular transformation following a first order rate equation. The rate constant at a given temperature is directly obtained from the slope of a linear regression of the -ln([*Z*]) vs. time data (Figure 12-14).

---

[k] Please note, half lifes reported in Table 2 were directly determined from the rate constants at the given temperature. Estimated errors for activation parameters are in the range of ±1 kcal mol^{-1} for $\Delta H^{\ddagger}$ and ±1 cal mol^{-1} K^{-1} for $\Delta S^{\ddagger}$. Rate constants and half lifes, which can be calculated from $\Delta H^{\ddagger}$ and $\Delta S^{\ddagger}$ by the thermodynamic formulation of the Eyring equation, are extremely sensitive to these quantities.

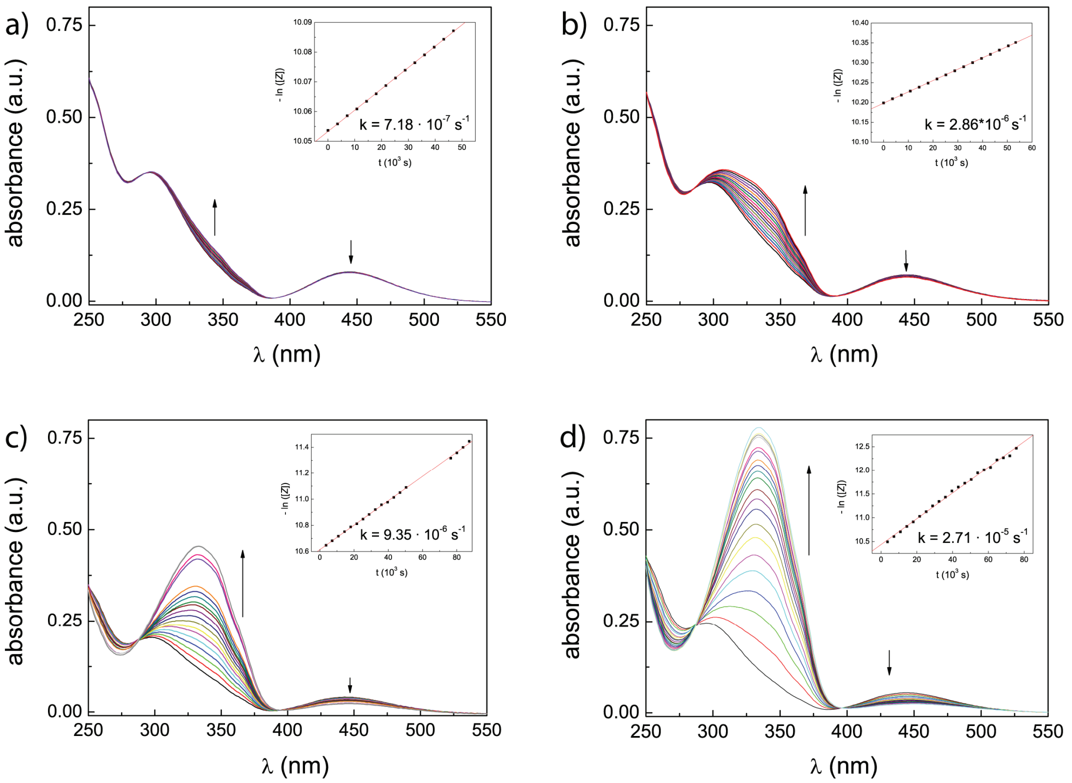

Figure 12: Thermal isomerization of *Z*-**1a** → *E*-**1a** at varying temperatures; insets show plots of -ln([*Z*]) vs. time and derived rate constants. a) 20 °C for 13 h ($4.51 \cdot 10^{-5}$ M in CH_3CN), b) 30 °C for 15 h ($4.11 \cdot 10^{-5}$ M in CH_3CN), c) 40 °C for 25 h ($2.70 \cdot 10^{-5}$ M in CH_3CN), d) 50 °C for 21 h ($2.71 \cdot 10^{-5}$ M in CH_3CN).

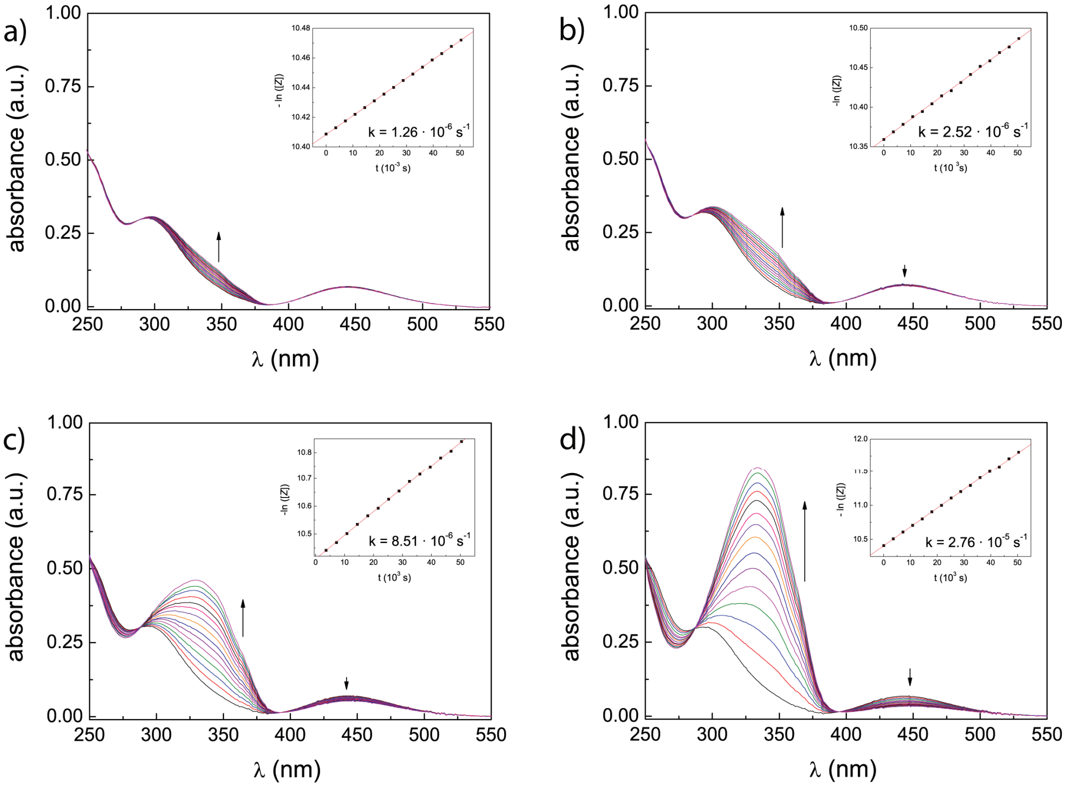

Figure 13: Thermal isomerization of *Z*-**1b** → *E*-**1b** at varying temperatures; insets show plots of -ln([*Z*]) vs. time and derived rate constants. a) 25 °C for 14 h ($3.17 \cdot 10^{-5}$ M in CH_3CN), b) 30 °C for 14 h ($2.52 \cdot 10^{-5}$ M in CH_3CN), c) 40 °C for 14 h ($3.20 \cdot 10^{-5}$ M in CH_3CN), d) 50 °C for 14 h ($2.76 \cdot 10^{-5}$ M in CH_3CN).

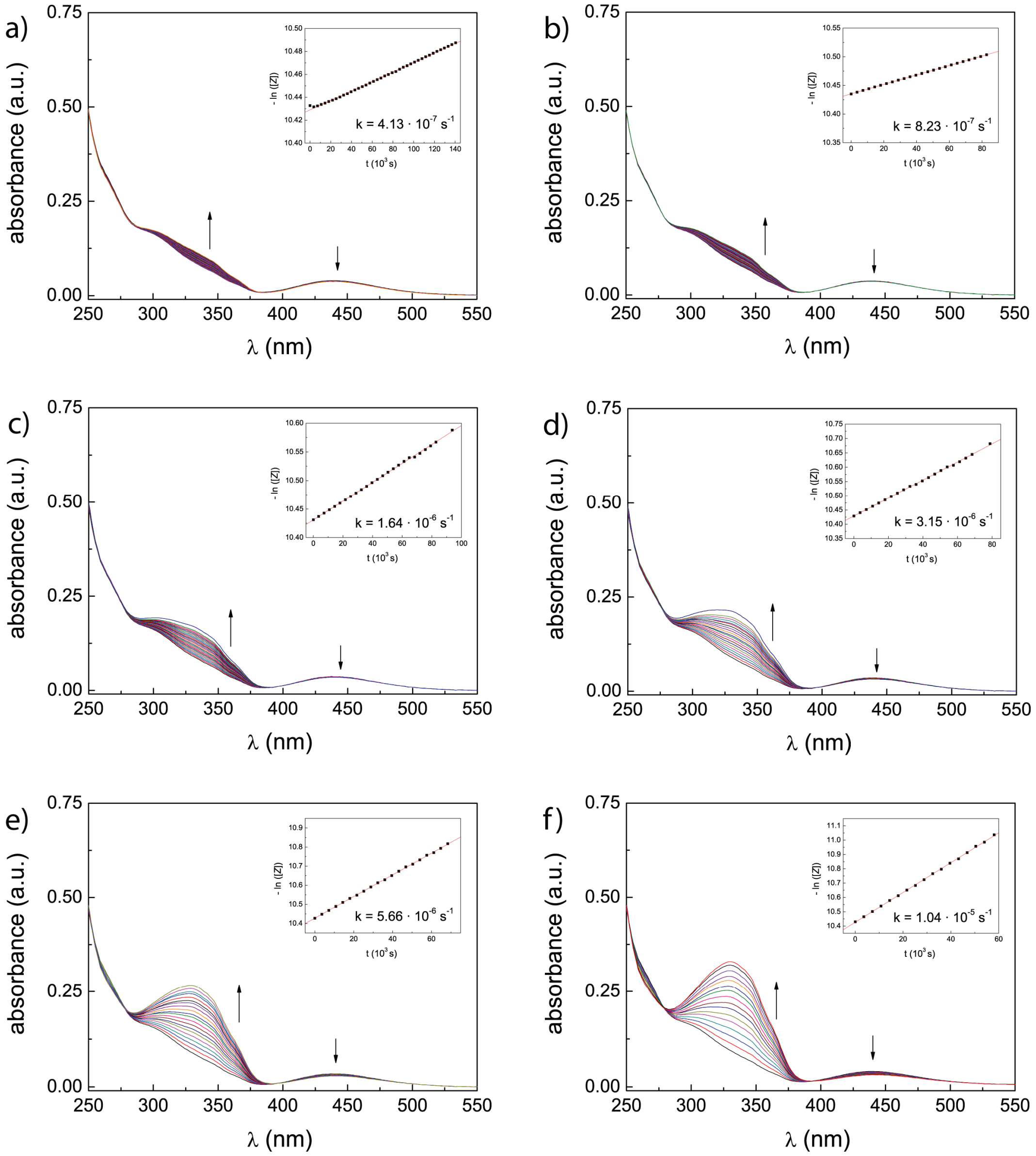

Figure 14: Thermal isomerization of *Z*-**1c** → *E*-**1c** at varying temperatures; insets show plots of -ln([*Z*]) vs. time and derived rate constants. a) 20 °C for 39 h ($1.28 \cdot 10^{-5}$ M in CH_3CN), b) 25 °C for 23 h ($1.28 \cdot 10^{-5}$ M in CH_3CN), c) 30 °C for 26 h ($1.28 \cdot 10^{-5}$ M in CH_3CN), d) 35 °C for 22 h ($1.28 \cdot 10^{-5}$ M in CH_3CN), e) 40 °C for 19 h ($1.28 \cdot 10^{-5}$ M in CH_3CN), f) 45 °C for 16 h ($1.28 \cdot 10^{-5}$ M in CH_3CN).

Conventional transition state theory treats the kinetics of a reaction in terms of an equilibrium between starting materials and an activated complex, commonly referred to as the transition state. According to Eyring,[32] this leads to the formulation given in equation 2: the rate constant is expressed as the product of an equilibrium constant $K^‡$

and the frequency factor $(k_B \cdot T) / h$. Thermodynamics allows to formulate a relation between the free enthalpy of activation and the equilibrium constant $K^{\ddagger}$ (equation 3). Combination of equations 2 and 3 gives the thermodynamical formulation of the Eyring equation (equation 5). Substitution with equation 4 allows to split the exponential term and to introduce two new quantities: the enthalpy of activation $\Delta H^{\ddagger}$ and the entropy of activation $\Delta S^{\ddagger}$.

$$k = \frac{k_B \cdot T}{h} \cdot K^{\ddagger} \tag{2}$$

$$\Delta G^{\ddagger} = -R \cdot T \cdot \ln\left(K^{\ddagger}\right) \tag{3}$$

$$\Delta G^{\ddagger} = \Delta H^{\ddagger} - T \cdot \Delta S^{\ddagger} \tag{4}$$

$$k = \frac{k_B \cdot T}{h} \cdot e^{-\frac{\Delta G^{\ddagger}}{R \cdot T}} = \frac{k_B \cdot T}{h} \cdot e^{-\frac{\Delta H^{\ddagger}}{R \cdot T}} \cdot e^{\frac{\Delta S^{\ddagger}}{R}} \tag{5}$$

The enthalpy of activation $\Delta H^{\ddagger}$ is a measure for the enthalpy difference between reactants and transition state, that is it describes the energetic situation of the activated complex. The entropic situation of the activated complex is described by the entropy of activation $\Delta S^{\ddagger}$. Strongly negative values of $\Delta S^{\ddagger}$ suggest a relatively high degree of order in the transition state compared to the reactants, a situation commonly encountered, if degrees of freedom are frozen when approaching the transition state. Conversely, weakly negative or positive values of $\Delta S^{\ddagger}$ are found, if degrees of freedom are gained when approaching the transition state. Combination of $\Delta H^{\ddagger}$ and $\Delta S^{\ddagger}$ gives the free enthalpy of activation $\Delta G^{\ddagger}$ (equation 4).

From equation 5, it becomes apparent that by plotting ln(k/T) versus 1/T a linear relation should be found, cf. equations 6 and 7. The slope of a linear regression allows to determine the enthalpy of activation $\Delta H^{\ddagger}$, whereas the interception with the ordinate gives the entropy of activation $\Delta S^{\ddagger}$. By application of Formula 4, the free enthalpy of activation can be determined. Plots of ln(k/T) versus 1/T are commonly referred to as van't Hoff plots.

$$\ln\left(\frac{k}{T}\right)+\ln\left(\frac{h}{k_B}\right)=-\frac{\Delta G^{\ddagger}}{R\cdot T}=-\frac{\Delta H^{\ddagger}}{R\cdot T}+\frac{\Delta S^{\ddagger}}{R} \tag{6}$$

$$\ln\left(\frac{k}{T}\right)=-\frac{\Delta H^{\ddagger}}{R\cdot T}+\frac{\Delta S^{\ddagger}}{R}-\ln\left(\frac{h}{k_B}\right) \tag{7}$$

Van't Hoff plots for the determination of activation parameters for catalysts **1a-c** are shown in Figure 15. Activation parameters derived from these plot are given in Table 2. All activation parameters obtained are in reasonable agreement with parameters determined for other azobenzene derivatives.[33,34]

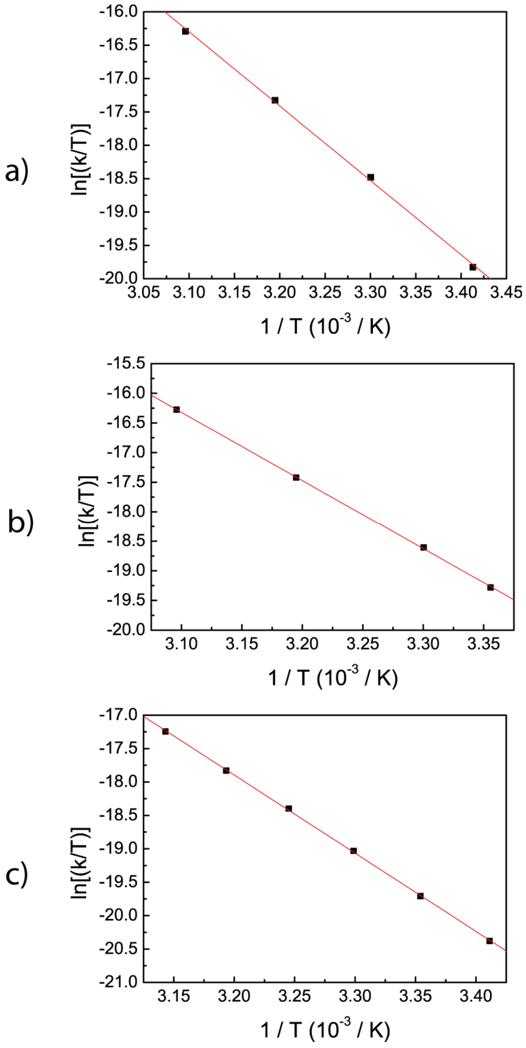

Figure 15: Van't Hoff plot for thermal $Z \rightarrow E$ isomerization of **1a-c** obtained by plotting ln (k/T) versus 1/T: a) *Z*-**1a** → *E*-**1a**; b) *Z*-**1b** → *E*-**1b**; c) *Z*-**1c** → *E*-**1c**. Obtained activation parameters are given in Table 2.

Thermal isomerization was also investigated computationally. For **1a**, the only *E/Z*-transition state that could be located is one that is associated with inversion at the diazo-N-atom bound to the spiro-annulated core (**1a**-TSEZ, see black path a in Scheme 7 and Figure 16).[35] That transition state was obtained even when the search started from a structure that would correspond to a rotation about the N=N axis. This finding is in line with earlier DFT results for azobenzene, according to which inversion has a lower barrier than rotation.[36] For the other derivatives, similar inversion transition states

1b,c-TSEZ were found. In all of these, the 3,5-disubsituted benzene ring is oriented almost perpendicular to the plane of the spiro-annulated benzene ring having a C-N=N-C torsional angle around 100° and N=N-C-C torsional angles close to 0° and 180°, respectively. Activation parameters for *Z* → *E* isomerization in the gas phase, calculated as the free energy of **1**-TSEZ relative to that of *Z*-**1** (Table 1), are 22.8, 21.8, and 23.0 kcal/mol for **1a**, **1b**, and **1c**, respectively. These numbers are slightly lower than the experimental estimates for $\Delta G^{\ddagger}$ in Table 2 and show no particular trend. Enthalpies of activations $\Delta H^{\ddagger}$ are fairly equal when comparing theoretical[1] and experimental values, indicating a comparable enthalpic loss when going from the strained *Z* isomer to the twisted transition state. Activation entropies $\Delta S^{\ddagger}$ for the gas phases reaction are small in all cases, suggesting that contributions to $\Delta S^{\ddagger}$ in condensed phase are mostly associated with solvation effects. From the negative values found experimentally for $\Delta S^{\ddagger}$, it can be deduced that the degree of order of solvated *Z*-**1a-c** increases by going to its respective transition state.

---

[1] The corresponding DFT values for $\Delta H^{\ddagger}$ (not included in Table 1) are 23.0, 22.9, and 23.6 kcal/mol for **1a**, **1b**, and **1c**, respectively.

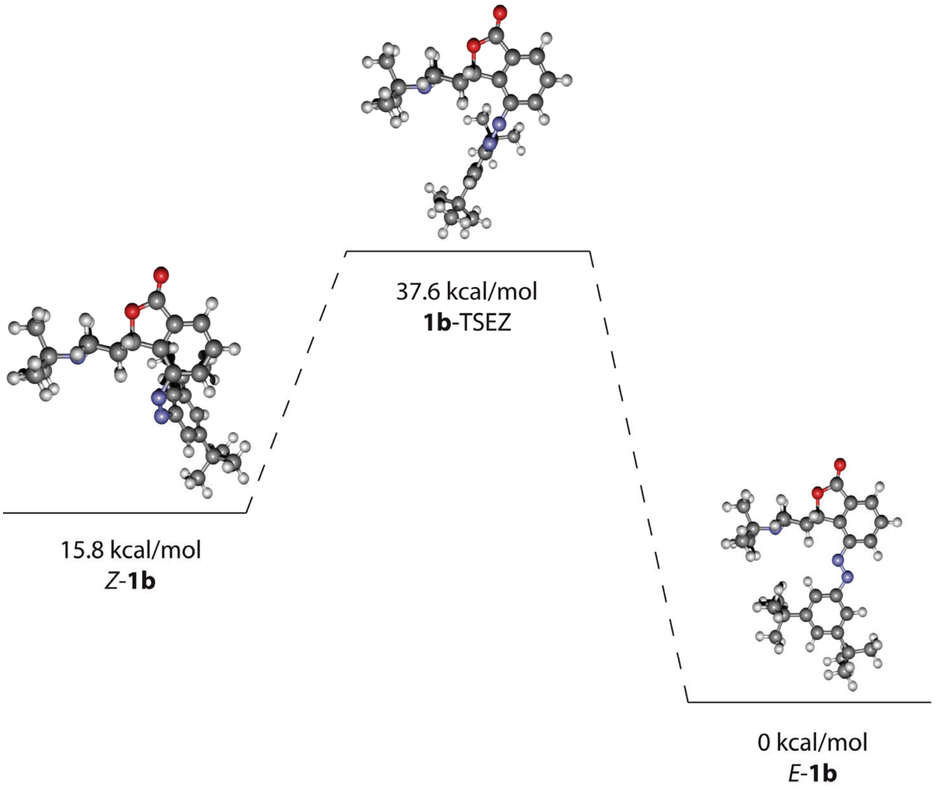

Figure 16: Energy level diagram of the calculated energies for *Z* → *E* isomerization of **1b** in the ground state. Free energies ΔG are given with respect to the energy of *E*-**1b** (see also Table 1; energies calculated on the B3LYP/6-31G* level of theory). Structures of stationary points along the reaction coordinate are shown as ball-stick models.

With regard to the prolonged half life of *Z*-**1c**, it is reasonable to assume a larger entropic contribution resulting in a decrease of $\Delta G^{\ddagger}$ ($\Delta G^{\ddagger} = \Delta H^{\ddagger} - \mathrm{T}\,\Delta S^{\ddagger}$) compared to **1a,b**, because the larger, more hydrophobic blocking group is more weakly solvated therefore requiring a smaller amount of reorganization in the solvation sphere. The small increase in half life observed experimentally for **1a** and **1b** is most likely due to a similar effect associated with the increase in hydrophobicity when exchanging the methyl substituent for the *tert*-butyl group. The effect is smaller, because the site of substituent exchange is more remote from the azo fragment causing differences in solvation having a smaller influence on the transition state of *E* → *Z* isomerization. In fact, experimentally determined values for $\Delta S^{\ddagger}$ increase by about 3 cal mol^{-1} K^{-1} going from **1a** to **1c**. However, this can only be seen as a trend and experimental uncertainties preclude any accurate quantification.

To avoid potential problems originating from the thermal instability of the *Z* isomer of the azobenzene based catalysts **1a-c**, stilbene based catalyst **2** was investigated. In contrast to azobenzene and its derivatives, stilbenes exhibit a photochromic behavior with both switching states being thermally stable (photochromism of the P type).[37] As expected, irradiation of **2** led to conversion of the *E* isomer to the *Z* isomer accompanied by a decrease of the absorption band around 300 nm and a small increase of absorption around 250 nm (Figure 17). Remarkably, the photostationary state mixture obtained by irradiation of analytical samples in acetonitrile with light of wavelength greater than 330 nm contained almost exclusively *Z* isomer, i.e. 97% as determined by HPLC.

As expected, thermal reversion of *Z*-**2** to *E*-**2** was not observed. Irradiation of the photostationary state mixture with light of 250 nm wavelength induced $Z \rightarrow E$ isomerization, yet only 22% *E* isomer could be recovered due to the marked absorption of the *E* isomer at 250 nm. No spectral region can be identified that would allow for satisfactory $Z \rightarrow E$ photoisomerization, since the *E* isomer's absorption is more significant throughout the entire wavelength range as compared to the *Z* isomer, precluding the use of **2** as a practical photoswitch. Implications of the small extent of $Z \rightarrow E$ switching on the catalytic performance of the stilbene catalyst **2** are discussed in the next section. The spectra of pure *Z*-**2** was calculated from the UV/vis spectra of pure *E*-**2** and the *Z* : *E* mixture at the photostationary state (Figure 18).

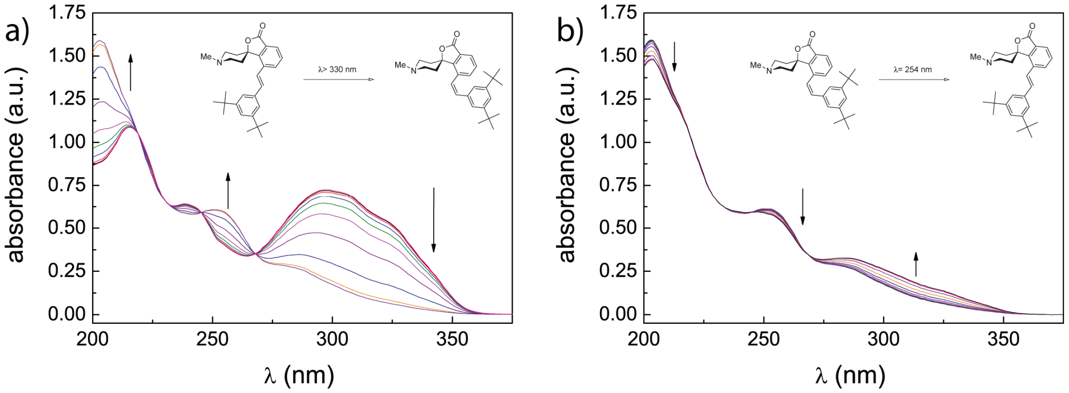

Figure 17: Irradiation of **2** ($1.9 \cdot 10^{-5}$ M in CH_3CN): a) Isomerization *E*-**2** → *Z*-**2**, (λ_{irr} > 330 nm, 57 min irradiation time); b) Isomerization *Z*-**2** → *E*-**2** (λ_{irr} = 254 nm, 8.5 min irradiation time).

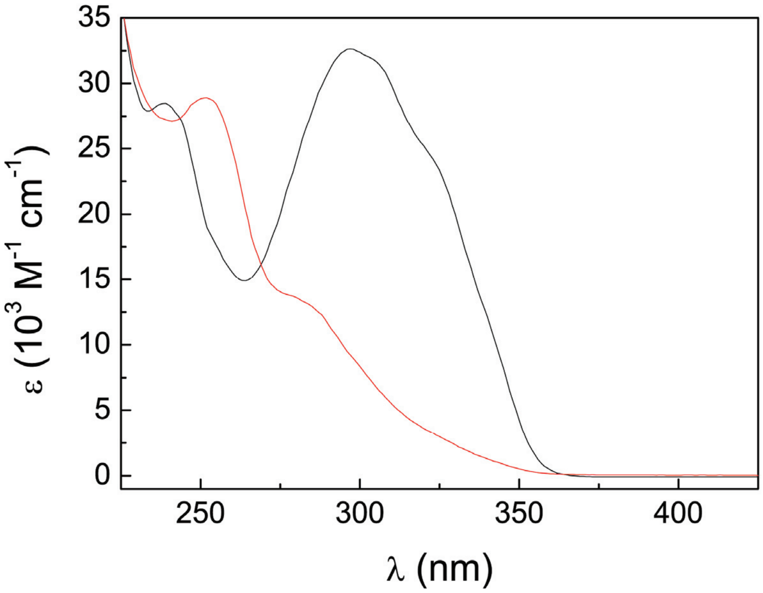

Figure 18: UV/vis-spectra of *E*-**2** (black, c = $3.7 \cdot 10^{-5}$ M, $\varepsilon_{333nm} = 21484\ M^{-1}\ cm^{-1}$) and *Z*-**2** (red, c = $3.7 \cdot 10^{-5}$ M, $\varepsilon_{440nm} = 1181\ M^{-1}\ cm^{-1}$) in CH_3CN. The spectrum of *Z*-**2** was calculated from the UV/vis spectra of pure *E*-**2** and the *Z* : *E* mixture at the photostationary state, for which the *Z* : *E* ratio was determined by HPLC separation.

3.5 Reactivity[m]

3.5.1 Basicity

The photochromic behavior of catalysts **1a-c** is associated with pronounced structural changes, which translate into differences in chemical reactivity of both isomers. In context with the desired general-base catalysis, the basicity of the amines and the extent to which it can be altered between the ON- and OFF-states are of great interest. A change in basicity upon isomerization could be expected due to the different stabilities of the corresponding acid-base adducts involved. However, it is important to note that the realization of a photoswitchable Brønsted base constitutes a formidable task since the proton represents the smallest possible electrophile and precludes strong steric interactions.

To compare the basicities of different switching states of compounds **1b,c**, titration experiments with trifluoromethanesulfonic acid were carried out (Scheme 8). Negligible changes in the absorption spectra of **1b** and **1c** upon protonation precluded a direct determination of the concentrations of the non-protonated and protonated forms, necessary for a direct evaluation of the pK_a-values. However, indirect determination of these concentrations was possible by using Neutral Red **Ind** (3-amino-7-dimethylamino-2-methylphenazin) as a reference base.[38] Neutral red displays distinct differences in the absorption spectra of the neutral and protonated form, having absorption maxima at λ_{max} (**Ind**) = 441 nm and λ_{max} (**Ind**-H^+) = 534 nm in acetonitrile solution.[39] This allows for a convenient determination of the concentration of **Ind** and **Ind**-H^+ by UV vis spectroscopy. The choice of the reference base is crucial, since a too large difference in basicity of catalyst and reference base precludes meaningful measurements. For optimal results, the pK_a of the reference base should not differ more than 2 pK_a units from the pK_a of the base to be measured. Neutral red meets these requirements, having a pK_a of 15.6 for the protonated form in acetonitrile, which is close to the pK_a values expected for substituted piperidines in the same solvent.

---

[m] Basicity and kinetic data of piperidine bases **1a,b** were determined by Maike Peters.[7]

Scheme 8: Equilibrium of *E*/*Z*-**1b,c**, *E*/*Z*-**1b,c**-H$^+$, **Ind**, and **Ind**-H$^+$ observed in titration experiments using trifluoromethanesulfonic acid in acetonitrile.

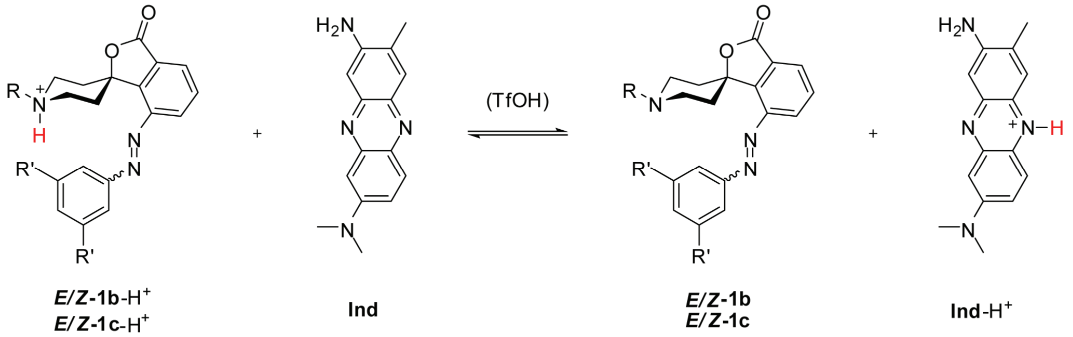

Considering equation 8, the protonation equilibrium given in Scheme 8 can be described as the quotient of the two acid dissociation constants K_a (*E*/*Z*-**1b,c**-H$^+$) and K_a (**Ind**-H$^+$) of the catalyst and Neutral Red, respectively. Rearrangement of equation 8 gives equation 9, which allows to determine the acid dissociation constant of the catalyst and, therefore, the pK_a value, defined as the negative decadal logarithm of K_a (*E*/*Z*-**1b,c**-H$^+$), from known quantities.

$$K = \frac{K_a\,(E/Z\text{-}\mathbf{1b,c}\text{-H}^+)}{K_a\,(\mathbf{Ind}\text{-H}^+)} = \frac{[E/Z\text{-}\mathbf{1b,c}]\,[\mathbf{Ind}\text{-H}^+]}{[E/Z\text{-}\mathbf{1b,c}\text{-H}^+]\,[\mathbf{Ind}]} \tag{8}$$

$$K_a\,(E/Z\text{-}\mathbf{1b,c}\text{-H}^+) = \frac{K_a\,(\mathbf{Ind}\text{-H}^+)\,[E/Z\text{-}\mathbf{1b,c}]\,[\mathbf{Ind}\text{-H}^+]}{[E/Z\text{-}\mathbf{1b,c}\text{-H}^+]\,[\mathbf{Ind}]} \tag{9}$$

Since the photophysical parameters of both forms of Neutral Red are known, the concentration of the protonated form **Ind**-H$^+$ can be determined from equation 10. Taking the known initial concentration of Neutral Red c_0(**Ind**) into account, the equilibrium concentration [**Ind**] is given by equation 11. The use of very strong trifluoromethanesulfonic acid precludes the presence of non-dissociated acid in the system, thereby allowing to determine the equilibrium concentration [*E*/*Z*-**1b,c**-H$^+$] of protonated catalyst (equation 12). Application of the mass balance for the system leads to equation 13 and the equilibrium concentration [*E*/*Z*-**1b,c**] of non-protonated catalyst.

$$\left[\mathbf{Ind}\text{-H}^+\right] = \frac{\mathrm{Abs}_{534\ \mathrm{nm}} - c_0\,(\mathbf{Ind}) \cdot \varepsilon_{534\ \mathrm{nm}}(\mathbf{Ind})}{\varepsilon_{534\ \mathrm{nm}}\,(\mathbf{Ind}\text{-H}^+) - \varepsilon_{534\ \mathrm{nm}}(\mathbf{Ind})} \tag{10}$$

$$\left[\mathbf{Ind}\right] = c_0(\mathbf{Ind}) - \left[\mathbf{Ind}\text{-H}^+\right] \tag{11}$$

$$\left[E/Z\text{-}\mathbf{1b,c}\text{-H}^+\right] = c(\mathrm{TfOH}) - \left[\mathbf{Ind}\text{-H}^+\right] \tag{12}$$

$$\left[E/Z\text{-}\mathbf{1b,c}\right] = c_0(E/Z\text{-}\mathbf{1b,c}) - \left[E/Z\text{-}\mathbf{1b,c}\text{-H}^+\right] \tag{13}$$

For the determination of the pK_a value of *E*/*Z*-**1b**, equimolar amounts of catalyst *E*/*Z*-**1b** and Neutral Red **Ind** were dissolved in acetonitrile and a solution of trifluoromethanesulfonic acid in acetonitrile was added in increments of 0.1 ml. A UV vis spectrum was recorded after each addition, allowing to monitor the formation of protonated Neutral Red **Ind**-H$^+$ (Figure 19). By application of equations 9 - 13, the pK_a value of *E*/*Z*-**1b** was determined (*vide infra*). A similar methodology was used for determination of pK_a values of *E*/*Z*-**1c** (Figure 20).

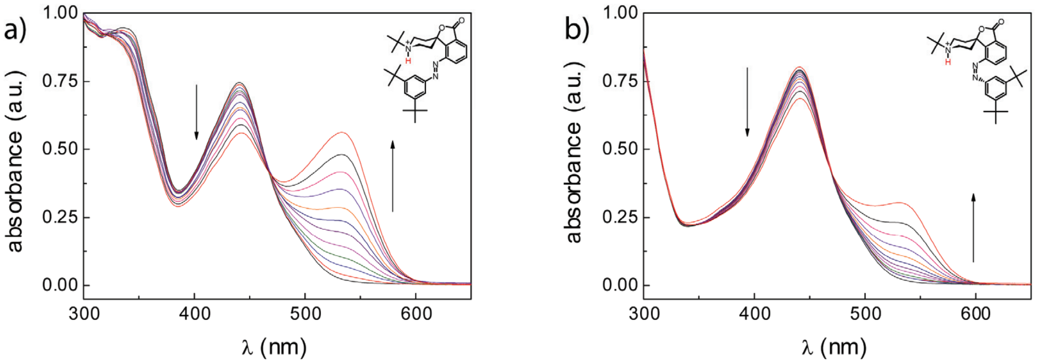

Figure 19: UV/vis titration of a solution of **1b** and neutral red **Ind** as indicator. The formation of the protonated form (**Ind**-H^+) of neutral red was followed upon addition of overall 1.1 mL (0.1 mL increment) of TfOH ($c = 3.15 \cdot 10^{-6}$ M). a) *E*-**1b** and neutral red (c_0 (*E*-**1b**) = c_0 (**Ind**) = $4.1 \cdot 10^{-5}$ M) resulted in a pK_a (*E*-**1b**) = 15.9 ± 0.1 and b) *Z*-**1b** and neutral red (c_0 (*Z*-**1b**) = c_0 (**Ind**) = $4.2 \cdot 10^{-5}$ M) resulted in pK_a (*Z*-**1b**) = 16.7 ± 0.1. *Z*-**1b** was used as mixture stated at the photostationary state (*Z*-**1b** : *E*-**1b** = 9 : 1).

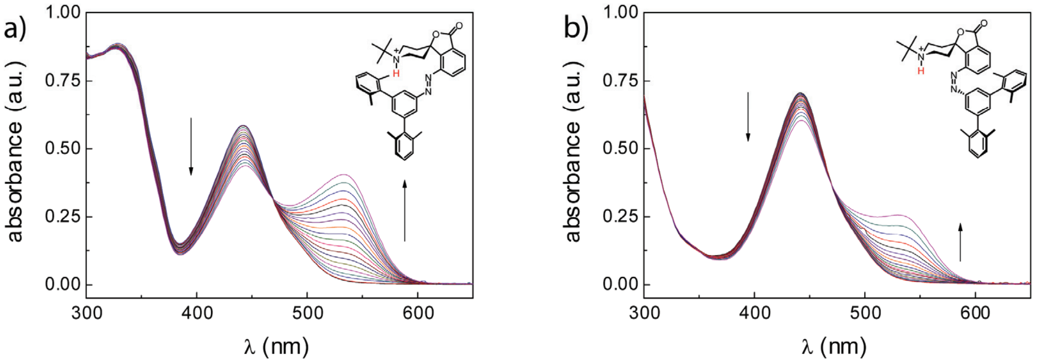

Figure 20: UV/vis titration of a solution of **1c** and neutral red **Ind** as indicator. The formation of the protonated form (**Ind**-H^+) of neutral red was followed upon addition of overall 180 µL (10 µL increment) of TfOH ($c = 5.86 \cdot 10^{-4}$ M). a) *E*-**1c** and neutral red (c_0 (*E*-**1c**) = c_0 (**Ind**) = $3.56 \cdot 10^{-5}$ M) resulted in a pK_a (*E*-**1c**) = 16.0 ± 0.1 and b) *Z*-**1c** and neutral red (c_0 (*Z*-**1c**) = c_0 (**Ind**) = $4.2 \cdot 10^{-5}$ M) resulted in pK_a (*Z*-**1c**) = 16.7 ± 0.1.

Indeed, pK_a-values of both isomers of **1b** differ significantly (Table 3). The basicity of *Z*-**1b** (ON-state) increased by almost one order of magnitude amounting to $pK_a = 15.9$ as compared to $pK_a = 16.7$ for the corresponding *E*-**1b** (OFF-state). For *E*-**1c** and *Z*-**1c** pK_a-values of 16.0 and 16.7, respectively, were found and are essentially identical to those of the respective **1b** analogues, when considering the uncertainty of these measurements of approximately ±0.1 pK_a units.

Protonation has no effect on the isomerization behavior of catalyst **1c**. Neither photochemical $E \rightarrow Z$ and $Z \rightarrow E$ switching, nor thermal $Z \rightarrow E$ reversion at 20 °C and 45 °C are disturbed by protonation, as is evident from the absorption spectra obtained while monitoring the respective process (Figure 21, Figure 22). It is reasonable to assume a similar behavior for the other azobenzene catalyst **1a** and **1b**.

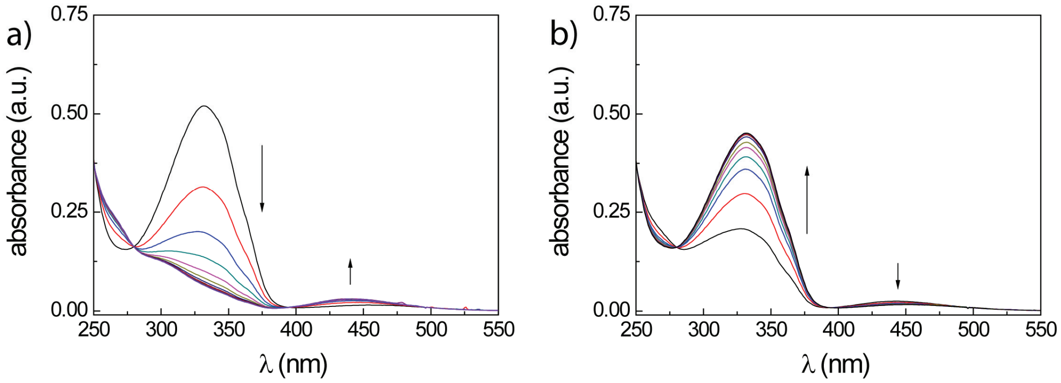

Figure 21: Irradiation of **1c**-H$^+$ ($2.75 \cdot 10^{-5}$ M in CH_3CN, obtained by addition of 1.2 equiv. of trifluoromethansulfonic acid to a solution of **1c** in acetonitrile): a) Isomerization *E*-**1c**-H$^+$ → *Z*-**1c**-H$^+$, (λ_{irr} = 365 nm, 16 min irradiation time); b) Isomerization *Z*-**1c**-H$^+$ → *E*-**1c**-H$^+$ (λ_{irr} > 400 nm, 4 min irradiation time).

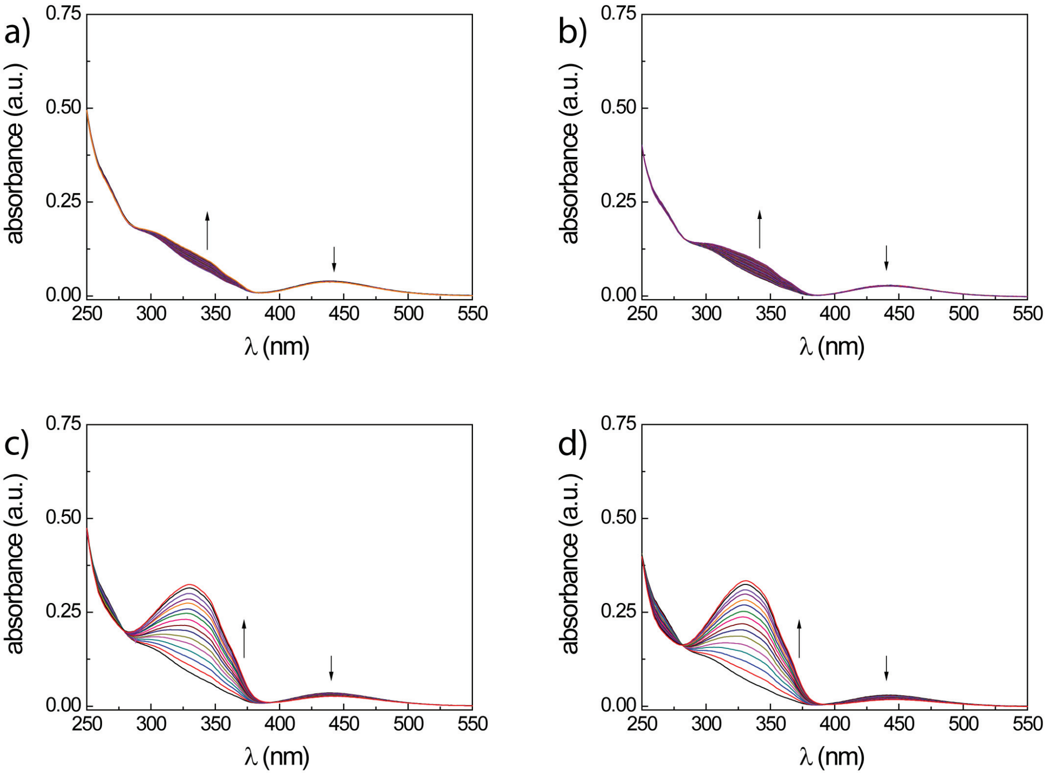

Figure 22: Thermal $Z \rightarrow E$ isomerization: a) 20 °C for 40 h, c(**1c**) = $2.98 \cdot 10^{-5}$ M in CH_3CN, b) 20 °C for 40 h, c(**1c**-H^+) = $2.75 \cdot 10^{-5}$ M in CH_3CN, b) 45 °C for 16 h, c(**1c**) = $2.98 \cdot 10^{-5}$ M in CH_3CN, b) 45 °C for 16 h, c(**1c**-H^+) = $2.75 \cdot 10^{-5}$ M in CH_3CN. Protonated samples were obtained by addition of 1.2 equiv. of trifluoromethansulfonic acid to a solution of **1c** in acetonitrile.

Table 3: Basicities of catalysts **1b** and **1c**.

	basicities		
	pK_a(OFF)[a]	**pK_a(ON)**[b]	**ΔpK_a**[c]
1b	15.9	16.7	0.8
1c	16.0	16.7	0.7

[a] pK_a-value of the E isomer representing the OFF-state. [b] pK_a-value of the photostationary state mixture representing the ON-state. [c] Difference of pK_a-values, i.e. pK_a(PSS) – pK_a(E).

3.5.2 General Base Catalysis

Reactivity differences associated with both switching states of compounds **1a-c** as well as **2** could be exploited to photocontrol the conversion in a general base catalyzed reaction. For this purpose, the nitroaldol reaction, commonly referred to as Henry reaction,[40] of nitroethane with 4-nitrobenzaldehyde was investigated as model reaction (Scheme 9) due to its low background rate in the absence of base catalyst. Using excess of the nitroethane substrate to ensure pseudo-first order kinetics, the build-up of *syn*- and *anti*-aldol products in the presence of 10 mol% of catalyst in [D_8]THF solution was monitored by ^{1}H-NMR spectroscopy. Exemplary NMR spectra taken form reaction mixtures containing *E*-**1c** and *Z*-**1c** are shown in Figure 23 and Figure 24, respectively. It is clearly evident from the build-up of product signals, that the *E* isomer corresponds to the OFF-state, whereas the *Z* isomer is much more reactive and therefore corresponds to the ON-state, as intended by the design of photoswitchable catalysts **1a-c**.

Scheme 9: Nitroaldol reaction of 4-nitrobenzaldehyde and nitroethane (Henry-reaction).

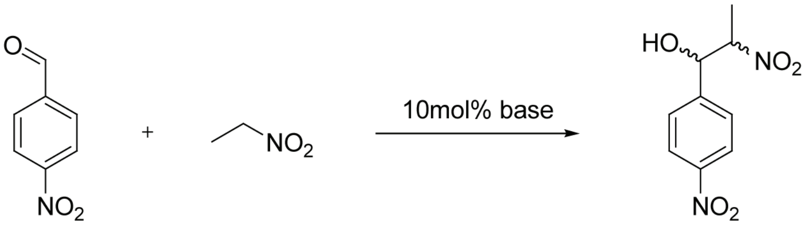

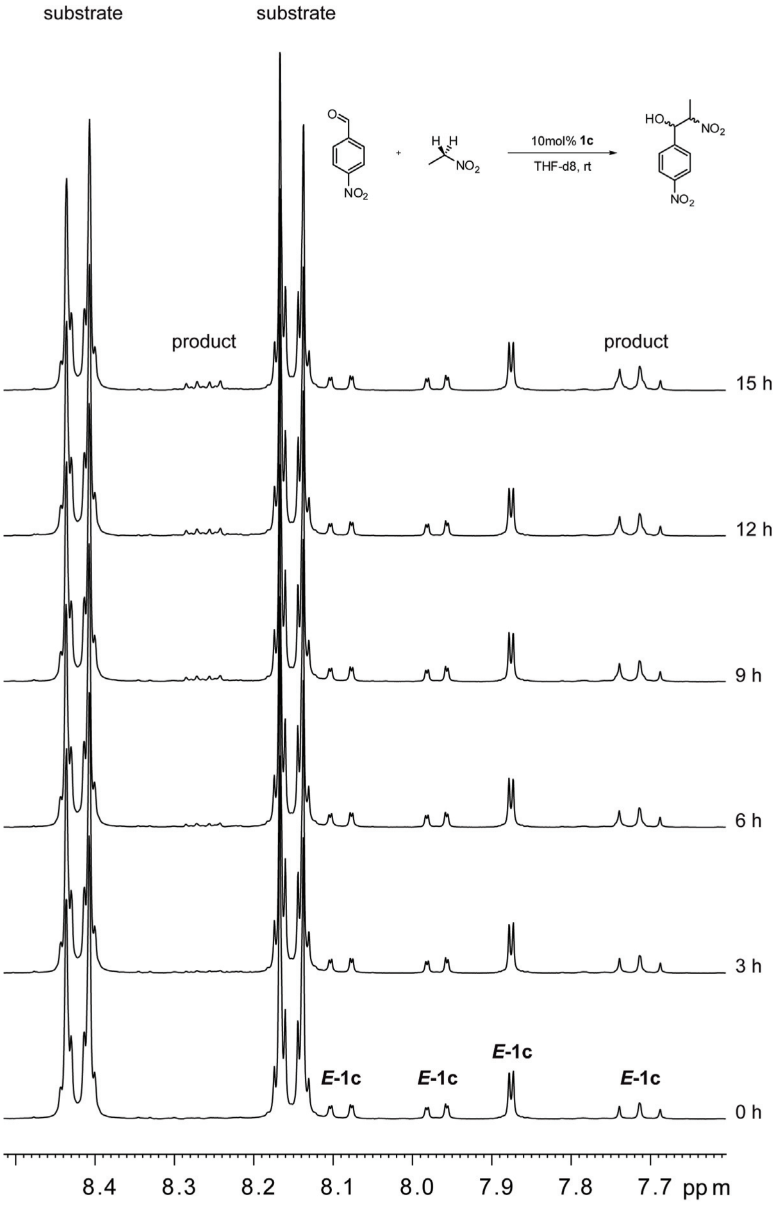

Figure 23: Monitoring of the Henry reaction of 1 equiv. of 4-nitrobenzaldehyde with 12 equiv. of nitroethane in the presence of 10 mol% *E*-**1c** by ^{1}H-NMR spectroscopy.

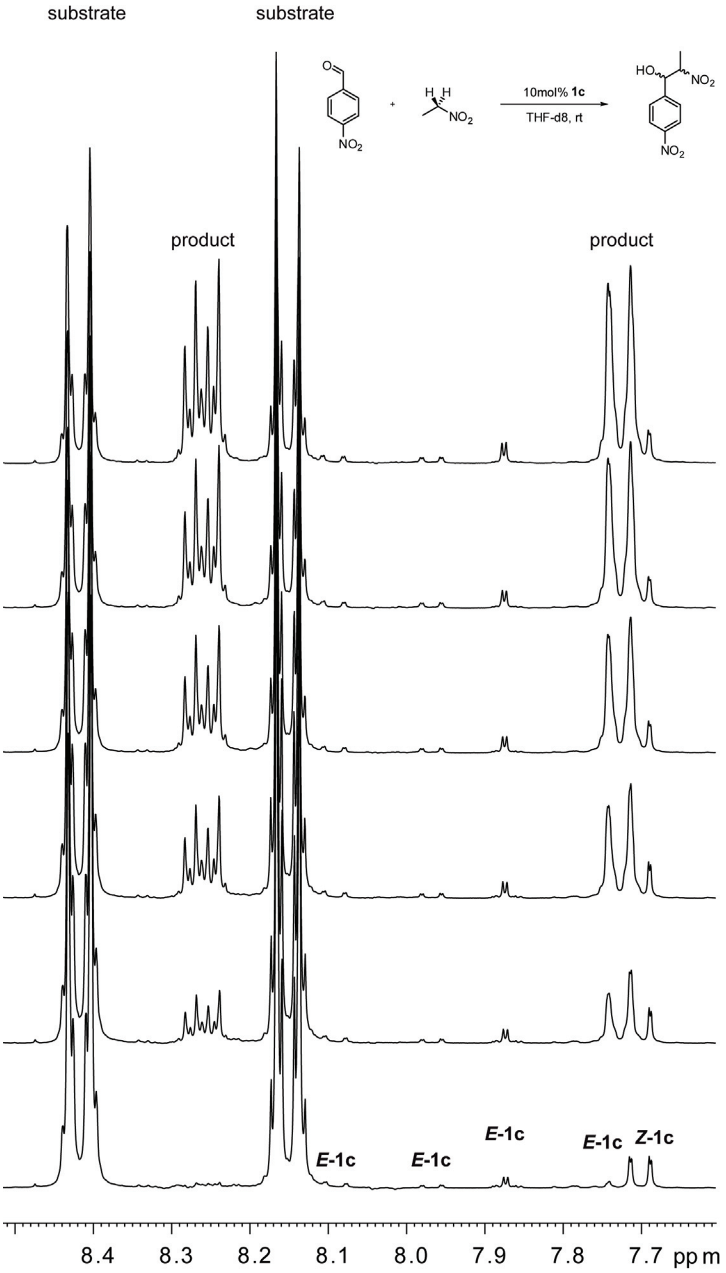

Figure 24: Monitoring of the Henry reaction of 1 equiv. of 4-nitrobenzaldehyde with 12 equiv. of nitroethane in the presence of 10 mol% *Z*-**1c** : *E*-**1c** (9 : 1) by ^{1}H-NMR spectroscopy.

Plots of product concentration derived from the NMR-spectra versus time revealed a similar behavior for the other catalysts **1a,b** and **2** as found for catalyst **1c**, that is the *Z* isomers are more reactive than the shielded *E* isomers (Figure 25-28). However, distinct differences in the relative reactivities become apparent and will be discussed below.

Assuming pseudo-first order kinetics, rate constants can be derived from the slope of plots of ln([product]) versus time. For comparison of the reactivity associated with the two switching states of a catalyst, k_{rel} was defined as the ratio of rate constants for use of either pure *Z* or pure *E* isomer, that is $k_{rel} = k_{ON} / k_{OFF}$ (Table 4). The rate constant for use of the pure *Z* isomer is not directly accessible by kinetic measurements, since the *Z* isomer can only be obtained as a mixture containing residual *E* isomer representing the photostationary state and thermal reversion to the thermodynamically more stable *E* isomer starts to contribute after prolonged reaction times. Therefore, initial kinetic data were corrected for reactivity attributed to residual *E* isomer and for thermal reversion of *Z* isomer to *E* isomer.

Table 4: Rate constants of the Henry reaction obtained for catalysts **1a-c** and **2**.

	Henry reaction				
	PSS[a] (*Z*/*E*)	k_{OFF}[b] [10^{-6} s^{-1}]	k_{obs}[c] [10^{-6} s^{-1}]	k_{ON}[d] [10^{-6} s^{-1}]	k_{rel} (k_{ON}/k_{OFF})
1a	80:20	4.96	15.0	21.5	4.3
1b	90:10	0.963	8.87	12.7	13.2
1c	90:10	0.391	10.6	13.9	35.5
2	93:7	12.9	-	25.4	2.0

[a] Photostationary state obtained by preparative irradiations at λ = 365 nm. [b] Rate constant of Henry reaction using pure *E* isomer. [c] Rate constant of Henry reaction using the photostationary state mixture obtained by preparative irradiations at λ = 365 nm. [d] Rate constant of Henry reaction extrapolated to 100% *Z* isomer.

Reactivity originating from the much less basic azochromophore could be ruled out by a control experiment using azobenzene itself as catalyst leading to no acceleration of product formation (Figure 25-28). The catalysts employed in the kinetic experiments were used in their isolated form, i.e. the *E* isomer was used in its pure form while the *Z* isomer was used as the photostationary state mixture containing minor amounts of residual *E* isomer. Note that the higher concentration used in preparative irradiation experiments increased the absorbance of the solution such that usually even after prolonged irradiation times the photostationary state mixtures contained a larger amount of *E* isomer as compared to irradiating analytical samples of much lower concentration. For these reasons, the conditions necessary to accurately determine the kinetics, i.e. the rather high catalyst concentrations employed in the NMR experiments, precluded switching of the catalysts *in situ*. However, this does only constitute a drawback in bulk or solution phase homogeneous catalysis associated with high optical densities – a drawback that photochemistry suffers from in general – yet an application utilizing mono- or multilayers of immobilized catalysts should be feasible (*vide infra*).

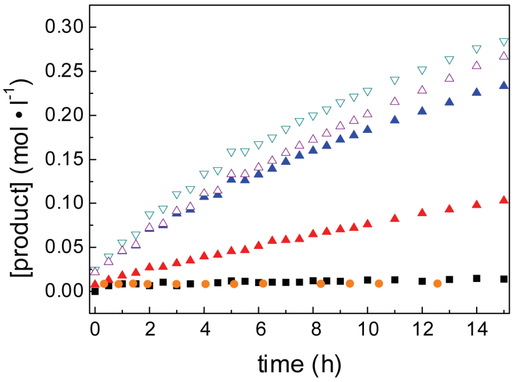

	catalyst (10mol%)	k [10^{-5} s^{-1}]	k$_{rel}$
▽	extrapol. 100% ***Z*-1a**	2.2	4.4
△	thermal corr. PSS	1.8	3.6
▲	PSS ***Z*-1a : *E*-1a = 8 : 2**	1.5	3.0
▲	***E*-1a**	0.50	1
●	*E*-azobenzene	0.0024	0.0048
■	no catalyst	0.039	0.078

Figure 25: Catalytic performance of **1a** in the Henry reaction calculated from product concentrations determined from NMR measurements (▲: *E*-**1c**, ▲: PSS: *Z*-**1a** : *E*-**1a** = 80 : 20, △: PSS with thermal correction for *Z* → *E* isomerization, ▽: extrapolation to 100% *Z*-**1a**, ■: no catalyst, ●: *E*-azobenzene).

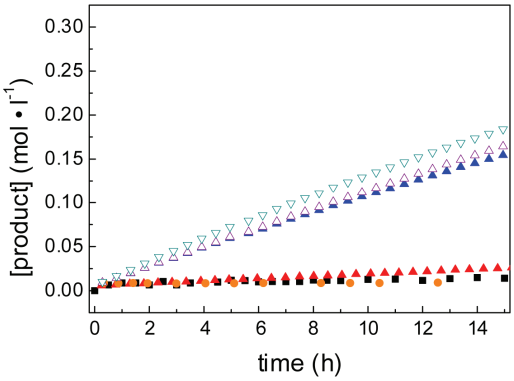

	catalyst (10mol%)	k [10^{-5} s^{-1}]	k$_{rel}$
▽	extrapol. 100% ***Z*-1b**	1.3	13.5
△	thermal corr. PSS	1.0	10.4
▲	PSS ***Z*-1b : *E*-1b = 9 : 1**	0.89	9.3
▲	***E*-1b**	0.096	1
●	*E*-azobenzene	0.0024	0.025
■	no catalyst	0.039	0.41

Figure 26: Catalytic performance of **1b** in the Henry reaction calculated from product concentrations determined from NMR measurements (▲: *E*-**1b**, ▲: PSS: *Z*-**1b** : *E*-**1b** = 90 : 10, △: PSS with thermal correction for *Z* → *E* isomerization, ▽: extrapolation to 100% *Z*-**1b**, ■: no catalyst, ●: *E*-azobenzene).

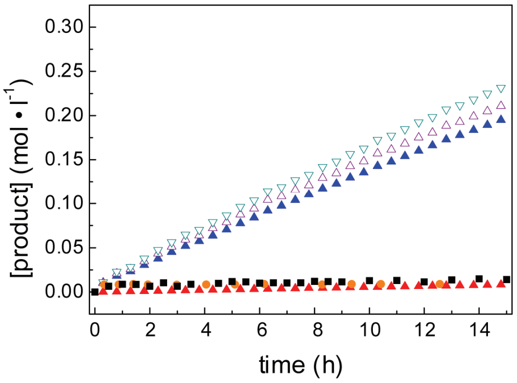

catalyst (10mol%)	k [10^{-5} s^{-1}]	k$_{rel}$
▽ extrapol. 100% ***Z*-1c**	1.4	35.9
△ thermal corr. PSS	1.2	30.8
▲ PSS ***Z*-1c : *E*-1c = 9 : 1**	1.1	28.2
▲ ***E*-1c**	0.039	1
● *E*-azobenzene	0.0024	0.062
■ no catalyst	0.039	1.0

Figure 27: Catalytic performance of **1c** in the Henry reaction calculated from product concentrations determined from NMR measurements (▲: *E*-**1c**, ▲: PSS: *Z*-**1c** : *E*-**1c** = 90 : 10, △: PSS with thermal correction for *Z* → *E* isomerization, ▽: extrapolation to 100% *Z*-**1c**, ■: no catalyst, ●: *E*-azobenzene).

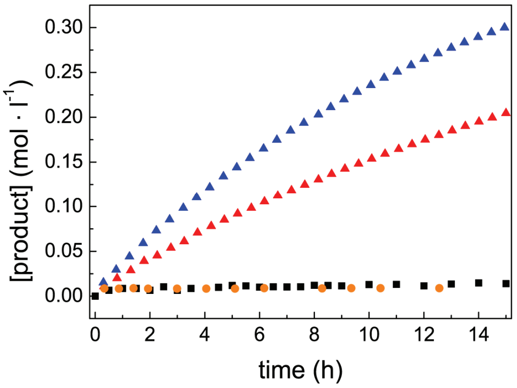

catalyst (10mol%)	k [10^{-5} s^{-1}]	k$_{rel}$
▲ PSS (***Z*-2 : *E*-2 = 9.4 : 0.6**)	1.1	28.2
▲ ***E*-2**	0.039	1
● *E*-azobenzene	0.0024	0.062
■ no catalyst	0.039	1.0

Figure 28: Catalytic performance of **2** in the Henry reaction calculated from product concentrations determined from NMR measurements (▲: *E*-**2**, ▲: PSS: *Z*-**2** : *E*-**2** = 94 : 6, ■: no catalyst, ●: *E*-azobenzene).

In all cases, use of the reactive *Z* isomer of catalysts **1a-c** as well as **2** led to a rate enhancement as compared to the use of *E* isomer (Table 3). Catalyst **1a** displayed only a moderate difference in activity between its ON- and OFF-state, resulting in a relatively small value of k$_{rel}$ = 4.3. It is evident from the kinetic data that use of the *E* isomer led to some residual activity not desirable for the OFF-state of a switchable catalyst. Most likely, the *E* isomer's reactivity originates from deprotonation of the nitroalkane, pointing to unwanted accessibility of the basic piperidine lone pair. Three pathways can be considered for the deprotonation of the nitroalkane by the catalyst's OFF-state: (1) inversion of the piperidine N-atom placing the lone pair in an equatorial position (i-**1a-c**), (2) chair flip leading to piperidine conformations with the basic lone pair in non-shielded equatorial or axial positions (f_{eq}-**1a-c** or f_{ax}-**1a-c**), and (3) a rotation of the blocking group allowing the nitroalkane to be deprotonated by the piperidine's most stable (chair) conformation with the lone pair in axial position. On the basis of computational and NMR studies (*vide supra*) the chair flip can be ruled out for catalysts **1a-c**. However, inversion of the nitrogen atom and/or rotation of the blocking group could in principle be responsible for residual catalytic activity of the OFF-state *E*-**1a** (Table 1).

In order to suppress *N*-inversion, the methyl group R was replaced with a more demanding *tert*-butyl group, known to act as an efficient conformational anchor for six-membered rings.[6] Indeed, N-inversion of the *E* isomer of catalyst **1b** could be ruled out by NMR spectroscopy as well as DFT calculations, which estimate a significant destabilization of i-**1b** over i-**1a** (Table 1). This leads to a roughly 200-fold decrease in population of the N-inverted isomer of catalyst **1b**, correlating with a significantly diminished residual activity, as compared to catalyst **1a**. In addition, the kinetic stability of i-**1b** is decreased due to the lowering of the N-inversion barrier as compared to i-**1a** (Table 1). Not unexpectedly, flipping of the piperidine chair is even more unlikely for **1b**. Investigation of the catalytic activity of catalyst **1b** in its ON- and OFF-state under identical conditions as used for **1a** revealed a significant improvement of the ON/OFF-ratio, reaching a value of k_{rel} = 13.2, corresponding to a reactivity difference of both switching states exceeding one order of magnitude (Table 3). The enhanced reactivity difference mainly originates from the pronounced decrease of the OFF-state's activity overcompensating the slightly reduced reactivity of the ON-state, which was attributed to the steric demand of the *tert*-butyl group in *Z*-**1b,** hindering the nitroalkane to approach the basic catalyst site.

Assuming the reactivity of *Z*-**1b** to be the maximum intrinsic reactivity of a *N*-*tert*-butyl substituted piperidine, the catalyst's ON/OFF-ratio can only be improved by further lowering the reactivity of the OFF-state. This could be realized by improving the efficiency of blocking, provided by the azobenzene shield. Inspection of models of *E*-**1b** as well as **1b**-TSrot, obtained from DFT calculation, led to the initial conclusion that a twist of the blocking group around the C-N bond leads to a less shielded *E* isomer, potentially causing some residual reactivity. To address this problem, the R’ substituents of the blocking group responsible for shielding were increased in size, i.e. from *tert*-butyl (**1b**) to 2,6-dimethylphenyl (**1c**), taking advantage of the modular synthetic route (Scheme 1). Indeed, no rate acceleration was observed by using the catalyst’s OFF-state *E*-**1c** as compared to the non-catalyzed reaction, while the reactivity of the ON-state *Z*-**1c** remained practically not affected. Both effects lead to an increased overall ON/OFF-ratio $k_{rel} = 35.5$.

It is interesting to note, that according to DFT calculations N-inversion of **1c** is energetically more favorable than inversion of **1b** indicated by a decrease of the relative free enthalpy of the inverted isomers from 7.1 kcal/mol to 5.4 kcal/mol on going from **1b** to **1c** in the gas phase.[n] Obviously, the reactivities of the OFF-states cannot simply be explained by differences in populating the N-inverted conformers i-**1** and show that additional effects have to be taken into account. In order to address this rather complicated issue in more detail, the proton affinities (PAs) of the bases **1a-c** were investigated by computational methods. Representative calculated protonation energies and enthalpies are summarized in Table 5. Noting that the trends of the protonation energies in the gas phase are comparable for the two basis sets employed (compare ΔE/6-31G* and ΔE/cc-pVTZ values), a discussion primarily based on the PAs obtained with the lower basis set seems appropriate. The latter are defined as the negative enthalpies of protonation of the free bases, i.e. the absolute value of the ΔH/6-31G* values of the protonated species in Table 5.

Table 5: Relative energies Δ*E* and enthalpies Δ*H* obtained at selected levels for key isomers of **1a-c** (with respect to the global minimum, *E*-**1**), as well as energies and enthalpies of protonation (relative to the respective minima *E*-**1**, *Z*-**1**, i-**1**).[a]

	Δ*E* 6-31G*	**Δ*H* (-PA)**[b] 6-31G*	**Δ*E*** cc-pVTZ	**Δ*E*** cc-pVTZ PCM(THF)[c]	**Δ*E*** cc-pVTZ PCM(MeCN)[d]
Z-**1a**	15.8	15.2	15.5	13.7	13.3
i-**1a**	3.8	3.8	4.4	4.0	3.9
E-**1a**-H$^+$	-244.1	-234.5	-242.4	-276.0	-280.9
Z-**1a**-H$^+$	-245.5	-235.6	-243.6	-281.8	-287.7
i-**1a**-H$^+$	-245.1	-236.1	-243.8	-282.5	-288.4
Z-**1b**	15.4	15.2	15.0	13.6	13.2
i-**1b**	6.0	5.8	6.3	5.9	5.8
E-**1b**-H$^+$	-250.5	-241.7	-248.5	-278.3	-282.8
Z-**1b**-H$^+$	-251.7	-242.3	-249.5	-281.3	-286.5
i-**1b**-H$^+$	-250.0	-240.3	-248.4	-282.5	-288.0
Z-**1c**	15.3	15.0	15.2	14.0	13.5
i-**1c**	5.5	5.4	6.0	5.9	5.8
E-**1c**-H$^+$	-252.0	-242.4	-249.6	-278.9	-283.3
Z-**1c**-H$^+$	-251.0	-241.5	-248.9	-281.2	-286.9
i-**1c**-H$^+$	-250.6	-240.8	-249.1	-282.6	-287.7

[a]In kcal/mol, employing the B3LYP functional and B3LYP/6-31G* optimized geometries. [b]Negative PA for the protonated species (298.15 K, 1 atm). [c]Continuum model employing the parameters of THF. [d]Continuum model employing the parameters of acetonitrile

---

[n] At the B3LYP/cc-pVTZ/PCM(acetonitrile) level, the relative energies of i-**1a**, i-**1b**, and i-**1c** are 3.9, 7.1, and 5.8 kcal/mol, respectively, i.e. quite similar to the gas-phase ΔE values in Table 5.

PAs of the global minimum conformation show a constant increase with increasing steric demand of the molecule on going from **1a** to **1c**. While the PA increases strongly on going from **1a** to **1b**, the difference between **1b** and **1c** is small, in line with the respective substitution at the piperidine nitrogen atom. Isomerization of the double bond leads to an increase of the PAs of **1a** and **1b** by 1.1 kcal/mol and 0.6 kcal/mol, respectively, whereas that of **1c** decreases by 0.9 kcal/mol upon $E \rightarrow Z$ isomerization. As the latter result cannot easily be rationalized on steric grounds alone, a potential explanation involves "internal solvation" of the protonated nitrogen center by the proximal R' groups of the blocking group, which in the case of E-**1c**-H^+ is somewhat more efficient due to a stabilizing interaction with the aromatic ring (Figure 29).[41] Upon solvation (modeled by a simple polarizable continuum), protonation of the *Z* isomers becomes much more favorable than that of the corresponding *E* isomers. Clearly, the protonated nitrogen center bearing the charge is more exposed to the solvent (or the continuum) in Z-**1**-H^+, increasing their stabilization by favorable interactions with the solvent. This computed increase in basicity of *Z* vs. *E* isomers is in qualitative agreement with the experimental pK_a measurements discussed above, where both **1b** and **1c** show an increase in pK_a upon $E \rightarrow Z$ isomerization (Table 3). Quantitatively, this increase in basicity is significantly overestimated by the DFT/PCM calculations for acetonitrile as the computed differences in protonation energies are on the order of -4 kcal/mol (e.g. from -282.8 to -286.5 kcal/mol for **1b** in Table 5), which would translate into changes by several pK_a units. Evidently, the continuum solvation model is too simplistic and specific interactions with the solvent (or its dynamics) would have to be taken into account for a better quantitative accuracy.

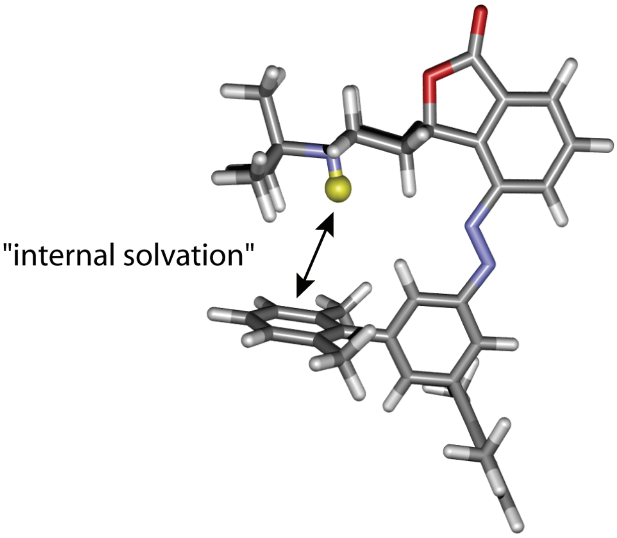

Figure 29: Schematic representation of the proposed effect of “internal solvation” in *E*-**1c**-H$^+$ (acidic proton is marked in yellow).

When assessing the PAs of the N-inverted isomers, it is assumed that protonation equilibria are fast relative to N-inversion. Although N-inversion is so rapid that practically only equilibria involving the global minima *E*-**1** would be observable, the question of the inherent basicity of i-**1** is of interest in the context of catalysis, as the more reactive species – even when present in small amounts – might constitute the more potent catalysts. In the gas phase, i-**1a** is indicated to be a stronger base than *E*-**1a**, whereas the opposite is found for i-**1b,c**. Steric reasons are likely to be responsible for this result, because the repulsion between the R and R' groups is so strong in i-**1b,c** that the amine nitrogen atom is significantly planarized, i.e. the angle sum at N amounts to 352° in both cases. When going from i-**1a** (angle sum of 339°) to i-**1b,c**, the s-character of the nitrogen lone pair and hence its basicity are decreased. In the polar continuum, this effect is overcompensated by the better stabilization of the i-**1**-H$^+$ isomers with their solvent-accessible cationic NH centers, and all i-**1** forms are computed to be stronger bases than their *E*-**1** counterparts.[o]

To summarize this part, the higher basicity of the inverted isomer of **1a** might account to some extent for the significant reactivity of the OFF-state, since a thermal population of the N-inverted isomer is possible. Even if the population of i-**1a** is small (at 298 K, a relative free energy of 4 kcal/mol would correspond to 0.1% in an equilibrium mixture), its contribution to the overall catalytic turnover would be noticeable because of the expected enhanced reactivity. Freezing the N-inversion by incorporation of the *tert*-butyl group lowers the population of the *N*-inverted isomers of **1b** and **1c** even more, thus strongly reducing their potential contribution to the residual activity. This interpretation is consistent with the experimental results, provided the relative reactivities reflect the respective thermodynamic driving forces (for a discussion of possible kinetic effects see below). By comparing catalysts **1b** and **1c**, it is evident that no further improvement of the activity ratio k_{rel} seems possible for the particular system under investigation. As mentioned, the reactivity of *Z*-**1b** and *Z*-**1c** represents the intrinsic reactivity of a *N*-*tert*-butyl substituted piperidine incorporated into the catalysts framework towards nitroethane, leaving no room for further improvement since a greater extent of deshielding is not possible. The lower limit of reactivity is given by *E*-**1c** displaying a reactivity not distinguishable from the reaction's background reactivity.

---

[o] For i-**1a**, this stabilization is predicted to be so strong that the protonated inverted isomer i-**1a**H$^+$ is even more stable than *E*-**1a**H$^+$. This particular result should be taken with care in light of the performance of the continuum model for predicting the basicities of *Z* vs. *E* isomers (*vide supra*). However, the qualitative finding that the N-inverted isomers i-**1** are more basic than their more stable chair conformers *E*-**1** forms should be reliable.

Since slow thermal reversion of the *Z* isomers of catalysts **1a-c** leads to unwanted catalyst deactivation upon prolonged reaction times, stilbene based catalyst **2** was devised to suppress thermal $Z \rightarrow E$ isomerization. Comparison of DFT-optimized structures of azobenzene-based catalysts *E*-**1a** and *E*-**2** reveals interesting differences (Figure 30). On going from the azobenzene to the stilbene, the elongation of the X=X distance and the opening of the X=X-C angle (115° and 126° for X = N and C, respectively) strongly increases the separation between the amine N-atom and the *tert*-butyl substituent of the blocking group, and is expected to lead to less efficient shielding and a higher reactivity of the *E* isomer. This was confirmed experimentally, observing a 2.6 times higher reactivity for *E*-**2** as compared to *E*-**1a** under otherwise identical conditions. Switching stilbene **2** to its corresponding *Z* isomer only moderately accelerated the rate of the reaction, i.e. $k_{rel} = 2$. In addition to this low ON/OFF-ratio the applicability of stilbene **2** as a photoswitchable catalyst is further narrowed by the inefficient photochemical $Z \rightarrow E$ isomerization (*vide supra*).

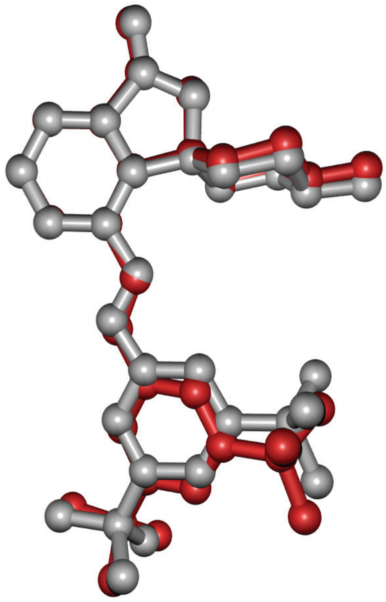

Figure 30: Overlay of DFT-optimized structures of catalysts **1a** and **2** (**1a** is shown in gray, **2** is shown in red, structures were optimized on the B3LYP/6-31G* level of theory).

In their OFF-state, catalysts **1b** and **1c** display a distinct difference in reactivity in the Henry reaction, even though they have almost equal basicities in acetonitrile. This observation suggests that under catalytic turnover, dictated by the kinetics of the rate-limiting step, the reaction barriers are influenced by other factors in addition to those solely grounded on thermodynamic driving forces for substrate deprotonation. The rate-determining step in the general-base catalyzed Henry reaction is the deprotonation of the nitroalkane by the amine base. The conformational flexibility of the systems under scrutiny as well as the need to properly account for solvation effects during the concomitant charge separation make a computational search for the relevant transition states for deprotonation very involved.[p] As a first step, representative adducts formed from *E*-**1a-c** and the simplest nitroalkane, nitromethane, which are likely to be involved in the early stages of deprotonation, were located (Figure 31). The raw nitromethane-complexation energies, uncorrected for zero-point energies and basis-set superposition error, are -4.0, -3.1, and -2.4 kcal/mol for **1a**, **1b**, and **1c**, respectively. As can be seen in the optimized structures in Figure 31, the blocking group has to rotate significantly about the C-N bond in order to allow coordination of the nitromethane to the lone pair. For a more quantitative analysis, the energies required to distort the free bases from their conformations in the fully optimized global minima to those in the nitromethane complexes were evaluated. These energies should be a good indication of the kinetic hindrance imposed by the substituents R and R' during the deprotonation step and amount to 1.4, 2.3, and 3.6 kcal/mol for **1a**, **1b**, and **1c**, respectively. These data are in very good qualitative agreement with the experimentally observed reactivity trend for the OFF-states of **1a-c**. The rather low energetic "penalty" for coordination of the nitroalkane to *E*-**1a** is noteworthy, as it implies that a substantial part of the residual activity of **1a** in its OFF-state is in fact due to the global *E* minimum itself, in addition to the part that may arise from traces of the N-inverted isomer (*vide supra*). Even though it is beyond the theoretical methods presently available to relate these rather modest changes in the energetics quantitatively to specific rate constants, the overall qualitative agreement between theory and experiment provides a solid basis for the interpretation of the observations given above.

---

[p] In a recent B3LYP study of the Henry reaction catalyzed by a Cinchona alkaloid, a barrier of 10.8 kcal/mol for deprotonation of nitromethane has been computed in a THF continuum.[42]

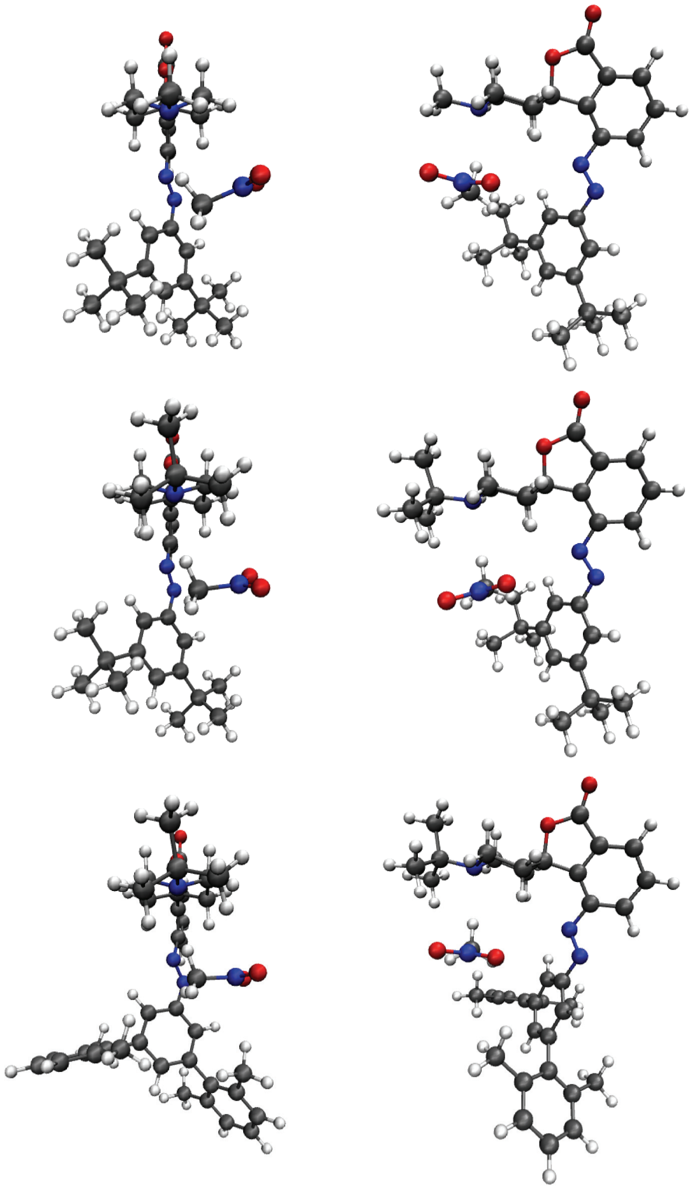

Figure 31: Adducts between nitromethane and *E*-**1a-c** illustrating the degree of twisting of the aromatic blocker group (left: front view along the N-R axis, right: side view; B3LYP/6-31G*optimized).

In the general context of comparing the competing reactivities of an equilibrating mixture of conformers, a scenario in which the activation barriers for interconverting the participating conformers, i.e. *E*-**1**, i-**1**, f_{ax}-**1**, and f_{eq}-**1**, are comparable to the activation barriers for proton abstraction from a nitroalkane is most likely valid.[42] For this reason, the simplest case of the reactivity schemes developed by Winstein and Holness on the basis of kinetic observations as well as Curtin and Hammett on the basis of product distributions,[6,43] probably does not apply and the system would be more appropriately described by the general treatment given by Seeman and Farone.[44]

3.6 Immobilization

3.6.1 Motivation and Strategy

Photoswitching of basicity by implementation of photochromic bases **1a-c** is described in section 3.5.1. Basicity differences were successfully translated into activity differences of general base catalysts **1a-c**, as exemplified by photoregulation of the conversion of the Henry model reaction (section 3.5.2). These experiments were performed in homogenous solution, consequently leading to general reactivity differences throughout the entire system. However, to exploit the advantages of light as an external stimulus offering superb spatial and temporal control over the energy input required for photoswitching, it is mandatory to prevent dissipation of the incident information by means of diffusion to other loci or compartments of the system/reactor. Efficient suppression of diffusion is achieved by covalently linking the base to a solid substrate, putting sophisticated applications in the fields of surface patterning or sensor technologies within reach.

Besides giving the switching process a spatially addressable component, immobilization of catalysts **1a-c** is anticipated to significantly improve catalyst handling. Most importantly, a drastic improvement of the switching performance is expected upon confining the photochromic bases to a surface, since problems encountered with photoswitching in solution under catalytic turnover conditions attributed to the employed concentrations and therefore high optical densities are overcome in single- or multilayer arrangements. In light of possible surface patterning tasks, the low loading on surfaces in comparison to loadings encountered in bulk or solution phase catalysis does not pose a drawback, since effective catalyst concentrations in vicinity to the surface are high and reactions should necessarily be confined to the substrate.

Numerous strategies for immobilization on all kinds of substrate have been devised (Figure 32). In principal, two different approaches can be distinguished: (a) surface-tethering by covalent bonds and (b) surface-tethering by non-covalent interactions. Utilization of non-covalent interactions allows assembly of largely defect-free monolayers, provided suitable adsorbents and substrates are chosen, since the assembly process follows the path to the global thermodynamic minimum. Typical forces, driving the system to the energy minimum, are π,π-interaction between the basal plane of high-oriented pyrolytic graphite (HOPG) and various aromatic molecules[45] as well as van-der-Waals interactions between the HOPG surface and aliphatic organic molecules (path *A* in Figure 32, exemplarily shown for HBC on HOPG), [46] or ionic interactions between oxide surfaces and carboxylates (path *B* in Figure 32).[47] The absence of covalent interactions limits the stability of the monolayers, that is the adsorbed molecules are easily washed away with an excess of solvent. Monolayers of high stability are obtained by covalently linking adsorbate and substrate, as for example encountered in numerous examples of thiol-monolayers on gold surfaces (path *C* in Figure 32).[47] However, this approach is limited to the application on gold single-crystal surfaces and was therefore rejected for the immobilization of photoswitchable bases **1a-c**. Numerous strategies for immobilization on silicon or silicon-oxide substrates have been developed and intensively utilized for the generation of functional surfaces. For examples, H-terminated silicon can be functionalized by chemically, thermally, or photochemically induced radical chemistry (path *D* in Figure 32).[48] This approach is again limited to precisely cut surfaces of silicon single crystals and the surface chemistry is very sensitive to impurities. Functionalization of silicon oxide substrates is much less sensitive to impurities and offers the unique advantage to immobilize on an optically transparent (and insulating) material, considerably facilitating characterization of the monolayers obtained. The scope is further broadened by the possibility to substitute the silicon oxide substrate with silicon wafers, which carry surface hydroxyl functions, if no special treatment was used to remove them. A variety of strategies for immobilization on silicon oxide substrates haven been developed and only selected examples shall be discussed here.[47] Monochlorosilanes react with hydroxyl groups on silicon oxide surfaces, allowing to obtain homogenous monolayers carrying a large variety of functional groups (path *E* in Figure 32). Easy access to monochlorosilanes is provided by hydrosilylation of C=C double bonds with chlorodimethylsilane. Alternatively, immobilization can be achieved by reaction of freshly oxidized silicon oxide surfaces with trialkoxy silanes (path *F* in Figure 32). Careful control of reaction conditions is required to avoid formation of inhomogeneous layers due to partial condensation of the precursors in solution. This approach is usually limited to the immobilization of simple derivatives of trialkoxy silanes, due to their low stability towards hydrolysis. However, the robust nature of the monolayers allows for convenient post-functionalization by standard solution phases techniques, exemplified by surface tethering of alkenes utilizing the thiol-ene reaction (pathway *G* in Figure 32).[49] The high tolerance towards functional groups designates pathways *E*, *F*, and *G* as ideal immobilization strategies for the immobilization of photoswitchable bases **1a-c**. Since catalyst **1c** exhibited the best performance in solution, it was chosen as the primarily target for surface tethering.

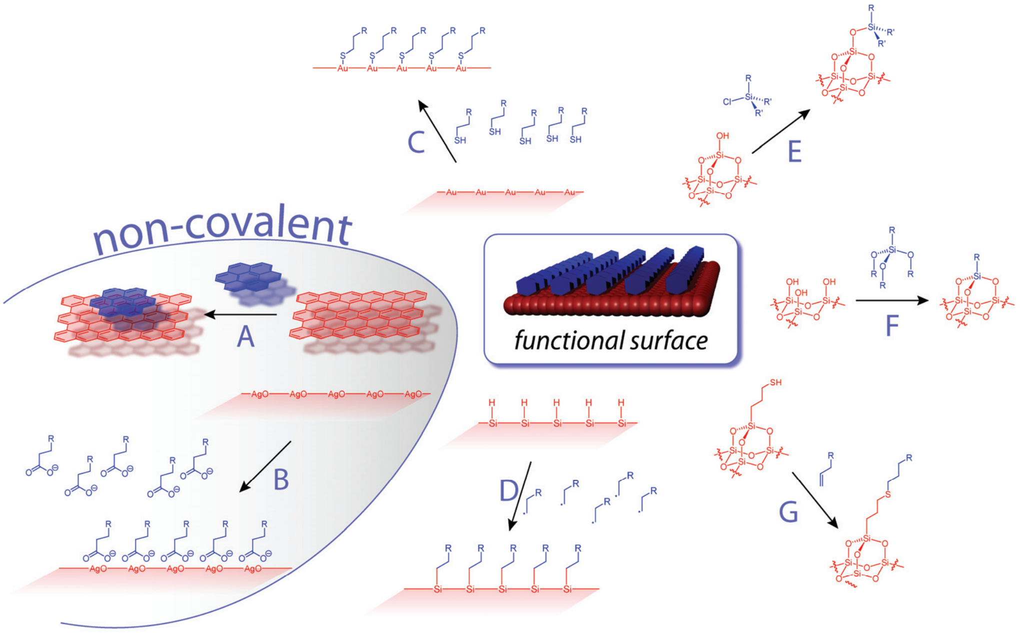

Figure 32: Summary of immobilization strategies on various substrates (red: substrate; blue: adsorbate; see text for details).

In general, immobilization of functional units such as organocatalysts requires an anchoring group, suitable for surface tethering, and a linker, necessary to provide a certain mobility to the catalyst to avoid unwanted deactivation by too close contact to the substrate.[50] The site of attachment of the linker to the catalyst is crucial, as it might negatively (or positively) interfere with the catalytic performance. Generally, a site far remote from the active center is expected to lead to minor influence of the linker on the catalyst's performance.

Initial attempts to replace the lactone-moiety with a lactame-moiety and to exploit the trivalency of nitrogen for attaching the linker failed due to synthetic problems (Scheme 10a). Alternative fixation of the linker in the 4-position of the blocker group failed as well. The Grignard-intermediate could not be quenched with undecenyl-bromide, although alkylation with allyl bromide was successful (Scheme 10b). However, the allyl-linker is presumably to short for efficient immobilization, therefore this approach was abandoned as well.

Scheme 10: Initial attempts to introduce the linker to catalyst **1c**.

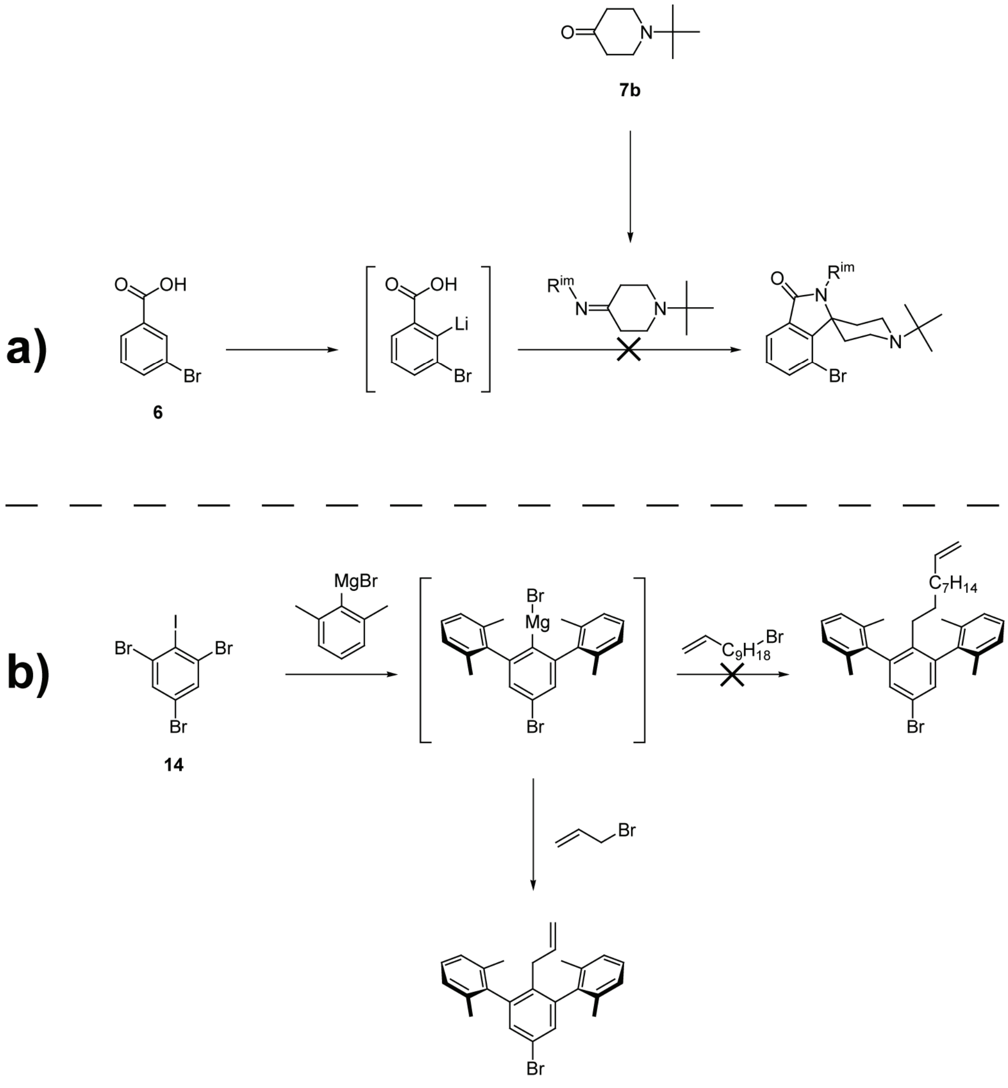

Accounting for these early failures to incorporate the linker into the framework of catalyst **1c**, new strategies were devised. Attachment of the linker to the benzene ring of the benzofuranone moiety by alkylation of a suitable phenol seems feasible. A possible target structure is given in Scheme 11 with a flexible undecenyl linker to allow for sufficient mobility of the catalytically active end-group on the surface. Furthermore, employing a undecenyl residue as linker precursor enables for two different tethering strategies either based on a hydrosilylation-immobilization sequence or utilizing the thio-ene reaction, cf. Figure 32.

Scheme 11: Target structure for a versatile immobilization precursor of catalyst **1c**.

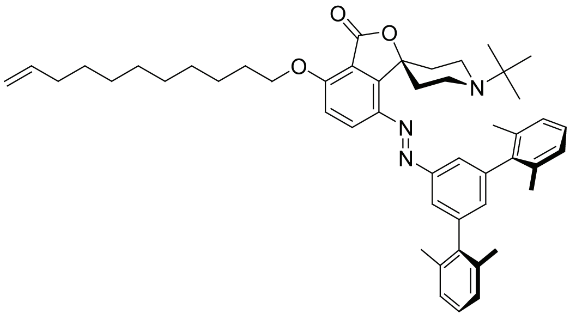

16

3.6.2 Synthesis

Immobilization Precursor

Retrosynthetic analysis of immobilization precursor **16** is straight forward (Scheme 12). Closely following the synthesis of catalyst **1c**, precursor **16** is derived by oxidation of a BOC-protected diarylhydrazine **17**, which is easily assembled from spiroannulated piperidine **18** and **4b**.

Scheme 12: Retrosynthesis of Immobilization precursor **16**.

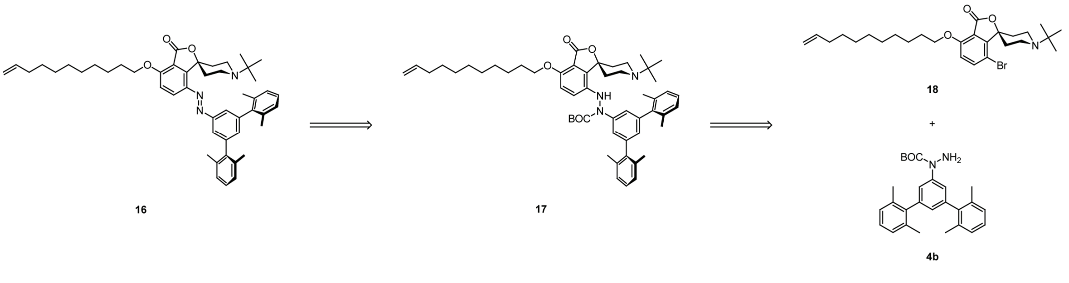

Spiroannulated piperidine **18** is obtained by adapting the protocols developed for synthesis of photoswitchable bases **1a-c**. Regioselective deprotonation of suitably alkylated 5-bromosalicylic acid **19** and subsequent reaction with piperidone **7b** is expected to give **18**. Alkylation of 5-bromosalicylic acid **20** with undecenyl bromide provides convenient access to intermediate **19**.

Scheme 13: Retrosynthesis of spiroannulated piperidine **18**.

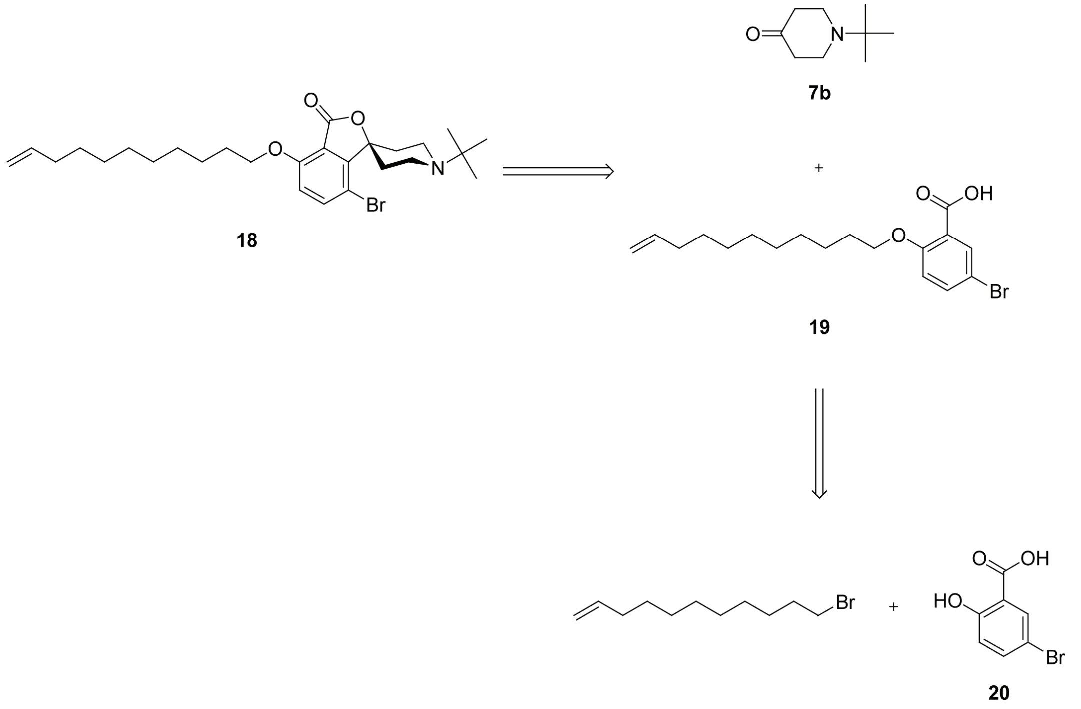
18
7b
19
20
O
N
Br
OH
HO
+

Indeed, alkylation of methyl 5-bromosalicylate **21** with undecenyl bromide proceeds smoothly to give the desired alkylated methyl ester **22**, which is easily hydrolyzed to give undecenyl 5-bromosalicylic acid **19**.[51]

Scheme 14: Synthesis of undecenyl 5-bromosalicylic acid **19**.

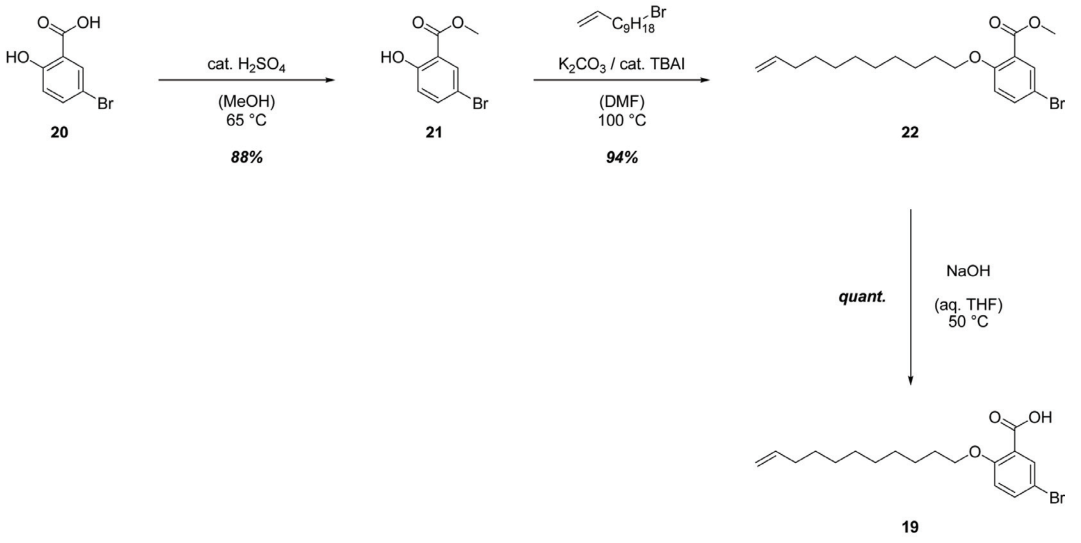
20
21
22
19
cat. H2SO4
(MeOH)
65 °C
88%
C9H18 Br
K2CO3 / cat. TBAI
(DMF)
100 °C
94%
NaOH
(aq. THF)
50 °C
quant.
HO
OH
Br

Synthesis of spiroannulated piperidine **18** was possible by lithiation of carboxylic acid **19** with two equivalents of LTMP and subsequent reaction with piperidone **7b** (Scheme 15).[8,9] Purification was complicated due to the formation of significant amounts of a carboxylic acid, presumably formed by addition of 2,2,6,6-tetramethylpiperidine to the aryne intermediate (*vide supra*). Therefore, the carboxylic acid byproduct was converted to the methyl ester prior to purification by reaction with EDC/DMAP in methanol. Afterwards, purification was straight forward and allowed to isolate target compound **18** in 36% yield.

Scheme 15: Synthesis of spiroannulated piperidine **18**.

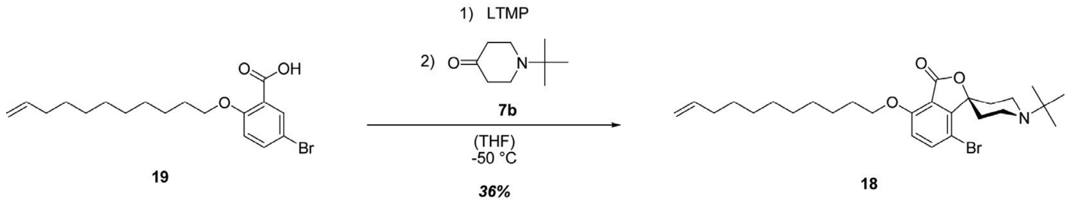

N-Arylation of terphenyl-based hydrazine **4b** with spiroannulated piperidine **18** proceeds in relatively low yields but allows for isolation of BOC-protected diarylhydrazine **17**,[15] which is subsequently oxidized to obtain small amounts of immobilization precursor **16** (Scheme 16).[16]

Scheme 16: Synthesis of immobilization precursor **16**.

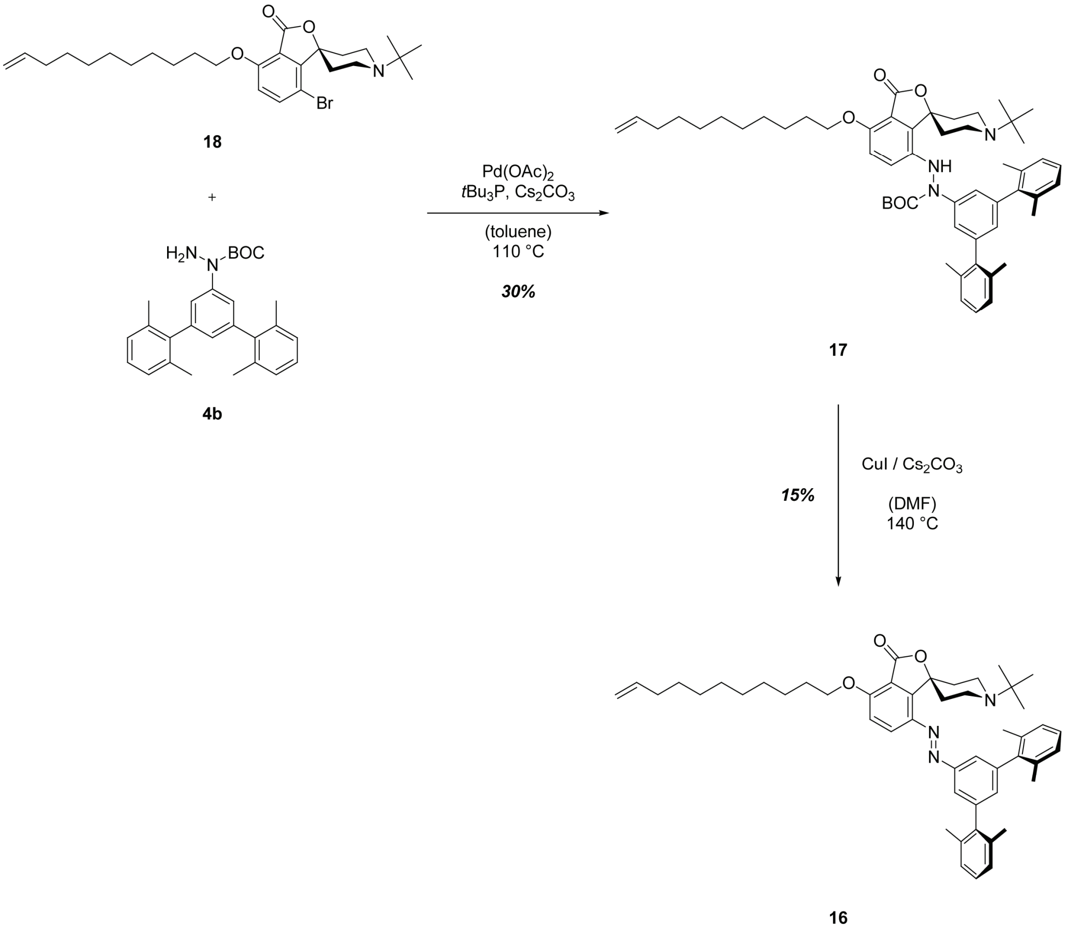

Immobilization

Considering silicon oxide substrates, a convenient way of immobilization is the reaction of surface hydroxyl groups with suitable monochlorosilanes, which can easily be derived from precursors carrying a C=C double bond on a flexible linker (cf. Section 3.6.1). Hydrosilylation of immobilization precursor **16** is easily achieved by reaction with excess chlorodimethylsilane in the presence of catalytic amounts of Karstedt's catalyst (Scheme 17).[52] The azobenzene chromophore is not destroyed under the conditions employed, as jugged from persistent orange/red coloration of the solution throughout the entire reaction. To avoid hydrolysis of monochlorosilane **23**, the orange material obtained was directly used without further characterization.

Scheme 17: Synthesis of monochlorosilane **23**.

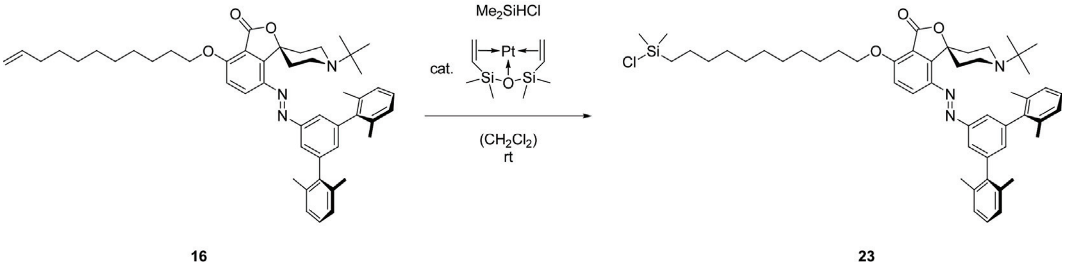

Immobilization on a solid support was easily achieved by reacting monochlorosilane **23** with conventional silica gel in the presence of triethyl amine (Scheme 18).[52] After repeated washing/sonication cycles, the supported catalyst **24** was isolated as a gray powder. Again, the red color of the solution was persistent throughout the entire reaction, indicative for the stability of the azobenzene chromophore towards the condition employed. The use of conventional silica gel as solid support with a high surface area and hence high loading capacity offers the advantage to use established solution phase spectroscopy to characterize the materials obtained, thereby circumventing problems associated with the characterization of monolayers on planar substrates, e.g. quartz slides or silicon wafers. However, for the construction of sophisticated surface architectures immobilization on planar substrates is inevitable. Therefore, monochlorosilane **23** was immobilized by the same methodology on quartz slides and silicon wafers as well.

Scheme 18: Immobilization of monochlorosilane **23** on silica gel to obtain supported catalyst **24**.

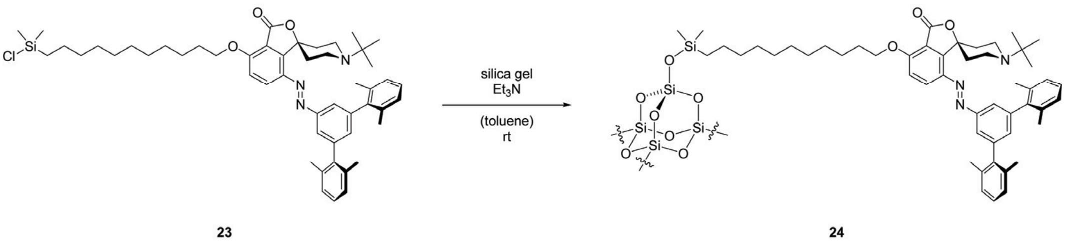

3.6.3 Photochromism in Solution

As for photoswitchable piperidines **1a-c**, the photochromic behavior of immobilization precursor **16** in solution was investigated in detail (Table 6). Irradiation of *E*-**16** with light of 365 nm wavelength causes isomerization of the azobenzene moiety, leading to a remarkable photostationary state comprised of 98% *Z*-**16** (Figure 33a). The photochemical back-reaction can be affected by irradiation with light of wavelengths >400 nm and proceeds cleanly until a photostationary state comprised of 77% *E*-**16** is reached (Figure 33b). No evidence for degradation of the photochrome upon light-induced switching was observed by either inspection of the absorption spectra or UPLC analysis of the irradiated mixtures.

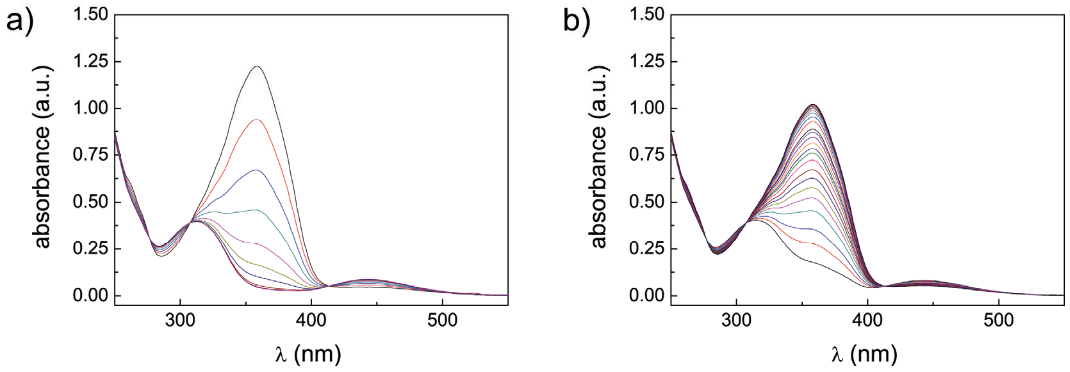

Figure 33: Irradiation of immobilization precursor **16**: a) isomerization *E*-**16** → *Z*-**16** (365 nm, 2 min 30 s irradiation time, $4.76 \cdot 10^{-5}$ M in CH_3CN); b) isomerization *Z*-**16** → *E*-**16** (400 nm, 5 min irradiation time, $4.76 \cdot 10^{-5}$ M in CH_3CN).

Table 6: Photochromic properties and activation parameters for thermal $Z \rightarrow E$ isomerization of **16** (values for **1c** are given for comparison).

	absorption		**PSS composition**	
	$\lambda_{max}(E)$[a] [nm]	**$\lambda_{max}(Z)$**[b] [nm]	**E → Z** (Z/E)	**Z → E** (Z/E)
1c	333	440	>99:1[e]	10:90
16	358	443	98:2	77:23

	thermal Z → E isomerization			
	$\tau_{1/2}$[c] [h]	**$\Delta G^{\ddagger}_{298\ K}$**[d] [kcal mol^{-1}]	**$\Delta H^{\ddagger}$**[d] [kcal mol^{-1}]	**$\Delta S^{\ddagger}$**[d] [cal mol^{-1} K^{-1}]
1c	466	25	23	-8
16	248	25	23	-6

[a] π,π*-Absorption. [b] n,π*-Absorption. [c] At 20 °C (293.15 K). [d] Obtained from kinetic data of the thermal $Z \rightarrow E$ isomerization at various temperatures and Eyring analysis of the data. [e] No *E* isomer was detected by UPLC analysis.

The absorption spectrum of pure *E*-**16** was readily obtained from a thermally equilibrated sample, whereas the spectrum of *Z*-**16** was calculated from the UV/vis spectra of pure *E*-**1b** and the *E* : *Z* mixture at the photostationary state, for which the *E* : *Z* ratio was determined by UPLC separation (Figure 34).

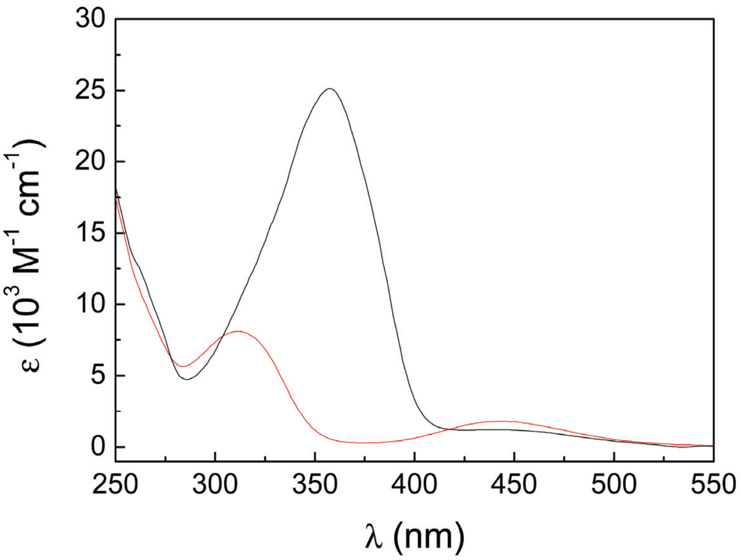

Figure 34: UV/vis-spectra of *E*-**16** (black, c = 3.2 · 10^{-5} M, $\varepsilon_{358\ \mathrm{nm}} = 25800\ \mathrm{M^{-1}\ cm^{-1}}$) and *Z*-**16** (red, c = 3.2 · 10^{-5} M, $\varepsilon_{443\ \mathrm{nm}} = 500\ \mathrm{M^{-1}\ cm^{-1}}$) in CH_3CN. The spectrum of *Z*-**16** was calculated from the UV/vis spectra of pure *E*-**16** and the *E* : *Z* mixture at the photostationary state, for which the *E* : *Z* ratio was determined by UPLC separation.

As observed for the azobenzene catalysts **1a-c**, the *Z* isomer of immobilization precursor **16** thermally reverts to the *E* isomer with prolonged half lifes of $\tau_{1/2}$ = 248 h at 20 °C, clearly exceeding the value determined for the parent azobenzene ($\tau_{1/2}$ = 16 h in benzene).[31] However, the thermal half life is decreased by almost a factor of two, when comparing $\tau_{1/2}$ for structurally related catalysts **1c** and **16** (Table 6). Such a decrease is expected for azobenzenes carrying an additional donor substituent in conjugation to the N=N double bond.[34,53]

Activation parameters for the thermal isomerization of *Z*-**16** were determined by following the $Z \rightarrow E$ isomerization by UV/vis spectroscopy at different temperatures (Figure 35). From the UV/vis spectra, the concentrations of *E* and *Z* isomers were calculated and subsequently the rate constants for the thermal $Z \rightarrow E$ isomerization were obtained from the slope of plots of -ln([*Z*]) versus time (see also Section 3.4).

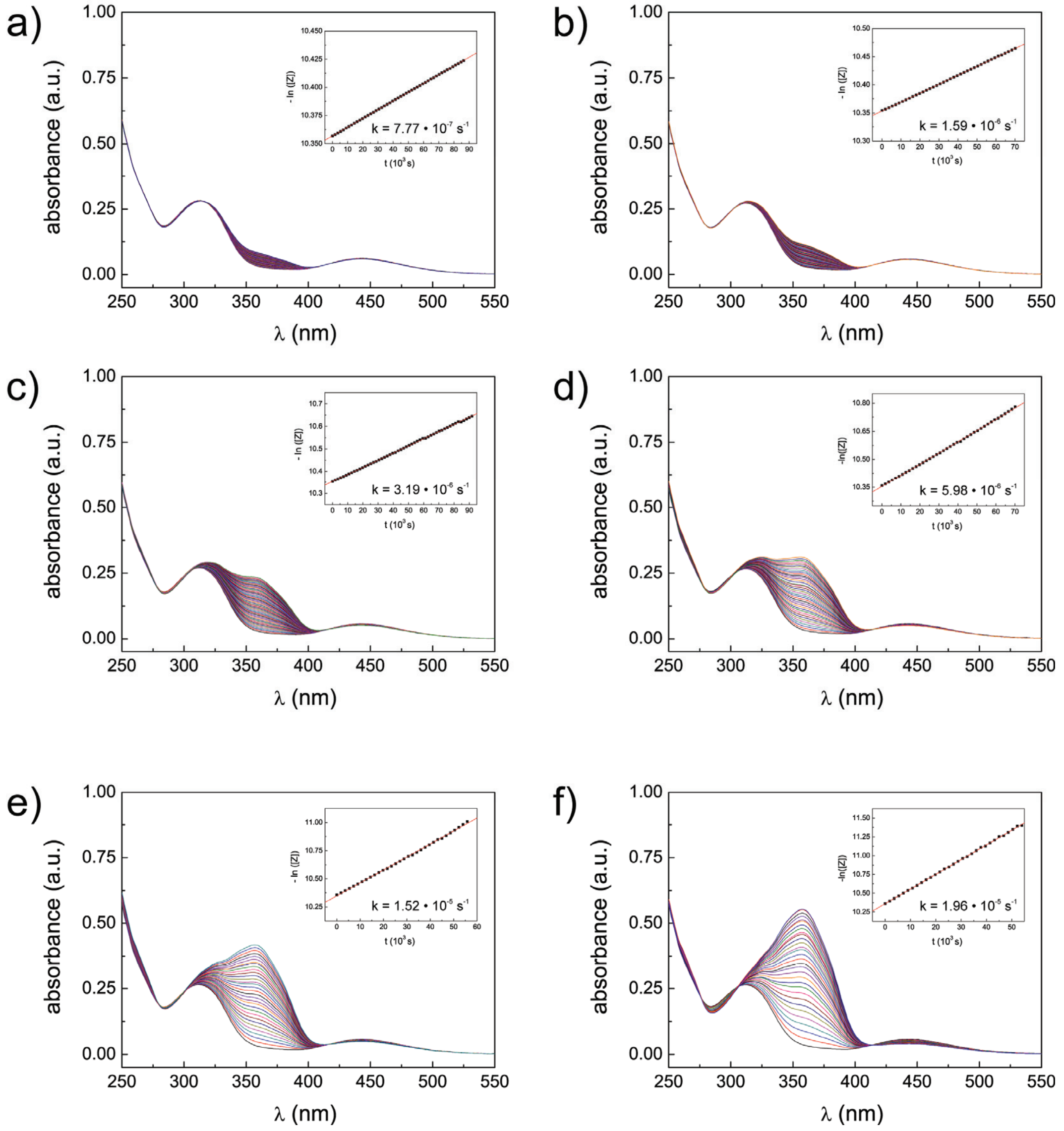

Figure 35: Thermal isomerization of *Z*-**16** → *E*-**16** at varying temperatures; insets show plots of -ln([*Z*]) vs. time and derived rate constants. a) 20 °C for 24 h ($3.24 \cdot 10^{-5}$ M in CH_3CN), b) 25 °C for 19.5 h ($3.24 \cdot 10^{-5}$ M in CH_3CN), c) 30 °C for 25.5 h ($3.24 \cdot 10^{-5}$ M in CH_3CN), d) 35 °C for 19.5 h ($3.24 \cdot 10^{-5}$ M in CH_3CN), e) 40 °C for 15.5 h ($3.24 \cdot 10^{-5}$ M in CH_3CN), f) 45 °C for 15 h ($3.24 \cdot 10^{-5}$ M in CH_3CN).

Following the approach described in Section 3.4, activation parameters for the thermal $Z \rightarrow E$ isomerization were determined by plotting ln(k/T) versus 1/T and are summarized in Table 6. Comparison of the activation parameters for structurally related catalysts **1c** and **16** reveals equal enthalpies of activation $\Delta H^{\ddagger}$, indicating a similar enthalpic loss when approaching the transition state. A slightly higher entropy of activation $\Delta S^{\ddagger}$ was found for **16** compared to **1c**, suggesting that differences in the thermal half lifes are entropic in origin. Values found for $\Delta S^{\ddagger}$ of **1c** and **16** are both negative, pointing to an increase in the degree of order of solvated catalysts *Z*-**1c** and *Z*-**16** by going to the respective transition states. Considering the long alkyl chain attached to immobilization precursor **16**, it is reasonable to assume a smaller increase in order (c.f. larger values for $\Delta S^{\ddagger}$) upon approaching the transition state, since numerous degrees of freedom associated with the alkyl chain are expected to be essentially unaffected by isomerization of the N=N double bond, thus decreasing the relative build-up of order upon isomerization as compared to catalyst **1c** (c.f. Section 3.4).

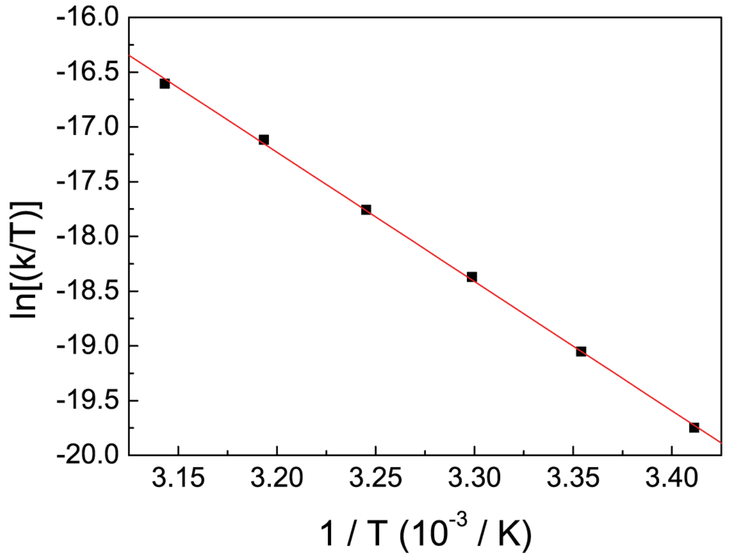

Figure 36: Van't Hoff plot for thermal $Z \rightarrow E$ isomerization of **16** obtained by plotting ln (k/T) versus 1/T. Obtained activation parameters are given in Table 6.

3.6.4 Photochromism on Solid-Support

The photoswitching behavior of silica gel supported catalyst **24** was investigated by UV/vis spectroscopy of suspensions of **24** in methylene chloride. Use of methylene chloride as solvent is crucial for obtaining satisfying results, because comparable refractive indices of solvent and silica gel diminish detrimental diffraction at the solid/liquid interface.[54] A distinct absorption around 360 nm is attributed to the $\pi \rightarrow \pi^*$ transition of *E*-**24** (black line, Figure 37). The symmetry forbidden and hence weak $n \rightarrow \pi^*$ transition can not be resolved due to the increased background absorption of the suspensions. Compared to homogenous solutions the spectra obtained from suspensions of **24** exhibit a substantial amount of noise, which is attributed to unavoidable scattering on large silica particles. Irradiation of *E*-**24** with light of 365 nm wavelength induces $E \rightarrow Z$ isomerization, as is evident from the bleaching of the absorption band around 360 nm. The expected increase of the $n \rightarrow \pi^*$ absorption attributed to *Z*-**24** can only be anticipated from a very slight increase of the absorbance around 450 nm (red line, Figure 37). Again, this is attributed to the increased background absorbance of the suspension. As for catalysts **1a-c** and **16**, irradiation of *Z*-**24** with light of wavelengths >400 nm induces $Z \rightarrow E$ isomerization leading to a photostationary state mainly comprised of *E*-**24** (blue line, Figure 37). Noteworthy, the initial spectrum obtain from a non-irradiated sample is almost completely restored, demonstrating the efficiency of the overall switching process.

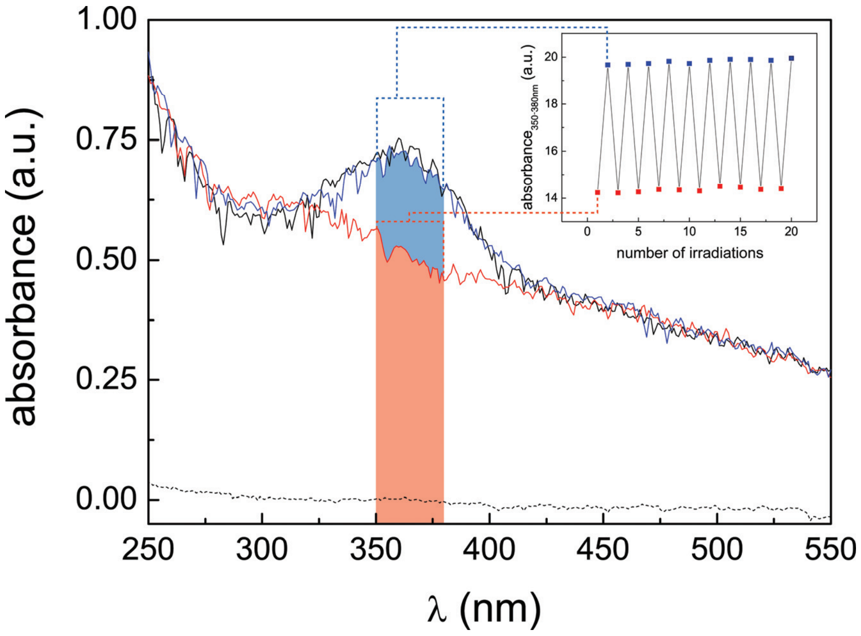

Figure 37: Switching of silica gel supported catalyst **24**.

Supported catalyst **24** exhibits an excellent fatigue resistance. Switching can be affected many times with out any detectable sign of degradation, as is evident from plots of the integral absorbance between 350 nm and 380 nm versus the number of irradiations (inset in Figure 37). The integral absorbance is plotted as an averaging equivalent to the absorbance at a single wavelength to compensate for the enhanced scattering of the suspension. No evidence for catalyst leaching from the solid support is found after repeated switching, as evidenced by the absence of any detectable absorption around 360 nm after filtration of the suspension (dotted line, Figure 37).

3.6.5 Characterization of Monolayers

Characterization of monolayers constitutes an inherently difficult task due to the very low loadings typically encountered on flat surfaces. In most cases, conventional spectroscopic methods to not provide sufficient sensitivity for a satisfactory characterization of these extremely thin films. However, a number of techniques for the characterization of monolayers have been developed to meet this analytical challenge. Standard techniques include for example the determination of contact angles, ATR-IR measurements, and ellipsometry. These methods are further complemented by the powerful tools of atomic force microscopy (AFM) and scanning tunneling microscopy (STM).

Contact angles of water on a functionalized surface provide some insights into the hydrophobicity of the surface, however structural information is only very limited. More structural information is available from AFM and STM investigations, however, these methods require flat and largely homogenous monolayers for obtaining reasonable results and require complex experimental setups. Furthermore, electronically conducting substrates are mandatory for STM experiments. Convenient access to structural information is possible by ATR-IR and ellipsometry measurements. Ellipsometry is a versatile and powerful optical technique for the investigation of the dielectric properties of thin films and can yield detailed spectral information in the UV/vis or IR range, if run in a proper set-up.

Currently, attempts to characterize monolayers on quartz slides and silicon wafers by IR-spectroscopic ellipsometry (IRSE) are underway and preliminary results point to the successful immobilization in the case of silicon wafers as substrates. Comparison of IR-spectra obtained from a KBr-tablet with data obtained by IR-ellipsometry reveal some bands present in both spectra (Figure 38). However, other bands from the IR-spectrum are missing in the ellipsometry spectrum, which might be attributed to orientational effects within the film. Unfortunately, ATR-IR spectra from monolayers on quartz slides could not be obtained.

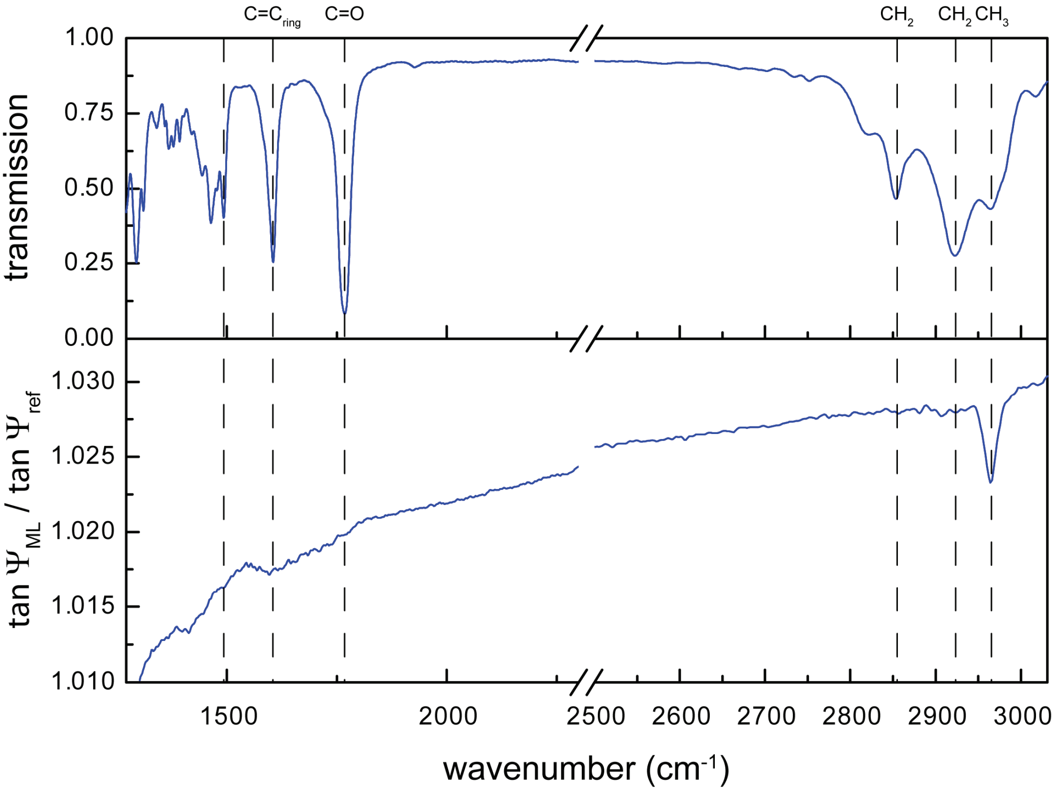

Figure 38: Comparison of IR-spectra obtained from a KBr-tablet (top) and IR-spectroscopic ellipsometry (bottom). The absence of bands in the IRSE-spectra might be attributable to orientational effects within the monolayer.

3.7 Conclusion and Outlook

In conclusion, a new conceptual design for photoswitchable catalyst systems has been developed. Photoswitchable catalysts on the basis of conformationally locked piperidine bases were synthesized and differences in basicity of the switching states involved were successfully exploited to photocontrol the catalysts' activities in general base catalysis, exemplified by photocontrolling conversion of the Henry reaction. A careful analysis of the dynamic structural behavior in solution using the recently introduced residual dipolar couplings in combination with quantum-chemical calculations allowed to formulate the structure-reactivity relation for the catalyst system, thereby facilitating tuning of the catalysts to enhance ON/OFF-ratios. Immobilization of the catalyst on solid substrates is expected to enable sophisticated surface pattering and functionalization tasks. Successful surface-tethering of the most active catalyst was demonstrated by repeated switching on silica gel. Current work is focused on the preparation and characterization of catalytically active monolayers on planar substrates to exploit the full potential of immobilized catalysts. Preliminary results obtained by IR-spectroscopic ellipsometry point the successful immobilization on silicon wafers.

3.8 Experimental

3.8.1 General Methods

Solvents and starting materials were used as received. Toluene and THF were distilled under an argon atmosphere over sodium prior to use. Dry DMF was purchased from Acros or distilled under an argon atmosphere from calcium hydride. All reactions were performed in an argon atmosphere. Column chromatography was carried out with 130 - 400 mesh silica gel. NMR spectra were recorded on a 400 MHz (100.6 MHz for ^{13}C) Bruker AV 400 or on a 300 MHz (75.6 MHz for ^{13}C) Bruker DPX 300 spectrometer at 27 °C using residual protonated solvent signals as internal standard (^{1}H-NMR: $\delta(CDCl_3) = 7.24$ ppm, $\delta(CD_3CN) = 1.94$ ppm, δ(THF-*d8*) = 3.58 ppm and ^{13}C-NMR: $\delta(CDCl_3) = 77.0$ ppm, $\delta(CD_3CN) = 1.32$ ppm). Mass spectrometry was performed on

Thermo LTQ FT instrument (ESI, ESI-HRMS: additives of mixtures of MeOH/H_2O 75/25 + 0.5% formic acid) and MSI concept 1H (EI, 70eV ionization) as well as on a QSTARXL Applied Q-TOF with a ISV of 950 V. HPLC separations were performed with Shimadzu LC-10A systems equipped with a photodiode array detector (PAD or DAD) or with Waters Alliance systems (mixtures and gradient mixtures of acetonitrile/water) equipped with 150 x 2 mm Luna columns (3 µm, phenyl-hexyl material). The Waters systems consisted of a Waters Separations Module 2695, a Waters Diode Array detector 996 and a Waters Mass Detector ZQ 2000. Conditions are specified when describing the corresponding substances. UPLC separations were preformed with a Waters Acquity system equipped with Acquity UPLC columns, a Water Diode Array detector, and a LCTPremierXE TOF-MS detector.

3.8.2 Spectroscopy

UV-visible absorption spectra were recorded using quartz cuvettes of 1 cm length on a Cary 50 spectrophotometer equipped with a Peltier-thermostated cell holder at 25 ± 0.05 °C. All solvents employed in optical spectroscopy studies were of spectrophotometric grade. Analytical irradiation experiments (see Figure 8, Figure 17, and Figure 33) were performed on degassed solutions (Ar for 5 min, $2 - 4 \cdot 10^{-5}$ M) of **1a-c**, **2**, and **16,** respectively, in CH_3CN using a LOT-Oriel 1000 W medium-pressure xenon lamp (XBO) equipped with an interference filter ($\lambda_{max\,T} = 365$ nm @ 10% T, FWHM = 10 nm) for irradiation of *E*-**1a**, with two cut-off filters resulting in a narrow spectral window ($\lambda_{max\,T} = 365$ nm @ 35% T, FWHM = 42 nm) for irradiation of *E*-**1b,c** and *E*-**16**, and with two cut-off filters resulting ($\lambda_{max\,T} = 356$ nm @ 55% T, FWHM = 78 nm) for irradiation of **2**. For photochemical $Z \rightarrow E$ isomerization of *Z*-**1a-c** and *Z*-**16** a cut-off filter was used ($\lambda_{max} > 400$ nm @ T = 65%). For photochemical $Z \rightarrow E$ isomerization of *Z*-**2** an interference filter was used ($\lambda_{max} = 254$ nm @ T = 33%). Thermal $Z \rightarrow E$ isomerization of *Z*-**1a-c** and ***Z*-16** was monitored by UV/vis spectroscopy (see Figure 12-14 and Figure 35). Quantitative UV/vis spectra of *Z*-**1a-c**, *Z*-**2**, and *Z*-**16** were determined combining spectroscopy and chromatography data (see

Figure 9-11, Figure 18, Figure 34). Photochemical $E \rightarrow Z$ and $Z \rightarrow E$ isomerization of **1c**-H$^+$ was monitored by UV/vis spectroscopy at 25 °C (see Figure 21). Thermal $Z \rightarrow E$ isomerization of *Z*-**1c**-H$^+$ was monitored by UV/vis spectroscopy at 20 °C and 45 °C (see Figure 22). The rate constants of thermal *Z*-**1a-c** → *E*-**1a-c** and *Z*-**16** → *E*-**16** isomerization at different temperatures were obtained by plotting -ln([*Z*-**1a-c**]) or -ln([*Z*-**16**]) calculated from UV-vis spectra versus time (see Figure 12-14 and Figure 35). Activation parameters were determined by plotting ln (k/T) versus 1/T (van't Hoff plot, Figure 15 and Figure 36).

3.8.3 pKa-Determination

The pK_a-values were determined using a reference base (indicator) with different absorptions of the neutral (**Ind**) and the protonated form (**Ind**-H$^+$) allowing to monitor the concentration of both species spectrophotometrically.[38] For optimal results, the pK_a of the reference base should not differ more than 2 pK_a units from the pK_a of the base to be measured. Neutral Red (3-amino-7-dimethylamino-2-methylphenazin) meets these requirements displaying absorption maxima at λ_{max} (**Ind**) = 441 nm and λ_{max} (**Ind**-H$^+$) = 534 nm in acetonitrile solution (further data: K_a (**Ind**-H$^+$) = $2.51 \cdot 10^{-16}$, pK_a (**Ind**-H$^+$) = 15.6, $\varepsilon_{534\,nm}$ (**Ind**-H$^+$) = 33350 $M^{-1}\,cm^{-1}$, and $\varepsilon_{534\,nm}$ (**Ind**) = 420 $M^{-1}\,cm^{-1}$).[39]

Neutral red was purchased in its protonated form. The free base was obtained by dissolving few milligrams of the protonated form in water, adjusting to basic pH using aq. 1N-NaOH solution, and extraction of the free base with methylene chloride. Drying over $MgSO_4$ and removal of solvent *in vacuo* afforded the free base indicator as a dark red solid.

Equimolar amounts of *E/Z*-**1b** and Neutral Red were dissolved in 100 mL of acetonitrile ($c_0 = 4.1 - 4.2 \cdot 10^{-5}$ M) and a solution of trifluoromethanesulfonic acid in acetonitrile (TfOH, $c = 3.15 \cdot 10^{-3}$ M) was added in increments of 0.1 ml (V_{tot} = 1.1 mL). Concentrations of *E/Z*-**1b**, *E/Z*-**1b**-H$^+$, **Ind**, and **Ind**-H$^+$ were determined from UV/vis spectra recorded after each addition (see Figure 19). Finally, pK_a values were obtained by applying the equations 8-13 (see page 99).

pK_a values for *E/Z*-**1c** were determined applying a similar methodology. Equimolar amounts of *E/Z*-**1c** and Neutral Red were dissolved in 3655 µL of acetonitrile (c_0 = $3.56 \cdot 10^{-5}$ M) and a solution of trifluoromethanesulfonic acid in acetonitrile (TfOH, c = $5.86 \cdot 10^{-4}$ M) was added in increments of 10 µL (V_{tot} = 180 µL, see Figure 10). Finally, pK_a values were obtained by applying the equations 8-13 (see page 99).

3.8.4 Kinetic Experiments

1 Equiv. of 4-nitrobenzaldehyde and 0.1 equiv. of catalyst **1a-c** and **2**, respectively, were dissolved in THF-d_8 (c_{cat} = 0.04 M), transferred to a NMR-tube, and 12 equiv. of nitroethane were added. ^{1}H-NMR spectra (300 MHz) were acquired at time intervals of 30 min over a period of 15 h. Plots of product formation, obtained from integration of ^{1}H-NMR spectra (exemplary shown in Figure 23 and 24) versus time yielded the rates of reaction (see Figure 25-28).

3.8.5 NMR Spectroscopy

All spectra of isotropic samples for variable temperature NMR, EXSY experiments and for the measurement of scalar couplings were recorded on a 500 MHz spectrometer (Bruker DRX-500) with a triple resonance inverse probe equipped with a z-gradient. All measurements were carried out without sample spinning at 303 K unless otherwise stated. For EXSY the standard NOESY (at ambient temperature or above) or ROESY (at low temperatures) pulse sequence from the Bruker pulse sequence library was used, with mixing times between 200 and 800 ms.

For the RDC measurements an oriented sample was prepared directly in a 5 mm o.d. NMR tube from 62 mg PBLG (M_n = 404.000 g/mol),[24] 13 mg *E*-**1b** and 600 mg CD_2Cl_2, which exhibited the quadrupolar splitting $\Delta\nu_Q$ = 134 Hz. As we observed strong coupling artefacts within the diastereotopic methylene groups, the RDCs of which, however, were crucial for our investigation, we used variable angle sample spinning to reduce the size of the RDCs.[25] For these experiments we transferred approximately half of the oriented sample into a 4 mm ZrO_2 rotor and used a Bruker dual HR-MAS probe equipped with z-gradient. Spectra were recorded at an angle of 51.8° with respect to the magnetic field (leading to a quadrupolar splitting $\Delta\nu_Q = 15$ Hz) and with a spinning frequency of 1400 Hz.

The one bond total coupling constants (^1T) and scalar coupling constants (^1J) were measured from ω_2 and ω_1 coupled HSQC experiments using an INEPT delay corresponding to 145 Hz. ω_2 coupled HSQCs were recorded without decoupling during acquisition using the Echo/Antiecho selection scheme. A total of 8 k data points were sampled in the direct dimension over a spectral width of 10 ppm to give a FID resolution of 0.61 Hz. In the indirect dimension 256 data points were sufficient to prevent signal overlap. The spectra were processed with use of an exponential window function with 1 Hz line broadening in the direct dimension. In the indirect dimension a $\pi/2$ shifted sine squared window function and zero filling by a factor of 4 was applied. ω_1 coupled HSQCs were recorded by removing the 180° proton pulse in the centre of the t_1 evolution period. A total of 1 k data points were sampled in the direct dimension over a spectral width of 10 ppm to give a FID resolution of 4.88 Hz. In the indirect dimension 512 k data points were sampled over a spectral width of 13 ppm to give a FID resolution of 3.19 Hz. The spectra were processed with use of an exponential window function with 3 Hz line broadening and zero filling to 2 k data points in the direct dimension. In the indirect dimension a $\pi/2$ shifted sine squared window function and zero filling by a factor of 2 was applied. For ^1H-^1H couplings XLOC spectra[55] were recorded with 8k data points in the direct dimension and 400 data points in the indirect dimension.

The dipolar coupling was calculated from the difference of the total coupling (anisotropic sample) and the scalar coupling (isotropic sample) by dividing by two, according to: $T = J + 2D$. Usually an error of 1 Hz was assumed for $^1D_{C\text{-}H}$.

The ${}^{1}D_{C\text{-}H}$ coupling of the rotable *tert*-butyl group (${}^{1}D_{\mathrm{C1\text{-}H1}}$) attached to the piperidine nitrogen is converted into the ${}^{1}D_{C\text{-}N}$ (${}^{1}D_{\mathrm{C2\text{-}N}}$) coupling using Eq.14.

$$ {}^{1}D_{C-N} = 9 \cdot \frac{\gamma_{{}^{15}N}}{\gamma_{{}^{1}H}} \cdot \frac{r_{C-H}^{3}}{r_{C-N}^{3}} \cdot {}^{1}D_{C-H} \tag{14} $$

with $\gamma_{N,H}$ being the two respective gyromagnetic ratios, $r_{C\text{-}H}$ being the C-H bond length within the methyl groups of the *tert*-butyl substituent, $r_{C\text{-}N}$ being the C-N bond length of the piperidine N to the attached quarternary *tert*-Bu carbon. This coupling was scaled by a factor of 1000 (see Section 3.3.2 of the main text and corresponding footnote); therefore its error is much larger (18 Hz in this case).

The ${}^{1}D_{\mathrm{CH}}$ of the *tert*-butyl groups on the steric blocker (${}^{1}D_{\mathrm{C18\text{-}H18}}$) was converted into the corresponding ${}^{1}D_{\mathrm{CC}}$ (${}^{1}D_{\mathrm{C15\text{-}C17}}$) according to Eq. 15.

$$ {}^{1}D_{C-C} = 9 \cdot \frac{\gamma_{{}^{13}C}}{\gamma_{{}^{1}H}} \cdot \frac{r_{C-H}^{3}}{r_{C-C}^{3}} \cdot {}^{1}D_{C-H} \tag{15} $$

The RDCs obtained in this way (for comments which RDCs were used for which purpose, see Section 3.3.2) were analyzed using the bestFit option in PALES.[26]

Table 7: Measured isotropic (*J*) and total couplings (*T*) and resulting dipolar couplings (*D*) together with corresponding numbering of atoms.

	J/Hz	*T*/Hz	*D*/Hz
C1H1	125	125.4	0.2
C3H3a	129	97	-16
C3H3b	134	155.63	10.815
C4H4a	126	145.26	9.63
C4H4b	126	93.6	-16.2
C9H9	166.2	144.13	-11.035
C10H10	163.3	164.56	0.63
C11H11	164.3	128.63	-17.835
C14H14	159.6	147.36	-6.12
C16H16	153.6	130.04	-11.78
C18H18	125.53	124.24	-0.645
H9H10	7.2	-2	-4.6
H10H11	7.5	-3.5	-5.5
H16H14	1.2	0	-0.6

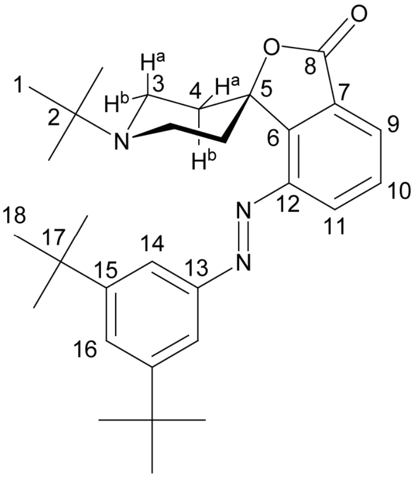

3.8.6 Computational Details

Geometries were fully optimized at the B3LYP/6-31G* level[56] of DFT, employing a fine integration grid (75 radial shells with 302 angular points per shell). The nature of the stationary points was verified by computations of the harmonic frequencies at the same level of theory. Transition states were characterized by a single imaginary frequency, and visual inspection of the corresponding vibrational modes ensured that the desired minima are connected. The computed harmonic frequencies were used to evaluate thermal and entropic contributions to enthalpies and Gibbs free energies. In selected cases, single-point energies were computed at the B3LYP level using cc-pVTZ basis,[57] and, to account for bulk solvation effects, employing the Polarized Continuum Model (PCM) of Tomasi and co-workers[58] with the parameters of THF and acetonitrile. All calculations were performed using the Gaussian03 suite of programs.[59]

3.8.7 Synthetic Procedures

3.8.7.1 Azobenzene Catalysts

Azobenzene based catalysts **1a-c** were synthesized adopting a procedure by Lim et al.[16]

*Azobenzene catalysts E-***1a**

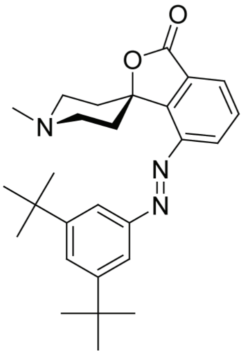

Spiro-hydrazo compound **8a** (100 mg, 0.19 mmol), copper(I) iodide (54 mg, 0.27 mmol), cesium carbonate (90 mg, 0.27 mmol), and 3 mL of dry DMF were mixed in a dry Schlenk tube and heated at 140 °C for 3 h. The mixture was diluted with methylene chloride and filtered through celite. Column chromatography (silica gel, Hex/EA, 3/1 + 0.1vol% NEt_3) afforded 48 mg of product as an orange solid (0.11 mmol, 58%). R_f (Hex/EA, 2/1 + 0.1vol% NEt_3) = 0.36. ^{1}H-NMR ($CDCl_3$, 400 MHz): δ (ppm) = 7.94 (m, 2H, Ar-*H*), 7.84 (d, ^4J = 1.8 Hz, 2H, Ar-*H*), 7.60 (m, 2H, Ar-*H*), 2.85 (broad m, 4H, pip-*H*), 2.53 (broad m, 2H, pip-*H*), 2.34 (s, 3H, C*H*$_3$), 1.77 (d, ^3J = 11Hz, 2H, pip-*H*), 1.39 (s, 18H, *t*-Bu-*H*). ^{13}C-NMR ($CDCl_3$, 100 MHz): δ (ppm) = 169.3, 152.8, 152.2, 146.1, 130.2, 127.7, 126.3, 120.0, 117.9, 109.8, 85.9, 51.8, 46.1, 36.0, 35.1, 31.3. MS (EI, 125 °C): *m/z* = 433 ($[M]^+$). HRMS (ESI pos.): *m/z* = 434.28009, (calc. 434.28019 for $C_{27}H_{36}N_3O_2$). HPLC (MeOH/10mmol TEAA pH 6.5 = 85/15, Nucleodur 100-5C18ec. 4 mm i.d.): t_R = 14.44 min (97% peak area). X-ray: $[C_{27}H_{35}N_3O_2]$, from dimethylformamide, M_r = 433.58, orange prism, crystal size: 0.085×0.055×0.015 mm^3; *a* = 13.051(7), *b* = 9.533(5), *c* = 20.391(11) Å,

β = 101.09(3)°, V = 2490(2) Å^3, T = 100 K, monoclinic, space group P2$_1$/c [no. 14], Z = 4, ρ_{calcd} = 1.157 Mg m^{-3}, F(000) = 936, Bruker-AXS X8-Proteum diffractometer, λ(Cu K$_\alpha$) = 1.54178 Å, μ = 0.575 mm^{-1}, 39082 measured and 3906 independent reflections (R_{int} = 0.1678), 1801 with $I > 2\sigma(I)$, θ_{max} = 68.86°, apparent $T_{\mathrm{min}}/T_{\mathrm{max}}$ = 0.8006 (SADABS, G. M. Sheldrick, 2007), direct methods (*SHELXS-97*) and least-squares refinement (*SHELXL-97*) on F_o^2, programs from G. M. Sheldrick, University of Göttingen, 2008. Because of the low signal-to-noise ratio in higher regions of reciprocal space due to the small size of the sample (thickness ca. 0.015 μm) it was difficult to determine where the actual reflections were located, and only 84.5% of the data to θ of 68.86° were determined to be measurable. Nevertheless, at resolutions of infinity to 0.96 \%A an average redundancy of 3.26 was obtained, with over six up to 1.75 Å. The Rint of 0.168 is also relatively high as a consequence of the low signal-to-noise ratio of the measured intensities from the small crystal. 290 parameters, H atoms calculated and refined using a riding model, R_1 = 0.0659 ($I > 2\sigma(I)$), wR_2 = 0.1977 (all data), $\Delta\rho_{\mathrm{max/min}}$ = 0.311/-0.251 eÅ^{-3}, CCDC 664577.

Azobenzene catalysts E-**1b**

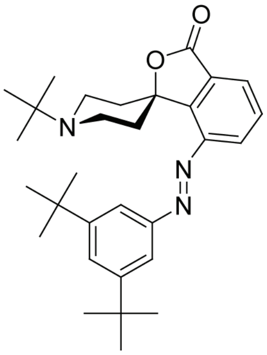

Spiro-hydrazo compound **8b** (166 mg, 0.29 mmol), copper(I) iodide (80 mg, 0.42 mmol), cesium carbonate (130 mg, 0.40 mmol), and 4.5 mL of dry DMF were mixed in a dry Schlenk tube and heated to 140 °C for 3 h. The mixture was diluted with methylene chloride and filtered through celite. Column chromatography (silica gel, Hex/EA, 2/1) afforded 71 mg of product as an orange solid (0.15 mmol, 52%). R_f (Hex/EA 5/1) = 0.1. ^{1}H-NMR (THF-d_8, 300 MHz): δ (ppm) = 8.05 (dd, 1H, ^{3}J = 8 Hz, ^{4}J = 0.8 Hz, Ar-*H*), 7.93 (m, 2H, Ar-*H*), 7.69 (t, 1H, ^{4}J = 1.8 Hz, Ar-*H*), 7.65 (t, 1H, ^{3}J = 7.7 Hz, Ar-*H*), 2.79 (m, 2H, pip-*H*), 3.10 (m, 2H, pip-*H*), 2.67 (m, 2H, pip-*H*), 1.83 (d, 2H, J =4.4 Hz, pip-*H*), 1.43 (s, 18H, *t*-Bu), 1.14 (s, 9H, *N*-*t*-Bu-*H*). ^{13}C-NMR (THF-d_8, 75 MHz): δ (ppm) = 167.2, 152.9, 152.2, 151.1, 146.1, 130.0, 128.6, 127.6, 126.1, 119.3, 117.9, 85.5, 53.7, 42.7, 37.7, 34.9, 30.9, 25.7. MS (ESI pos): *m/z* = 476.4 $[M+H]^+$. HRMS (ESI pos): *m/z* = 476.3274 (calculated 476.3272 for $C_{30}H_{42}N_3O_2$). HPLC (LUNA Phenyl-Hexyl, 3 µm, 2 x 150, gradient 5→95% CH_3CN/H_2O): t_R = 17.14 min (96.8% peak area). X-ray: $[C_{30}H_{41}N_3O_2]$, from acetonitrile, M_r = 475.67, orange plates, crystal size: 0.40×0.32×0.16 mm^3; $a = 51.292(4)$, $b = 13.2238(11)$, $c = 29.0236(19)$ Å, $\beta = 118.497(7)°$, $V = 17301(2)$ Å^3, $T = 180$ K, monoclinic, space group *C*2/c, $Z = 24$, $\rho_{calcd} = 1.096$ Mg m^{-3}, $F(000) = 6192$, Stoe IPDS diffractometer, λ(Mo K_α) = 0.71073 Å, $\mu = 0.069$ mm^{-1}, 35186 measured and 11173 independent reflections ($R_{int} = 0.0647$), 6292 with $I > 2\sigma(I)$, $\theta_{max} = 22.47°$, apparent $T_{min/max} = 0.9731/0.9891$, direct methods (*SHELXS-97*) and least-squares refinement (*SHELXL-97*) on F_o^2, programs from G. Sheldrick, University of Göttingen, 1997. Three independent molecules are in the crystal structure leading to an unusually large unit cell. 974 parameters, H atoms riding, $R_1 = 0.0438$ ($I > 2\sigma(I)$), $wR_2 = 0.0949$ (all data), $\Delta\rho_{max/min} = 0.376/-0.227$ eÅ^{-3}, CCDC 686676.

*Azobenzene catalysts E-***1c**

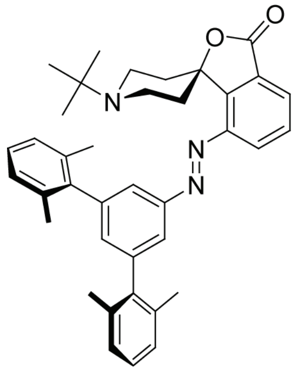

Spiro-hydrazo compound **8c** (300 mg, 0.45 mmol), copper(I) iodide (127 mg, 0.67 mmol), cesium carbonate (217 mg, 0.67 mmol), and 5 mL of dry DMF were mixed in a dry Schlenk tube and heated to 140 °C for 14 h. The mixture was diluted with methylene chloride and filtered through celite. Column chromatography (silica gel, Hex/EA, 9/1 + 0.1vol% NEt_3) afforded 125 mg of product as an orange solid (0.45 mmol, 49%). R_f (Hex/EA, 9/1 + 0.1vol% NEt_3) = 0.36. ^{1}H-NMR ($CDCl_3$, 300 MHz): δ (ppm) = 8.03 (d, ^3J = 7.9 Hz, 1H, Ar-*H*), 7.99 (d, ^3J = 7.9 Hz, 1H, Ar-*H*), 7.81 (d, ^4J = 1.6 Hz, 2H, Ar-*H*), 7.63 (t, ^3J = 7.9 Hz, 1H, Ar-*H*), 7.24 - 7.12 (m, 7H Ar-*H*), 2.99 (m, 2H, pip-*H*), 2.71 (m, 2H, pip-*H*), 2.58 (m, 2H, pip-*H*), 2.18 (s, 12H, C*H*$_3$), 1.82 (m, 2H, pip-*H*), 0.95 (s, 9H, *t*-Bu-*H*). ^{13}C-NMR ($CDCl_3$, 75 MHz): δ (ppm) = 169.4, 153.3, 151.5 146.1, 142.7, 140.7, 135.8, 133.9, 130.2, 128.2, 128.0, 127.7, 127.5, 122.8, 120.1, 87.1, 53.7, 42.8, 37.8, 26.3, 21.2. DEPT135-NMR ($CDCl_3$): δ (ppm) = 130.2 (pos.), 128.2 (pos.), 127.7 (pos.), 127.5 (pos.), 122.8 (pos.), 120.1 (pos.), 42.8 (neg.), 37.8 (neg.), 26.3 (pos.), 21.2 (pos.). MS (ESI pos): *m/z* = 572 ($[M + H]^+$). HRMS (ESI pos): *m/z* = 572.3278 (calc. 572.3272 for $C_{38}H_{42}N_3O_4$). HPLC (LUNA Phenyl-Hexyl, 3 µm, 2 x 150, gradient 40 → 95% CH_3CN/H_2O): t_R = 11.75 min (100% peak area). X-ray: [$C_{38}H_{41}N_3O_2$], from methylene chloride, M_r = 571.74, orange plate, crystal size: 0.12×0.08×0.02 mm^3, a = 11.3812(4), b = 24.8447(10), c = 12.4766(4), β = 116.154(3)°, V = 3166.7(2) Å^3, T = 150 K, monoclinic, space group P21/c, Z = 4, ρ_{calcd} = 1.199 Mg m^{-3}, F(000) = 1224, Stoe IPDS-2t diffractometer,

λ(Mo K_α) = 0.71073 Å, μ = 0.074 mm^{-1}, 50374 measured and 5732 independent reflections (R_{int} = 0.1288), 3690 with $I > 2\sigma(I)$, θ_{max} = 25.25°, apparent $T_{min/max}$ = 0.9912/0.9982, direct methods (*SHELXS-97*) and least-squares refinement (*SHELXL-97*) on F_o^2, programs from G. Sheldrick, University of Göttingen, 1997. 396 parameters, H atoms calculated, R_1 = 0.0392 ($I > 2\sigma(I)$), wR_2 = 0.0773 (all data), $\Delta\rho_{max/min}$ = 0.180/-0.212 eÅ^{-3}, CCDC 703183.

*Azobenzene catalysts Z-***1a**

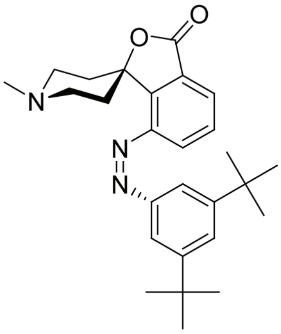

Azobenzene catalysts *E*-**1a** (20 mg, 0.04 mmol) was dissolved in 100 mL of acetonitrile and degassed by bubbling argon through the solution for 10 min. Subsequently, the solution was irradiated using a LOT-Oriel 1000 W medium-pressure xenon lamp (XBO) equipped with a cut-off filter (365 nm) and a solution filter (0.31 M aqueous $CoSO_4$, 5 cm path length) for 25 min. Afterwards, the solvent was evaporated *in vacuo* at 18 °C. For scale-up purposes, this procedure was repeated five times. Column chromatography of the collected samples (neutral alumina, gradient Hex/EA, 10/1 → EA, evaporation of the solvent at 0 °C) gave 44 mg (44%) of mainly *Z* isomer *Z*-**1a** (80% *Z*-**1a** according to ^{1}H-NMR). ^{1}H-NMR (CD_3CN, 400 MHz): δ (ppm) = 7.64 (dd, ^{3}J = 7.6 Hz, ^{4}J = 0.9 Hz, 1H, Ar-*H*), 7.34 (t, ^{4}J = 1.7 Hz, 1H, Ar-*H*), 7.22 (t, ^{3}J = 7.7 Hz, 1H, Ar-*H*), 6,75 (d, ^{4}J = 1.7 Hz, 2H, Ar-*H*), 6.35 (dd, ^{3}J = 7.8 Hz, ^{4}J = 0.9 Hz, 1H, Ar-*H*), 2.87 (m, 2H, pip-*H*), 2.66 (m, 2H, pip-*H*), 2.43 (s, 2H, pip-*H*), 2.33 (s, 3H, CH_3), 1.83 (m, 2H, pip-*H*), 1.15 (s, 18H, t-Bu-*H*). HPLC (MeOH, 10mM TEAA pH 6.8 = 85/15, Nucleodur, 4 mm i.d.) = 4.25 min (90.0% peak area).

Azobenzene catalysts *Z*-**1b**

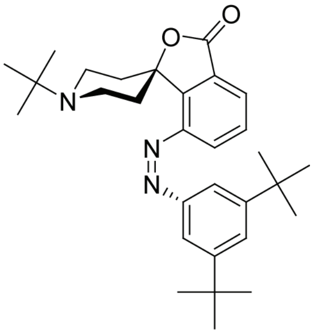

Azobenzene catalysts *E*-**1b** (20 mg, 0.04 mmol) was dissolved in 100 mL of acetonitrile and degassed by bubbling argon through the solution for 10 min. Subsequently, the solution was irradiated at $\lambda_{max} = 365$ nm for 60 min (two cut-off filters, $\lambda_{max\ T} = 365$ nm @ 35% T, FWHM = 42 nm). Afterwards, the solvent was evaporated *in vacuo* at 18 °C to afford *Z*-**1b** (with PSS *Z*-**1b** : *E*-**1b** 86 : 14 according to ^{1}H-NMR). ^{1}H-NMR (CD_3CN, 400 MHz): δ (ppm) = 7.62 (dd, $^3J = 7.6$ Hz, $^4J = 0.9$ Hz, 1H, Ar-*H*), 7.33 (t, $^4J = 1.7$ Hz, 1H, Ar-*H*), 7.21 (t, $^3J = 7.7$ Hz, 1H,--*H*), 3.12 (m, 2H, pip-*H*), 2.55 (m, 4H, pip-*H*), 1.85 (m, 2H, pip-*H*), 1.15 (s, 18H, *t*-Bu-*H*), 1.11 (s, 9H, *N*-*t*-Bu-*H*). ^{13}C-NMR (CD_3CN, 75 MHz): δ (ppm) = 169.2, 153.4, 152.9, 148.9, 147.3, 130.7, 123.4, 122.2, 116.4, 86.4, 54.6, 43.3, 36.4, 35.6, 31.3, 26.4. HPLC (LUNA Phenyl-Hexyl, 3 µm, 2 x 150, gradient 20→75% CH_3CN/H_2O): $t_R = 17.03$ min (88.5% peak area). X-ray: [$C_{30}H_{41}N_3O_2$], from acetonitrile, $M_r = 475.66$, orange prisms, crystal size: 0.60×0.40×0.24 mm^3; $a = 7.5388(13)$, $b = 13.771(2)$, $c = 14.573(2)$ Å, $\alpha = 93.35(2)°$, $\beta = 102.371°$, $\gamma = 100.33(2)°$, $V = 1446.4(4)$ Å^3, $T = 180$ K, triclinic, space group P-1, $Z = 2$, $\rho_{calcd} = 1.092$ Mg m^{-3}, $F(000) = 516$, Stoe IPDS diffractometer, $\lambda(\text{Mo K}_\alpha) = 0.71073$ Å, $\mu = 0.068$ mm^{-1}, 10441 measured and 5273 independent reflections ($R_{int} = 0.0678$), 2397 with $I > 2\sigma(I)$, $\theta_{max} = 26.04°$, apparent $T_{min/max} = 0.9601/0.9838$, direct methods (*SHELXS-97*) and least-squares refinement (*SHELXL-97*) on F_o^2, programs from G. Sheldrick, University of Göttingen, 1997. 422

parameters, H atoms determined, R_1 = 0.0463 ($I > 2\sigma(I)$), wR_2 = 0.1037 (all data), $\Delta\rho_{max/min}$ = 0.363/-0.192 eÅ^{-3}, CCDC 686677.

*Azobenzene catalysts Z-***1c**

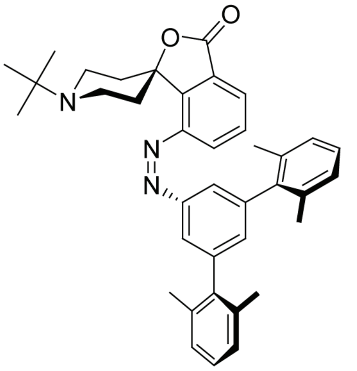

Azobenzene catalysts *E*-**1c** (14 mg, 0.03 mmol) was dissolved in 100 mL of acetonitrile and degassed by bubbling argon through the solution for 10 min. Subsequently, the solution was irradiated at λ_{max} = 365 nm for 120 min (two cut-off filters, $\lambda_{max\ T}$ = 365 nm @ 35% T, FWHM = 42 nm). Afterwards, the solvent was evaporated *in vacuo* at 10 °C to afford ***Z*-1c** (with PSS *Z*-**1c** : *Z*-**1c** 91 : 9 according to ^{1}H-NMR). ^{1}H-NMR (CD_3CN, 300 MHz): δ (ppm) = 7.64 (d, ^3J = 7.6 Hz, 1H, Ar-*H*), 7.30 (t, ^3J = 7.8 Hz, 1H, Ar-*H*), 7.10 - 7.00 (m, 6H, Ar-*H*), 6.78 (t, ^4J = 1.5 Hz, 1H, Ar-*H*), 6.65 (d, ^4J = 1.5 Hz, 2H, Ar-*H*), 6.61 (d, ^3J = 7.6 Hz, 1H, Ar-*H*), 3.08 - 3.05 (m, 2H, pip-*H*), 2.59 - 2.5 (m, 4H, pip-*H*), 1.92 (s, 12H, CH_3), 1.68 (m, 2H, pip-*H*), 1.10 (s, 9H, *t*-Bu-*H*).

3.8.7.2 Stilbene Catalyst

*E-Stilbene catalyst E-***2**

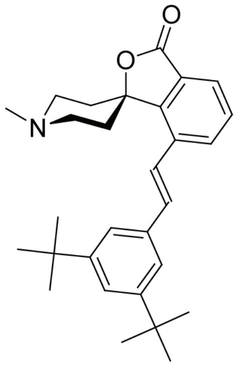

Bromo-spiro building block **3a** (755 mg, 2.6 mmol) and 2-(3,5-di-*tert*-butylstyryl)benzo[d][1,3,2]dioxaborole **5** (855 mg, 2.6 mmol) were dissolved in 47 mL of dry toluene. Addition of 1M aqueous NaOH solution (23 mL) and, tetrakis(triphenyl-phosphine)palladium(0) (100 mg, 0.112 mmol) was followed by degassing the mixture by three successive freeze-pump-thaw cycles. The resulting mixture was heated to 110 °C for 17 h. The phases were separated and the aqueous layer was washed with toluene once. Combined organic layers were washed with brine, dried over $MgSO_4$, and the solvent was evaporated under reduced pressure. The crude mixture was purified by column chromatography (silica gel, Hex/CH_2Cl_2, 100/1) to afford 620 mg of product as a colorless solid (1.44 mmol, 60%). R_f (CH_2Cl_2 / MeOH, 50/1) = 0.24. ^{1}H-NMR ($CDCl_3$, 300 MHz): δ (ppm) = 7.84 (d, ^3J = 7.7 Hz, 1H, Ar-*H*), 7.80 (dd, ^3J = 7.6 Hz, ^4J = 1 Hz, 1H, Ar-*H*), 7.52 (t, ^3J = 7.6 Hz, 1H, Ar-*H*), 7.43 (t, ^4J = 1.8 Hz, 1H, Ar-*H*), 7.37 (broad d, ^3J = 1.2 Hz, 2H, Ar-*H*), 7.35 (d, ^3J = 16 Hz, 1H, -C*H*), 7.13 (d, ^3J = 16 Hz, 1H, -C*H*), 2.85 (m, 2H, pip-*H*), 2.57 (broad m, 4H, pip-*H*), 2.36 (d, ^3J = 11.1 Hz, 2H, pip-*H*), 1.69 (s, 3H, -C*H₃*), 1.38 (s, 18 H, *t*-bu-*H*). ^{13}C-NMR ($CDCl_3$, 75 MHz): δ (ppm) = 151.3, 135.9, 134.9, 131.7, 129.6, 126.4, 124.7, 123.1, 122.5, 121.4, 85.4, 46.1, 34.9, 34.8, 31.4, 51.7. MS (EI, 40-50 °C): m/z = 432.29 ($[M + H]^+$). HRMS (ESI pos): 432.2897 (calc. 432.2903 for $C_{29}H_{38}N_1O_2$). HPLC (LUNA Phenyl-

Hexyl, 3 µm, 2 x 150, gradient 20 → 60% CH_3CN/H_2O): t_R = 18.6 min (96.8% peak area).

*Z-Stilbene catalyst Z-***2**

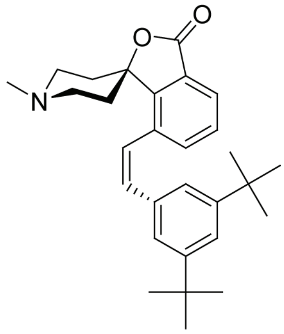

E-Stilbene catalyst *E*-**2** (20.92 mg, 0.047 mmol) was dissolved in 100 mL of acetonitrile and degassed by bubbling argon through the solution for 10 min. Subsequently, the solution was irradiated at $\lambda > 327$ nm (cut-off filter, T = 70%) for 57 min. The solvent was evaporated *in vacuo* to afford *Z*-**2** (with PSS *Z*-**2** : *E*-**2** 93.6 : 6.4 according to HPLC). R_f (CH_2Cl_2/MeOH, 50/1) = 0.24. ^{1}H-NMR ($CDCl_3$, 300 MHz): δ (ppm) = 7.8 (dd, ^3J = 7.3, ^4J = 1.2 Hz, 1H, Ar-*H*), 7.45 (dd, ^3J = 7.5 Hz, ^4J = 1.2 Hz, 1H, Ar-*H*), 7.37 (t, ^3J = 7.5 Hz, 1H, Ar-*H*), 7.20 (t, ^4J = 1.8 Hz, 1H, Ar-*H*), 6.84 (t, ^4J = 1.8 Hz, 2H, Ar-*H*), 6.78 (s, 2H, C-*H*), 2.88 (m, 2H, pip-*H*) 2.61 (m, 4H, pip-*H*), 2.39 (s, 3H, -C*H*$_3$), 1.64 (d, ^3J = 12, 2H, pip-*H*), 1.12 (s, 18H, C(C*H*$_3$)$_3$). ^{13}C-NMR ($CDCl_3$, 75 MHz): δ (ppm) = 169.6, 150.5, 135.8, 134.8, 134.5, 133.8, 129.5, 124.7, 123.9, 123.7, 121.8, 85.0, 51.6, 46.2, 34.5, 33.8, 31.1. HPLC (C LUNA Phenyl-Hexyl, 3 µm, 2 x 150, gradient 20 → 60% CH_3CN/H_2O): t_R = 17.75 min (93.6% peak area).

3.8.7.3 Bromo-Spiro Building Blocks

Syntheses of bromo-spiro building blocks **3a,b** were inspired by the procedures developed by Gohier et al.[8] and Parham et al.[9]

Bromo-spiro building block **3a**

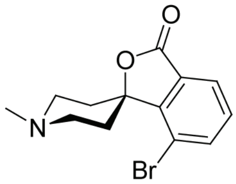

2,2,6,6-Tetramethylpiperidine (22.5 mL, 132 mmol) was dissolved in 100 mL of dry THF and cooled to -5 °C. *n*-Butyl lithium (82 mL, 1.6 M in hexane, 132 mmol) was added dropwise and stirring was continued for 1 h at -5 °C. After cooling to -50 °C, a solution of 3-bromobenzoic acid **6** (12.06 g, 60 mmol) in 30 mL of THF was added dropwise and the solution was stirred at -50 °C for 10 min. *N*-methyl-4-piperidinone **7a** **(**28 mL, 240 mmol) dissolved in 25 mL of THF was added rapidly and the solution was stirred at -50 °C for 1 h. The mixture was acidified to pH ~2 using 1N aq. HCl-solution and was stirred at room temperature over night. The organic solvent was removed *in vacuo* and the remaining aqueous layer was extracted with diethyl ether twice. The aqueous phase was adjusted to basic pH with solid $NaHCO_3$ and washed again with diethyl ether several times. Combined organic phases were washed with sat. aq. $NaHCO_3$-solution and water three times, respectively. Drying over $MgSO_4$ and evaporation of the solvent gave the crude product. Dissolution in methylene chloride and repetitive washing with ~800 mL of sat. aq. $NaHCO_3$-solution, followed by drying over $MgSO_4$, and evaporation of the solvent gave 2.5 g of product as nearly colorless solid (8.4 mmol, 14%). R_f (CH_2Cl_2/MeOH, 10/1) = 0.4. ^{1}H-NMR ($CDCl_3$, 400 MHz): δ (ppm) = 7.80 (dd, ^4J = 1 Hz, ^3J = 7.6 Hz, 1H, Ar-*H*), 7.78 (dd, ^4J = 1 Hz, ^3J = 7.8 Hz, 1H, Ar-*H*), 7.39 (t, ^3J = 7.7 Hz, 1H, Ar-*H*), 3.0 (broad m, 4H, pip-*H*), 2.62 (broad m, 2H, pip-*H*), 2.44 (s, 3H, -CH_3), 1.60 (d, 2H, ^3J = 16 Hz, pip-*H*). ^{13}C-NMR ($CDCl_3$, 100 MHz): δ (ppm) = 138.8, 131.1, 128.3, 125.2, 116.4, 95.9, 51.4, 46.0, 32.3. MS (EI, 90 °C): *m/z* = 296 ($[M]^+$), 216 ($[M - Br]^+$), 129. HRMS (ESI pos.): *m/z* = 318.01004 (calc. 318.01002 for $C_{13}H_{14}N_1O_2NaBr$).

Bromo-spiro building block **3b**

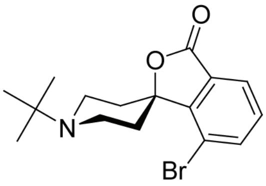

2,2,6,6-Tetramethylpiperidine (1.87 mL, 11 mmol) was dissolved in 8.4 mL of dry THF and cooled to -5 °C. *n*-Butyl lithium (6.83 mL, 1.6 M in hexane, 11 mmol) was added dropwise and stirring was continued for 1 h at -5 °C. After cooling to -50 °C, a solution of 3-bromobenzoic acid **6** (1.00 g, 5 mmol) in 2.5 mL of THF was added dropwise and the solution was stirred at -50 °C for 10 min. *N*-*tert*-butyl-4-piperidinone **7b (**1.55 g, 10 mmol) dissolved in 2.1 mL of THF was added rapidly and the solution was stirred at -50 °C for 1 h. The mixture was acidified to pH ~2 using 1N aq. HCl-solution and was stirred at room temperature over night. The organic solvent was removed *in vacuo* and the remaining aqueous layer was extracted with diethyl ether twice, adjusted to basic pH by addition of solid $NaHCO_3$, and extracted with diethyl ether again. Combined organic layers were washed with sat. aq. $NaHCO_3$-solution four times, three times with water, and dried over $MgSO_4$. Column chromatography (silica gel, CH_2Cl_2/MeOH, 20/1) afforded 0.45 g of product as an off-white solid (2.9 mmol, 26%). R_f (CH_2Cl_2/MeOH, 10/1) = 0.52. ^{1}H-NMR ($CDCl_3$, 300 MHz): δ (ppm) = 7.86 (dd, 1H, ^{4}J = 1 Hz, ^{3}J = 7.5 Hz, Ar-*H*), 7.81 (dd, 1H, ^{4}J = 1 Hz, ^{3}J = 7.9 Hz, Ar-*H*), 7.40 (t, 1H, ^{3}J = 7.7 Hz, Ar-*H*), 3.09 (d, 2H, ^{3}J = 8.7 Hz, pip-*H*), 2.83 (d, 2H, ^{3}J = 11.8 Hz, pip-*H*), 2.65 (t, 2H, J = 11.2 Hz, pip-*H*), 1.60 (d, 2H, ^{3}J = 12.5 Hz, pip-*H*), 1.14 (s, 9H, *N*-*t*-Bu-*H*)). ^{13}C-NMR ($CDCl_3$, 75 MHz): δ (ppm) = 138.6, 130.7, 128.6, 125.0, 116.4, 42.1, 33.6, 26.2. MS (EI, 80°C): *m/z* = 337 ($[M]^+$), 322 ($[M - CH_3]^+$). HRMS (ESI pos):

m/z = 337.0677 (calc. 337.0677 for $C_{16}H_{20}N_1O_2Br$). HPLC (LUNA Phenyl-Hexyl, 3 µm, 2 x 150, gradient 5→95% CH_3CN/H_2O): t_R = 10.58 min (97% peak area).

3.8.7.4 BOC-Protected Hydrazines

BOC-protected hydrazines **4a,b** were synthesized according to a procedure developed by Wolter et al.[12]

1-tert-Butoxycarbonyl-1-(3,5-di-tert-butylphenyl)hydrazine **4a**

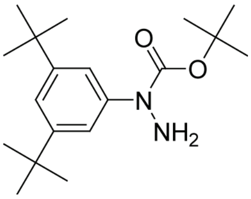

3,5-Di-*tert*-butyliodobenzene **10** (1.43 g, 8.25 mmol), *tert*-butyl-carbazate (1.32 g, 10 mmol), copper(I) iodide (22 mg, 0.12 mmol), 1,10-phenanthroline (170 mg, 0.9 mmol), cesium carbonate (3.72 g, 11.5 mmol), and 8.5 mL of dry DMF were mixed in a dry Schlenk tube and heated to 80 °C for 23 h. After cooling to room temperature, the solvent was evaporated and the crude mixture was purified by column chromatography (silica gel, gradient Hex/EA, 7/1 → 5/1) to afford 1.30 g of product as a yellow oil, which slowly solidified upon standing (4.01 mmol, 49%). R_f (Hex/EA, 5/1) = 0.16. ^{1}H-NMR ($CDCl_3$, 400 MHz): δ (ppm) = 7.31 (d, 2H, ^4J = 1.5 Hz, Ar-*H*), 7.16 (t, 1H, ^4J = 1.5 Hz, Ar-*H*) 1.48 (s, 9H, *t*-Bu-*H*), 1.30 (s, 18H, *t*-Bu-*H*). ^{13}C-NMR ($CDCl_3$, 100 MHz): δ (ppm) = 150.9, 119.3, 118.7, 81.8, 35.3, 31.8, 28.8. MS (EI, 45 °C): *m/z* = 320 ($[M]^+$), 262 ($[M - C(CH_3)_3]^+$), 220 ($[M - CO_2C(CH_3)_3]$). HRMS (ESI pos): *m/z* = 343.2355 (calc. 343.2355 for $C_{19}H_{32}N_2O_2Na$).

1-tert-Butoxycarbonyl-1-(3,5-bis(2,6-dimethylphenyl)phenyl)hydrazine **4b**

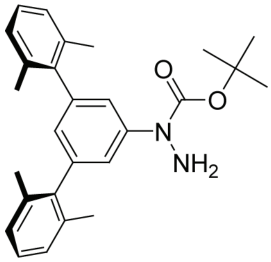

1-Iodo-3,5-bis(2,6-dimethylphenyl)benzene **12** (4.28 g, 10.37 mmol), *tert*-butyl-carbazate (1.71 g, 12.97 mmol), copper(I) iodide (198 mg, 1.04 mmol), 1,10-phenanthroline (374 mg, 2.07 mmol), cesium carbonate (4.73 g, 14.52 mmol), and 10 mL of dry DMF were mixed in a dry Schlenk tube and heated to 80 °C. Small amounts of copper(I) iodide and *tert*-butyl-carbazate were added after 16 h and heating to 80 °C was continued for additional 4 h. After cooling to room temperature, water was added and the aqueous layer was extracted with ethyl acetate three times. Combined organic layers were washed with brine three times and dried over $MgSO_4$. Removal of solvent *in vacuo* and purification of the material obtained by column chromatography (silica gel, gradient Hex/EA, 9/1 → 8/2) afforded 3.20 g of product as a colorless solid (7.25 mmol, 70%). R_f (Hex/EA, 8/2) = 0.46. ^{1}H-NMR ($CDCl_3$, 300 MHz): δ (ppm) = 7.25 (d, ^4J = 1.5 Hz, 2H, Ar-*H*), 7.19 - 7.09 (m, 6H, Ar-*H*), 6.72 (t, ^4J = 1.5 Hz, 1H, Ar-*H*), 4.51 (broad s, 2H, N*H*$_2$), 2.12 (s, 12H, C*H*$_3$), 1.49 (s, 9H, *t*--Bu-*H*). ^{13}C-NMR ($CDCl_3$, 75 MHz): δ (ppm) = 155.4, 143.5, 141.6, 141.4, 136.0, 127.4, 127.2, 126.4, 122.8, 81.9, 28.5, 21.0. DEPT135-NMR ($CDCl_3$): δ (ppm) = 127.4 (pos.), 127.2 (pos.), 126.4 (pos.), 122.8 (pos.), 28.5 (pos.), 21.0 (pos.). MS (ESI pos.): *m/z* = 439 ($[M + Na]^+$). HRMS (ESI pos.): *m/z* = 439.2357 (calc. 439.2356 for $C_{27}H_{32}O_2N_2Na$). HPLC (LUNA Phenyl-Hexyl, 3 µm, 2 x 150, gradient 5→95% CH_3CN/H_2O): t_R = 24.94 min (93.5% peak area).

3.8.7.5 Styryl Boronic Ester

2-(3,5-Di-tert-butylstyryl)benzo[d][1,3,2]dioxaborole **5**

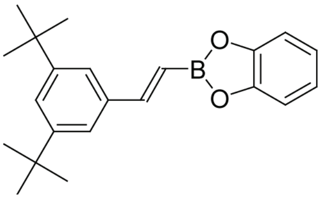

3,5-Di-tert-butyl-phenylacetylene **15** (399 mg, 1.85 mmol) was mixed with catecholborane (1.85 mL, 1.85 mmol, 1M in THF) in a dry Schlenk tube under an argon atmosphere and heated at 75 °C for 13 h. The solution was diluted with methylene chloride and the solvent was evaporated. Column chromatography (silica gel, CH_2Cl_2/MeOH, 100/1) afforded 304 mg of product as an off-white solid (0.91 mmol, 50%). R_f (CH_2Cl_2/MeOH, 50/1) = 0.6. ^{1}H-NMR (DMSO, 300 MHz): δ (ppm) = 1.29 (s, 18H, *t*-Bu-*H*), 6.10 (d, ^{3}J = 18.4 Hz, 1H, C-*H*), 6.59 (m, 2H, Ar-*H*), 6.71 (m, 2H, Ar-*H*), 7.27 (d, ^{3}J = 18.3 Hz, C-*H*), 7.29 (d, ^{4}J = 1.8 Hz, 2H, Ar-*H*), 7.35 (t, ^{4}J = 1.8 Hz, 1H, Ar--*H*). ^{13}C-NMR (DMSO, 75.5 MHz): δ (ppm) = 31.7, 34.9, 116.1, 119.7, 121.2, 122.8, 137.4, 145.7, 151.0. MS (EI, 40-50 °C): m/z = 334.3 ([M]$^+$), 319 ([M - Me]$^+$).

3.8.7.6 *N*-tert-Butyl-4-piperidone

Synthesis of *N*-*tert*-butyl-4-piperidone **7b** inspired by a procedure developed by Amato et. al.[11]

N,N-Dimethyl-4-oxopiperidinium iodide.

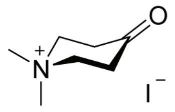

N-Methyl-4-piperidinone **7a** (10.4 mL, 90 mmol) was dissolved in 135 mL of acetone and cooled to 0 °C. Methyl iodide (6.7 mL, 100 mmol) was added under vigorous stirring and the resulting mixture was stirred for 10 min at 0 °C. The solution was warmed to room temperature and stirring was continued for 1 h. Isolation of the bright yellow precipitate by filtration, washing with small amounts of acetone three times, and drying over night afforded 22.3 g of product as a colorless solid (87.3 mmol, 97%). The analytical data agree with the literature.[11]

N-tert-Butyl-4-piperidinone **7b**

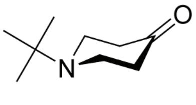

Water (40 mL) and acrylic acid (13.7 mL, 200 mmol) were mixed in a round bottom flask and 18.5 mL of a 10 M NaOH solution were added dropwise under vigorous stirring. *N*,*N*-Dimethyl-4-oxopiperidinium iodide (10.2 g, 40 mmol) and *tert*-butylamine (80 mL, 755 mmol) were added and the solution was heated to reflux (65 °C) for 3 h. After cooling to 0 °C (ice/water bath), remaining *tert*-butylamine was removed quickly at 0 °C *in vacuo* using a rotary evaporator. The cold solution was extracted with ethyl acetate three times. Combined organic layers were washed with brine three times and dried over $MgSO_4$. Evaporation of solvent at max. 30 °C and column chromatography (silica gel, CH_2Cl_2/MeOH, 20/1, evaporation at max. 30 °C) afforded 4.67 g of product as a yellow oil (30 mmol, 75%). Alternatively, analytically pure product can be obtained by distillation of the crude material *in vacuo*. ^{1}H-NMR ($CDCl_3$, 300 MHz): δ (ppm) = 2.80 (t, ^3J = 6.1 Hz, 4H, pip-*H*), 2.38 (t, ^3J = 6.1 Hz, 4H, pip-*H*), 1.08 (s, 9H, *t*-Bu-*H*). ^{13}C-NMR ($CDCl_3$, 75 MHz): δ (ppm) = 210, 54.1, 46.2, 42.2, 26.4. MS (ESI pos) *m/z* = 311 ($[2M + H]^+$), 188, 156 ($[M + H]^+$). HRMS (ESI pos): *m/z* = 156.1394 (calculated 156.1388 for $C_9H_{18}NO$), 311.2697 (calculated 311.2693 for $C_{18}H_{35}N_2O_2$).

3.8.7.7 Spiro-Hydrazo Compounds

Spiro-hydrazo building blocks **8a-c** were synthesized following a protocol developed by Lim et al.[15]

Spiro-hydrazo compound **8a**

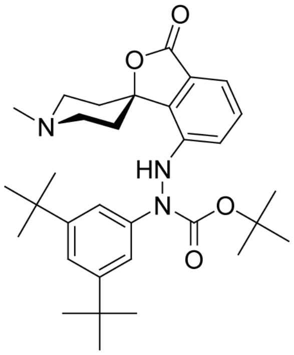

Bromo-spiro building block **3a** (75 mg, 0.26 mmol), 1-*tert*-butoxycarbonyl-1-(3,5-di-*tert*-butylphenyl)hydrazine **4a** (102 mg, 0.309 mmol), palladium(II) acetate (3 mg, 0.02 mmol), cesium carbonate (138 mg, 0.4 mmol), tri-*tert*-butyl phosphine (3 mg, 0.014 mmol), and 3.2 mL of toluene were mixed under an argon atmosphere in a sealed tube and stirred at room temperature for 0.5 h followed by heating to 120 °C for 2 h. After cooling to room temperature and diluting with methylene chloride, the reaction mixture was passed through a celite plug using methylene chloride and the solvent was evaporated. Column chromatography (silica gel, CH_2Cl_2/MeOH, 30/1) afforded 77 mg of the product as a colorless oil (55%). R_f (CH_2Cl_2/MeOH, 10/1) = 0.6. ^{1}H-NMR ($CDCl_3$, 400 MHz): δ (ppm) = 7.37 (m, 2H, Ar-*H*), 7.31 (d, ^4J = 1.6 Hz, 2H, Ar-*H*), 7.18 (t, ^4J = 1.6 Hz, 1H, Ar-*H*), 7.11 (dd, ^3J = 7.5 Hz, ^4J = 1.2 Hz, 1H, Ar-*H*), 6.90 (s, 1H, N-*H*), 2.92 (broad d, ^3J = 8.8 Hz, pip-*H*), 2.70 (m, 2H, pip-*H*), 2.57 (broad t, ^3J = 10 Hz, 2H, pip-*H*), 2.4 (s, 3H, -C*H*$_3$), 1.74 (broad d, ^3J = 13.5 Hz, 2H, pip-*H*), 1.41 (s, 9H, *t*-Bu-*H*), 1.28 (s, 18H, *t*-Bu-*H*). ^{13}C-NMR ($CDCl_3$, 100.62 MHz): δ (ppm) = 169.5, 153.9, 150.9, 142.5, 141.2, 136.9, 130.6, 126.8, 119.4, 117.4, 117,2, 116.7, 83.1, 82.5, 53.3, 51.6, 46.1, 34.9, 31.3, 28.2. MS (EI, 150°C): *m/z* = 535 ([M]$^+$), 435 ([M - BOC]$^+$), 185. HRMS (ESI pos.): *m/z* = 536.34844, (calculated 536.34827 for $C_{32}H_{46}N_3O_4$).

Spiro-hydrazo compound **8b**

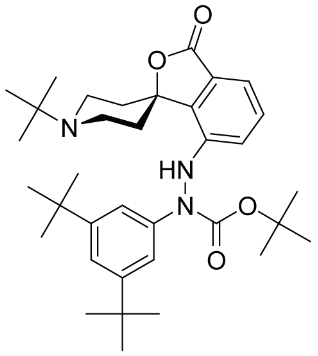

Bromo-spiro building block **3b** (200 mg, 0.6 mmol), 1-*tert*-butoxycarbonyl-1-(3,5-di-*tert*-butylphenyl)hydrazine **4a** (230 mg, 0.72 mmol), cesium carbonate (330 mg, 1 mmol), palladium(II) acetate (7 mg, 0.03 mmol), tri-*tert*-butylphosphine (7 mg, 0.03 mmol), and 7 mL of toluene were mixed in a sealed tube under an argon atmosphere and heated at 120 °C for 3 h. After cooling to room temperature and diluting with methylene chloride, the reaction mixture was passed through a celite plug using methylene chloride and the solvent was evaporated. Column chromatography (silica gel, CH_2Cl_2/MeOH, 100/1) afforded 190 mg of product as a colorless solid (0.32 mmol, 54%). R_f (CH_2Cl_2/MeOH, 50/1) = 0.24. ^{1}H-NMR ($CDCl_3$, 300 MHz): δ (ppm) = 7.39 (m, 4H, Ar-*H*), 7.20 (t, 1H, ^4J=1.7 Hz, Ar-*H*), 7.12 (m, 2H, Ar-*H*), 3.10 (d, 2H, ^3J = 9.6 Hz, pip-*H*), 2.67 (dd, 4H, ^3J = 13.9 Hz, ^3J = 25.1 Hz, pip-*H*), 1.76 (d, 2H,

^3J = 12.4 Hz, pip-*H*), 1.44 (s, 9H, *t*-Bu-*H*), 1.30 (s, 18H, *t*-Bu-*H*), 1.15 (s, 9H, *N*-*t*-Bu-*H*). ^{13}C-NMR ($CDCl_3$, 75 MHz): δ (ppm) = 150.9, 142.6, 130.5, 119.2, 117.2, 116.9, 84.4, 82.5, 54.4, 42.3, 34.9, 31.4, 28.2, 26.1. MS (ESI pos): *m/z* = 578 ($[M + H]^+$), 522 ($[M - C_4H_8]^+$). HRMS (ESI pos): *m/z* = 578.3948 (calc. 578.3952 for $C_{35}H_{52}N_3O_4$).

Spiro-hydrazo compound **8c**

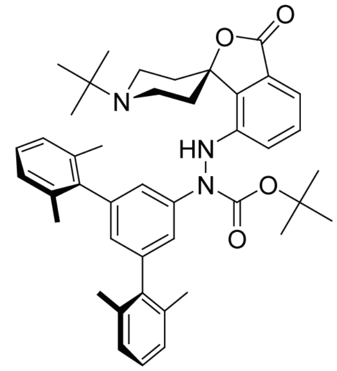

Bromo-spiro building block **3b** (488 mg, 1.44 mmol), 1-*tert*-butoxycarbonyl-1-(3,5-bis(2,6-dimethylphenyl)-phenyl)hydrazine **4b** (721 mg, 1.73 mmol), cesium carbonate (940 mg, 2.88 mmol), palladium(II) acetate (65 mg, 0.29 mmol), tri-*tert*-butylphosphine (58 mg, 0.29 mmol), and 10 mL of toluene were mixed in a sealed tube under an argon atmosphere. The mixture was degassed by three successive freeze-pump-thaw cycles and heated at 120 °C for 12 h. After cooling to room temperature and diluting with methylene chloride, the reaction mixture was passed through a celite plug using methylene chloride and the solvent was evaporated. Column chromatography (silica gel, CH_2Cl_2/MeOH, 99/1 containing 0.1vol% NEt_3) afforded 811 mg of product as a colorless solid (1.44 mmol, 83%). R_f (CH_2Cl_2/MeOH, 99/1) = 0.18. ^{1}H-NMR ($CDCl_3$, 300 MHz): δ (ppm) = 7.43 - 7.28 (m, 5H, Ar-*H* + N-*H*), 7.20 - 7.06 (m, 7H, Ar-*H*), 6.74 (broad t, ^4J = 1.5 Hz, Ar-*H*), 3.20 - 3.05(m, 2H, pip-*H*), 2.78 - 2.63 (m, 2H, pip-*H*), 2.63 - 2.45 (m, 2H, pip-*H*), 2.11 (s, 12H, C*H*$_3$), 1.84 - 1.70 (m, 2H, pip-*H*), 1.39 (s, 9H, *t*-Bu-*H*), 1.15 (s, 9H, *t*-Bu-*H*). ^{13}C-NMR ($CDCl_3$, 75 MHz): δ (ppm) = 169.7, 153.6, 142.8, 142.7, 141.7, 141.4, 136.9, 136.1, 130.7, 127.4, 127.3, 126.6, 121.2, 117.5, 117.3, 116.3, 84.4, 82.9, 54.6, 42.4, 34.4, 28.3, 26.3, 21.0. DEPT135-NMR ($CDCl_3$): δ (ppm) = 130.7 (pos.), 124.4 (pos.), 127.3 (pos.), 126.6 (pos.), 121.2 (pos.), 117.4 (pos.), 116.3 (pos.), 42.4 (neg.), 34.4 (neg.), 28.3 (pos.), 26.3 (pos.), 21.0 (pos.). MS (ESI pos): *m/z* = 674 ($[M + H]^+$), 572 ($[M - BOC]^+$). HRMS (ESI pos): *m/z* = 674.3963 (calc. 674.3958 for $C_{43}H_{52}N_3O_4$). HPLC (LUNA Phenyl-Hexyl, 3 µm, 2 x 150, gradient 40→95% CH_3CN/H_2O): t_R = 12.00 min (95% peak area).

3.8.7.8 Blocking-Group Precursors

3,5-Di-tert-butyliodobenzene **10**

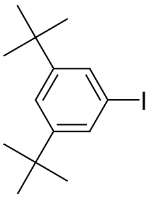

3,5-Di-*tert*-butylbromobenzene **9** (5.40 g, 20 mmol) was dissolved in 160 mL of THF and cooled to -78 °C. *n*-Butyl lithium (16.5 mL, 1.6 M in hexane, 26 mmol) was added and the solution was stirred at -78 °C for 1 h. Iodine (6.59 g, 26 mmol) was dissolved in THF and added at -78 °C. The cooling bath was removed and the colored solution was stirred at room temperature overnight. After washing with aq. $Na_2S_2O_3$-solution and drying over $MgSO_4$, 6.24 g of product were obtained as a colorless oil, which solidified upon standing (20 mmol, 99%). R_f (Hex/EA, 10/1) = 0.66. ^{1}H-NMR ($CDCl_3$, 300 MHz): δ (ppm) = 7.51 (d, 2H, Ar-*H*), 7.35 (s, 1H, Ar-*H*), 1.28 (s, 18H, *t*-Bu-*H*). MS (EI, 20 °C): *m/z* = 316 ($[M]^+$), 207 ($[M - CH_3]^+$). GC**:** 87.9 % peak area.

1-Bromo-3,5-bis(2,6-dimethylphenyl)benzene **11**

1-Bromo-3,5-bis(2,6-dimethylphenyl)-benzene **11** was synthesized according to a procedure by Vinod and Hart.[14]

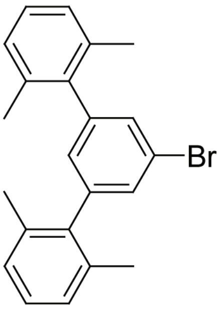

A dry 3N-flask equipped with a reflux condenser and an addition funnel was charged with magnesium (1.70 g, 70 mmol) and 20 mL dry THF. A solution of bromo-2,6-dimethylbenzene (8.05 mL, 11.10 g, 60 mmol) in 100 mL of dry THF was slowly added. Formation of the Grignard reagent was aided by gentle heating. The mixture was stirred for 1 h at room temperature and transferred to a second dry 3N-flask equipped with a reflux condenser and an addition funnel via a filter cannula followed by heating to reflux (65 °C). A mixture of 2,4,6-tribromoiodobenzene **14** (8.81 g, 20 mmol) and 60 mL of dry THF was added via the addition funnel over the course of 60 min. Stirring at 65 °C was continued for 3 h. The mixture was cooled in ice/water followed by addition of 100 mL of aq. 1N-HCl solution. Phases were separated and the aqueous layer was extracted with ethyl acetate three times. Combined organic layers were washed with brine three times, dried over $MgSO_4$, and the solvent was removed *in vacuo*. The crude product was purified by column chromatography (silica gel, Hex) to afford 4.28 g of pure product as a colorless oil (12 mmol, 59%). R_f (Hex) = 0.2. ^{1}H-NMR ($CDCl_3$, 300 MHz): δ (ppm) = 7.35 (d, ^4J = 1.5 Hz, 2H, Ar-*H*), 7.22 - 7.11 (m, 6H, Ar-*H*), 6.92 (t, ^4J = 1.5 Hz, 1H, Ar-*H*), 2.12 (s, 12H, C*H*$_3$). ^{13}C-NMR ($CDCl_3$, 75 MHz): δ (ppm) = 143.4, 140.4, 135.9, 130.4, 128.9, 127.6, 127.5, 122.7, 21.0. DEPT135-NMR ($CDCl_3$): δ (ppm) = 130.4 (pos.), 128.9 (pos.), 127.6 (pos.), 127.5

(pos.), 21.0 (pos.). MS (EI, 35 °C): *m/z* = 364 ($[M]^+$), 285 ($[M - Br]^+$), 270 ($[M - Br - CH_3]^+$), 255 ($[M - Br - 2\ CH_3]^+$). HRMS (EI): *m/z* = 364.0827 (calc. 364.0827 for $C_{22}H_{21}Br^{79}$).

1-Iodo-3,5-bis(2,6-dimethylphenyl)benzene **12**

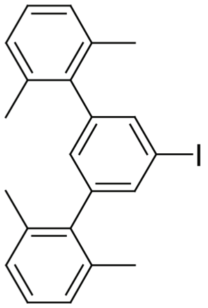

1-Bromo-3,5-bis(2,6-dimethylphenyl)benzene **11** (4.15 g, 11.4 mmol) was dissolved in 50 mL of THF and cooled to -78 °C. *n*-Butyl lithium (9.2 mL, 1.6 M in hexane, 14.8 mmol) was added and the solution was stirred at - 78 °C for 1 h. Iodine (3.75 g, 14.8 mmol) was dissolved in 10 mL of THF and added at - 78 °C. Stirring at -78 °C was continued for 1 h. The cooling bath was removed and the colored solution was quenched with sat. aq. $NaHSO_3$-solution. The organic layer was washed with sat. aq. $NaHSO_3$-solution three times and dried over $MgSO_4$. Removal of solvent *in vacuo* afforded 4.41 g of pure product as a colorless wax (10.3 mmol, 94%). R_f (Hex/EA, 9/1) = 0.8. ^{1}H-NMR ($CDCl_3$, 300 MHz): δ (ppm) = 7.56 (d, ^4J = 1.5 Hz, 2H, Ar-*H*), 7.22 - 7.11 (m, 6H, Ar-*H*), 6.96 (t, ^4J = 1.5 Hz, 1H, Ar-*H*), 2.12 (s, 12H, C*H*$_3$). ^{13}C-NMR ($CDCl_3$, 75 MHz): δ (ppm) = 143.4, 140.3, 136.3, 135.9, 129.5, 127.6, 127.5, 94.7, 21.0. DEPT135-NMR ($CDCl_3$): δ (ppm) = 136.3 (pos.), 129.5 (pos.), 127.6 (pos.), 127.5 (pos.), 21.0 (pos.). MS (EI): *m/z* = 412 ($[M]^+$), 285 ($[M - I]^+$), 255 ($[M - I - 2\ CH_3]^+$), 207, 179. HRMS (EI): *m/z* = 412.0689 (calc. 412.0689 for $C_{22}H_{21}I$).

2,4,6-Tribromoiodobenzene **14**

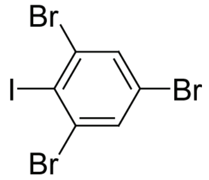

2,4,6-Tribromoaniline **13** (24.7 g, 75 mmol) was dissolved in 120 mL of concentrated sulfuric acid and cooled to 0 °C. A concentrated solution of sodium nitrite (11.4 g, 165 mmol) in water was added in portions and stirring at 0 °C was continued for 3.5 h. The mixture was poured into ice/water followed by immediate addition of a mixture of potassium iodide (74.7 g, 450 mmol) with water and ice (gas evolution). The mixture was transferred to a separation funnel and extracted with ethyl acetate five times. Combined organic layers were washed with sat. aq. $NaHSO_3$-solution five times and with water and brine three times, respectively. Drying over $MgSO_4$ and removal of solvent *in vacuo* afforded a crude, reddish material which could be further purified by fractionated crystallization from ethanol/water mixtures to obtain 20.8 g of pure product (47 mmol, 63%). R_f (Hex) = 0.5. ^{1}H-NMR ($CDCl_3$, 300 MHz): δ (ppm) = 7.70 (s, 2H, Ar-*H*). ^{13}C-NMR ($CDCl_3$, 75 MHz): δ (ppm) = 133.7, 132.0, 123.1, 108.2. DEPT135-NMR ($CDCl_3$): δ (ppm) = 133.7 (pos.). MS (EI, 35 °C): *m/z* = 440 ($[M]^+$), 360, 312, 234, 153, 74. HRMS (EI): *m/z* = 439.6732 (calc. 439.6732 for $C_6H_2Br^{79}{}_2Br^{81}I$). HPLC (LUNA Phenyl-Hexyl, 3 µm, 2 x 150, gradient 30→70% CH_3CN/H_2O): t_R = 33.32 min (100% peak area).

3,5-Di-tert-butyl-trimethylsilyl-phenylacetylene

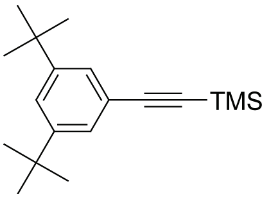

Di-*tert*-butylbromobenzene **9** (2.16 g, 8.02 mmol), tetrakis(triphenylphosphine)-palladium(0) (363 mg, 0.41 mmol), copper(I) iodide (78 mg, 0.4 mmol), triphenylphosphine (117 mg, 0.45 mmol) and 35 mL of triethylamine were mixed in a dry Schlenk tube under an argon atmosphere and degassed by three successive freeze-pump-thaw cycles. TMS-acetylene (1.7 mL, 12 mmol) was added and the reaction mixture was heated to 90 °C for 2 h. After cooling to room temperature the mixture was filtered through celite and the solvent was evaporated (raw yield 760 mg). After column chromatography (Hex), 2.01 g of product were obtained as a colorless solid in (7.02 mmol, 88%). The ^{1}H-NMR is in accordance with the literature.[60] ^{13}C-NMR ($CDCl_3$, 75 MHz): δ (ppm) = 150.7, 126.2, 123.0, 122.0, 106.4, 92.5, 34.8, 31.3, 0.1. MS (EI, 40-45 °C): *m/z* = 286.2 ($[M]^+$), 271.2 ($[M - Me]^+$).

3,5-Di-tert-butyl-phenylacetylene **15**

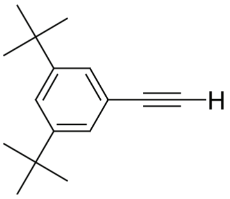

3,5-Di-*tert*-butyl-trimethylsilyl-phenylacetylene (1.01 g, 3.52 mmol) and potassium carbonate (735 mg, 5.3 mmol) were placed in a Schlenk tube under an argon atmosphere followed by addition of 18 mL of methanol and 4 mL methylene chloride. The mixture was stirred at room temperature for 1 h, diluted with methylene chloride, and the solid was filtered off. The organic phase was washed with saturated aqueous

NH_4Cl-solution twice and with water once. After drying with $MgSO_4$, the solvent was evaporated to obtain 0.75 g of product as a colorless solid (3.52 mmol, quantitative). R_f (Hex) = 0.31. The ^{1}H-NMR is in accordance with the literature.[60] ^{13}C-NMR ($CDCl_3$, 75 MHz): δ (ppm) = 150.9, 126.4, 123.3, 121.0, 84.8, 34.8, 31.3.

3.8.7.9 Immobilization Precursor

Immobilization Precursor **16**

Immobilization precursor **16** was synthesized adopting a procedure by Lim et al.[16]

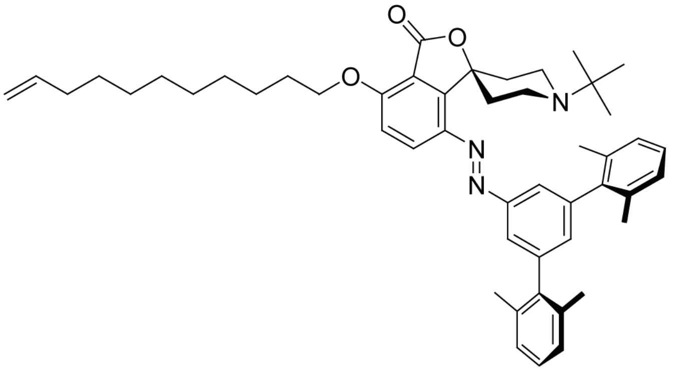

A dry sealable tube was charged with diarylhydrazine **17** (75 mg, 0.089 mmol), copper(I) iodide (25 mg, 0.134 mmol), ceasium carbonate (43 mg, 0.134 mmol), and 1 mL of dry DMF. The tube was flushed with argon several times, sealed, and heated to 140 °C for 8 h. The mixture was passed through a plug of Celite using methylene chloride and the solvent was removed *in vacuo*. The residue was purified by column chromatography (silica gel, CH_2Cl_2/MeOH, 9.9/0.1 + 0.1 vol% Et_3N) to afford the product as an orange solid (10 mg, 15%). An additional fraction of slightly impure product could be isolated as well (14 mg). The samples obtained could be further purified by repeated recrystallization from methanol. R_F (CH_2Cl_2/MeOH, 9.7/0.3 + 0.1 vol% Et_3N) = 0.34. ^{1}H-NMR ($CDCl_3$, 300 MHz): δ (ppm) = 8.04 (d, ^{3}J = 9.0 Hz, 1H, Ar-*H*), 7.72 (d, ^{4}J = 1.6 Hz, 2H, Ar-*H*), 7.18-7.09 (m, 6H, Ar-*H*), 7.08 (t, ^{4}J = 1.6 Hz, 1H, Ar-*H*), 7.00 (d, ^{3}J = 9.0 Hz, 1H, Ar-*H*), 5.42-5.38 (m, 3H, =C*H*), 4.19 (t,

^{3}J = 6.7 Hz, 2H, CH_2), 2.98-2.94 (m, 2H, CH_2), 2.72-2.62 (m, 2H, CH_2), 2.52-2.44 (m, 2H, CH_2), 2.14 (s, 12H, CH_3), 2.09-1.84 (m, 6H, CH_2), 1.77-1.72 (m, 2H, CH_2), 1.54-1.26 (m, 10H, CH_2), 0.90 (s, 9H, CH_3). ^{13}C-NMR (CDCl$_3$, 75 MHz): δ (ppm) = 166.56, 160.48, 154.91, 153.41, 142.54, 141.01, 139.40, 135.88, 133.01, 131.72, 130.89, 127.51, 127.36, 124.56, 122.43, 114.24, 112.64, 85.00, 69.64, 42.83, 37.87, 32.66, 29.70, 29.63, 29.48, 29.35, 29.19, 28.95, 26.87, 25.98, 25.84, 20.88. DEPT135-NMR (CDCl$_3$): δ (ppm) = 133.01 (pos.), 131.72 (pos.), 127.51 (pos.), 127.36 (pos.), 124.56 (pos.), 122.43 (pos.), 112.64 (pos.), 69.64 (neg.), 42.83 (neg.), 37.87 (neg.), 32.66 (neg.), 29.70 (neg.), 29.63 (neg.), 29.48 (neg.), 29.35 (neg.), 29.19 (neg.), 28.95 (neg.), 26.87 (neg.), 25.98 (pos.), 25.84 (neg.), 20.88 (pos.). MS (ESI pos.): *m/z* = 741 ([M + H]$^+$). HRMS (ESI pos.): *m/z* = 740.4789 (calc. 740.4791 for $C_{49}H_{62}O_3N_3$). UPLC (Acquity UPLC column, gradient 60→95% CH_3CN/H_2O): t_R = 4.47 min (100% peak area).

Diarylhydrazine **17**

Diarylhydrazine **17** was synthesized following a protocol developed by Lim et al.[15]

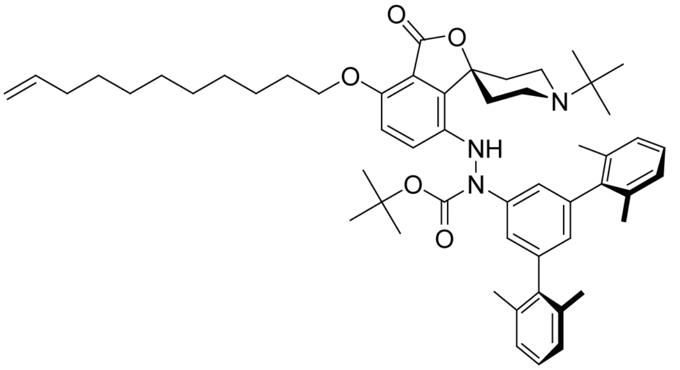

A dry sealable tube was charged with spiroannulated piperidine **18** (483 mg, 0.952 mmol), 1-*tert*-butoxycarbonyl-1-(3,5-bis(2,6-dimethylphenyl)phenyl)hydrazine **4b** (476 mg, 1.144 mmol), palladium(II) acetate (43 mg, 0.191 mmol), tri-*tert*-butylphosphine (solution in toluene, 39 mg, 0.191 mmol), cesium carbonate (621 mg, 1.906 mmol), and 10 mL of dry toluene. The tube was sealed and heated to 120 °C for 21 h. The mixture was passed through a plug of Celite using methylene chloride and the solvent was removed *in vacuo*. Purification of the raw material by column chromatography (silica gel, gradient CH_2Cl_2/MeOH, 9.9/0.1→9.8/0.2 + 0.1 vol% Et_3N) afforded the product as a colorless solid (240 mg, 30%). R_F (CH_2Cl_2/MeOH, 9.8/0.2 + 0.1 vol% Et_3N) = 0.30. ^{1}H-NMR: despite repeated attempts no conclusive ^{1}H-NMR of the title compound could be obtained. ^{13}C-NMR ($CDCl_3$, 75 MHz): δ (ppm) = 167.26, 153.83, 152.53, 142.85, 141.55, 141.43, 136.04, 135.56, 131.04, 135.56, 131.75, 130.96, 127.41, 127.24, 126.51, 124.65, 123.72, 121.32, 118.84, 113.80, 82.69, 69.48, 46.33, 42.40, 32.69, 29.70, 29.51, 29.44, 29.32, 29.21, 29.06, 28.34, 26.93, 26.21, 25.93, 21.01, 18.04. DEPT135-NMR ($CDCl_3$): δ (ppm) = 131.75 (pos.), 130.96 (pos.), 127.41(pos.), 127.24 (pos.), 126.51 (pos.), 124.65 (pos.), 121.32 (pos.), 118.87 (pos.), 113.80 (pos.), 69.48 (neg.), 46.33 (neg.), 42.40 (neg.), 32.69 (neg.), 29.70 (neg.), 29.51 (neg.), 29.44 (neg.), 29.32 (neg.), 29.21 (neg.), 29.06 (neg.), 28.34 (pos.), 26.93 (neg.), 26.21 (pos.), 25.93 (neg.), 21.01 (pos.), 18.04 (pos.). MS (ESI pos.): *m/z* = 842 ([M + H]$^+$). HRMS (ESI pos.): *m/z* = 842.5458 (calc. 842.5466 for $C_{54}H_{72}O_5N_3$). UPLC (Acquity UPLC column, gradient 50→90% CH_3CN/H_2O): t_R = 5.08 min (91% peak area).

Spiroannulated Piperidine **18**

Syntheses of spiroannulated piperidine **18** was inspired by the procedures developed by Gohier et al.[8] and Parham et al.[9]

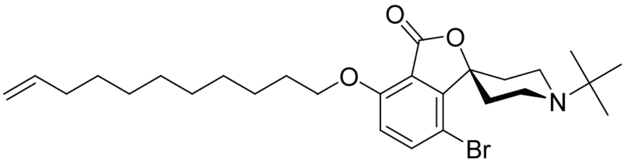

A dry Schlenk tube was charged with tetramethylpiperidine (4.63 mL, 27.21 mmol) and 16 mL of dry THF. The mixture was cooled to 0 °C, *n*-butyl lithium (1.6 M in hexanes, 17.01 mL, 27.21 mmol) were added dropwise, and the mixture was stirred at 0 °C for 1 h. After cooling to -50 °C, a solution of 5-bromo-2-(undec-10-enyloxy)benzoic acid **19** (4.57 g, 12.37 mmol) in 15 mL of dry THF was added dropwise over the course of 10 min. Stirring at -50 °C was continued for 7 min and a solution of *tert*-butyl piperidone **7b** (3.84 g, 24.74 mmol) in 5 mL of dry THF was added dropwise. After stirring at -50 °C for 1 h, the mixture was allowed to warm to room temperature and stirring was continued for 1 h. The mixture was quenched with 1N aq. HCl-solution, acidified with conc. aq.-HCl, and stirred for 18 h at room temperature. After adjusting the mixture to basic pH by addition of, phases were separated and the aqueous layer was extracted with ethyl acetate three times. Combined organic layers were washed with sat. aq. $NaHCO_3$-solution and brine three times, respectively, dried over $MgSO_4$, and the solvent was removed *in vacuo* to obtain 12.37 g of a crude mixture of products. Free carboxylic acids present in the crude mixture prevented successful purification and were therefore transformed into their respective methyl ester by the following procedure. The crude product mixture was dissolved in 50 mL of methanol, cooled to 0 °C, and EDC-HCl (3.32 g, 17.32 mmol) was added together with DMAP (0.53 g, 4.33 mmol). The mixture was allowed to warm to room temperature for 18 h and the solvent was removed *in vacuo*. The residue was collected in methylene chloride and the organic layer was washed with 1N aq. citric acid-solution three times, sat. aq. $NaHCO_3$-solution four-times, and brine three times. Drying of the organic layer over $MgSO_4$ and subsequent removal of the solvent *in vacuo* afforded a crude mixture, which was purified by column chromatography (silica gel, Hex/EA, 6/4 + 0.1 vol% Et_3N) to afford the product as a colorless solid (1.72 g, 36%). R_f (Hex/EA, 6/4 + 0.1 vol% Et_3N) = 0.30. ^{1}H-NMR ($CDCl_3$, 300 MHz): δ (ppm) = 7.63 (d, ^3J = 8.7 Hz, 1H, Ar-*H*), 6.80 (d, ^3J = 8.7 Hz, 1H, Ar-*H*), 5.85-5.72 (m, 1, =C*H*), 4.99-4.89 (m, 2H, =C*H*), 4.10 (t, ^3J = 6.8 Hz, 2H, $\mathrm{C}H_2$), 3.01-3.01 (m, 2H, $\mathrm{C}H_2$), 2.83-2.75 (m, 2H, $\mathrm{C}H_2$), 2.64-2.56 (m, 2H, $\mathrm{C}H_2$), 2.05-2.00 (m, 2H, $\mathrm{C}H_2$), 1.91-1.81 (m, 2H, $\mathrm{C}H_2$), 1.55-1.28 (m, 14H, $\mathrm{C}H_2$), 1.09 (s, 9H, $\mathrm{C}H_3$). ^{13}C-NMR ($CDCl_3$, 75 MHz): δ (ppm) = 166.15, 157.88, 152.93, 140.13, 139.28, 115.98, 114.22, 113.96, 105.43, 85.19, 69.44, 54.14, 42.19, 33.88, 33.59, 29.51, 29.47, 29.36, 29.18, 28.98, 28.80, 26.35, 25.83. DEPT135-NMR ($CDCl_3$): δ (ppm) = 140.13 (pos.), 139.28 (pos.), 114.22 (neg.), 113.96 (pos.), 69.44 (neg.), 42.19 (neg.), 33.88 (neg.), 33.59 (neg.), 29.51 (neg.), 29.47 (neg.), 29.36 (neg.), 29.18 (neg.), 28.98 (neg.), 28.80 (neg.), 26.35 (neg.), 25.83 (neg.). MS (ESI pos.): *m/z* = 508 ([M + H]$^+$), 506 ([M + H]$^+$). HRMS (ESI pos.): *m/z* = 506.2267 (calc. 506.2264 for $C_{27}H_{41}O_3N^{79}Br$). UPLC (Acquity UPLC column, gradient 50→95% CH_3CN/H_2O): t_R = 3.30 min (96% peak area).

5-Bromo-2-(undec-10-enyloxy)benzoic acid **19**

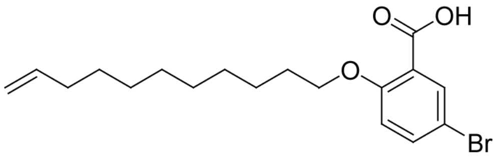

Methyl 5-bromo-2-(undec-10-enyloxy)benzoate **22** (3.71 g, 9.68 mmol) was dissolved in a mixture of 50 mL of THF and 25 mL of water. Addition of sodium hydroxide (6.78 g, 169.37 mmol) was followed by stirring at 50 °C for 16 h. The mixture was adjusted to acidic pH using conc. aq.-HCl. Phases were separated and the aqueous layer was extracted with ethyl acetate three times. Combined organic layers were washed with brine three times, dried over $MgSO_4$, and the solvent was removed *in vacuo*.

Recrystallization of the crude material from cold hexane afforded pure product as a colorless solid (3.57 g, 100%). R_f (Hex/EA, 8/2) = 0.16. ^{1}H-NMR ($CDCl_3$, 300 MHz): δ (ppm) = 10.54 (s, broad, 1H, CO_2*H*), 8.24 (d, ^4J = 2.63 Hz, 1H, Ar-*H*), 7.61 (dd, ^3J = 8.86 Hz, ^4J = 2.63 Hz, 1H, Ar-*H*), 6.93 (d, ^3J = 8.86 Hz, 1H, Ar-*H*), 5.85-5.72 (m, 1H, =C*H*), 5.01-4.88 (m, 2H, =C*H*), 4.21 (t, ^3J = 6.6 Hz, 2H, CH_2), 2.05-2.01 (m, 2H, CH_2), 1.98-1.84 (m, 2H, CH_2), 1.51-1.23 (m, 12H, CH_2). ^{13}C-NMR ($CDCl_3$, 75 MHz): δ (ppm) = 164.42, 156.74, 139.19, 137.64, 136.12, 119.41, 114.61, 114.48, 114.25, 70.79, 33.84, 29.41, 29.39, 29.22, 29.11, 28.94, 28.89, 25.86. DEPT135-NMR ($CDCl_3$): δ (ppm) = 139.19 (pos.), 137.64 (pos.), 136.12 (pos.), 114.61 (pos.), 114.25 (neg.), 70.79 (neg.), 33.84 (neg.), 29.41 (neg.), 29.39 (neg.), 29.22 (neg.), 29.11 (neg.), 28.94 (neg.), 28.89 (neg.), 25.86 (neg.). MS (ESI pos.): *m/z* = 371 ($[M + H]^+$), 369 ($[M + H]^+$). HRMS (ESI pos.): *m/z* = 369.1055 (calc. 369.1060 for $C_{18}H_{26}O_3{}^{79}Br$). UPLC (Acquity UPLC column, gradient 50→95% CH_3CN/H_2O): t_R = 5.72 min (98% peak area).

Methyl 5-bromo-2-hydroxybenzoate **21**

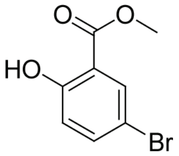

5-Bromo-2-hydroxybenzoic acid **20** (21.70 g, 100.0 mmol) was dissolved in 50 mL of methanol and 10 mL of conc. sulfuric acid were added in portions. The mixture was heated to reflux for 6 h. The mixture was poured on ice and the aqueous layer was extracted with methylene chloride three times. Combined organic layers were washed with sat. aq. $NaHCO_3$-solution and brine three times, respectively, and subsequently dried over $MgSO_4$. Removal of solvent afforded 20.28 g of product as a colorless solid (88.0 mmol, 88%). R_f (CH_2Cl_2/Hex, 2/8) = 0.28. ^{1}H-NMR ($CDCl_3$, 300 MHz): δ (ppm) = 10.69 (s, 1H, O*H*), 7.94 (d, ^4J = 2.5 Hz, 1H, Ar-*H*), 7.51 (dd, ^3J = 8.9 Hz, ^4J = 2.53 Hz, 1H, Ar-*H*), 6.88 (d, ^3J = 8.9 Hz, 1H, Ar-*H*), 3.95 (s, 3H, CH_3). ^{13}C-NMR ($CDCl_3$, 75 MHz): δ (ppm) = 169.6, 169.7, 138.5, 132.3, 119.7, 113.9, 110.9, 52.7.

DEPT135-NMR ($CDCl_3$): δ (ppm) =138.5 (pos.), 132.2 (pos.), 119.7 (pos.), 52.73 (pos.). MS (ESI neg.): *m/z* = 231 ($[M - H]^-$), 229 ($[M - H]^-$). HRMS (ESI neg.): *m/z* = 228.9503 (calc. 228.9506 for $C_8H_6O_3{}^{79}Br$). UPLC (Acquity UPLC column, gradient 5→50% CH_3CN/H_2O): t_R = 6.95 min (90% peak area).

Methyl 5-bromo-2-(undec-10-enyloxy)benzoate **22**

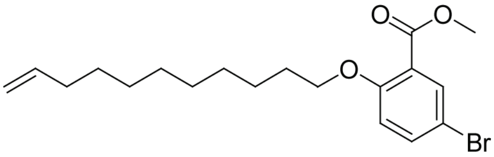

Methyl 5-bromo-2-hydroxybenzoate **21** (11.55 g, 50.0 mmol), K_2CO_3 (16.59 g, 120.0 mmol), and tetrabutylammonium iodide (1.85 g, 0.1 mmol) were dissolved in 80 mL of dry DMF and 11-bromo-1-undecane was added to the stirring mixture. The mixture was heated to 100 °C for 18 h and the majority of the solvent was subsequently removed by vacuum distillation. The residue was dissolved in water and the aqueous layer was extracted with methylene chloride three times. Combined organic layers were washed with brine three times, dried over $MgSO_4$, and the solvent was removed *in vacuo*. Purification of the residue by column chromatography (silica gel, CH_2Cl_2/Hex, 3/7) afforded the product as a colorless solid (18.07 g, 94%).). R_f (CH_2Cl_2/Hex, 3/7) = 0.20. ^{1}H-NMR ($CDCl_3$, 300 MHz): δ (ppm) = 7.87 (d, ^4J = 2.43 Hz, 1H, Ar-*H*), 7.48 (dd, ^3J = 8.85 Hz, ^4J = 2.43 Hz, 1H, Ar-*H*), 6.81 (d, ^3J = 8.85 Hz, 1H, Ar-*H*), 5.86-5.72 (m, 1H, =C*H*), 5.00-4.89 (m, 2H, =C*H*), 3.97 (t, ^3J = 6.5 Hz, 2H, CH_2), 3.86 (s, 3H, CH_3), 2.05-1.99 (m, 2H, CH_2), 1.84-1.75 (m, 2H, CH_2), 1.45-1.29 (m, 10H, CH_2). ^{13}C-NMR ($CDCl_3$, 75 MHz): δ (ppm) = 165.54, 157.82, 139.20, 135.96, 134.19, 122.07, 115.01, 114.21, 112.02, 69.30, 52.17, 33.86, 29.56, 29.47, 29.35, 29.17, 29.11, 28.98, 25.93. DEPT135-NMR ($CDCl_3$): δ (ppm) = 139.20 (pos.), 135.96 (pos.), 134.19 (pos.), 115.01 (pos.), 114.21 (neg.), 69.30 (neg), 52.17 (neg.), 33.86 (neg.), 29.56 (neg.), 29.47 (neg.), 29.34 (neg.), 29.17 (neg.), 29.10 (neg.), 28.98 (neg.), 25.86 (neg.). MS (ESI pos.): *m/z* = 385 ($[M + H]^+$), 383 ($[M + H]^+$). HRMS (ESI pos.): *m/z* = 383.1221 (calc.

383.1219 for $C_{19}H_{28}O_3{}^{79}Br$). UPLC (Acquity UPLC column, gradient 40→95% CH_3CN/H_2O): t_R = 5.33 min (95% peak area).

Monochlorosilane **23**

Monochlorosilane **23** was synthesized adopting a synthesis described by Tully et. al.[52]

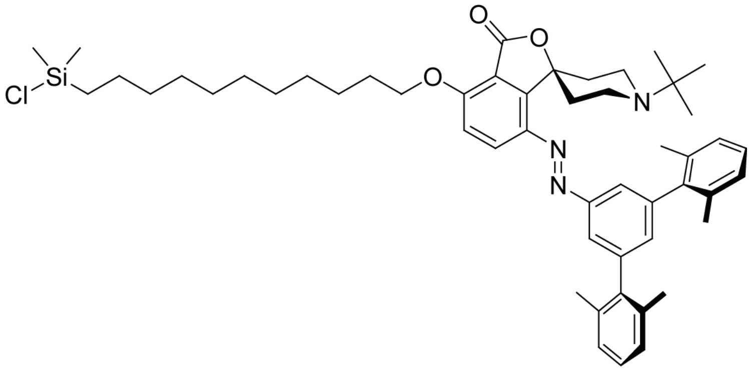

A dry Schlenk tube was charged with 10 mg of immobilization precursor **16** (0.013 mmol, 1 equiv.), one drop of Karsted's catalyst (platinum(0)-1,3-divinyl-1,1,3,3-tetramethyldisiloxane complex, 0.10 M solution in xylene), and 1 mL of methylene chloride under an atmosphere of argon. The mixture was stirred at room temperature for 25 min and 145 µL dimethylchlorosilane (1.30 mmol, 100 equiv.) were added in one portion. The mixture was stirred for 18 h at room temperature. The solvent was removed *in vacuo* and the orange material obtained was directly used without further characterization.

3.8.7.10 Supported Catalysts

Catalysts supported on different substrates were synthesized adopting a procedure described by Tully et. al.[52]

Supported catalyst **24**

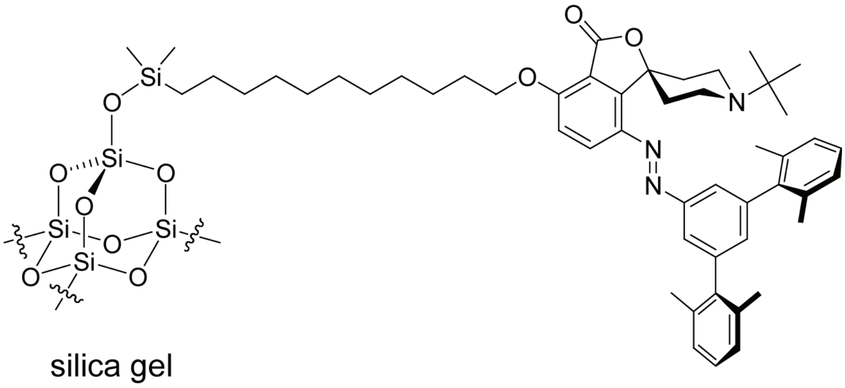

A dry Schlenk flask was charged with 11 mg of monochlorsilane **23** (0.013 mmol), 200 mg of silica gel (as received), and 2 mL of dry toluene. After addition of 3 drops of dry triethyl amine, the mixture was stirred under an atmosphere of argon at room temperature for 24 h. The solid was collected by centrifugation and extensively washed with toluene, ethyl acetate, and methylene chloride/methanol mixtures, respectively. The gray powder was dried *in vacuo*. For characterization by UV/vis spectroscopy, see Section 3.6.5.

Immobilization in quartz slides

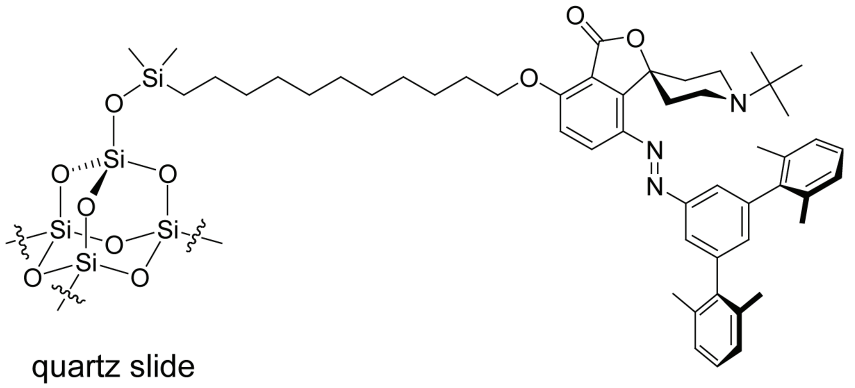

For surface activation, a quartz slide was immersed in mixtures of concentrated sulfuric acid with 30% hydrogen peroxide (1/1 = vol/vol) for 45 minutes. Subsequently, the slides were extensively washed with water, acetone, and diethyl ether, blown dry under a stream of argon, and immediately used for functionalization with freshly prepared monochlorosilane **23**. Therefore, the quartz slide was immersed in a solution of approx. 10 mg of monochlorosilane **23** in 2 mL of dry toluene and 3 drops of dry triethyl amine were added. The flask was sealed under an atmosphere of argon and the mixture was carefully stirred for 3 days. The slide was removed from the mixture and extensively washed with toluene, ethyl acetate, ethanol, ethyl acetate, toluene, and diethyl ether in the given order. The slide was blown dry under a stream of argon and carefully dried *in vacuo*. For characterization attempts, see section 3.6.5.

Immobilization of silicon wafers

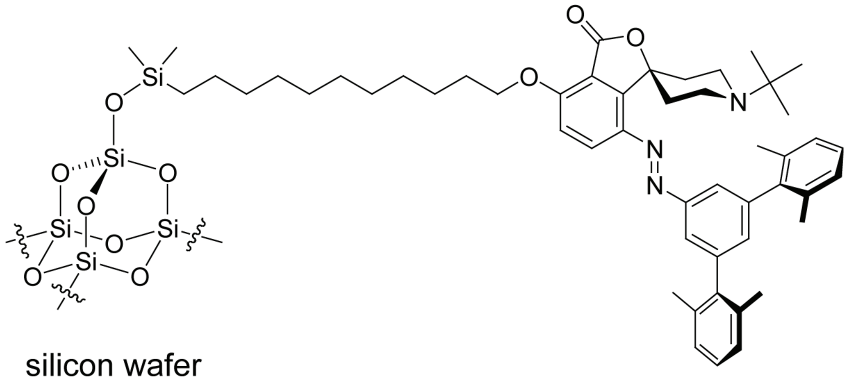

A silicon wafer was carefully washed with ethanol, ethyl acetate, acetone, and diethyl ether, respectively, and blown dry under a stream of argon. Subsequently, the silicon wafer was immersed in a solution of approx. 10 mg of monochlorosilane **23** (0.013 mmol) in 2 mL of dry toluene and 3 drops of dry triethyl amine were added. The flask was sealed under an atmosphere of argon and the mixture was carefully stirred for 3 days. The wafer was removed from the mixture and extensively washed with toluene, ethyl acetate, ethanol, ethyl acetate, toluene, and diethyl ether in the given order. The slide was blown dry under a stream of argon and carefully dried *in vacuo*. For characterization attempts, see section 3.6.5.

3.9 Literature

(1) Ueno, A.; Takahashi, K.; Osa, T. *Chem. Commun.* **1981**, 94-96; Ueno, A.; Takahashi, K.; Osa, T. *Chem. Commun.* **1980**, 837-838; Würthner, F.; Rebek, J., Jr. *Angew. Chem., Int. Ed. Engl.* **1995**, *34*, 446-450; Würthner, F.; Rebek, J., Jr. *J. Chem. Soc., Perkin Trans. 2* **1995**, 1727-1734; Sugimoto, H.; Kimura, T.; Inoue, S. *J. Am. Chem. Soc.* **1999**, *121*, 2325-2326; Cacciapaglia, R.; Di Stefano, S.; Mandolini, L. *J. Am. Chem. Soc.* **2003**, *125*, 2224-2227; Sud, D.; Norsten, T. B.; Branda, N. R. *Angew. Chem., Int. Ed. Engl.* **2005**, *44*, 2019-2021. The only exception relates to a photoswitchable Lewis acid, however no catalysis was reported: Lemieux, V.;

Spantulescu, M. D.; Baldridge, K. K.; Branda, N. R. *Angew. Chem., Int. Ed. Engl.* **2008**, *47*, 5034-5037.

(2) Peters, M. V.; Stoll, R. S.; Kuehn, A.; Hecht, S. *Angew. Chem., Int. Ed. Engl.* **2008**, *47*, 5968-5972.

(3) Peters, M. V.; Goddard, R.; Hecht, S. *J. Org. Chem.* **2006**, *71*, 7846-7849; Peters, M. V.; Stoll, R. S.; Goddard, R.; Buth, G.; Hecht, S. *J. Org. Chem.* **2006**, *71*, 7840-7845.

(4) Dondoni, A.; Massi, A. *Angew. Chem., Int. Ed. Engl.* **2008**, *47*, 4638-4660.

(5) Dove, A. P.; Pratt, R. C.; Lohmeijer, B. G. G.; Waymouth, R. M.; Hedrick, J. L. *J. Am. Chem. Soc.* **2005**, *127*, 13798-13799; Kamber, N. E.; Jeong, W.; Waymouth, R. M.; Pratt, R. C.; Lohmeijer, B. G. G.; Hedrick, J. L. *Chem. Rev.* **2007**, *107*, 5813-5840.

(6) Eliel, E. L.; Wilen, S. H. *Stereochemistry of Organic Compounds*; Wiley: New York, 1994.

(7) Peters, M., V. Dissertation, Humboldt-Universität zu Berlin, 2008.

(8) Gohier, F.; Mortier, J. *J. Org. Chem.* **2003**, *68*, 2030-2033.

(9) Parham, W. E.; Egberg, D. C.; Sayed, Y. A.; Thraikill, R. W.; Keyser, G. E.; Neu, M.; Montgomery, W. C.; Jones, L. D. *J. Org. Chem.* **1976**, *41*, 2628-2633.

(10) Amato, J. S.; Chung, J. Y. L.; Cvetovich, R. J.; Reamer, R. A.; Zhao, D.; Zhou, G.; Gong, X. *Org. Process Res. Dev.*. **2004**, *8*, 939-941.

(11) Amato, J. S.; Chung, J. Y. L.; Cvetovich, R. J.; Gong, X.; McLaughlin, M.; Reamer, R. A. *J. Org. Chem.* **2005**, *70*, 1930-1933.

(12) Wolter, M.; Klapars, A.; Buchwald, S. L. *Org. Lett.* **2001**, *3*, 3803-3805.

(13) Du, C. J. F.; Hart, H.; Ng, K. K. D. *J. Org. Chem.* **1986**, *51*, 3162-3165.

(14) Vinod, T. K.; Hart, H. *J. Org. Chem.* **1991**, *56*, 5630-5640.

(15) Lim, Y.-K.; Lee, K.-S.; Cho, C.-G. *Org. Lett.* **2003**, *5*, 979-982.

(16) Lim, Y.-K.; Choi, S.; Park, K. B.; Cho, C.-G. *J. Org. Chem.* **2004**, *69*, 2603-2606.

(17) Brown, H. C.; Gupta, S. K. *J. Am. Chem. Soc.* **1972**, *94*, 4370-4371.

(18) Kessler, H. *Angew. Chem., Int. Ed. Engl.* **1970**, *9*, 219-235.

(19) Perrin, C. L.; Dwyer, T. J. *Chem. Rev.* **1990**, *90*, 935-967.

(20) Thiele, C. M. *Concepts Magn. Reson.* **2007**, *30A*, 65-80.

(21) Thiele, C. M.; Berger, S. *Org. Lett.* **2003**, *5*, 705-708; Thiele, C. M. *Eur. J. Org. Chem.* **2008**, 5673-5685.

(22) dos Santos, F. P.; Tormena, C. F. *Theochem* **2006**, *763*, 145-148.

(23) Crowley, P. J.; Robinson, M. J. T.; Ward, M. G. *Tetrahedron* **1977**, *33*, 915-925.

(24) Thiele, C. M.; Marx, A. *Chem. Eur. J.* **2009**, *15*, 254-260.

(25) Thiele, C. M. *Angew. Chem., Int. Ed. Engl.* **2005**, *44*, 2787-2790.

(26) Zweckstetter, M.; Bax, A. *J. Am. Chem. Soc.* **2000**, *122*, 3791-3792.

(27) Thiele, C. M. *J. Org. Chem.* **2004**, *69*, 7403-7413.

(28) Leong, M. K.; Mastryukov, V. S.; Boggs, J. E. *J. Phys. Chem.* **1994**, *98*, 6961-6966.

(29) Leuthäußer, S.; Schmidts, V.; Thiele, C. M.; Plenio, H. *Chem. Eur. J.* **2008**, *14*, 5465-5481.

(30) Dürr, H.; Bouas-Laurent, H. *Photochromism: Molecules and Systems: Revised Edition*, 2003; El'tsov, A. V. *Organic Photochromes*; 1. ed.; Consultants Bureau: New York, 1990.

(31) Schulte-Fröhlinde, D. *Liebigs Ann. Chem.* **1958**, *612*, 131-138.

(32) Eyring, H. *Chem. Rev.* **1935**, *17*, 65-77; Eyring, H. *J. Chem. Phys.* **1935**, *3*, 107-115.

(33) Gegiou, D.; Muszkat, K. A.; Fischer, E. *J. Am. Chem. Soc.* **1968**, *90*, 3907-3918.

(34) Le Fèvre, R. J. W.; Northcott, J. *J. Chem. Soc.* **1953**, 867-870.

(35) Gonzalez, C.; Schlegel, H. B. *J. Phys. Chem.* **1990**, *94*, 5523-5527; Gonzalez, C.; Schlegel, H. B. *J. Chem. Phys.* **1989**, *90*, 2154-2161.

(36) Crecca, C. R.; Roitberg, A. E. *J. Phys. Chem. A* **2006**, *110*, 8188-8203.

(37) Bouas-Laurent, H.; Dürr, H. *Pure Appl. Chem.* **2001**, *73*, 639-665.

(38) Biondic, M. C.; Erra-Balsells, R. *J. Chem. Soc., Perkin Trans. 2* **1997**, 1323-1327; Leito, I.; Kaljurand, I.; Koppel, I. A.; Yagupolskii, L. M.; Vlasov, V. M. *J. Org.*

Chem. **1998**, *63*, 7868-7874; Kaljurand, I.; Rodima, T.; Leito, I.; Koppel, I. A.; Schwesinger, R. *J. Org. Chem.* **2000**, *65*, 6202-6208.

(39) Kolthoff, I. M.; Chantooni, M. K., Jr.; Bhowmik, S. *Anal. Chem.* **1967**, *39*, 315-320.

(40) Henry, L. *Comptes Rendus Hebdomadaires des Seances de l'Academie des Sciences* **1895**, *120*, 1265-8; Luzzio, F. A. *Tetrahedron* **2001**, *57*, 915-945.

(41) Hunter, C. A.; Lawson, K. R.; Perkins, J.; Urch, C. J. *J. Chem. Soc., Perkin Trans. 2* **2001**, 651-669; Meyer, E. A.; Castellano, R. K.; Diederich, F. *Angew. Chem., Int. Ed. Engl.* **2003**, *42*, 1210-1250.

(42) In a recent B3LYP study of the Henry reaction catalyzed by a Cinchona alkaloid, a barrier of 10.8 kcal/mol for deprotonation of nitromethane has been computed in a THF continuum: Hammar, P.; Marcelli, T.; Hiemstra, H.; Himo, F. *Adv. Synt. Cataly.* **2007**, *349*, 2537-2548.

(43) Seeman, J. I. *Chem. Rev.* **1983**, *83*, 83-134.

(44) Seeman, J. I.; Farone, W. A. *J. Org. Chem.* **1978**, *43*, 1854-1864.

(45) Samori, P. *J. Mater. Chem.* **2004**, *14*, 1353-1366; Grimsdale, A. C.; Mullen, K. *Angew. Chem., Int. Ed. Engl.* **2005**, *44*, 5592-5629.

(46) Rabe, J. P.; Buchholz, S. *Phys. Rev. Lett.* **1991**, *66*, 2096-2099; Rabe, J. P.; Buchholz, S. *Science* **1991**, *253*, 424-427.

(47) Ulman, A. *Chem. Rev.* **1996**, *96*, 1533-1554.

(48) Buriak, J. M. *Chem. Rev.* **2002**, *102*, 1271-1308; Linford, M. R.; Chidsey, C. E. D. *J. Am. Chem. Soc.* **1993**, *115*, 12631-12632; Cleland, G.; Horrocks, B. R.;

Houlton, A. *J. Chem. Soc., Faraday Trans.* **1995**, *91*, 4001-4003; Cicero, R. L.; Linford, M. R.; Chidsey, C. E. D. *Langmuir* **2000**, *16*, 5688-5695; Boukherroub, R.; Morin, S.; Sharpe, P.; Wayner, D. D. M.; Allongue, P. *Langmuir* **2000**, *16*, 7429-7434; Wayner, D. D. M.; Wolkow, R. A. *J. Chem. Soc., Perkin Trans. 2* **2002**, 23-34.

(49) Khire, V. S.; Yi, Y.; Clark, N. A.; Bowman, C. N. *Adv. Mater.* **2008**, *20*, 3308-3313; Khire, V. S.; Lee, T. Y.; Bowman, C. N. *Macromolecules* **2008**, *41*, 7440-7447; Jonkheijm, P.; Weinrich, D.; Koehn, M.; Engelkamp, H.; Christianen, P. C. M.; Kuhlmann, J.; Maan, J. C.; Nuesse, D.; Schroeder, H.; Wacker, R.; Breinbauer, R.; Niemeyer, C. M.; Waldmann, H. *Angew. Chem., Int. Ed. Engl.* **2008**, *47*, 4421-4424; Campos, L. M.; Meinel, I.; Guino, R. G.; Schierhorn, M.; Gupta, N.; Stucky, G. D.; Hawker, C. J. *Adv. Mater.* **2008**, *20*, 3728-3733; Killops, K. L.; Campos, L. M.; Hawker, C. J. *J. Am. Chem. Soc.* **2008**, *130*, 5062-5064; Campos, L. M.; Killops, K. L.; Sakai, R.; Paulusse, J. M. J.; Damiron, D.; Drockenmuller, E.; Messmore, B. W.; Hawker, C. J. *Macromolecules* **2008**, *41*, 7063-7070.

(50) Cozzi, F. *Adv. Synt. Cataly.* **2006**, *348*, 1367-1390; Benaglia, M.; Puglisi, A.; Cozzi, F. *Chem. Rev.* **2003**, *103*, 3401-3429.

(51) Andersch, J.; Tschierske, C.; Diele, S.; Lose, D. *J. Mater. Chem.* **1996**, *6*, 1297-1307.

(52) Tully, D. C.; Wilder, K.; Fréchet, J. M. J.; Trimble, A. R.; Quate, C. F. *Adv. Mater.* **1999**, *11*, 314-318.

(53) Nishimura, N.; Sueyoshi, T.; Yamanaka, H.; Imai, E.; Yamamoto, S.; Hasegawa, S. *Bull. Chem. Soc. Jpn.* **1976**, *49*, 1381; Dri, C.; Peters, M. V.; Schwarz, J.; Hecht, S.; Grill, L. *Nature Nanotechnology* **2008**, *3*, 649-653.

(54) *Handbook of Chemistry and Physics*; 76 ed.; Lide, D. R., Ed.; CRC Press: New York, 1995.

(55) Meissner, A.; Sorensen, O. W. *Magn. Reson. Chem.* **2001**, *39*, 49-52.

(56) Becke, A. D. *J. Chem. Phys.* **1993**, *98*, 5648-5652; Lee, C. T.; Yang, W. T.; Parr, R. G. *Physical Review B* **1988**, *37*, 785-789.

(57) Dunning, T. H. *J. Chem. Phys.* **1989**, *90*, 1007-1023.

(58) Barone, V.; Cossi, M.; Tomasi, J. *J. Comput. Chem.* **1998**, *19*, 404-417; Cossi, M.; Scalmani, G.; Rega, N.; Barone, V. *J. Chem. Phys.* **2002**, *117*, 43-54; Cossi, M.; Crescenzi, O. *J. Chem. Phys.* **2003**, *118*, 8863-8872.

(59) Frisch, M. J.; Trucks, G. W.; Schlegel, H. B.; Scuseria, G. E.; Robb, M. A.; Cheeseman, J. R.; J. A. Montgomery, J.; Vreven, T.; Kudin, K. N.; Burant, J. C.; Millam, J. M.; Iyengar, S. S.; Tomasi, J.; Barone, V.; Mennucci, B.; Cossi, M.; Scalmani, G.; Rega, N.; Petersson, G. A.; Nakatsuji, H.; Hada, M.; Ehara, M.; Toyota, K.; Fukuda, R.; Hasegawa, J.; Ishida, M.; Nakajima, T.; Honda, Y.; Kitao, O.; Nakai, H.; Klene, M.; Li, X.; Knox, J. E.; Hratchian, H. P.; Cross, J. B.; Adamo, C.; Jaramillo, J.; Gomperts, R.; Stratmann, R. E.; Yazyev, O.; Austin, A. J.; Cammi, R.; Pomelli, C.; Ochterski, J. W.; Ayala, P. Y.; Morokuma, K.; Voth, G. A.; Salvador, P.; Dannenberg, J. J.; Zakrzewski, V. G.; Dapprich, S.; Daniels, A. D.; Strain, M. C.; Farkas, O.; Malick, D. K.; Rabuck, A. D.; Raghavachari, K.; Foresman, J. B.; Ortiz, J. V.; Cui, Q.; A. G. Baboul; Clifford, S.; Cioslowski, J.; Stefanov, B. B.; Liu, G.; Liashenko, A.; Piskorz, P.; Komaromi, I.; Martin, R. L.; Fox, D. J.; Keith, T.; Al-Laham, M. A.; Peng, C. Y.; Nanayakkara, A.; Challacombe, M.; Gill, P. M. W.; Johnson, B.; W. Chen, M.; Wong, W.; Gonzalez, C.; Pople, J. A.; Gaussian, Inc.: Pittsburgh PA, 2003.

(60) Miura, Y.; Matsumoto, M.; Ushitani, Y.; Teki, Y.; Takui, T.; Itoh, K. *Macromolecules* **1993**, *26*, 6673-6675.

4 Towards Photoswitchable *N*-Heterocyclic Carbenes

4.1 Introduction

4.1.1 *N*-Heterocyclic Carbenes

Carbenes are defined as neutral compounds of divalent carbon, with the carbon atom having only six valence electrons.[1-3] The structure of carbenes can vary from linear to bent geometry, depending on the substituents. Linear carbenes possess two degenerate p-orbitals p_x and p_y on a sp-hybridized carbon atom (Figure 1). Degeneracy of the two p-orbitals leads to a triplet ground state, giving these carbenes substantial diradical character. However, most carbenes adopt a bent geometry and the carbon atom is therefore sp^2-hypridized. Compared to the sp-hybridized carbenes, one p-orbital remains essentially unperturbed, while the other p-orbital is mixed with a set of symmetrical σ-orbitals to yield a net stabilization of the orbital due to the increased s-character. These orbitals are referred to as p_π and σ, respectively. Depending on the energetic difference of p_π and σ, bent carbenes can either exits in a triplet or singlet ground state (Figure 1).

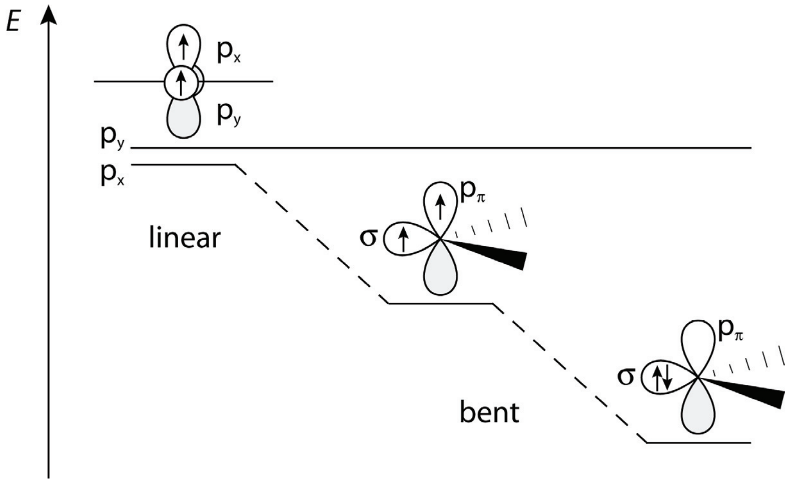

Figure 1: Schematic representation of frontier orbitals of carbenes having different geometries. Possible electron configurations are given as well.

The ground state multiplicity of sp^2-hybridized carbenes is influenced by the substituents on the divalent carbon atom. A large energy difference between p_π and σ is favored by σ-electron-withdrawing, that is electronegative, substituents, whereas σ-electron-donating substituents have the opposite effect. In addition to inductive effects, mesomeric effect influence the electronic situation of the carbene. In the following, only five-membered heterocyclic carbenes with π-donating substituents will be discussed due to their exceptional importance in organic chemistry. For other carbenes, the reader is referred to the literature.[3]

Singlet carbenes with two strongly π-donating substituents on the carbene center are strongly bent and experience an exceptional stabilization due to the substantial transfer of electron density from the π-donors to the electron-deficient carbene carbon (Figure 2). Most frequently encountered π-donors are nitrogen atoms, while sulfur, oxygen, or phosphorus atoms have been used much less. Incorporation of the carbene into a heterocyclic ring further increases the extent of mesomeric stabilization due to the enhanced conjugation between the donor p_π orbitals and the vacant carbene p_π orbital (Figure 2). In heterocyclic five-membered systems it is possible to replace one nitrogen donor with a CR_2-moiety without loosing too much stabilization, rendering these species relatively stable and observable under "normal" inert conditions. Five-membered heterocyclic carbenes based on the imidazole- or imidazolinium-framework are commonly referred to as N-heterocyclic carbenes (NHCs).[1-3]

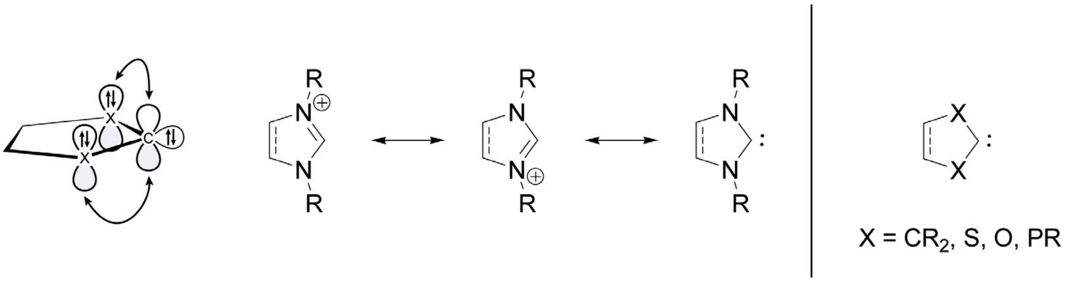

Figure 2: Mesomeric effects operating in five-membered heterocyclic carbenes.

The search for stable carbenes was initiated in the early 1960s by Wanzlick's report on the α-elimination of chloroform from 2-(trichloromethyl)-1,3-diphenylimidazolidine (Scheme 1).[4] However, it was not possible to isolate the free diphenylimidazolidin-2-ylidene from the reaction mixture. Instead, the corresponding dimer was isolated in good yields. Cross-metathesis experiments with dimers carrying distinguishable substituents revealed no cross-over between the electron-rich entetramines, thereby excluding an equilibrium between dimer and free carbene.[5] Much later, equilibria between electron-rich tetraaminoethylenes and carbenes could be identified and were investigated in great detail.[6]

Scheme 1: Wanzlick's synthesis of the dimer of diphenylimidazolidin-2-ylidene.

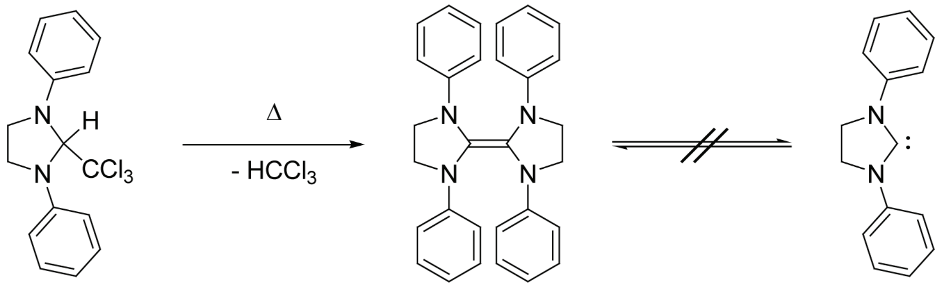

The first stable carbene was isolated by Arduengo and co-workers in 1990 by deprotonation of *N,N'*-diadamantyl imidazolium chloride (Scheme 2).[7] The carbene was unambiguously identified by x-ray crystal structural analysis. Since this first report on stable carbenes, numerous derivatives of the initial NHC have been synthesized[1-3,8] and found widespread use as ligands for complexes of outstanding catalytic performance.[9-11] Applications of NHC complexes in C-C cross-coupling reactions[12] and their use in highly efficient metathesis catalysts[13] constitute excellent examples for their performance as ligands. The application of NHC ligands in Grubb's second generation Ru-catalyst for olefin metathesis largely improved the utility of this powerful methodology, finally leading to the Nobel Prize in 2005 for Grubbs, Schrock, and Chauvin.

Scheme 2: Synthesis of the first stable carbene by Arduengo and co-workers.

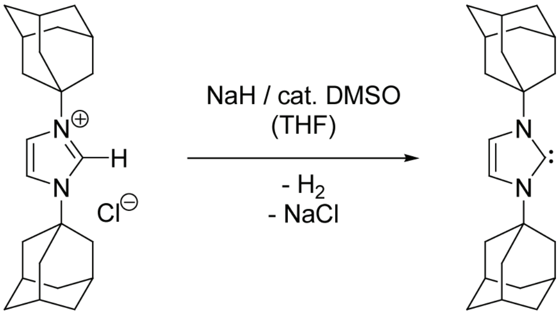

Beyond their application as ligands in organometallic complexes, NHCs found widespread application as organocatalysts.[11,14] The benzoin condensation is generally catalyzed by cyanide ions, but can also be brought about by use of catalytic amounts of thiazolium salts (Scheme 3). Classical "Umpolung" intermediates are encountered in the cyanide catalyzed reaction, whereas the mechanism of the reaction catalyzed by thiazolium salts was discussed controversially.

Scheme 3: Benzoin condensation catalyzed by cyanide ions or thiazolium Salts.

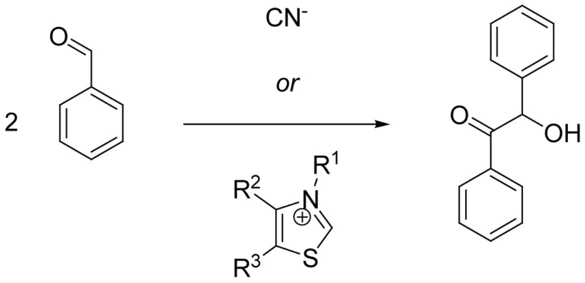

Breslow was the first to formulate a mechanism involving carbene intermediates for the benzoin condensation brought about by thiazolium salts (Scheme 4).[15] He assumed that the thiazolium salt is deprotonated at its most acidic position between the two heteroatoms to give a *N*-heterocyclic carbene, namely a thiazolin-2-ylidene. Addition of the nucleophilic carbene to benzaldehyde gives a zwitterionic intermediate, which subsequently tautomerizes to a neutral species. The resonance-stabilized enaminol-type intermediate is nucleophilic enough to add to another benzaldehyde electrophile. Elimination of benzoin from the zwitterionic intermediate regenerates the catalyst.

Scheme 4: Breslow's mechanism for the benzoin condensation catalyzed by thiazolium salts.

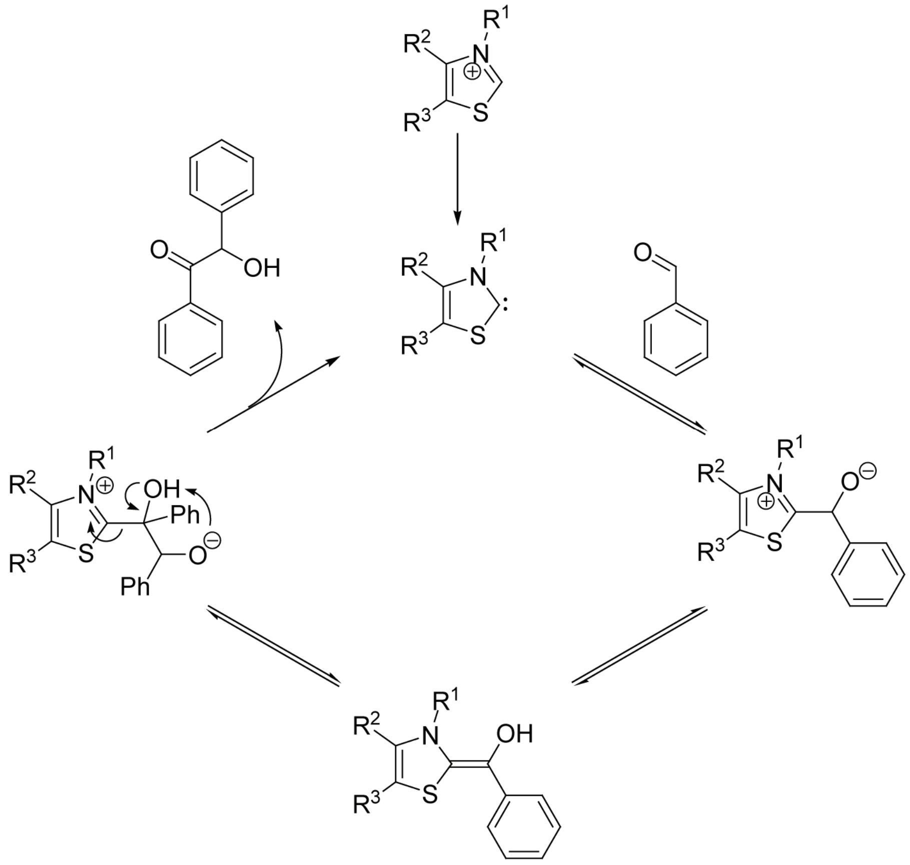

The mechanism proposed by Breslow is closely related to the mode of action of certain transketolase enzymes in the presence of the coenzyme thiamine (vitamin B_1, Scheme 5). Inter alia, this coenzyme is present in baker's yeast and might serve as an example for highly selective chemical reactions that can be accomplished *in vivo*.

Scheme 5: Coenzyme Thiamine (Vitamin B_1).

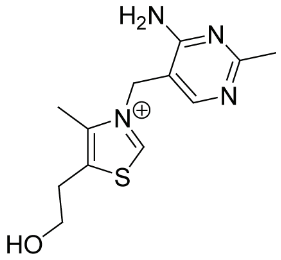

After the discovery of the thiazolium salt-mediated benzoin condensation, many other organic transformation catalyzed by NHCs were reported. It is beyond the scope of this text to give a complete review, so only a few exemplary transformation will be discussed. For comprehensive reviews of organocatalytic properties of NHCs the reader is referred to the literature.[11,14]

The benzoin condensation is an example of an highly efficient C-C bond formation brought about by NHCs (Scheme 6, path *A*). Chiral NHC catalysts efficiently transfer their stereogenic information to the substrate, thereby controlling the stereochemical outcome of the reaction. Electron-rich enaminol intermediates involved in the initial steps of the reaction can also be trapped by α,β-unsaturated carbonyl compounds in the Stetter reaction (Scheme 6, path *B*). As for the benzoin condensation, use of chiral NHC derivatives allows to control the stereogenic outcome of the reaction. The benzoin condensation and the Stetter reaction constitute important transformations in natural product synthesis, since the products constitute valuable intermediates in the synthesis of many natural products. The scope of NHCs as organocatalysts was markedly expanded by recognizing their ability to form homoenolates upon reaction with α,β-unsaturated carbonyl compounds. Homoenolates are interesting intermediates for numerous transformation, e.g. for cross-condensations with aldehydes (Scheme 6, path *C*) or for trapping with nucleophiles after protonation (Scheme 6, path *D*).

Scheme 6: Selected NHC-mediated transformations: benzoin condensation (*A*), Stetter reaction (*B*), condensation of enals with aldehydes (*C*), and trapping of homoenolates with nucleophiles (*D*).

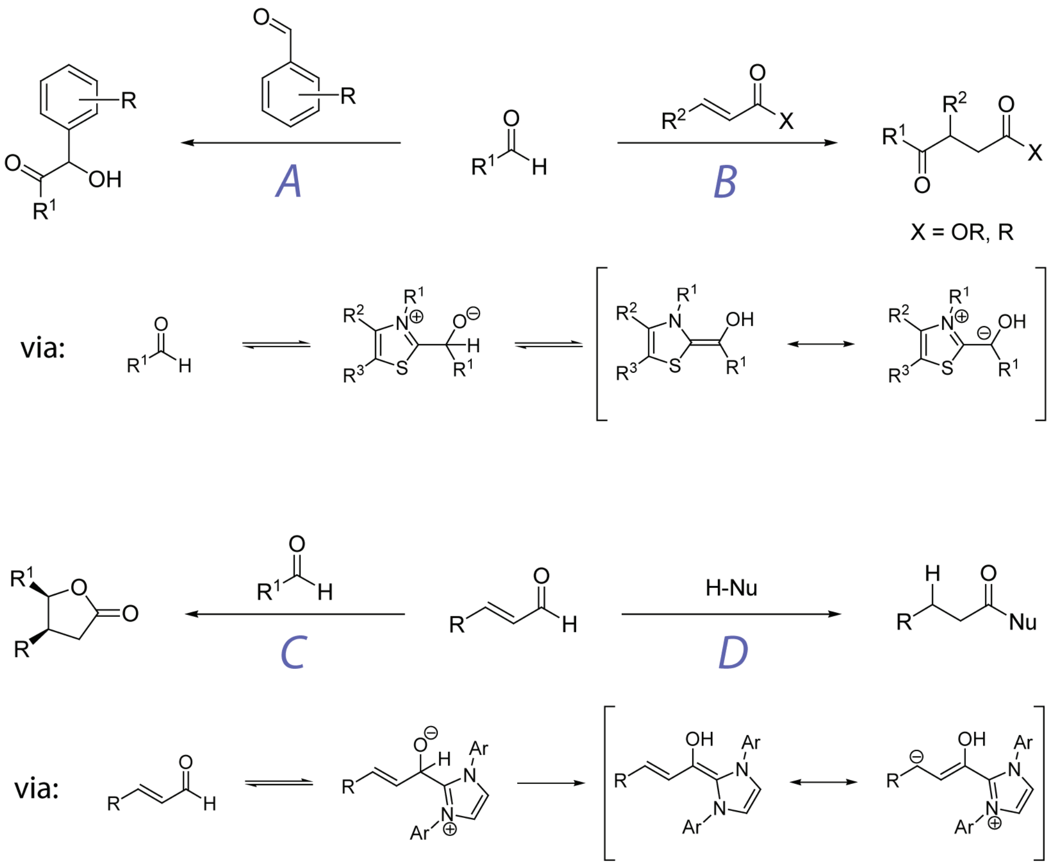

Transesterifications constitute another important transformation catalyzed by a number of NHCs (Scheme 7). The reaction does not proceed via acylated-NHC intermediates, but through hydrogen-bonded carbene-alcohol complexes.[16] A key intermediate is shown in Scheme 7.

Scheme 7: Transesterification reactions catalyzed by NHCs.

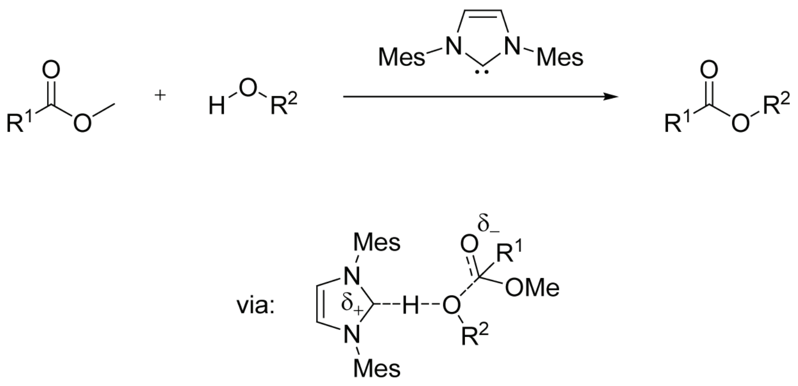

Ring-opening polymerization (ROP) of lactide and other cyclic esters provides a convenient access to interesting biodegradable polyesters. These materials found wide application in fibers, coatings, surgical sutures, and compounding medicines for the controlled release of drugs.[17] Especially in light of medicinal applications, organocatalytic pathways offer the advantage of obtaining materials not contaminated with potentially toxic metals. Several organocatalytic pathways towards ROP of cyclic esters have been developed, ranging from enzymatic reactions to NHC-catalyzed polymerizations.[18] NHCs are extremely efficient catalysts for the ROP of lactide (Scheme 8). High molecular weights and narrow polydispersities of the polymers obtained point to the living character of the polymerization.[19-22] For the ROP of lactide, the mechanism involves initial attack of the carbene at the electrophilic carbonyl carbon of lactide (Scheme 8). The initial adduct is in equilibrium with a ring-opened analogue, which is protonated by the initiator or the polymer chain in the next step. Some sort of interaction is believed to occur between the activated monomer and the alcohol, finally leading to an acyl group transfer and regeneration of the catalyst. Noteworthy, preparation of NHC-alcohol adducts renders use of the initiators obsolete, because the catalyst as well as the initiator can be generated from this one-component precursor by heating.[19,21] Since the process of adduct decomposition is reversible, the polymerization behavior can be controlled thermally.

Scheme 8: Ring-opening-polymerization of lactide: reaction (top) and mechanism (bottom).

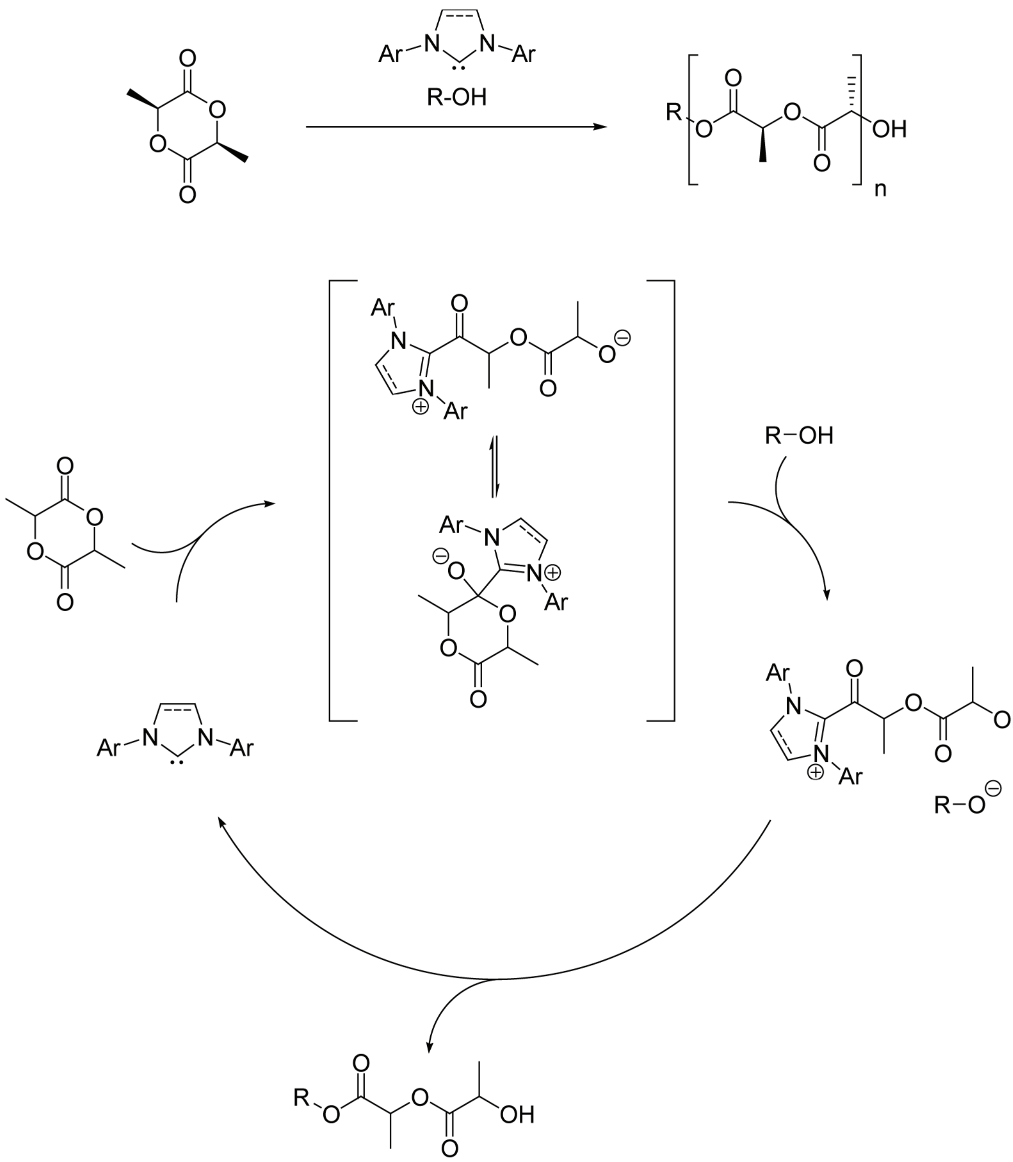

4.1.2 Synthesis of *N*-Heterocyclic Carbenes

The broad range of possible applications of N-heterocyclic carbenes demands for various synthetic pathways to access these highly reactive species. The overview given in the following section shall limit on the synthesis of the free carbene itself. For comprehensive overviews over numerous ways to access NHC-complexes from suitable precursors the reader is referred to the literature. [9-11]

N-Heterocyclic carbenes are most conveniently accessed from their respective salts by deprotonation with strong bases, such as sodium hydride or potassium *tert*-butoxide (Scheme 9).[2,10] Imidazolium salts give imidazolin-2-ylidenes upon action of base, whereas imidazolidin-2-ylidenes are derived from imidazolinium salts. Beside this main approach, several other pathways have been devised, two of which are depicted exemplarily in Scheme 9. Reduction of imidazolin-2-thiones with potassium gives the corresponding imidazolin-2-ylidenes.[23] However, this approach is limited by the harsh reaction conditions in the sodium/potassium melt, significantly restricting the number of substituents tolerated. Convenient alternative access to imidazolidin-2-ylidenes is provided by thermal decomposition of NHC-adducts with compounds bearing an acidic hydrogen, e.g. chloroform, alcohols, or perfluorinated benzene derivatives.[19,24,25] These adducts are either prepared directly from suitable ethylenediamine precursors (*vide infra*) or by quenching a NHC generated by some other way with a species carrying an activated hydrogen. The latter possibility offers the advantage to transform a reactive carbene to a less reactive, dormant species, which can regenerate the carbene on demand by simple heating.

Scheme 9: Synthetic pathways leading to: a) imidazolin-2-ylidenes and b) imidazolidin-2-ylidenes.

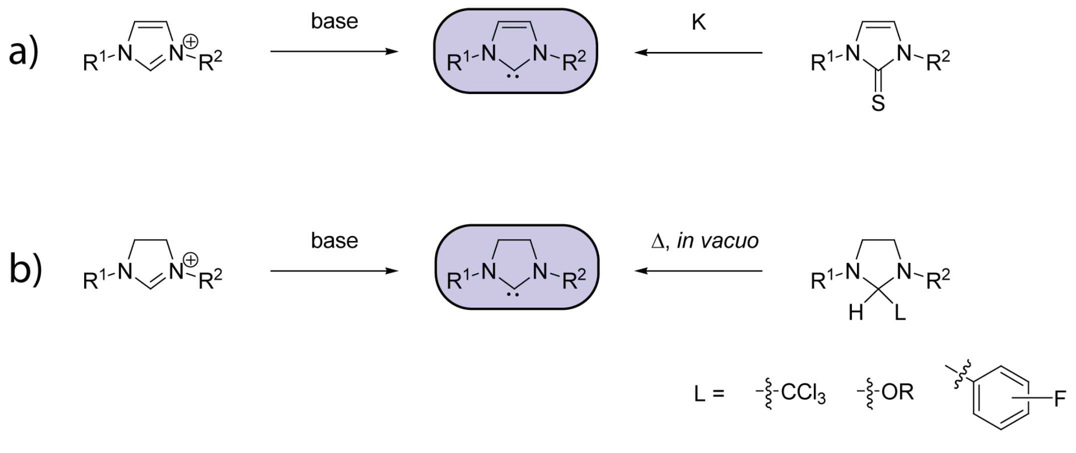

Imidazolium salts with symmetrical ($R^1 = R^2$ in Scheme 10) and non-symmetrical ($R^1 \neq R^2$) substitution pattern are readily available from different precursors (Scheme 10).[2,10] Alkylation of imidazole with alkyl halides and related alkylating agents in the presence of base allows convenient access of alkylated imidazolium salts (path *A* in Scheme 10, R^1 = alkyl, R^2 = alkyl). Exploiting the reactivity differences of the two imidazole nitrogen atoms allows the preparation of non-symmetrical imidazolium salts. Aromatic substituents can be introduced by assembly of the imidazole core from glyoxal, ammonium chloride, formaldehyde, and an aromatic amine. Final alkylation gives a non-symmetrical product (path *B* in Scheme 10, R^1 = aryl, R^2 = alkyl). Following a related strategy, symmetrical imidazolium salts can be directly assembled from two amines, glyoxal, and formaldehyde (path *C* in Scheme 10). The reaction can also be achieved by a multistep procedure, involving initial reaction of the amines with glyoxal to give a bisimine and subsequent cyclization with formaldehyde or an equivalent (path *D* in Scheme 10).

Scheme 10: Some possible synthetic pathways leading to imidazolium salts.

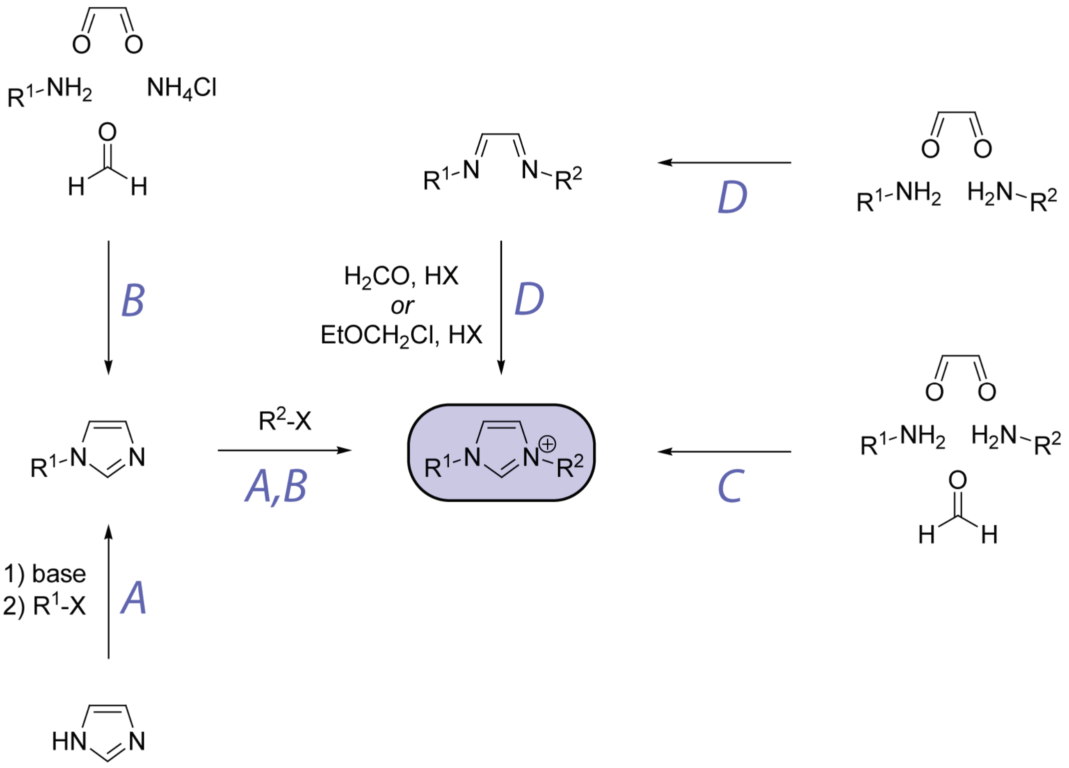

Several pathways grant access to imidazolinium salts (Scheme 11).[2,10] Commonly, ethylenediamines are cyclized to imidazolinium salts by reaction with orthoformates under acidic conditions (path *A* in Scheme 11). This route benefits from the numerous synthetic pathways towards ethylenediamines. Convenient access to symmetrical products is provided by mild reduction of bisimines derived from glyoxal and suitable anilines (path *B* in Scheme 11, $R^1 = R^2 =$ aryl). Non-symmetrical products can be obtained from anilines and other amines by initially reacting one amine with ethyl oxalyl chloride, followed by a saponification-activation sequence to introduce the second amine.[26] The non-symmetrical oxalamide gives the corresponding ethylenediamine upon reduction, e.g. with borane complexes (path *C* in Scheme 11, $R^1 =$ aryl, $R^2 =$ aryl). Similarly, symmetric products can be obtained by reaction of two equivalents of amine with oxalyl chloride followed by reduction of the symmetrical oxalamide (path *D* in Scheme 11). In a conceptually different approach, substituted ethylenediamines can be obtained from parent ethylenediamine and aryl bromides by palladium-catalyzed C-N cross-coupling (path *E* in Scheme 11).

Alternatively, imidazolinium salts can be accessed from formamidines by reaction with 1,2-dichloroethane.[27] Symmetrical as well as non-symmetrical formamidines can easily be prepared from anilines and triethyl orthoformate (path *F* in Scheme 11).

Scheme 11: Some synthetic pathways leading to imidazolinium salts.

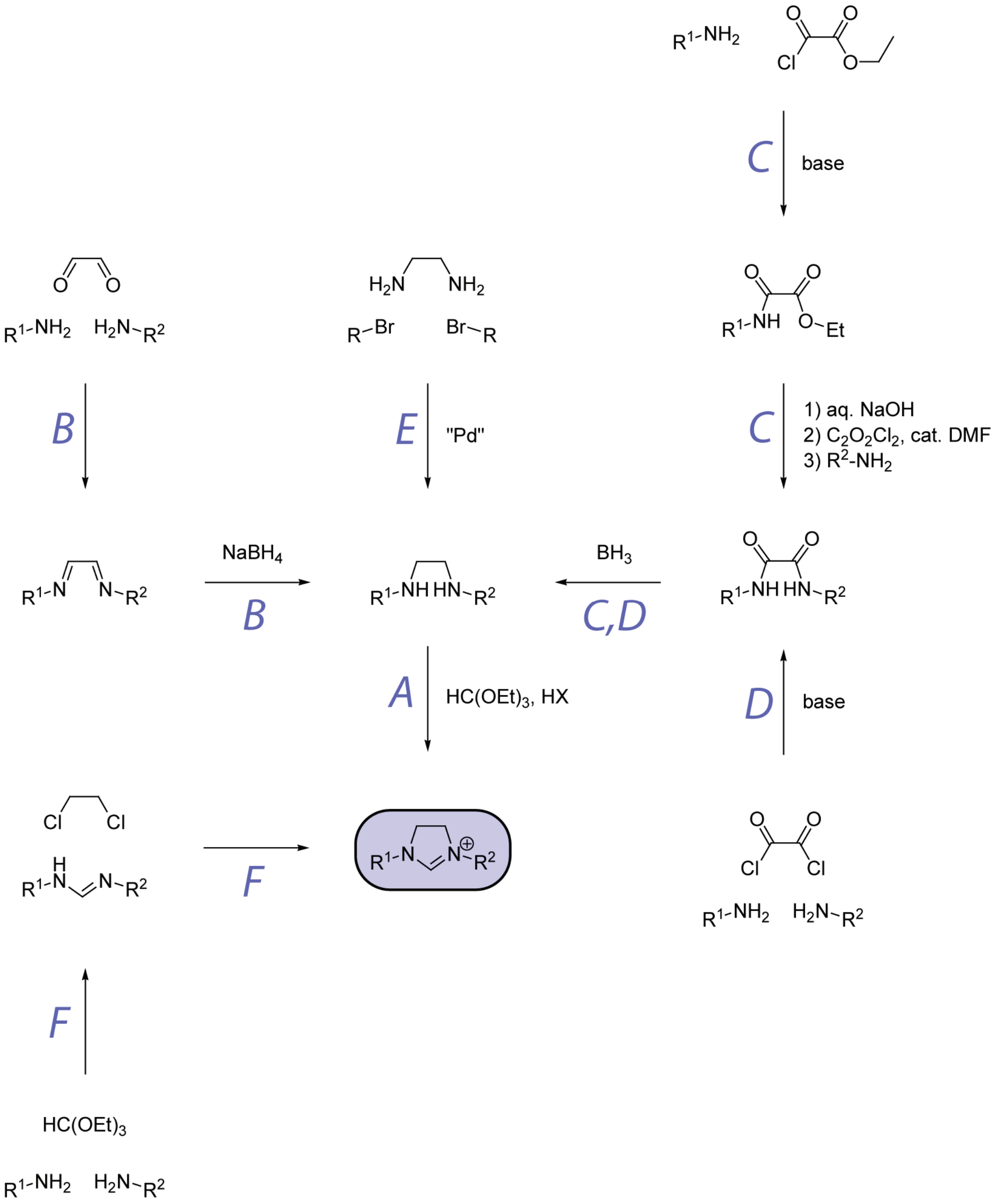
C
base
B
E
"Pd"
C
1) aq. NaOH
2) C2O2Cl2, cat. DMF
3) R2-NH2
NaBH4
B
BH3
C,D
A
HC(OEt)3, HX
D
base
F
F
HC(OEt)3

4.1.3 Application of the Concept of Reversible Steric Shielding

Taking the overwhelming number of possible applications as organocatalysts into account (*vide supra*), *N*-heterocyclic carbenes constitute an attractive target for the development of photoswitchable catalysts. Beside their broad applicability, NHCs possess several additional features, qualifying them as ideal targets for photocontrollable catalyst design. High intrinsic reactivities allow low catalyst loadings and this is expected to facilitate *in situ* switching, since low optical densities can thus be achieved (*vide supra*). The tricyclic structure of imidazolin-2-ylidenes and imidazolidin-2-ylidenes carrying two *N*-aryl substituents is expected to lead to relatively rigid frameworks, ideal for application of the reversible steric shielding concept. Further facilitation of efficient shielding is expected from the strong directionality of the catalytically active carbene lone pair. Convenient synthetic accessibility of imidazolium and imidazolinium salts should enable easy variation of the aryl rings' substituents, thereby allowing to incorporate the necessary switching and shielding elements. Especially their high intrinsic reactivity renders NHCs superior to the only moderately reactive piperidine bases discussed in Chapter 3, offering the possibility to substantially improve the ON/OFF-ratio.

Low OFF-rates are at least as important as high ON-rates in order to obtain high ON/OFF-ratios. High ON-rates are ensured by the NHCs' high intrinsic reactivities, whereas low OFF-rates require for efficient steric shielding of the reactive site. Considering the NHC's orientation in Figure 3, the catalytically active lone-pair is located in the plane of the five-membered ring (green). The most efficient trajectory to the lone pair is hence expected to be in the green plane as indicated by the green arrow. Reversible steric shielding should therefore predominantly block this trajectory to achieve low OFF-rates, as schematically shown by the red ball in Figure 3 (bottom, right). Pulling the red blocking group away from its initial location renders free access to the active site (Figure 3, bottom, left). Azobenzenes are attractive photochromes for this task, due to the large geometrical changes accompanying the switching process. Trajectories to the active site with substantial components parallel to the red plane presumably lead to less efficient encounters. Nevertheless, background reactivity may originate from these approaches, if these trajectories are not efficiently blocked. Therefore, a shielding torus is necessary to guarantee low OFF-rates and high ON/OFF-ratios. The shielding concept for NHCs is summarized in Figure 3. Several shielding strategies were developed and are discussed in the next sections.

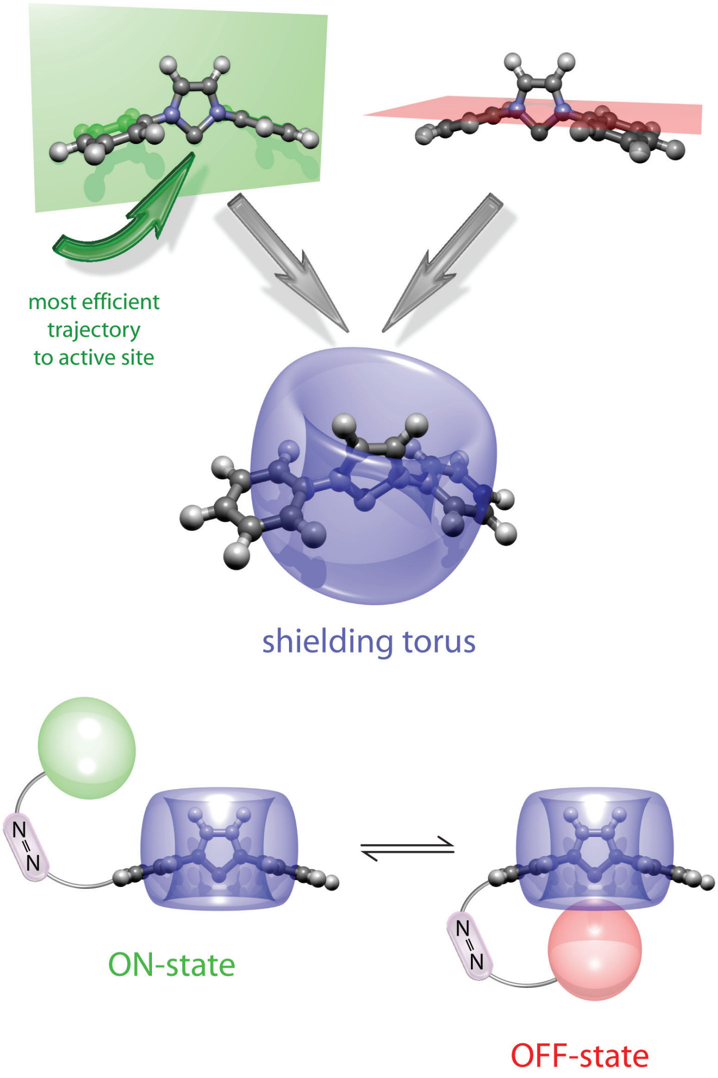
most efficient
trajectory
to active site
shielding torus
N=N
ON-state
N=N
OFF-state

Figure 3: Shielding concept for *N*-heterocyclic carbenes.

4.2 Pentiptycene-Based *N*-Heterocyclic Carbenes

4.2.1 Shielding Concept

From Figure 3 it is immediately apparent that the *N*-aryl substituents are ideal anchors for installing the shielding torus. Inspired by work of Swager and co-workers,[28] a pentiptycene-derived blocking group was devised to ensure efficient blocking of the five-membered core of the NHC (Figure 4). The NHC-core and its active site are completely shielded, preventing attacks coming from outside of the core's plane (cf. green plane in Figure 3), as can be deduced from the right-hand part of Figure 4, which shows a van-der-Waals radii overlay. In fact, two opponent pentiptycene-residues would sterically interfere in the simple, non-optimized model of Figure 4, presumably leading to some distortions of the real structure (most likely by a widening of the $C_{carbene}$-N-C_{aryl} angle).

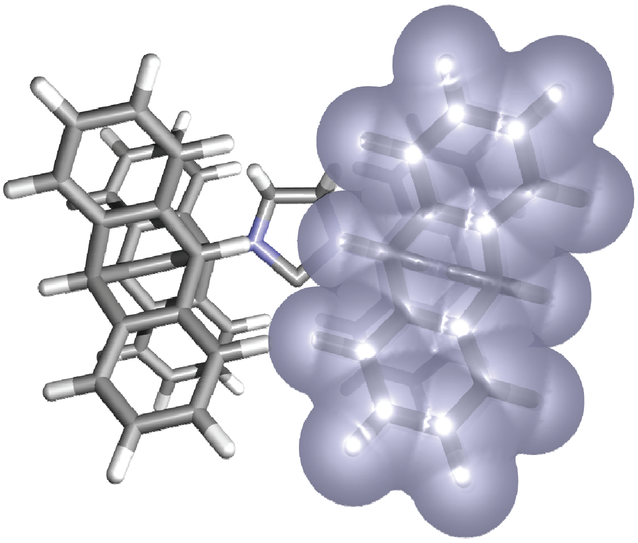

Figure 4: Sterical shielding of a NHC by pentiptycene-residues. The right-hand side shows a spacefill overlay. The model's geometry is not optimized.

The shielding strategy visualized in Figure 4 does not include any switching functionality. Adapting the concept given in Figure 3, it is necessary to block approaches following the direction of the green arrow, since all other trajectories are efficiently blocked by the pentiptycene-residues. Correct placement of the blocking group can be achieved by fusing a suitable azobenzene to the unoccupied *para*-positions of the pentiptycene-moieties, exploiting the perpendicular orientation of the two rings in biphenyl structures (Scheme 12). Rigid, orthogonal orientation of the azobenzene photochrome is ensured by the substituent R. Unfortunately, if R is different from the azobenzene photochrome attached to the other *ortho*-position, atropisomerism is expected to occur upon ring-closure leading to the five-membered core. However, polarity differences of the atropisomers should enable successful chromatographic separation on the stage of the imidazolium- or imidazolinium salt, depending on the exact synthetic strategy. On the other hand, if R equals the azobenzene photochrome, no atropisomerisim is expected, however, the presence of four photochromes inevitably leads to an extremely complex switching behaviour, due to the presence of 8 different switching states.

Scheme 12: Blocking concept for pentiptycene-based NHC **1** (wavy lines denote the pentiptycene "wings").

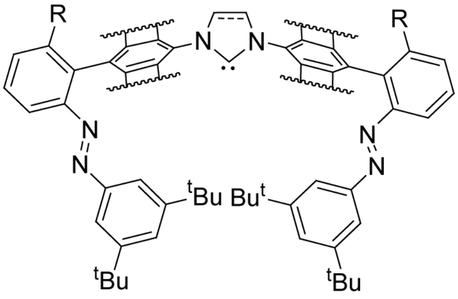

1

4.2.2 Synthesis

Considering Scheme 9, imidazolium- and imidazolinium salts were identified as promising precursors for NHC **1** with substituted anilines **2** being key-intermediates in the synthesis of these salts (Scheme 10, Scheme 11). Following the retrosynthetic route presented in Scheme 13, aniline **2** is obtained by a C-C cross-coupling, *N*-arylation sequence from pentiptycenediol bistriflate **3**, which is available from the hydroquinone

4. Twofold Diels-Alder cycloaddition of anthracene **5** to benzoquinone **6** is known to give pentiptycenedione **7**, which can easily be reduced to the corresponding hydroquinone **4**.

Scheme 13: Retrosynthetic analysis of the key-building block **2** of pentiptycene-NHC **1**.

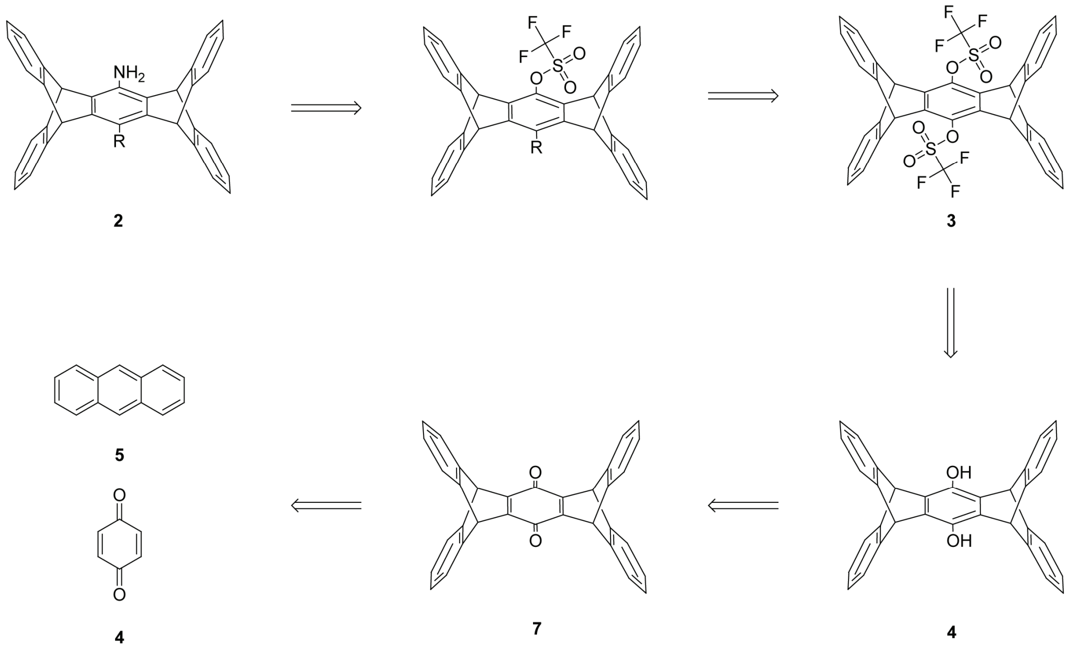

Addition of anthracene **5** to benzoquinone **6** gives pentiptycenedione **7** in moderate yields after oxidation of the initial Diels-Alder adduct (Scheme 14).[29,30] Initial attempts to achieve oxidation by *p*-chloranil were hampered by incomplete conversion, but subsequent oxidation with potassium bromate was successful. Separation of pure pentiptycenedione **7** from by-products was difficult, due to the intrinsic low solubility, accounting for the low yield obtained.

Scheme 14: Synthesis of pentiptycenedione **7**.

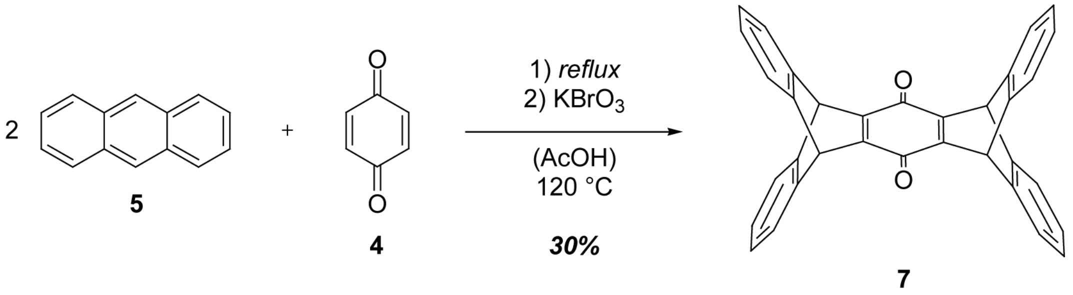
2
5
+
4
1) reflux
2) KBrO3
(AcOH)
120 °C
30%
7

Reduction of pentiptycenedione **7** with zinc in the presence of zinc chloride proceeds smoothly to give pentiptycenediol **4** in quantitative yield.[31]

Scheme 15: Synthesis of pentiptycenediol **4**.

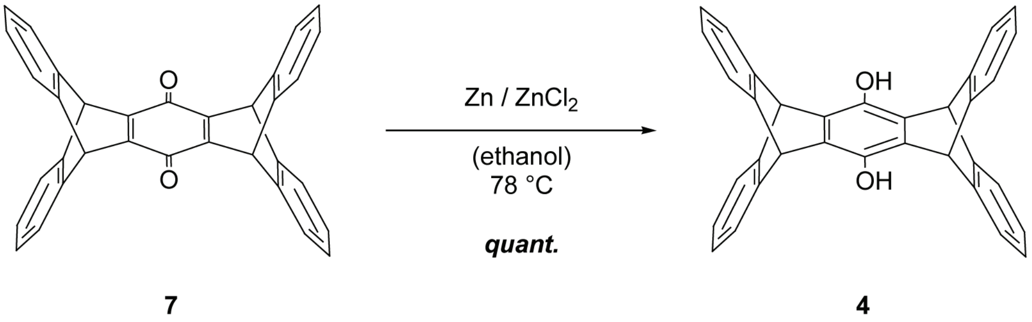
7
Zn / ZnCl2
(ethanol)
78 °C
quant.
OH
OH
4

Pentiptycenediol bistriflate **3** was obtained from pentiptycenediol **4** by reaction with triflic anhydride in the presence of triethyl amine. The product was isolated in good yields after column chromatography.[32]

Scheme 16: Synthesis of pentiptycenediol bistriflate **3**.

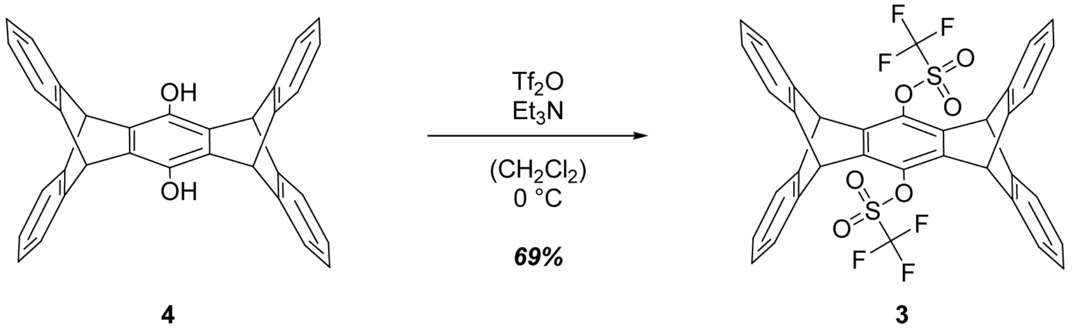
OH
OH
4
Tf2O
Et3N
(CH2Cl2)
0 °C
69%
3

Pentiptycenediol bistriflate **3** proved to be extremely unreactive towards palladium-catalyzed C-C cross-coupling reactions or *N*-arylations. Presumably, bistriflate **3** is sterically too encumbered for successful cross-couplings. The intrinsically low reactivity of aryl triflates towards oxidative addition of palladium species might constitute another reason for the failure to transform bistriflate **3**. However, the basic principles of reversible steric shielding developed for the initial NHC-target **1** were transferred to other design concepts devised to overcome these early synthetic problems encountered in the efforts to obtain NHC **1**.

4.3 Tetramethyl-Terphenyl-Based *N*-Heterocyclic Carbenes

4.3.1 Shielding Concept

Inspection of Figure 4 reveals a great extent of steric bulk originating from the pentiptycene moieties, which is not mandatory for steric shielding of the NHC core. In fact, introduction of *ortho*,*ortho'*-aryl substituents on the *N*-phenyl rings leads to very efficient shielding of the active site without encumbering the nitrogens' *para*-positions (Figure 5). Incorporation of methyl groups in the 2- and 6-positions of the shielding phenyl rings is expected to ensure a rigid, orthogonal orientation of the rings. Installation of photochromic blocker groups in analogy to Scheme 12 is not perturbed by unnecessary steric bulk next to the site of attachment (Figure 5). Please note that the structure shown in Figure 5 is not optimized, but only intends to visualize the shielding effect of the *ortho*-aryl substituents. Therefore, distortions of the structure are expected to avoid clashes of the shielding phenyl rings. However, the main shielding principles are expected to be preserved.

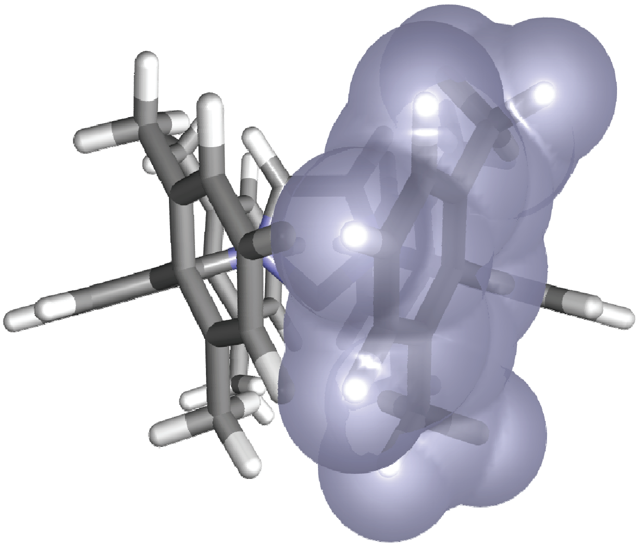

Figure 5: Sterical shielding of a NHC by terphenyl-residues. The right-hand side shows a spacefill overlay. The model's geometry is not optimized.

In analogy to the blocking strategy developed for NHC **1**, the switching units are installed in the nitrogens' *para*-positions. Reversible steric shielding of the active site is granted by bulky azobenzene photochromes held in a coplanar orientation to the five-membered NHC core by doubly exploiting the perpendicular biphenyl twist, as illustrated by structure of Me_4terphenyl-based NHC **8** (Scheme 17). As discussed in section 4.2, the nature of the R-group in NHC **8** is variable. Inert residues introduced to lock rotation of the bond connecting the phenyl rings are expected to give rise to atropisomerism upon formation of the five-membered core. Installation of a second azobenzene circumvents atropisomerism, but significantly increases the number of possible switching states (*vide supra*).

Scheme 17: Blocking concept for Me$_4$terphenyl-based NHC **8**.

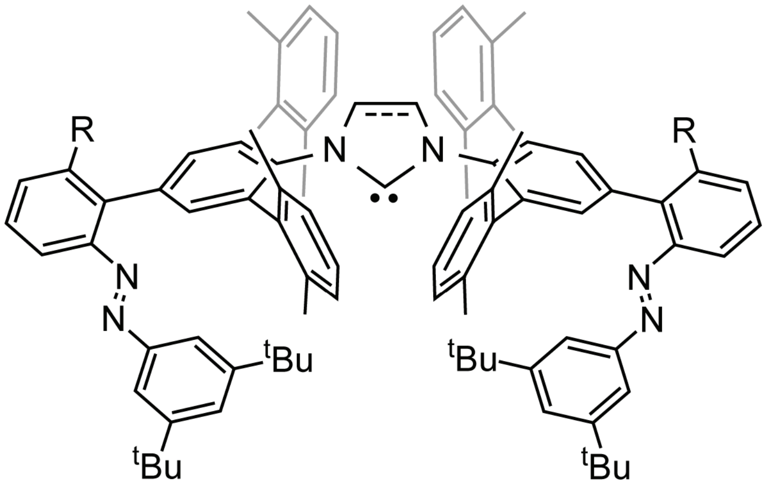

8

4.3.2 Synthesis

Analogous to the retrosynthetic analysis of pentiptycene-based NHC **1**, aniline **9** is a key-intermediate in the synthesis of carbene **8**, allowing to access either imidazolin-2-ylidenes or imidazolidin-2-ylidenes from the corresponding precursors. Aniline **9** can be retrosynthetically devided into 4-iodo-2,6-bis(2,6-dimethylphenyl)aniline **10** and a boronic acid **11** carrying the switching unit. Further analysis of **10** reveals 2,6-bis(2,6-dimethylphenyl)aniline **13** as an immediate precursor, which can be assembled from 2,6-dibromoaniline **14** and 2,6-dimethylphenylboronic acid **15**.

Scheme 18: Retrosynthetic analysis of the key-building block **9** of Me$_4$terphenyl-based NHC **8**.

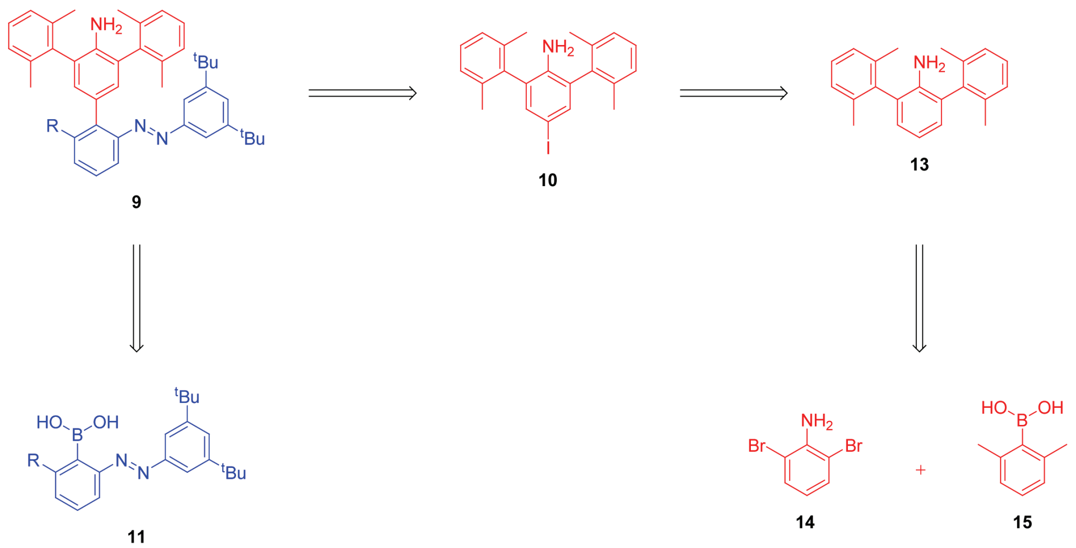

Ring-closure of C$_2$-bridged precursors of imidazolium and imidazolinium salts is expected to be a crucial step in the synthesis of *N*-heterocyclic carbenes of the Me$_4$terphenyl-type due to the substantial amount of steric bulk around the reacting sites (Figure 5). Considering the initial retrosynthetic analysis in Scheme 18, 2,6-bis(2,6-dimethylphenyl)aniline **13** was identified as a valuable building-block for testing the synthetic accessibility of the Me$_4$terphenyl-NHC framework of model carbene **16** (Scheme 19). Starting from aniline **13**, the glyoxal bisimine **17** constitutes the next key-intermediate in the synthesis of **16**.

Scheme 19: Retrosynthetic analysis of model-carbene **16**.

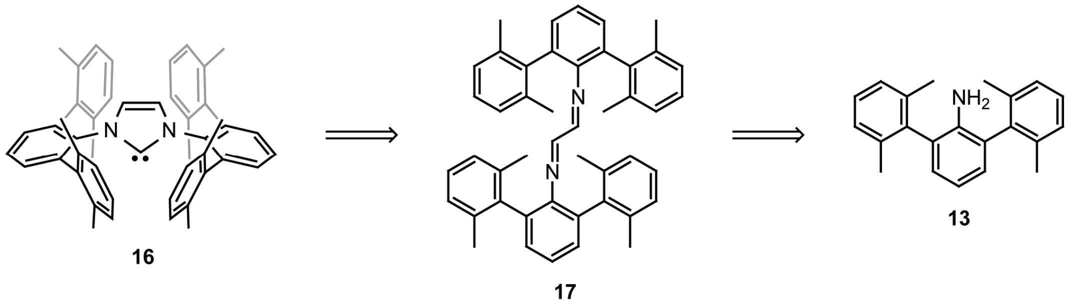

Utilizing Suzuki-type cross-coupling protocols developed by Buchwald and co-workers, 2,6-bis(2,6-dimethylphenyl)aniline **13** was easily obtained from 2,6-dibromoaniline **14** and 2,6-dimethylphenylboronic acid **15** in excellent yield (Scheme 20).[33]

Scheme 20: Synthesis of 2,6-bis(2,6-dimethylphenyl)aniline **13** (S-Phos: 2-dicyclohexylphosphino-2′,6′-dimethoxybiphenyl).

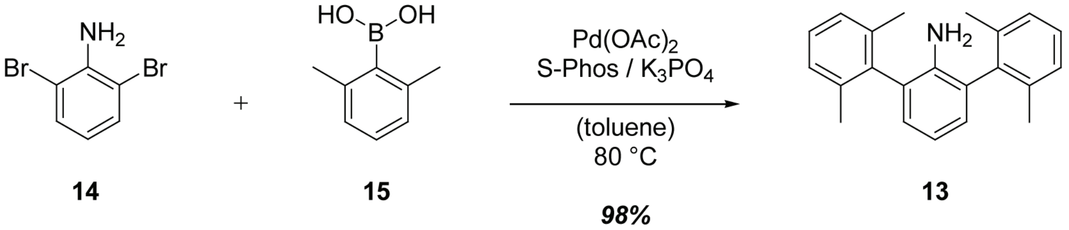

Terphenyl aniline **13** turned out to be a valueless precursor for the synthesis of model carbene **16**, nevertheless exhibiting interesting chemistry (Scheme 21). Reaction of glyoxal with sterically less hindered anilines usually is a very feasible reaction, giving the desired bisimines in good yields. However, aniline **13** did not react with glyoxal to a significant extent under standard conditions.[24,34] Even after prolonged reaction times and at elevated temperatures, only trace amounts of bisimine **18** could be isolated. A full characterization of the material obtained was prevented by its very low solubility in common organic solvent. However, the material was unambiguously identified as bisimine **18** by x-ray structural analysis of very small crystals obtained from very diluted, hot toluene solutions (Figure 6). The limited availability together with the low solubility make bisimine **18** an inadequate precursor of model carbene **16**.

Scheme 21: Reactivity scheme of aniline **13** towards glyoxal and oxalylic chloride.

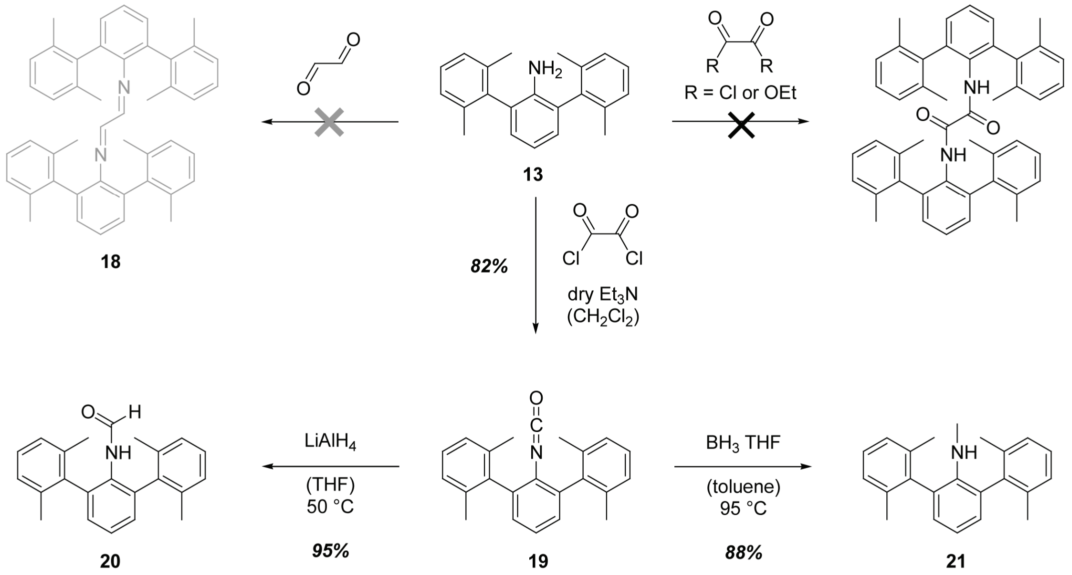
NH2
13
R = Cl or OEt
NH
NH
18
82%
Cl
Cl
dry Et3N
(CH2Cl2)
O=C=N
LiAlH4
(THF)
50 °C
95%
BH3 THF
(toluene)
95 °C
88%
20
19
21

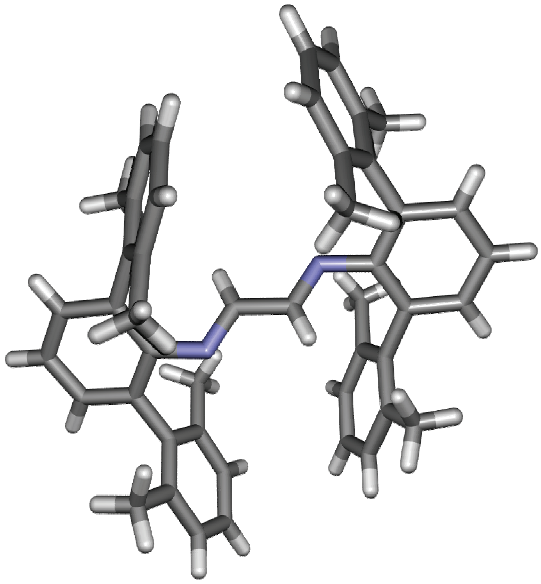

Figure 6: X-ray structure of terphenyl bisimine **18**.

Considering Scheme 11, reaction of anilines with oxalyl chloride or related reagents should lead to oxalamides, which upon reduction give ethylenediamines as valuable precursors of imidazolinium salts.[26] Reaction of terphenyl aniline **13** with either oxalyl chloride or diethyl oxalate did not give the desired oxalamide. After 5 days, no reaction was observed between diethyl oxalate and aniline **13** in the presence of catalytic amounts of PTSA. Unexpectedly, reaction of aniline **13** with oxalyl chloride gave terphenyl isocyanate **19** (Scheme 21). The reaction is assumed to proceed via a defragmentation of the initial mono-oxalamide (Scheme 22). Isocyanate **19** was unambiguously identified by IR-spectroscopy, revealing a typical band around 2251 cm^{-1} indicative for isocyanates.

Scheme 22: Assumed mechanism of formation of isocyanate **19**.

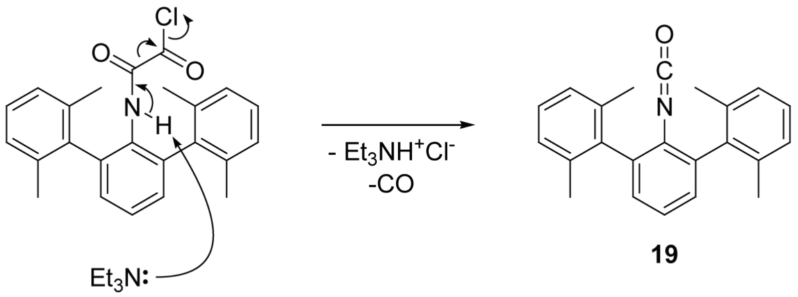

Reduction of terphenyl isocyanate **19** proceeds to different products depending on the reducing agent (Scheme 21). While *N*-formyl-2,6-bis(2,6-dimethylphenyl)aniline **20** is cleanly obtained with lithium aluminumhydride, reduction with borane-THF complex proceeds further to yield *N*-methyl-2,6-bis(2,6-dimethylphenyl)aniline **21**.

Since the installation of the C$_2$-linker starting from terphenyl aniline **13** was unsuccessful, new strategies for its introduction were devised. Installation of the linker before introduction of the sterically demanding phenyl substituents was thought to give easier access to the desired ethylenediamine or bisimine key intermediates. In contrast to 2,4,6-trimethyl aniline, bisimine formation from 2,6-dibromoaniline and glyoxal could not be achieved, probably due to the increased steric bulk of the bromine atoms compared to the methyl substituents in 2,4,6-trimethyl aniline (Scheme 23).[24,34] Access to the glyoxal bisamide of 2,6-dibromoaniline is also very limited in scope since only small amounts of product could be isolated by reaction with oxalyl chloride.[26] Furthermore, the presence of halogen substituents is expected to strongly interfere with the conditions necessary for reduction of the amide functionalities. No reaction was observed using diethyl oxalate.

Scheme 23: Reactivity of 2,6-dibromoaniline.

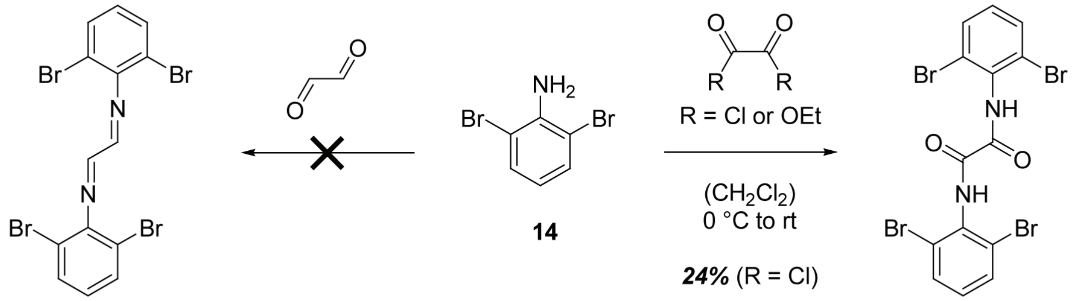

Problems originating from the sterically demanding bromine atoms were circumvented by introduction of the bromine substituents after establishing the C_2-linker (Scheme 24). Model ethylenediamine **22** was obtained starting from *para*-toluidine **23** by a sequence involving initial formation of glyoxal bisimine **24** and subsequent reduction with sodium borohydride to give ethylenediamine **25**.[24,34] Taking advantage from the activating, *ortho*/*para*-directing amino substituent and the methyl group, which blocks the *para*-position, bromination of **25** with elemental bromine gave tetrabromoethylenediamine **22**. Successful introduction of four bromo-substituents was only possible by a two-step procedure. Initial bromination of **25** using 3.95 equivalents of bromine gave a mixture of products, from which **22** could be isolated in 18% yield by chromatography. Other fractions contained partially brominated products according to GC-MS analysis. The overall yield could be significantly improved by reacting the combined, partially brominated products with an exact equimolar amount of bromine, based on the vacant *ortho*-positions as determined by GC-MS.

Scheme 24: Synthesis of model ethylenediamine **22**.

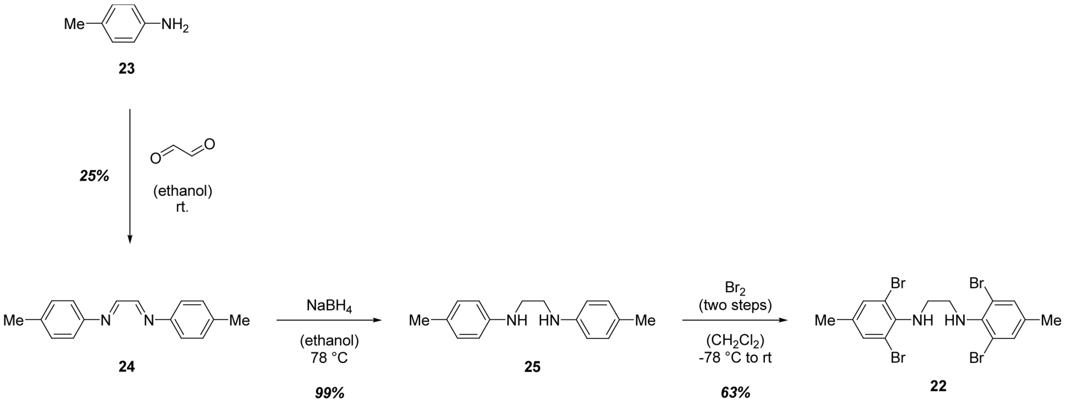
Me
NH2
23
25%
O
O
(ethanol)
rt.
Me
N
N
Me
24
NaBH4
(ethanol)
78 °C
99%
Me
NH
HN
Me
25
Br2
(two steps)
(CH2Cl2)
-78 °C to rt
63%
Br
Br
Me
NH
HN
Me
Br
Br
22

Application of the Suzuki-protocol, which enabled successful synthesis of aniline **13**, to tetrabromoethylenediamine **22** allowed convenient access of *N*,*N'*-bis-(2,6-bis(2,6-dimethylphenyl)-4-methylphenyl)ethylenediamine **26**.[33] Notably, the product was obtained in 64% yield, corresponding to an average yield per cross-coupling of around 90%, which is remarkable in light of the steric bulk build-up during the course of the reaction. X-ray structural analysis reveals significant planarization of the N-atoms (angle sum 360.1°), attributed to the clash of the 2,6-dimethylphenyl groups (Figure 7).

Scheme 25: Synthesis of *N*,*N'*-bis-(2,6-bis(2,6-dimethylphenyl)-4-methylphenyl)ethylenediamine **26** (S-Phos: 2-dicyclohexylphosphino-2′,6′-dimethoxybiphenyl).

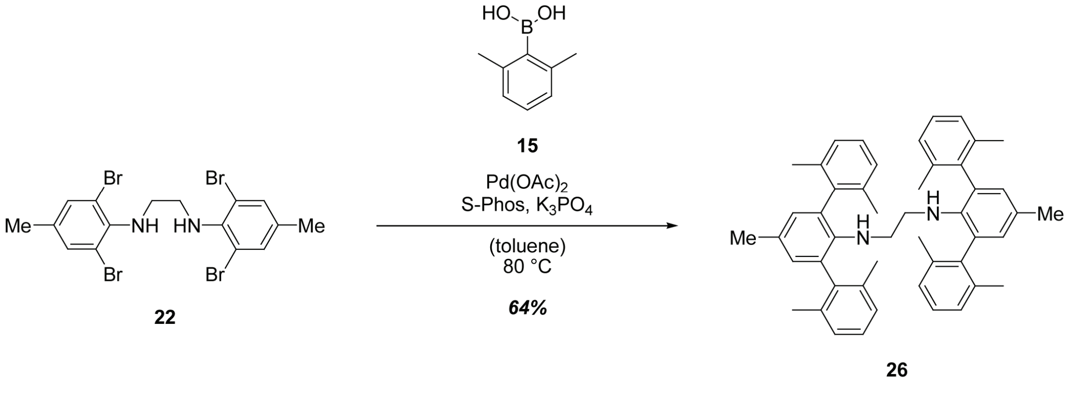
HO
B
OH
15
Pd(OAc)2
S-Phos, K3PO4
(toluene)
80 °C
64%
Br
Br
Me
NH
HN
Me
Br
Br
22
H
N
H
N
Me
Me
26

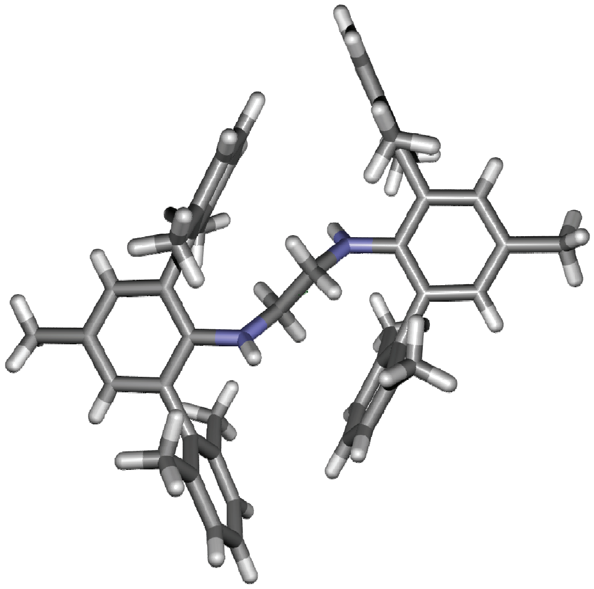

Figure 7: X-ray structure of *N,N'*-bis-(2,6-bis(2,6-dimethylphenyl)-4-methylphenyl)ethylenediamine **26**.

Cyclization of terphenylethylenediamine **26** to yield the imidazolinium salt **27** was not successful (Scheme 26).[35,36] A number synthetic attempts solely allowed for either re-isolation of the unreacted starting material or isolation of undefined, completely insoluble solids, presumably being comprised of inorganic by-products obtained by hydrolysis of BF_4^--anions under the harsh reaction conditions (HBF_4, sealed tube, 140 °C, duration up to two days). Scheme 26 gives an overview of the conditions tested.[a] Severe steric crowding of terphenylethylenediamine **26** apparently prevents cyclization. Therefore, new synthetic strategies were developed.

---

[a] Deprotonation of the amine functionality was expected to increase the nitrogen atom's nucleophilicity, thereby facilitating the reaction with triethyl orthoformate (red pathway in Scheme 26).

Scheme 26: Attempted syntheses of imidazolinium salt **27**.

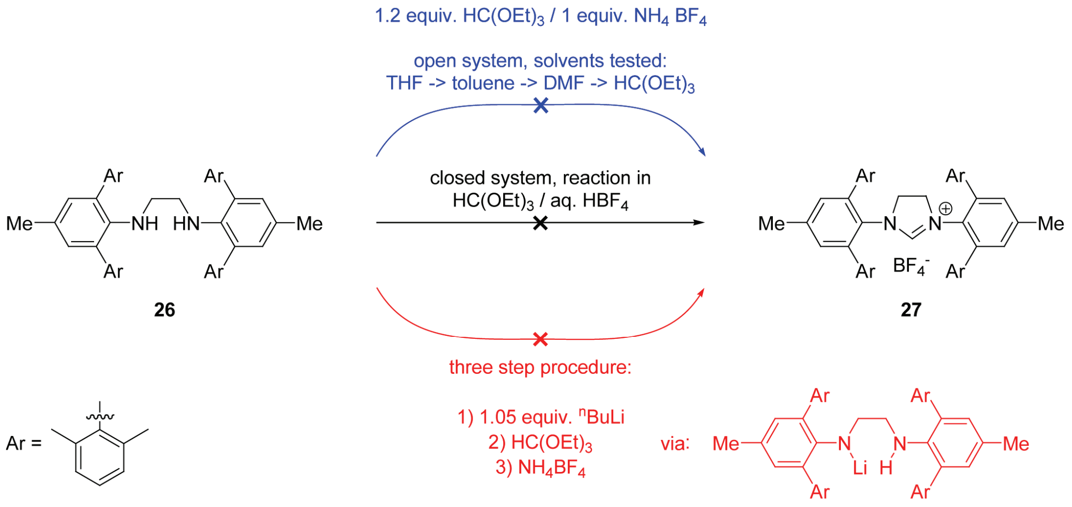
1.2 equiv. HC(OEt)3 / 1 equiv. NH4 BF4
open system, solvents tested:
THF -> toluene -> DMF -> HC(OEt)3
closed system, reaction in
HC(OEt)3 / aq. HBF4
three step procedure:
1) 1.05 equiv. nBuLi
2) HC(OEt)3
3) NH4BF4
via:
Ar
Me
NH
HN
Li
H
BF4-
26
27
Ar =

4.4 Terphenyl-Based *N*-Heterocyclic Carbenes

4.4.1 Shielding Concept

Cyclization of the Me4terphenyl-ethylenediamine **26** was hampered by the build-up detrimental steric strain during ring-closure to the imidazolinium core. Omission of the *ortho*-methyl groups in **26** is anticipated to lead to some relieve of steric strain by attenuating the orthogonal fixation of the biphenyl twist observed in **26** (cf. Figure 7). However, efficient steric shielding should still be granted by the *ortho*-phenyl substituents. Initially, no attempts were made to incorporate a switching functionality, since preliminary efforts were directed towards the synthesis of model terphenyl-based NHC **28** (Scheme 27). By the close similarity of the designs of NHCs **16** and **28**, it is evident that incorporation of switching functionalities would be carried out similarly as outlined in Scheme 18.

Scheme 27: Model terphenyl NHC **28**.

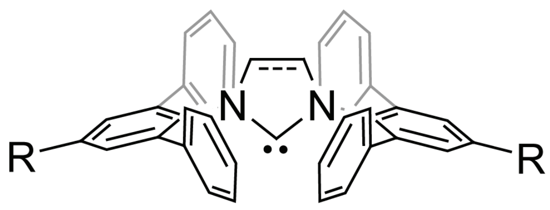

28

4.4.2 Synthesis

Depending on the nature of the five-membered heterocyclic core, retrosynthetic analysis of terphenyl NHC **28** reveals bisimine **29** or ethylenediamine **30** as key intermediates, both obtainable from 2,6-diphenylaniline **31**.

Scheme 28: Retrosynthetic analysis of terphenyl NHC **28**.

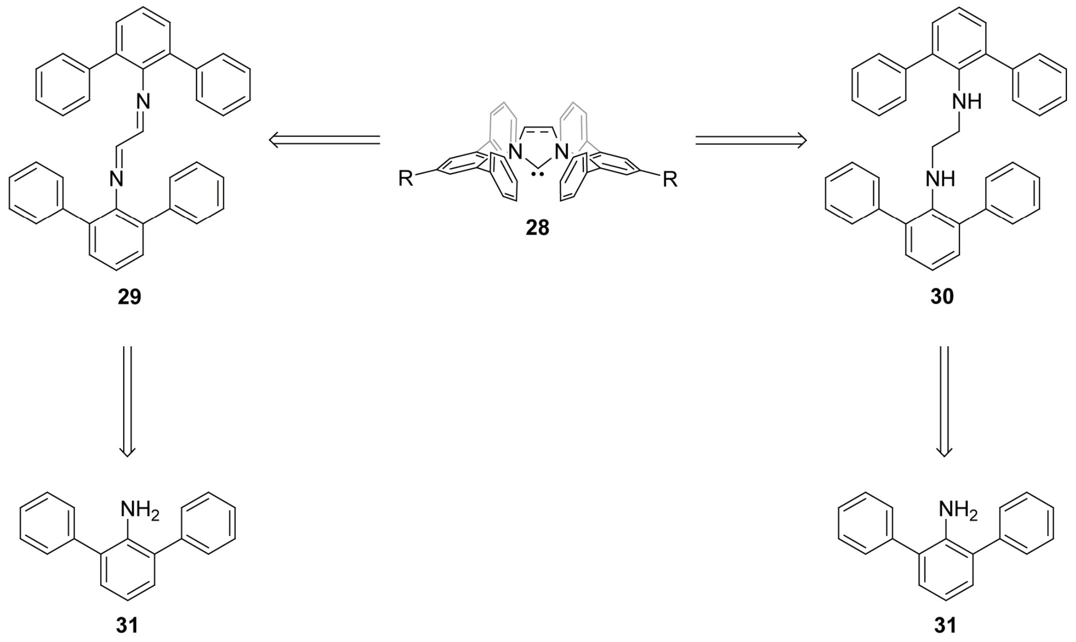

Suzuki-type cross-coupling protocols developed by Buchwald and co-workers, enabled convenient synthesis of 2,6-diphenylaniline **31** from commercially available 2,6-dibromoaniline **14** and phenylboronic acid **32** in excellent yield (Scheme 29).[33]

Scheme 29: Synthesis of 2,6-diphenylaniline **31** (S-Phos: 2-dicyclohexylphosphino-2′,6′-dimethoxybiphenyl).

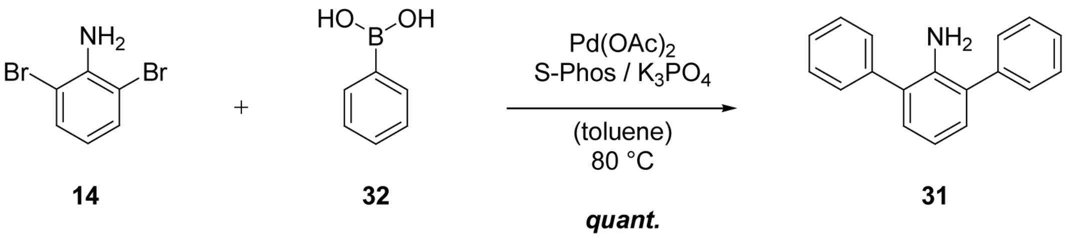

Glyoxal bisimine **29** was easily obtained from aniline **31** by standard procedures (Scheme 30).[24,34] Yields were only moderate and the outcome of the reaction seems to be quite sensitively dependent to the concentrations employed. High yields were obtained at high concentrations. Considering the labile nature of bisimine towards hydrolysis, no efforts were undertaken to obtain the imidazolium salt derived from **29**. Instead, reduction of bisimine **29** was attempted, but proved to be rather difficult. A range of reagents were tested ($LiAlH_4$ in THF, $NaBH_4$ in ethanol, BH_3-THF complex in THF with or without phthalic acid as additive),[37] but no ethylenediamine could be obtained. Presumably, the shielding effect of the *ortho*,*ortho'*-substituents prevents reduction. Synthesis of ethylenediamine **30** by reduction of the corresponding oxalamide was not attempted, because efficient shielding should inhibit reduction of these species as well.

Scheme 30: Synthesis of glyoxal bisimine **29**.

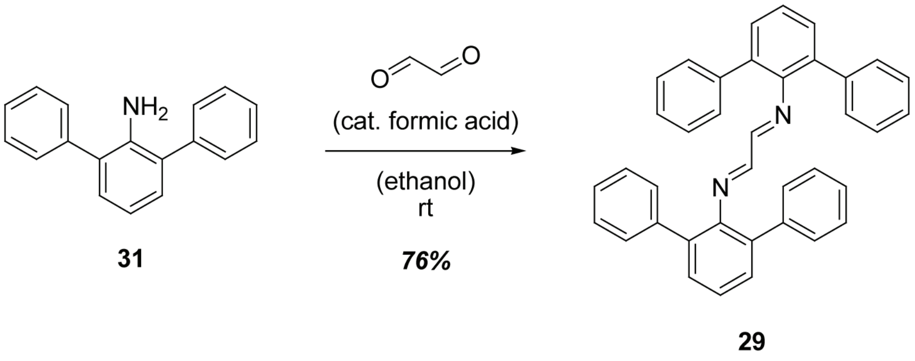

Considering the good results obtained for the fourfold Suzuki-type cross-coupling presented in Scheme 25, a similar approach to terphenyl-based NHC **28** (with R = Me) was devised. Indeed, cross-coupling of tetrabromoethylenediamine **22** with phenyl boronic acid **32** gave the desired *N*,*N'*-bis-(4-methyl-2,6-diphenylphenyl)ethylenediamine **33** in good yields.[33] X-ray structural analysis reveals a significant planarization of the nitrogen atoms (Figure 8a, angle sum 334.6°), even though the effect is less pronounced as compared to ethylenediamine **26**. The initially intended higher flexibility of ethylenediamine **33** is reflected in the significant twisting of the aryl rings in the terphenyl moiety (Figure 8b).

Scheme 31: Synthesis of *N*,*N'*-bis-(4-methyl-2,6-diphenylphenyl)ethylenediamine **33**.

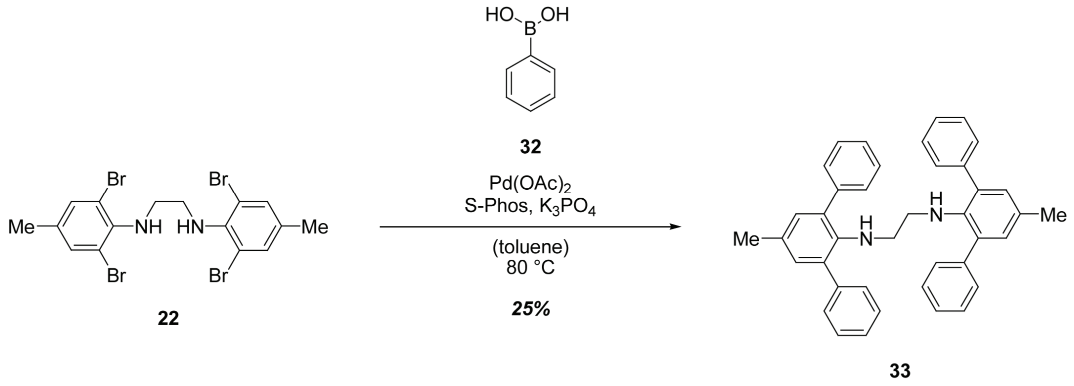

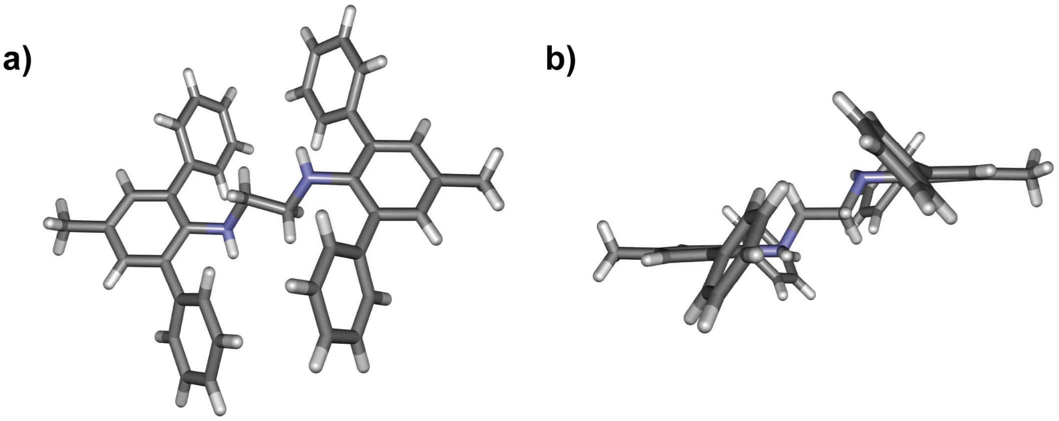

Figure 8: X-ray structure of *N*,*N'*-bis(4-methyl-2,6-diphenylphenyl)ethylenediamine **33**: a) top view, b) side view.

Formation of the imidazolinium salt corresponding to terphenylethylenediamine **33** utilizing triethyl orthoformate and aqueous HBF_4-solution was not possible, even under forcing conditions.[36] Presumably, ethylenediamine **33** is still sterically too crowded for successful cyclization to occur.

Therefore, the last two synthetic steps were reversed and four-fold Suzuki-coupling of *N*,*N'*-2,6-dibromo-4-methyl-phenyl imidazolinium tetrafluoroborate **34** with phenyl boronic acid **32** was attempted. Imidazolinium salt **34** is obtained by reacting tetrabromoethylenediamine **22** with triethyl orthoformate in the presence of aqueous HBF_4-solution (Scheme 32).[36] The product is obtained in moderate yields as a gray powder.

Scheme 32: Synthesis of *N*,*N'*-2,6-dibromo-4-methyl-phenyl imidazolinium tetrafluoroborate **34**.

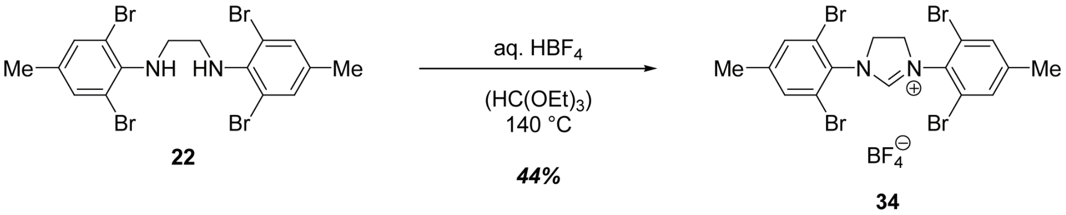

Four-fold Suzuki-coupling of imidazolinium salt **34** with phenyl boronic acid **32** was however not successful employing conditions developed by Ma.[38] A mixture of products was obtained, which could not be separated. NMR-spectroscopy reveals the presence of several by-products in the sample. ESIpos MS, HPLC, and electrophoresis point to the presence of one charged compound in the mixture with a mass equal to that of the expected product. However, as stated above, the product could not be purified and detection of a charged species by MS, HPLC, and electrophoresis may conceal the presence of uncharged species. Furthermore, it has to mentioned that HPLC and electrophoresis methods are hard to validate for charged species, which are accompanied by a complex matrix of numerous uncharged by-products. Intensive work directed in this direction in the HPLC service-department at the MPI für Kohlenforschung in Mülheim/Ruhr did not succeed to set-up a completely trustworthy method, underlining the analytical problems encountered. Application of the Suzuki-protocol developed by Buchwald,[33] led to a mixture of products, none of which could be identified as the target compound. Due to the synthetic difficulties in isolating **34**, a separation of atropisomers of imidazolinium salts seems to be impossible. Therefore, alternative routes towards photoswitchable NHC-catalysts were developed.

4.5 Non-symmetrical Terphenyl-Based *N*-Heterocyclic Carbenes

4.5.1 Shielding Concept

Shielding of the NHC-core by two more or less rigid terphenyl units is an unsuitable strategy (*vide supra*), since substantial crowding prevents formation of the five-membered NHC core. Considering Figure 9, a significant relieve of steric strain is expected for nonsymmetrically substituted NHCs bearing only one terphenyl unit, because clashes of opposing terphenyl-residues are avoided. Furthermore, the presence of a variable, smaller substituent allows for a precise fine-tuning of the steric interactions between opposing residues. Sufficient shielding of the NHC's five-membered ring is kept up mainly by the terphenyl-residue, with smaller contributions from the second substituent (2,4,6-trimethylphenyl in Figure 9). Nevertheless, shielding is expected to be sufficient to suppress in unwanted side-reactivity in a switchable NHC.

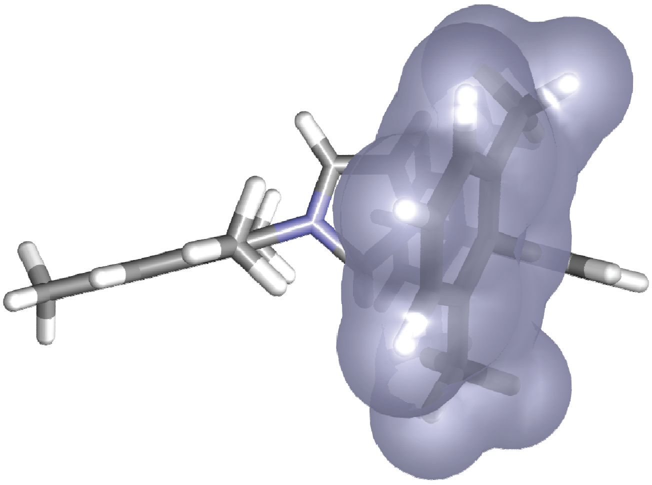

Figure 9: Sterical shielding of a nonsymmetrical NHC carrying one terphenyl-residue and one 2,4,6-trimethylphenyl-residue. The right-hand side shows a spacefill overlay. The model's geometry is not optimized.

Considering problems encountered during purification of imidazolinium salt **34** and cross-coupling products derived thereof, it seems appropriate to avoid unnecessary chromatographic purifications steps at the stage of the imidazolium or imidazolinium salts. Especially, separation of atropisomers obtained by incorporation of nonsymmetrical switching units seems to be an insurmountable difficulty. Therefore, new shielding strategies were devised to avoid problems originating from atropisomerism and a confusing number of possible switching states, if atropisomerism is circumvented by introduction of symmetrical switching units.

From Figure 9 it is evident that approaches to the active site with substantial components in the red plane of Figure 3 are effectively blocked by the terphenyl moiety. Therefore, switchable shielding components remain to be introduced. Previous designs were based on two switchable blocker units, each fused to one aryl-ring of the NHC framework. However, spacefill models reveal a significant extent of shielding by a single switchable blocking unit (Figure 10b). A C_2-symmetrical design of the blocking unit renders it invariable towards rotation, while the presence of two photochromes diminishes the number of possible switching states to three (Figure 10a). In summary, the structure of NHC **35** presented in Figure 10 combines an effectively shielded active site with a reversible shielding concept, which allows to decrease the number of possible switching states while simultaneously avoiding potential formation of atropisomers.

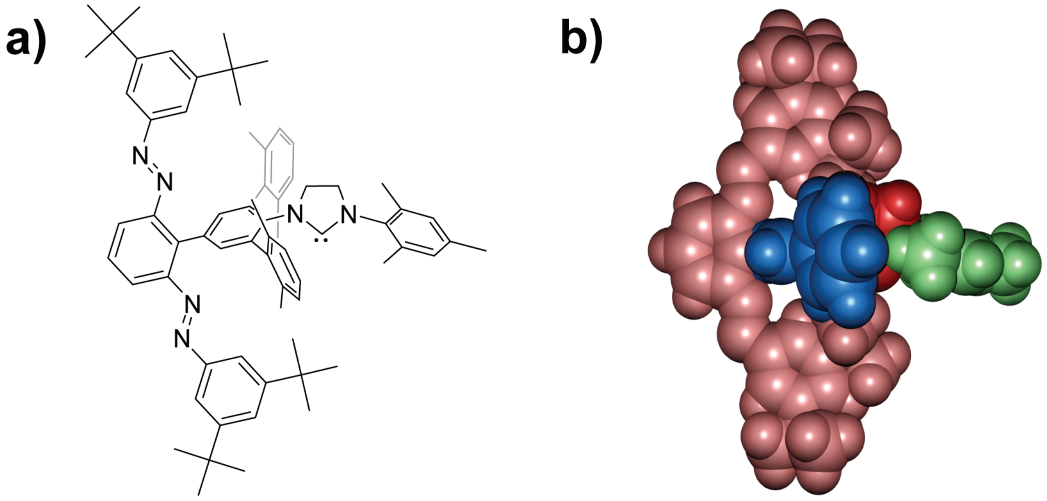

35

Figure 10: Nonsymmetrical NHC **35** carrying a C_2-symmetrical blocking group unit: a) potential target structure, b) spacefill-model of NHC **35** revealing efficient shielding of the active site in the OFF-state (*E*-azobenzenes; red: NHC core; blue: terphenyl-residue; green: 2,4,6-trimethylphenyl-residue; pink: switchable blocker unit).

4.5.2 Synthesis

Imidazolinium salts are versatile precursors for nonsymmetrical NHCs. Following the synthetic path *C* in Scheme 11, nonsymmetrically substituted ethylenediamines constitute direct precursors of NHCs with different aryl substituents on the nitrogen atoms. Retrosynthetic analysis of NHC **35** or of its precursor, the corresponding imidazolinium salt **36**, is therefore straight forward (Scheme 33). Ethylenediamine **37** is a direct precursor of imidazolium salt **36** and is derived from its corresponding oxalamide **38** by reduction. Oxalamide **38** is assembled following an established four-step sequence from photochromic terphenyl aniline **39** carrying the blocking units, mesityl amine **40**, and ethyl oxalyl chloride.[26] No synthesis of imidazolium salts carrying different aryl substituents on both nitrogen atoms has been described so far (Scheme 10). Therefore, this possibility was not considered.

Scheme 33: Retrosynthetic analysis of imidazolinium salt **36**.

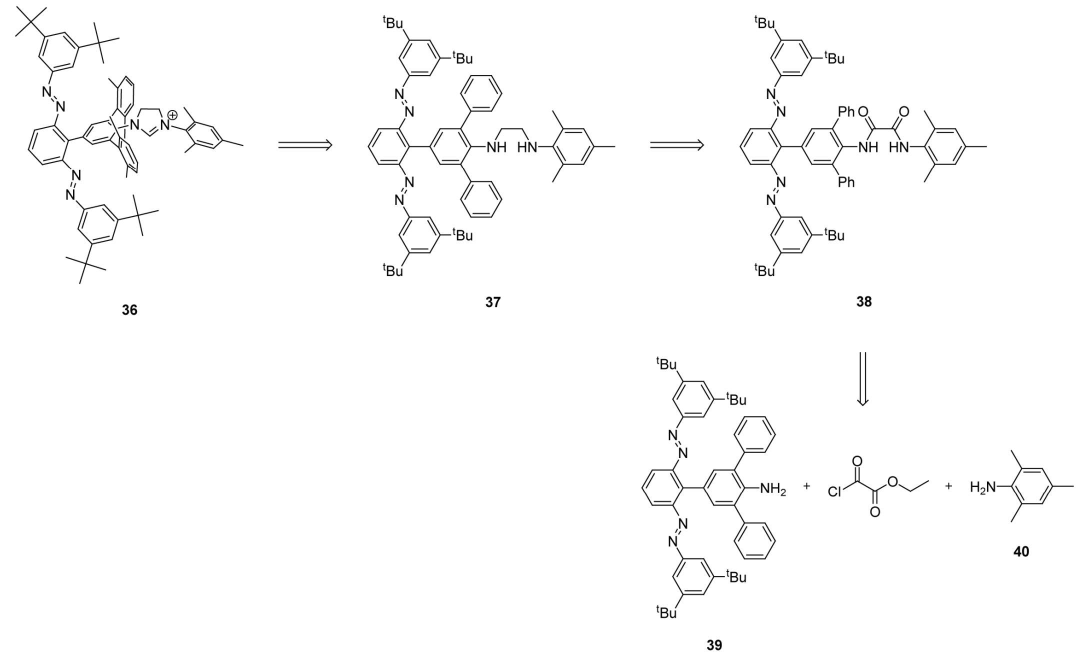

The photochromic terphenyl aniline **39** constitutes a key-intermediate in the synthesis of carbene **35**. Introduction of the azobenzene functionalities is possible via the efficient sequence utilized for the synthesis of the photoswitchable bases (Chapter 3), that is initial palladium-catalyzed N-arylation of dibromoaniline **42** with the *N*-BOC-*N*-(3,5-di-*tert*-butylphenyl)hydrazine **43** is followed by oxidation of the hydrazine derivative **41**, which is expected to give **39**. Dibromoaniline **42** can be obtained from 4-iodo-2,6-diphenylaniline **44** and an organometallic species **45**, for example a boronic acid or an organotin reagent. The higher reactivity of the iodo substituent towards palladium-mediated cross-coupling reactions is exploited for regionselective coupling of **44** and **45**. The retrosynthetic analysis is completed by recognizing the *para*-directing nature of the amino substituent in 2,6-diphenylaniline **31**, which should facilitate iodination and direct the new substituent into the desired 4-position to give 4-iodo-2,6-diphenylaniline **44**.

Scheme 34: Retrosynthetic analysis of photochromic terphenyl aniline **39** (Met: for example a boronic acid or an organotin reagent).

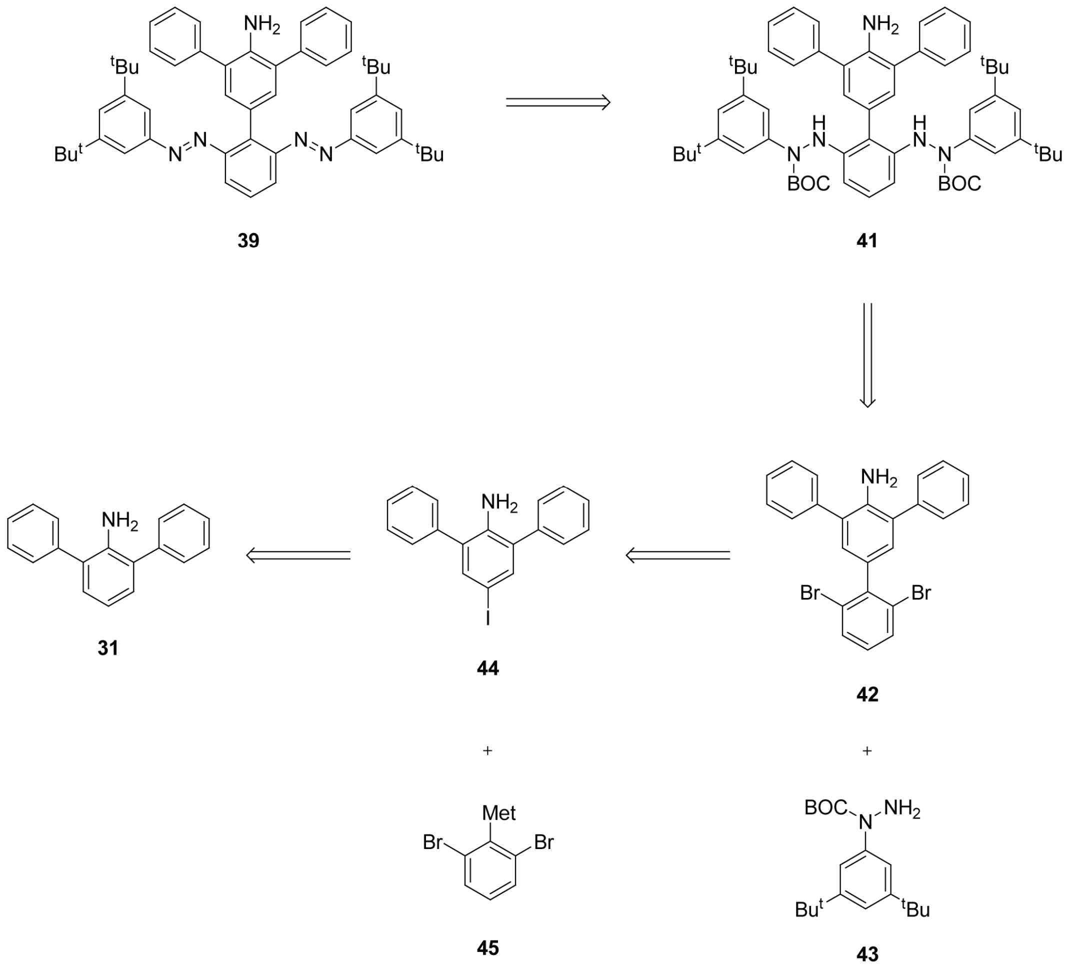

The synthesis of target NHC **35** was tackled along two lines: (a) synthesis of the photochromic aniline **39** according to Scheme 34, and (b) synthesis of a model compound to find access to the basic NHC framework of **35** without photochromic substituents, in strong analogy to the synthetic pathways followed towards NHC **28**. In the following, synthetic efforts directed in these directions will be discussed separately.

4.5.2.1 Synthesis of the Photochromic Terphenyl Aniline

The first key-intermediate in the synthesis of the photochromic terphenyl aniline **39** is easily obtained from 2,6-diphenylaniline **31** (see Scheme 29) by iodination with iodomonochloride in glacial acetic acid (Scheme 35).[39]

Scheme 35: Synthesis of 4-iodo-2,6-diphenylaniline **44**.

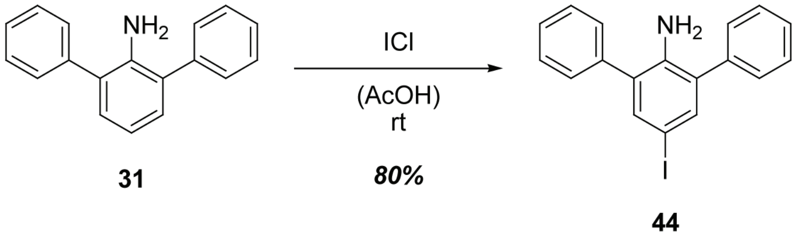

Initially, it was intended to connected 4-iodo-2,6-diphenylaniline **44** and the organometallic building block **45** via Negishi cross-coupling as outlined in Scheme 36.[40] Deprotonation of 1,3-dibromobenzene **46** using LDA at low temperature was expected to generate an unstable 2-lithiated intermediate, which is subsequently trapped by addition of dried zinc chloride. Cross-coupling of the more stable zinc intermediate with 4-iodo-2,6-phenylaniline **44** catalyzed by $Pd(PPh_3)_4$ did not lead to the expected dibromo quaterphenyl **42** in satisfying yields. The lithiation step could be ruled out as a source of failure, since the lithiated species could be successfully trapped by tri-*n*-butylstannylchloride (*vide infra*). Analysis of the crude product mixture by HPLC-MS indicated only very low conversion (64% starting material; maximum 13% product; many side-products). Moreover, HPLC and TLC analysis indicated a serious separation problem. Since no efficient access to the desired quaterphenyl by Negishi cross-coupling could be found,[b] new coupling strategies were devised.

Scheme 36: Attempted synthesis of dibromoaniline **42** by Negishi coupling.

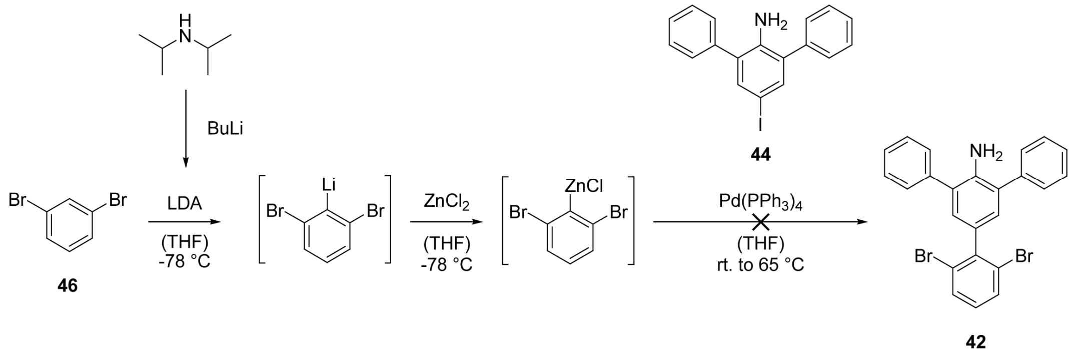

Stille-type cross-coupling is known to have a distinct selectivity for iodine over bromine.[41] Therefore, 1,3-dibromo-2-tri-*n*-butylstannylbenzene **47** was synthesized by deprotonation of 1,3-dibromobenzene **46** and subsequent trapping of the intermediate with tri-*n*-butylstannylchloride (Scheme 37).[42] Purification attempts of the crude product mixture by Kugelrohr distillation were unsuccessful but the mixture was sufficiently pure for further use without purification.

---

[b] The coupling is one of the key reactions in a multistep synthesis. Therefore, higher yields are required to give access to a sufficient amount of material.

Scheme 37: Synthesis of 1,3-dibromo-2-tri-*n*-butylstannylbenzene **47**.

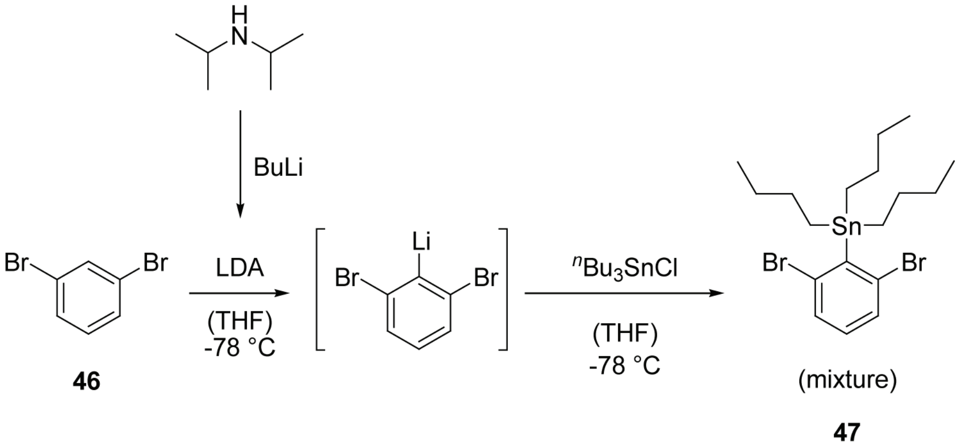

Coupling of the dibromo stannyl **47** with 4-iodo-2,6-diphenylaniline **44** in dry DMF applying standard conditions was not successful (Scheme 38).[43] No product formation could be detected by TLC monitoring.

Scheme 38: Attempted synthesis of 4-(2,6-dibromophenyl)-2,6-diphenylaniline **42**.

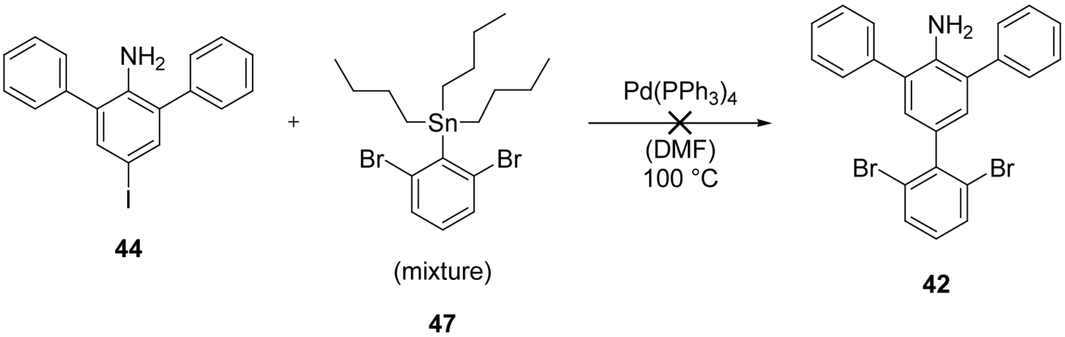

Electron-rich aryl halides are difficult substrates for palladium-catalyzed cross-coupling reactions, since the oxidative addition of the metal center to the aryl-halogen bond is slow. A partial deactivation of the amine-donor in **44** can be achieved by amide bond formation. Therefore, 4-iodo-2,6-diphenylaniline **44** was converted into *N*-(4-iodo-2,6-diphenylphenyl)-*O*-ethyl-oxalyl monoamide **48**, anticipating the necessary formation of related species when establishing the C_2-linker between the two aniline moieties according to Scheme 33 (see also Scheme 11). The oxalyl monoamide **48** was easily accessible by reaction of 4-iodo-2,6-diphenylaniline **44** with ethyl oxalyl chloride (Scheme 39). [26]

Scheme 39: Synthesis of *N*-(4-iodo-2,6-diphenylphenyl)-*O*-ethyl-oxalyl monoamide **48**.

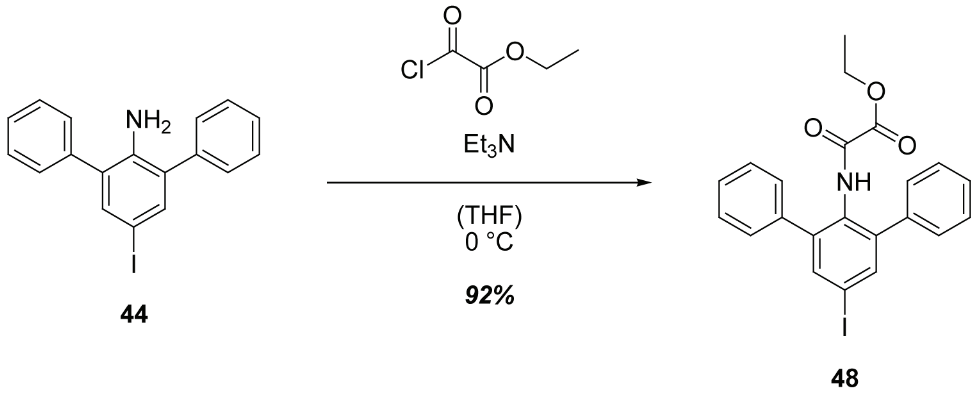

Palladium mediated cross-coupling of iodo oxalyl monoamide **48** and 1,3-dibromo-2-tri-*n*-butylstannylbenzene **47** to give *N*-(4-(2,6-dibromophenyl)-2,6-diphenylphenyl)-*O*-ethyl-oxalyl monoamide **49** was not successful (Scheme 40). Several conditions were tested but either the stannyl decomposed before coupling or no reaction took place at all. Conditions tested include use of $Pd(PPh_3)_4$ without additives[43] and use of $Pd(PPh_3)_4$ with CuI as well as CuI and CsF additives.[44,45] Replacing dibromostannyl compound **47** with an organozinc species derived from 1,3-dibromobenzene **46** (Scheme 36) and employing it in a subsequent Negishi-type cross-coupling was not successful as well (Scheme 41). [40]

Scheme 40: Attempted syntheses of *N*-(4-(2,6-dibromophenyl)-2,6-diphenylphenyl)-*O*-ethyl-oxalyl monoamide **49** via Stille coupling - Part I.

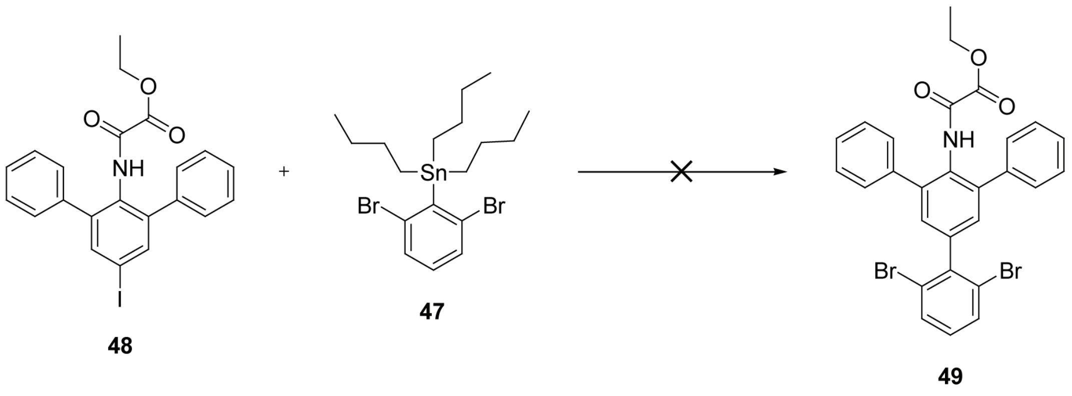

conditions:
(a) cat. $Pd(PPh_3)_4$ / dry DMF
(b) cat. $Pd(PPh_3)_4$ + cat. CuI / dry DMF
(c) cat. $Pd(PPh_3)_4$ + cat. CuI + 2 equiv. CsF / dry DMF

Scheme 41: Attempted synthesis of *N*-(4-(2,6-dibromophenyl)-2,6-diphenylphenyl)-*O*-ethyl-oxalyl monoamide **49** via Negishi coupling.

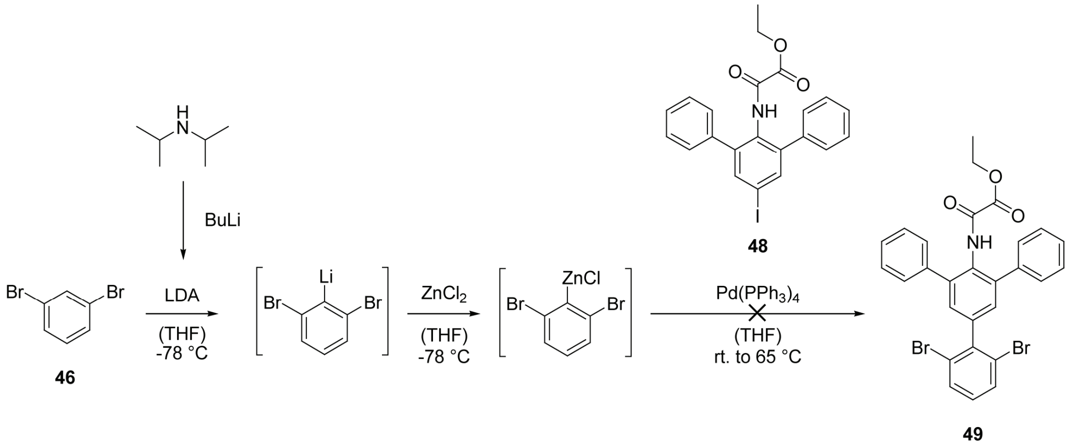

So far, all attempts to access dibromoaniline **42** or its corresponding amide **49** from terphenyl iodides and organometallic species **45** failed. Possible reasons are either a strong deactivation of the terphenyl iodides by electronic factors and/or a pronounced reactivity drop of the organometallic species by equally unknown factors, either of electronic or steric origin. To rule out these factors, functionalities were switched between both coupling components. *N*-(4-tri-*n*-butylstannyl-2,6-diphenylphenyl)-*O*-ethyl-oxalyl monoamide **50** was conveniently obtained by palladium-mediated cross-coupling of *N*-(4-iodo-2,6-diphenylphenyl)-*O*-ethyl-oxalyl monoamide **48** with hexa-*n*-butylditin **51** (Scheme 42).[45] Sandmeyer-reaction with 2,6-dibromoaniline **14** provided easy access to the second coupling component 2,6-dibromoiodobenzene **52** (Scheme 43).[46]

Scheme 42: Synthesis of *N*-(4-tri-*n*-butylstannyl-2,6-diphenylphenyl)-*O*-oxalyl monoamide **50**.

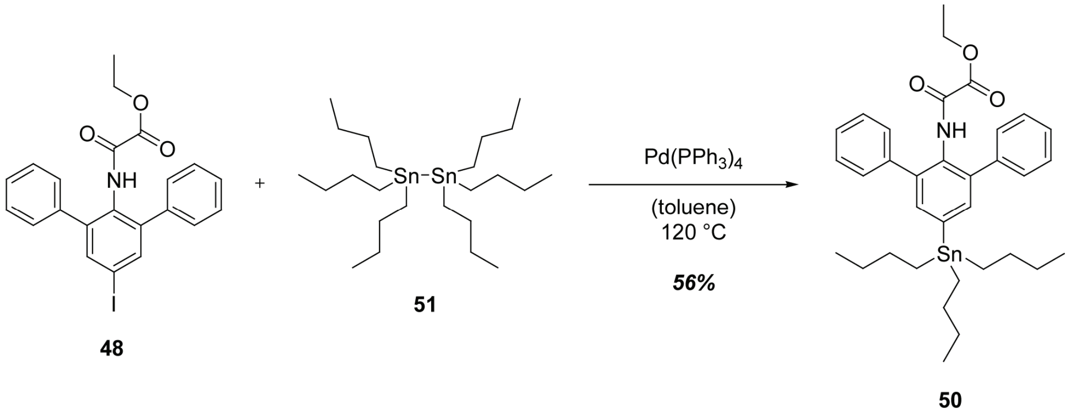

Scheme 43: Synthesis of 2,6-dibromoiodobenzene **52**.

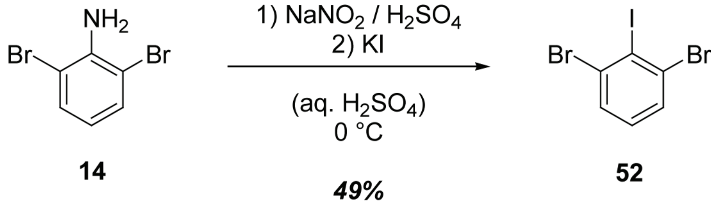

Stille coupling of the stannyl terphenyl amide **50** with 2,6-dibromoiodobenzene **52** was not successful (Scheme 44). No product could be isolated by employing either pure $Pd(PPh_3)_4$ as catalyst[43] or $Pd(PPh_3)_4$ in combination with catalytic amounts of CuI and stoichometric amounts of CsF.[44,45] Microwave irradiation of samples containing the $Pd(PPh_3)_4$-catalyst did not facilitate the reaction. TLC and HPLC-MS analysis of the crude mixture indicated no reaction at all.

Scheme 44: Attempted syntheses of *N*-(4-(2,6-dibromophenyl)-2,6-diphenylphenyl)-*O*-ethyl-oxalyl monoamide **49** via Stille coupling - Part II.

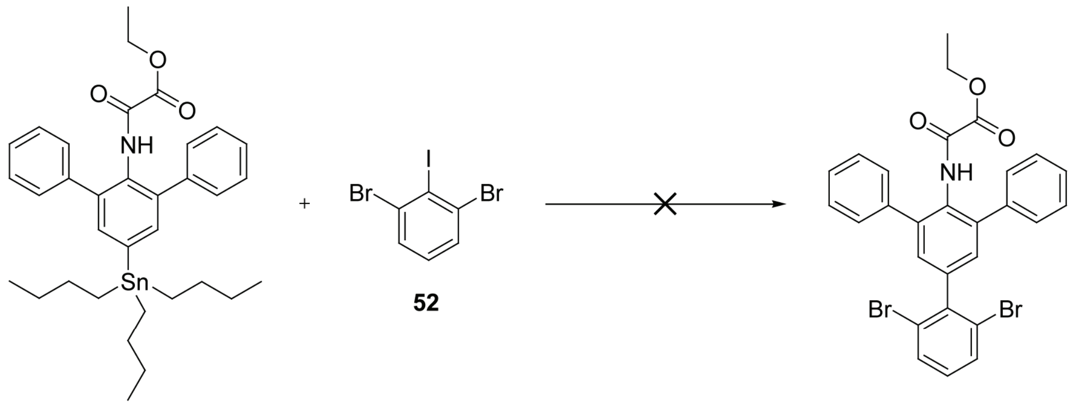

50 **52** **49**

conditions:
(a) cat. $Pd(PPh_3)_4$ / dry DMF
(b) cat. $Pd(PPh_3)_4$ + µw irradiation / dry DMF
(c) cat. $Pd(PPh_3)_4$ + cat. CuI + 2 equiv. CsF / dry DMF

Organotin reagents proved to be unsuitable coupling components for obtaining terphenyls **42** or **49**. Therefore, synthetic pathways towards these components based on boronic esters were developed to exploit the higher reactivity of these substrates in Suzuki-type cross-coupling reactions.[47,48] Considering the low reactivity of terphenyl iodide **44** in Stille-type reactions (Scheme 38), amino-terphenyl boronic esters or related amides were identified as promising coupling reagents. Boronic esters are frequently obtained by quenching of lithiated species with suitable borates (*vide infra*). The presence of an unprotected amine in 4-iodo-2,6-diphenylaniline **44** precludes this pathway, making cross-coupling strategies necessary to introduce the boronic ester. Indeed, 4-amino-3,5-diphenylphenyl-4,4,5,5-tetramethyl-1,3,2-dioxaborolane **53** was obtained from 4-iodo-2,6-diphenylaniline **44** by reaction with pinacolborane **54** in the presence of a palladium-catalyst (Scheme 45). However, yields were very low, not exceeding 8%, and amino boronic ester **53** was not used in cross-coupling attempts.[49]

Scheme 45: Synthesis of 4-amino-3,5-diphenylphenyl-4,4,5,5-tetramethyl-1,3,2-dioxaborolane **53** (DPEphos: bis(2-diphenylphosphinophenyl)ether).

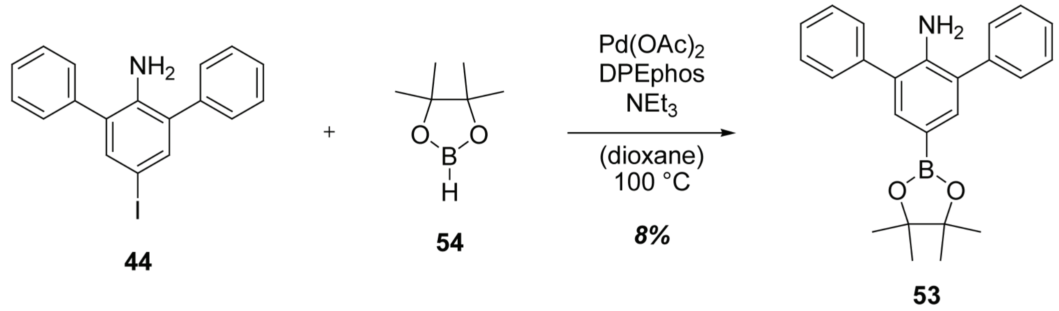
NH2
I
44
+
O
B
O
H
54
Pd(OAc)2
DPEphos
NEt3
(dioxane)
100 °C
8%
NH2
B
O
O
53

The less deactivated *N*-(4-iodo-2,6-diphenylphenyl)-*O*-ethyl-oxalyl monoamide **48** was reactive enough to obtain the desired boronic ester. Use of pinacol diborane **55** proved to be more effective in this case, despite the fact of being less atom economic, allowing to isolate (4-ethyloxalylamido-3,5-diphenylphenyl)-4,4,5,5-tetramethyl-1,3,2-dioxaborolane **56** in 50% yield.[50]

Scheme 46: Synthesis of (4-ethyloxalylamido-3,5-diphenylphenyl)-4,4,5,5-tetramethyl-1,3,2-dioxaborolane **56**.

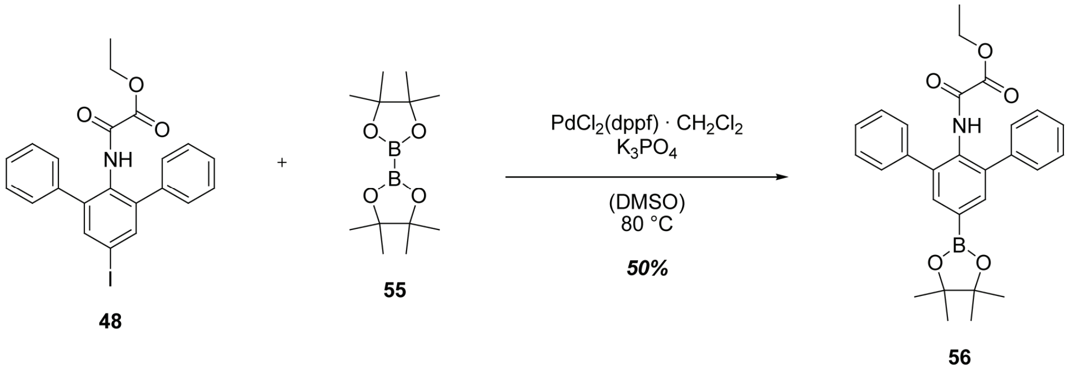
O
O
O
NH
I
48
+
O
B
O
B
O
O
55
PdCl2(dppf) · CH2Cl2
K3PO4
(DMSO)
80 °C
50%
O
O
O
NH
B
O
O
56

Cross-coupling attempts of boronic ester **56** with 2,6-dibromoiodobenzene **52** were not successful. Use of standard conditions in a biphasic solvent mixture (toluene/aq. $NaHCO_3$)[51] as well as Buchwald conditions[33] did not give desired *N*-(4-(2,6-dibromophenyl)-2,6-diphenylphenyl)-*O*-ethyl-oxalyl monoamide **49** (Scheme 47). No product could be identified by MS and NMR analysis of the crude product mixture obtained from standard conditions. Buchwald conditions gave no conversion at all.

Scheme 47: Attempted syntheses of *N*-(4-(2,6-dibromophenyl)-2,6-diphenylphenyl)-*O*-ethyl-oxalyl monoamide **49** via Suzuki-coupling (S-Phos: 2-dicyclohexylphosphino-2′,6′-dimethoxybiphenyl).

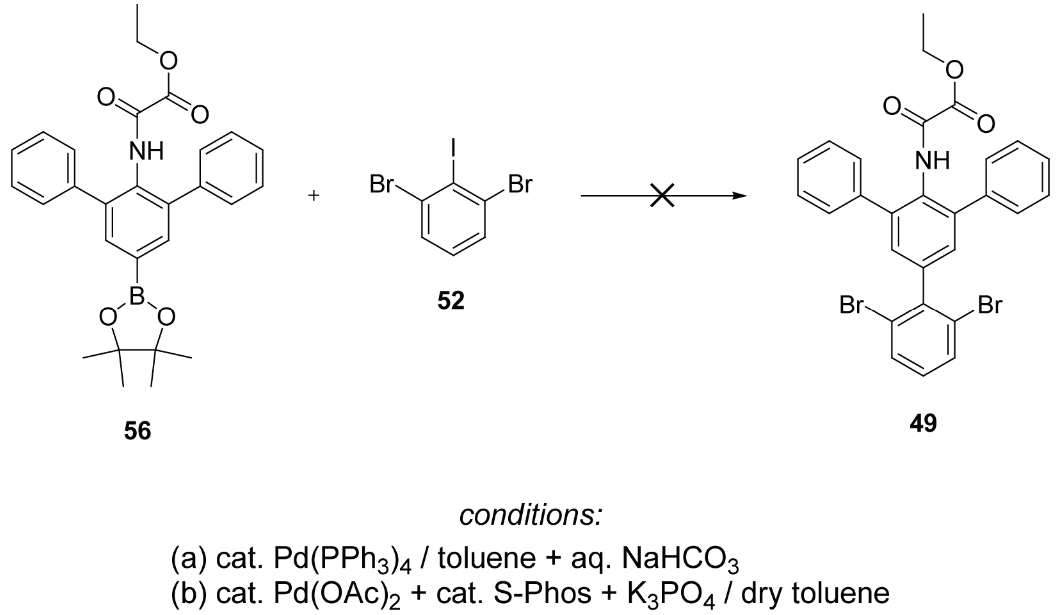
O
O
O
NH
B
O
O
56
+
I
Br
Br
52
O
O
O
NH
Br
Br
49
conditions:
(a) cat. Pd(PPh3)4 / toluene + aq. NaHCO3
(b) cat. Pd(OAc)2 + cat. S-Phos + K3PO4 / dry toluene

Changing the functionalities of the coupling partners as attempted for the Stille-substrates was not successful as well. Attempts to access (2,6-dibromophenyl)-4,4,5,5-tetramethyl-1,3,2-dioxaborolane **57** from 1,3-dibromobenzene **46** were hampered by aryne formation.[52] The reactive intermediate was trapped by reaction with diisopropyl amine formed in the reaction to give *N*,*N’*-di-*iso*-propyl-3-bromoaniline **58**, which was unambiguously confirmed by NMR.

Scheme 48: Attempted synthesis of (2,6-dibromophenyl)-4,4,5,5-tetramethyl-1,3,2-dioxaborolane **57**.

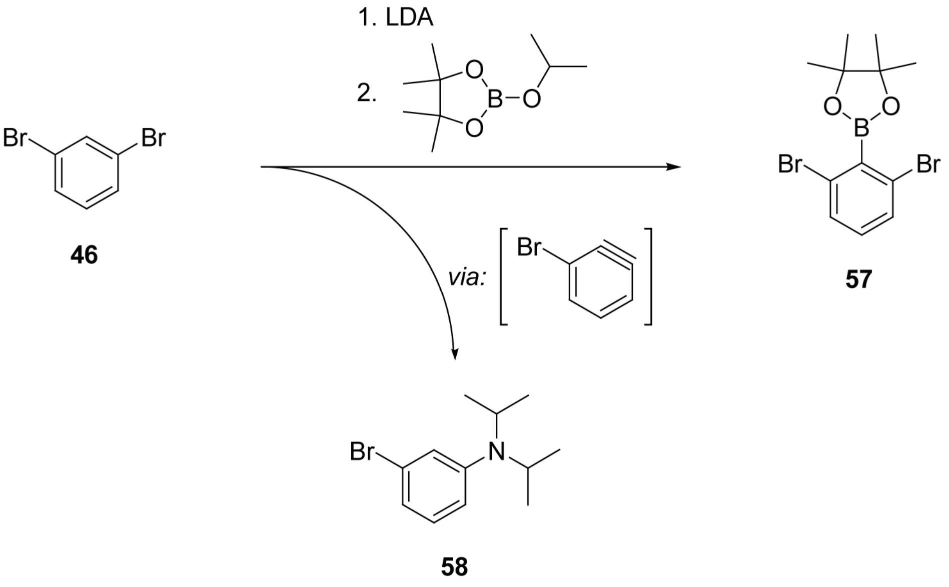

In summary, no synthetic access to the photochromic aniline **39** could be established. All attempts to construct the quaterphenyl framework of **39** by cross-coupling reactions failed. Presumably, the substrates were either too hindered by (electronically) unfavorable *ortho*-substituents or the aryl iodides were only poorly activated for cross-coupling and hence did not display the necessary reactivity.

Nonetheless, the basic NHC framework of **35** without photochromic substituents is an interesting synthetic target with potentially interesting coordination behavior and catalytic properties. Therefore, synthetic attempts were directed towards the synthesis of a nonsymmetrical NHC derived from 2,6-diphenylaniline **31** or one simple derivative thereof.

4.5.2.2 Synthesis of the Nonsymmetrical NHC-Framework

Nonsymmetrical NHCs of the general type shown in Scheme 49 are interesting compounds, because the extreme steric bulk around the carbene carbon atom is expected to lead to unusual coordination behavior and catalytic properties. For example, polymerization of lactide by NHCs was found to be extremely sensitive towards the steric surrounding of the active site and to electronic factors.[22]

Scheme 49: Target structure of a nonsymmetrical NHC carrying one terphenyl-substituent **59**.

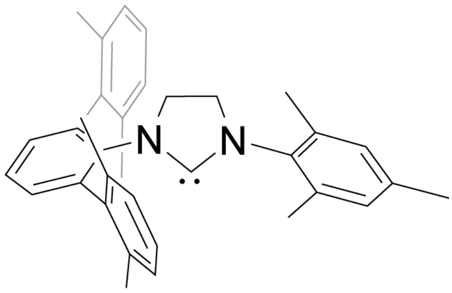

59

Retrosynthetic analysis of the nonsymmetrical NHC **59** is straight forward (Scheme 50). Carbene **59** is derived from its corresponding imidazolinium salts **60** by deprotonation. Ethylenediamine **61** is the direct precursor of salt **60** and can be obtained from the nonsymmetrical oxalamide **62** by reduction. Oxalamide **62** is easily assembled from 2,6-diphenylaniline **31**, mesityl amine **40**, and ethyl oxalyl chloride.[26]

Scheme 50: Retrosynthetic analysis of imidazolium salt **60**.

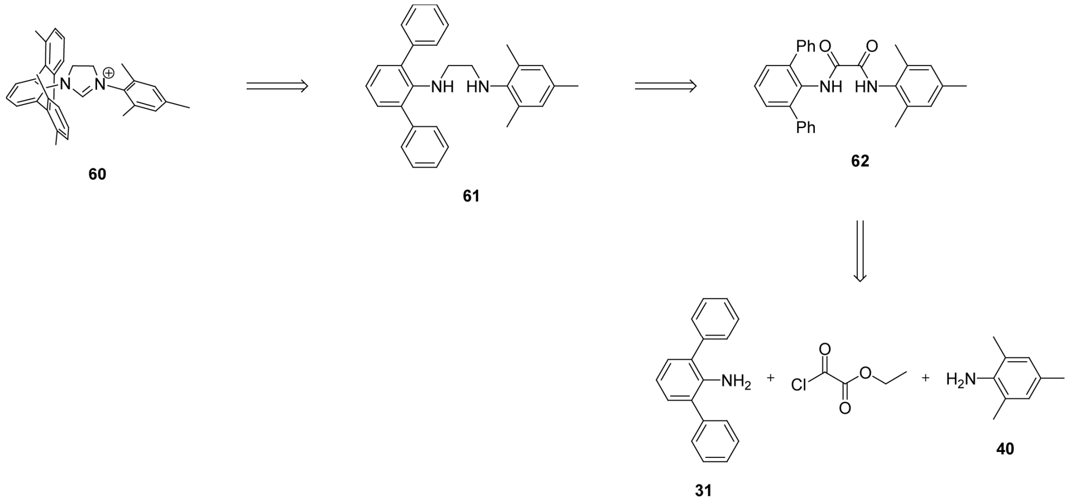

Reaction of 2,6-diphenylaniline **31** with ethyl oxalyl chloride proceeds smoothly to give *N*-(2,6-diphenylphenyl)oxanilic acid **63** (Scheme 51). Simplifying the reported two step procedures, the product was obtained in an one-pot/two-step sequence involving initial formation of the ethyl ester of **63**, which was hydrolyzed to give the free acid **63** in the same pot by addition of aqueous NaOH-solution.[26]

Scheme 51: Synthesis of *N*-(2,6-diphenylphenyl)oxanilic acid **63**.

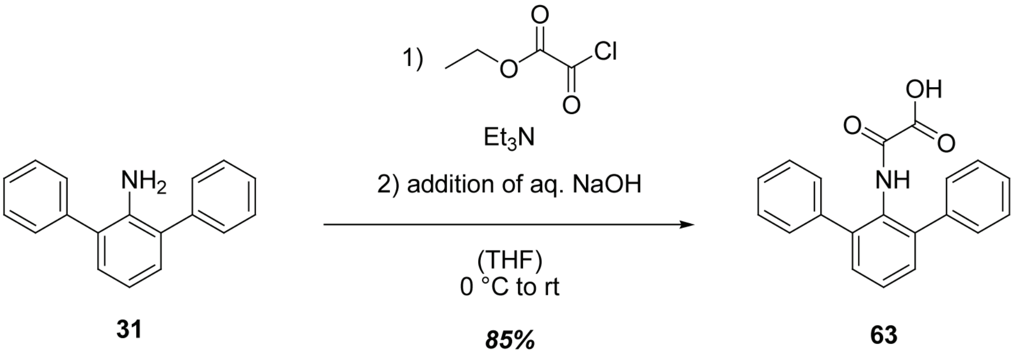
NH2
1)
O
Cl
O
O
Et3N
2) addition of aq. NaOH
(THF)
0 °C to rt
85%
OH
O
O
NH
31
63

Reaction of *N*-(2,6-diphenylphenyl)oxanilic acid **63** with oxalylic chloride and subsequent reaction of the acid chloride with mesityl aniline **40** allowed easy access of *N*-(2,6-diphenylphenyl)-*N'*-(2,4,6-trimethylphenyl)oxalamide **64** (Scheme 52).[26]

Scheme 52: Synthesis of *N*-(2,6-diphenylphenyl)-*N'*-(2,4,6-trimethylphenyl)oxalamide **64**.

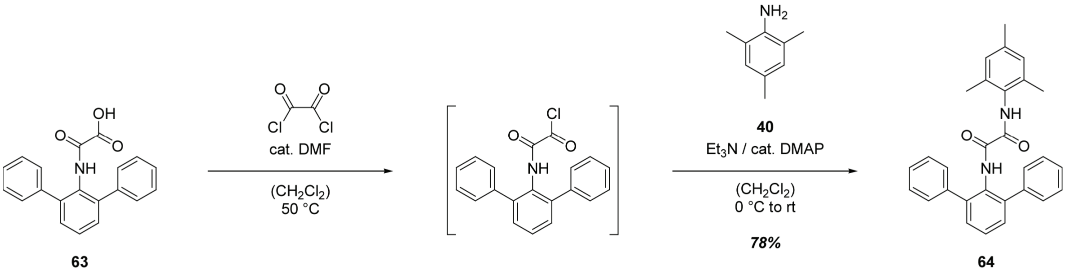
OH
O
O
NH
63
O
O
Cl
Cl
cat. DMF
(CH2Cl2)
50 °C
Cl
O
O
NH
NH2
40
Et3N / cat. DMAP
(CH2Cl2)
0 °C to rt
78%
NH
O
O
NH
64

Reduction of oxalamide **64** was not straight forward. Initial attempts to reduce **64** with lithium aluminumhydride in refluxing THF just allowed for re-isolation of unreacted starting material even after prolonged reaction times. Promising results obtained for reductions of other substrates with borane-THF-complex (*vide infra*) could not be reproduced for oxalamide **64**. An extremely complex reaction mixture was obtained instead. However, reduction can be achieved by employing diisobutylaluminium hydride (DIBAL) in refluxing THF allowing to isolate *N*-(2,6-diphenylphenyl)-*N'*-(2,4,6-trimethylphenyl)ethylenediamine **65** in 90% yield. (Scheme 53). The reaction could be driven to high conversion by dropwise addition of a large excess of DIBAL in two major batches and prolonged reaction times. Considering the low reactivity of lithium aluminumhydride and the contrasting reactivities of borane and DIBAL, it can be concluded that an electrophilic reducing agents helps the reduction step, presumably by pre-coordination to the amide functionality.

Scheme 53: Synthesis of *N*-(2,6-diphenylphenyl)-*N'*-(2,4,6-trimethylphenyl)ethylenediamine **65**.

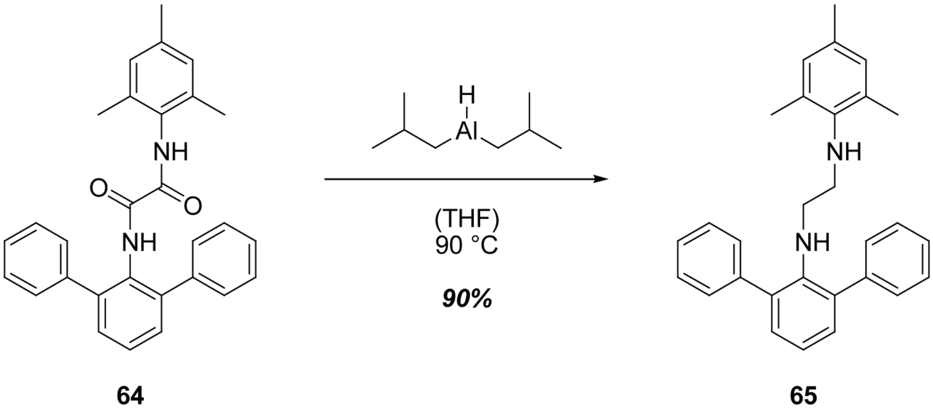

It is worth mentioning that reduction of an oxalamide analogous to **64**, but derived from 4-iodo-2,6-diphenylaniline **44**, was even more complicated. Aluminumhydride reagents are not suitable, since reduction of the iodine functionality is to be expected. Therefore, reduction was accomplished by use of borane-THF complex as a relatively mild reducing agent. However, the reaction proceeds with low reproducibility in extremely varying yields.

To facilitate reduction, alternative pathways to ethylenediamine **65** were devised. Upon monitoring the reduction of oxalamide **64** it becomes evident that one reduction proceeds quite fast, whereas the second reduction is significantly slower. Although no unambiguous proof can be given, it seems reasonable to assume a fast reduction of the amide next to the mesitylene group due to the smaller extent of shielding. Reduction of the amide functionality next to the terphenyl residue is expected to be substantially hindered by the great extent of steric shielding. Therefore, reduction of the ethyl (2,6-diphenylphenylamino)acetate **66** is assumed to proceed more smoothly. Possible access to monoamide **66** is provided by alkylation of 2,6-diphenylaniline **31** with ethyl chloroacetate (Scheme 54). However, steric crowding prevents an alkylation of aniline **31** and the starting material was completely recovered from the reaction mixture. Attempts to enhance the nucleophilicity of **31** by deprotonation with *n*-butyl lithium were not successful, giving 2-chloro-*N*-(2,6-diphenylphenyl)acetamide instead, which is expected to be difficult to reduce based on the concerns raised above.

Scheme 54: Attempted synthesis of ethyl (2,6-diphenylphenylamino)acetate **66**.

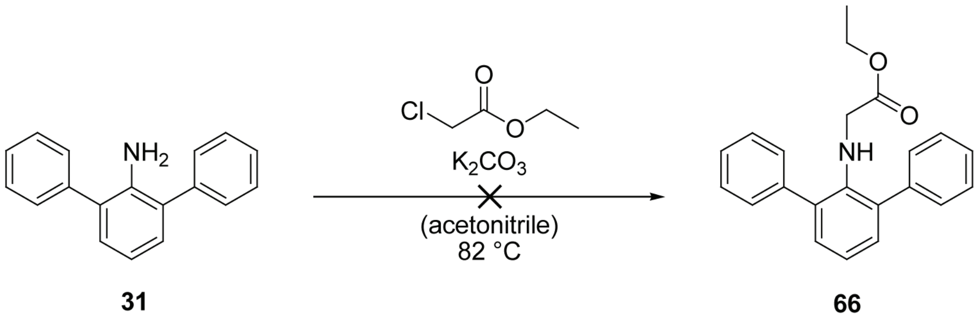

Imidazolinium salt **60** could not be obtained starting from ethylenediamine **65** (Scheme 55). A variety of conditions were tested, but either just allowed to recover unreacted starting material or to obtain hardly soluble materials, which revealed no organic protons by NMR. Attempts to separate charged from uncharged species utilizing ion exchange resins only led to unsatisfying results. Conditions tested were based on variations of a protocol developed by Bielawski and co-workers:[36] ethylenediamine **60** was reacted with triethyl orthoformate in the presence of strong mineral acids, such as HBF_4 or HCl at high temperatures in either closed or open systems. No enhanced reactivity was observed upon microwave irradiation of selected samples.

Scheme 55: Attempted syntheses of imidazolinium salt **60**.

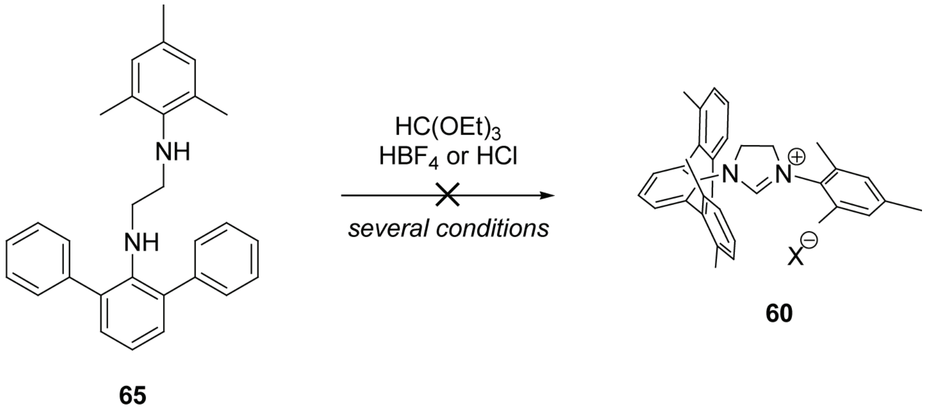

Considering Scheme 11, an alternative approach towards imidazolinium salts utilizes formamidines, which upon double alkylation by 1,2-dichloroethane give the respective imidazolinium salts.[27] Adapting the reported two-step procedure, 2,6-diphenylaniline **31** was reacted with triethyl orthoformate followed by addition of mesityl amine **40** to form the formamidine **67**. Indeed, UPLC analysis of a colorless solid obtained by recrystallization from acetone revealed *N*-(2,6-diphenylphenyl)-*N'*-(2,4,6-trimethylphenyl)formamidine **67**. NMR-analysis is hampered by complex equilibria between several tautomeric forms and therefore provides limited information.

Scheme 56: Synthesis *N*-(2,6-diphenylphenyl)-*N'*-(2,4,6-trimethylphenyl)formamidine **67**.

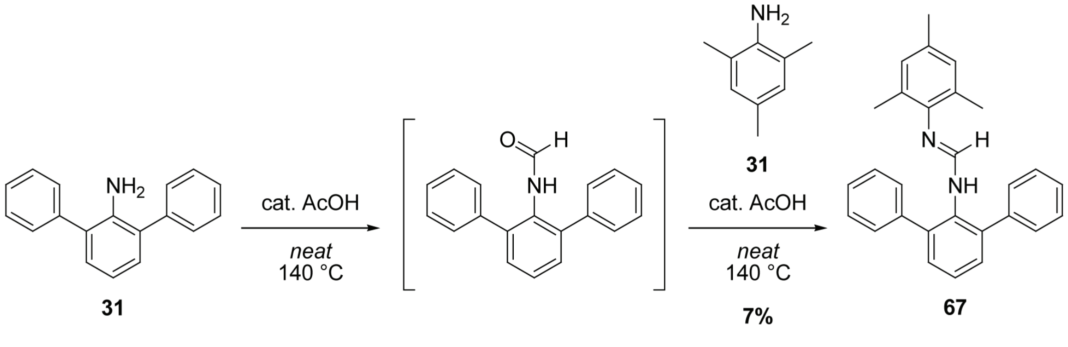

Formation of imidazolium salt **60** from formamidines **67** was not possible. Reaction with 1,2-dichloroethane gave a mixture of various products. However, purification by recrystallization was not possible and UPLC-analysis of the materials obtained was not conclusive, revealing several products. Despite the fact that UPLC points to the presence of the desired product in the mixture, this is only weak evidence, since the method was not verified for charged compounds, retention times were very short, and peak shapes as well as peak separation were doubtful (*vide supra*). These investigations were hampered by the availability of only small amounts of material, making isolation and characterization extremely difficult. Future work will be directed towards a final evaluation of the findings reported above.

Scheme 57: Attempted synthesis of imidazolinium salt **60**.

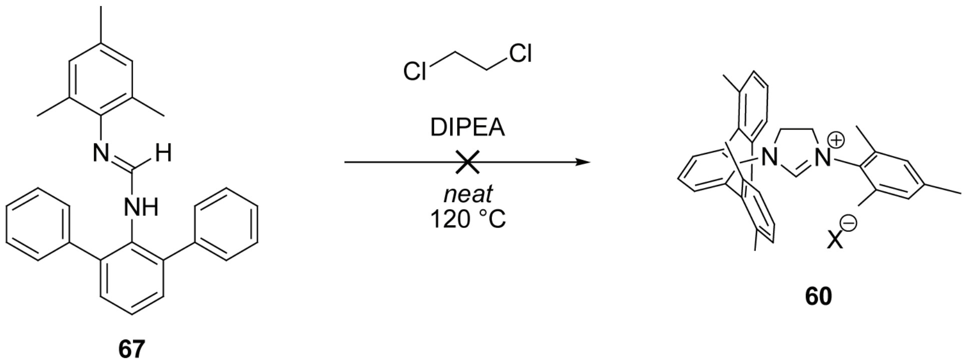

4.6 Concluding Remarks

The synthesis of photoswitchable *N*-heterocyclic carbenes bearing one or two *meta*-terphenyl-based moieties to ensure shielding of the carbene's active site could not be accomplished. Consequently reducing the degree of steric shielding in the carbenes **8**, **28**, and **35** did not succeed in enabling successful synthesis. Even the basic framework of the sterically least encumbered carbene **35** was not accessible in several attempts involving conceptually different pathways. Therefore, it seems reasonable to conclude that carbenes bearing 2,6-phenyl substituents on one or both aryl rings are not accessible by known conventional synthetic efforts. Detection of ions corresponding to the desired imidazolinium salts by MS, eventually coupled to a HPLC-system, is evidence for the formation of - at least - trace amounts of the desired products. Accordingly, the target structure might be accessible by other, unconventional synthetic routes in combination with sophisticated purification methods. Thus, future synthetic work might succeed in successfully synthesizing carbenes of the terphenyl-type.

Introduction of the switching unit for reversible steric blocking of the active site constitutes another task to be overcome. Intensive attempts to assemble the switching unit failed due to the low reactivity of various functionalized substrates towards cross-coupling. Again, future synthetic efforts might allow to access suitable precursors for photoswitchable NHCs by finding appropriate synthetic protocols.

4.7 Experimental

4.8 General Methods

Solvents and starting materials were used as received. Toluene and THF were distilled under an argon atmosphere over sodium prior to use. Dry DMF was purchased from Acros or distilled under an argon atmosphere from calcium hydride. All reactions were performed in an argon atmosphere. Column chromatography was carried out with 130 - 400 mesh silica gel. NMR spectra were recorded on a 400 MHz (100.6 MHz for ^{13}C) Bruker AV 400 or on a 300 MHz (75.6 MHz for ^{13}C) Bruker DPX 300 spectrometer at 27 °C using residual protonated solvent signals as internal standard (^{1}H-NMR: $\delta(CDCl_3) = 7.24$ ppm, $\delta(CD_3CN) = 1.94$ ppm, δ(THF-*d8*) = 3.58 ppm and ^{13}C-NMR: $\delta(CDCl_3) = 77.0$ ppm, $\delta(CD_3CN) = 1.32$ ppm). Mass spectrometry was performed on Thermo LTQ FT instrument (ESI, ESI-HRMS: additives of mixtures of MeOH/H_2O 75/25 + 0.5% formic acid) and MSI concept 1H (EI, 70eV ionization) as well as on a QSTARXL Applied Q-TOF with a ISV of 950 V. HPLC separations were performed with Shimadzu LC-10A systems equipped with a photodiode array detector (PAD or DAD) or with Waters Alliance systems (mixtures and gradient mixtures of acetonitrile/water) equipped with 150 x 2 mm Luna columns (3 µm, phenyl-hexyl material). The Waters systems consisted of a Waters Separations Module 2695, a Waters Diode Array detector 996 and a Waters Mass Detector ZQ 2000. Conditions are specified when describing the corresponding substances. UPLC separations were preformed with a Waters Acquity system equipped with Acquity UPLC columns, a Water Diode Array detector, and a LCTPremierXE TOF-MS detector.

4.9 Synthetic Procedures

Pentiptycenediol bistriflate **3**

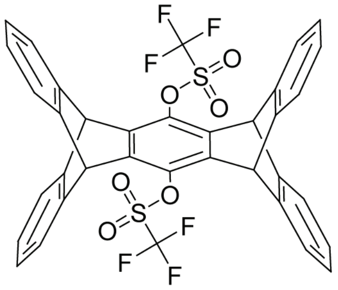

A dry Schlenk-tube was charged with 231 mg of pentiptycenediol **4** (0.50 mmol, 1 equiv.), 1.1 mL of dry triethylamine, and 15 mL of dry methylene chloride at 0 °C. After addition of 0.21 mL of triflic anhydride (1.25 mmol, 2.5 equiv.), the now red/black colored mixture was stirred at room temperature for 30 min. The mixture was poured onto ice/water, phases were separated, and the aqueous layer was extracted with methylene chloride three times. Combined organic layers were washed with 1N aq. HCl solution and brine three times, respectively. Drying over $MgSO_4$ and removal of solvent *in vacuo* gave a violet product which was further purified by column chromatography using a CH_2Cl_2/Hex (1.5/8.5) eluent mixture to give 252 mg of colorless product (69%). R_f (CH_2Cl_2/Hex, 2/8) = 0.32. ^{1}H-NMR ($CDCl_3$, 400 MHz): δ (ppm) = 7.40 (dd, $^3J = 5.30$ Hz, $^4J = 3.23$ Hz, 8H, Ar*H*), 7.02 (dd, $^3J = 5.41$ Hz, $^4J = 3.14$ Hz, 8H, Ar*H*), 5.74 (s, 4H, C-*H*). ^{13}C-NMR ($CDCl_3$, 100 MHz): δ (ppm) = 143.38 (*C*-OTf), 139.51 (C_{Ar}), 137.32 (C_{Ar}), 126.08 (C_{Ar}), 124.57 (C_{Ar}), 120.59 (CF_3), 48.93 (*C*-H). DEPT135 ($CDCl_3$): δ (ppm) = 126.08 (pos., C_{Ar}), 124.57 (pos., C_{Ar}), 48.93 (pos., *C*-H). MS (EI, 230 °C): m/z = 726 ($[M]^+$), 415, 202. HRMS (ESIpos): *calculated for* $C_{36}H_{20}O_6S_2F_6$ + Na: 749.049775, *found*: 749.049279. HPLC (methanol/water = 90/10, 0.8 mL/min, 125 mm Nucleodur 100-5-C18ec, DAD 220 nm): 26.03 min (100% peak area).

Pentiptycenediol **4**

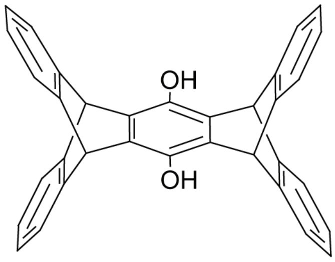

A one-necked flask equipped with a reflux condenser was charged with 230 mg of pentiptycenedione **7** (0.50 mmol), 230 mg zinc powder, and 230 mg zinc chloride. After addition of 5 mL of ethanol and flushing the mixture with argon three times, it was heated to reflux for 1.5 h. Water was added and the aqueous layer was extracted with methylene chloride three times. Combined organic layers were washed with water three times, dried over $MgSO_4$, and solvent was removed *in vacuo* to 232 mg give pure product (100%). R_f (CH_2Cl_2/Hex, 8/2) = 0.18. ^{1}H-NMR ($CDCl_3$, 400 MHz): δ (ppm) = 7.32 (dd, $^3J = 5.10$ Hz, $^4J = 3.31$ Hz, 8H, Ar*H*), 6.93 (dd, $^3J = 5.26$ Hz, $^4J = 3.14$ Hz, 8H, Ar*H*), 5.62 (s, 4H, C-*H*), 4.55 (s, broad, 2H, O*H*). ^{13}C-NMR and DEPT135 spectra could not be obtained due to intrinsic low solubility of pentiptycenediol in all common NMR solvents. MS (EI, 310 °C): m/z = 462 ($[M]^+$), 445 ($[M - OH]^+$), 427 ($[M - 2\,OH]^+$), 339, 284, 231, 207, 178. HRMS (ESIpos): *calculated for* $C_{34}H_{22}O_2$ + H: 463.169252, *found*: 463.169595. HPLC (methanol/water = 65/35, 0.8 mL/min, 125 mm Nucleodur 100-5-C18ec, DAD 220 nm): 13.51 min (100% peak area).

Pentiptycenedione **7**

Pentiptycenedione **7** was synthesized adopting procedures developed by Williams et. al.[29] and Zhu et. al.[30]

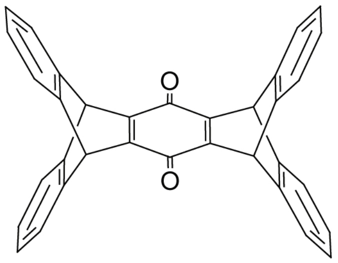

A one-necked flask was charged with 50 mL of glacial acetic acid, 5.41 g of benzoquinone **4** (50 mmol, 1 equiv.), and 17.82 g of anthracene **5** (100 mmol, 2 equiv.). The mixture was heated to reflux for 3 days. After cooling to room temperature, 12.29 g of *p*-chloranil (50 mmol, 1 equiv.) were added in one portion and heating to reflux was continued for one day. Again, the mixture was cooled to room temperature and 8.35 g of potassium bromate were added in one portion. Heating to reflux was continued for another day. The mixture was cooled to room temperature and a yellow-brown solid was isolated by filtration. The solid was washed with plenty of water. A small amount of yellow product could be obtained by recrystallization from chloroform. The larger part was obtained by Soxhlet extraction of the remaining solid over the course of 5 days using toluene as solvent. Both product fractions were combined to give 6.92 g of yellow product (30%). R_f (CH_2Cl_2/Hex, 3/7) = 0.66. ^{1}H-NMR ($CDCl_3$, 400 MHz): δ (ppm) = 7.37 (dd, $^3J = 5.21$ Hz, $^4J = 3.18$ Hz, 8H, Ar*H*), 6.98 (dd, $^3J = 5.32$ Hz, $^4J = 3.10$ Hz, 8H, Ar*H*), 5.76 (s, 4H, C*H*). ^{13}C-NMR ($CDCl_3$, 100 MHz): δ (ppm) = 180.12 (*C*=O), 151.09, 143.80, 125.62 (C_{Ar}), 124.40 (C_{Ar}), 47.52 (*C*-H). DEPT135 ($CDCl_3$): δ (ppm) = 125.62 (pos., C_{Ar}), 124.40 (pos., C_{Ar}), 47.52 (pos., *C*-H). MS (EI, 295°C): m/z = 460 ($[M]^+$), 432 ($[M - CO]^+$), 404 ($[C_{32}H_{20}]^+$), 230 ($[C_{17}H_{10}O]^+$), 202 ($[C_{17}H_{10}O - CO]^+$), 178 ($[C_{14}H_{10}]^+$). HRMS (ESIpos): *calculated for* $C_{34}H_{20}O_2$ + H:

461.153603, *found*: 461.153466. HPLC (methanol/water = 90/10, 0.8 mL/min, 125 mm Nucleodur 100-5-C18ec, DAD 220 nm): 7.03 min (100% peak area).

2,6-Bis(2,6-dimethylphenyl)aniline **13**

Synthesis of 2,6-bis(2,6-dimethylphenyl)aniline **13** followed a synthetic protocol developed by Walker et. al.[33]

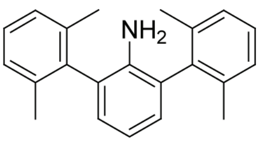

A dry sealable tube was charged with 1.033 g of 2,6-dibromoaniline **14** (4.12 mmol, 1 equiv.), 1.853 g of 2,6-dimethylphenylboronic acid **15** (12.35 mmol, 3 equiv.), 18 mg of palladium(II)acetate (0.082 mmol, 0.02 equiv.), 68 mg of 2-dicyclohexylphosphino-2′,6′-dimethoxybiphenyl (0.17 mmol, 0.04 equiv., S-Phos), and 2.622 g of finely ground, dry potassium phosphate (12.35 mmol, 3 equiv.). The tube was flushed with argon three times. Addition of 25 mL of dry toluene was followed by three freeze-pump-thaw cycles. The mixture was heated to 80 °C for 10 h with constant stirring. After dilution with toluene and addition of silica, the mixture was passed through a silica plug using ethyl acetate as eluent. The solvent was removed *in vacuo* to give crude product which was further purified by column chromatography using a CH_2Cl_2/Hex (2/8) eluent mixture to give 1.222 g of pure, colorless product (98%). R_f (CH_2Cl_2/Hex, 2/8) = 0.2. ^{1}H-NMR ($CDCl_3$, 400 MHz): δ (ppm) = 7.18 (m, 6H, Ar*H*), 6.92 (m, 3H, Ar*H*), 3.09 (s, broad, 2H, NH_2), 2.12 (s, 12H, CH_3). ^{13}C-NMR ($CDCl_3$, 100 MHz): δ (ppm) = 140.39 (C_{Ar}), 138.38 (C_{Ar}), 137.31 (C_{Ar}), 128.62 (C_{Ar}), 127.77 (C_{Ar}), 127.58 (C_{Ar}), 126.12 (C_{Ar}), 118.34 (C_{Ar}), 20.31 (CH_3). DEPT135 ($CDCl_3$): δ (ppm) = 128.62 (pos., C_{Ar}), 127.77 (pos., C_{Ar}), 127.58 (pos., C_{Ar}), 118.34 (pos., C_{Ar}), 20.31 (pos., CH_3). MS (EI, 70 °C): m/z = 301 ($[M]^+$), 286 ($[M - CH_3]^+$), 271 ($[M - 2\ CH_3]^+$), 254, 239. HRMS (ESIpos): *calculated for* $C_{22}H_{23}N$: 301.183051, *found*:

301.183348. HPLC (methanol/water = 80/20, 0.8 mL/min, 125 mm Nucleodur 100-5-C18ec, DAD 220 nm): 21.95 min (97% peak area).

N,N'-Bis-(2,6-di(2,6-dimethylphenyl)phenyl)glyoxal bisimine **18**

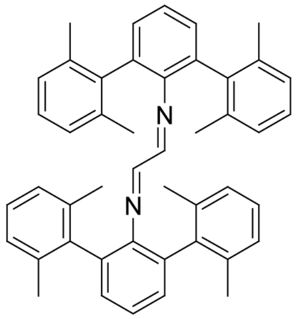

A one-necked flask was charged with 2 mL of ethanol, 211 mg of 2,6-bis(2,6-dimethylphenyl)aniline **13** (0.70 mmol, 2 equiv.), and 0.04 mL of glyoxal (0.35 mmol, 1 equiv., 40 wt% in water). The mixture was heated to 40°C under a steady stream of argon for 4 days followed by heating the mixture to reflux to additional 4 days. A very fine yellow powder formed, which was isolated by filtration and recrystallized from refluxing toluene to give 15 mg of the title compound as a yellow powder (7%). No NMR or MS spectra could be obtained due to the intrinsic insolubility of the material in all organic solvent. The identity of the title compound was confirmed by x-ray analysis of small crystals grown from refluxing toluene. X-Ray: [$C_{46}H_{44}N_2$], from toluene, M_r = 624.86, yellow crystals, *a* = 11.9531(3) Å, *b* = 11.9130(2) Å, *c* = 13.4631(2) Å, space group P 2_1/n, β = 113.948, U = 1752.07 $Å^3$.

2,6-Bis(2,6-dimethylphenyl)phenylisocyanate **19**

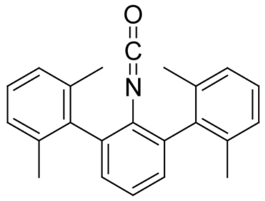

A dry Schlenk-tube was charged with 665 mg of 2,6-bis(2,6-dimethylphenyl)aniline **13** (2.21 mmol, 2.1 equiv.), 0.44 mL of dry triethylamine (3.15 mmmol, 3 equiv.), and 5 mL of dry methylene chloride. The mixture was cooled to 0 °C and 0.10 mL of oxalyl chloride (1.05 mmol, 1 equiv.) were added dropwise. The mixture was allowed to warm to room temperature over night. Solvent and excess oxalyl chloride were removed *in vacuo*. The residue was collected in diethyl ether, a colorless solid was filtered off, and the filtrate was concentrated *in vacuo* to obtain crude, colorless product which was further purified by flash column chromatography using a CH_2Cl_2/Hex (1/9) eluent mixture. The title compound was isolated as a colorless solid, the yield was 567 mg (82%). R_f (CH_2Cl_2/Hex, 3/7) = 0.5. ^{1}H-NMR ($CDCl_3$, 400 MHz): δ (ppm) = 7.36 (m, 1H, Ar*H*), 7.25 (m, 2H, Ar*H*), 7.17 (m, 6H, Ar*H*), 2.08 (s, 12H, C*H*$_3$). ^{13}C-NMR ($CDCl_3$, 100 MHz): δ (ppm) = 138.09, 137.02, 136.54, 131.35, 129.18 (C_{Ar}), 128.24 (C_{Ar}), 127.64 (C_{Ar}), 126.27 (C_{Ar}), 125.75, 20.40 (CH_3). DEPT135 ($CDCl_3$): δ (ppm) = 129.18 (pos., C_{Ar}), 128.24 (pos., C_{Ar}), 127.64 (pos., C_{Ar}), 126.27 (pos., C_{Ar}), 20.40 (pos., CH_3). MS (EI, 65°C): m/z = 327 ($[M]^+$), 312 ($[M - CH_3]^+$), 298 ($[M - 2\ CH_3]^+$), 284 ($[M - 3\ CH_3]^+$), 267 ($[M - 4\ CH_3]^+$), 254, 193, 156, 127. MS (ESIpos, MeOH): m/z = 350 ($[M + Na]^+$), 382 ($[M + MeOH + Na]^+$), 677 ($[2\ M + Na]^+$). HPLC (methanol/water = 80/20, 0.8 mL/min, 125 mm Nucleodur 100-5-C18ec, DAD 220 nm): 7.98 min (27% as methanol adduct by HPLC-APCI-MS) and 20.27 min (72% as isocyanate by HPLC-APCI-MS), methanol adduct is formed on the column, i.e. overall purity is 99%. IR (KBr): $\tilde{\nu}$ (cm^{-1}) = 3062 (C-H), 3022 (C-H), 2948 (Ar-CH_3), 2920 (Ar-CH_3), 2855, 2733, 2251 (-N=C=O), 1582 (C_{Ar}=C_{Ar}), 1490

(C_{Ar}=C_{Ar}), 1460 (C_{Ar}=C_{Ar}), 1390, 1380, 1270, 1164, 1124, 1055, 1030, 825 (C_{Ar}-H), 804 (C_{Ar}-H), 777 (C_{Ar}-H), 758 (C_{Ar}-H), 697, 626, 564.

N-Formyl-2,6-bis(2,6-dimethylphenyl)aniline **20**

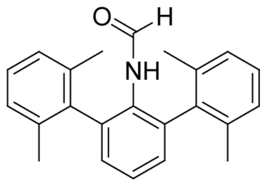

A dry Schlenk-tube was charged with 99 mg of 2,6-bis(2,6-dimethylphenyl)-phenylisocyanate **19** (0.30 mmol, 1 equiv.) and 5 mL of dry THF. The tube was placed in an ice/water bath and 300 mg of lithium aluminumhydride (0.30 mmol, 1 equiv.) were added in portions. Stirring at 0 °C was continued for 45 min followed by heating to 50 °C for 7 h. The mixture was diluted with THF and quenched with Baeckström's reagent. Filtration and removal of solvent *in vacuo* gave 150 mg of crude product. Column chromatography using a CH_2Cl_2/Hex (7/3) eluent mixture containing 0.1 vol% triethylamine afforded 90 mg of the title compound as a colorless solid (91%). R_f (CH_2Cl_2/Hex, 7/3 + 1 vol% TEA) = 0.24. ^{1}H-NMR ($CDCl_3$, 400 MHz): δ (ppm) = 7.62 (d, J^2 = 11.05, 1H, C*H*O), 7.34 (t, J^3 = 7.54, 1H, Ar*H*), 7.20 (m, 8H, Ar*H*), 6.58 (s, 1H, N*H*), 2.06 (s, 12H, C*H*$_3$). ^{13}C-NMR ($CDCl_3$, 100 MHz): δ (ppm) = 162.49 (*C*=O), 137.45 (*C*$_{Ar}$), 136.09 (*C*$_{Ar}$), 133.63 (*C*$_{Ar}$), 132.08 (*C*$_{Ar}$), 130.23 (*C*$_{Ar}$), 128.44 (*C*$_{Ar}$),128.24 (*C*$_{Ar}$), 126.23 (*C*$_{Ar}$), 20.56 (*C*H$_3$). DEPT135 ($CDCl_3$): δ (ppm) = 162.49 (pos., *C*=O), 130.23 (pos., *C*$_{Ar}$), 128.44 (pos., *C*$_{Ar}$),128.24 (pos., *C*$_{Ar}$), 126.23 (pos., *C*$_{Ar}$), 20.56 (pos., *C*H$_3$). MS (EI, 105°C): m/z = 329 ($[M]^+$), 314 ($[M - CH_3]^+$), 301 ($[M - CO]^+$), 286 ($[M - CO - CH_3]^+$), 271 ($[M - CO - 2\ CH_3]^+$), 254, 194, 180, 142, 127. IR (KBr): $\tilde{\nu}$ (cm^{-1}) = 3203 (N-H), 3022, 2967, 2919, 2861, 2785, 2744, 2687, 1931, 1865, 1693 (C=O), 1663 (C=O), 1639 (C=C), 1534 (δ(N-H)), 1461 (C=C), 1383, 1263, 1157, 1084, 1032, 1008, 968, 899, 826, 802, 778, 765, 754, 733, 699, 602, 551, 491.

N-Methyl-2,6-bis(2,6-dimethylphenyl)aniline **21**

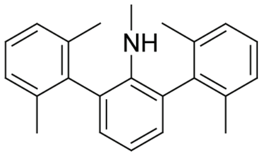

A dry Schlenk-tube was charged with 300 mg of 2,6-bis(2,6-dimethylphenyl)-phenylisocyanate **19** (0.92 mmol, 1 equiv.) and 5 mL of dry toluene. Addition of 2.02 mL of borane-THF-complex (2.02 mmol, 2.2 equiv., 1 M in THF) was followed by stirring the mixture at 95 °C for 5 h. The mixture was cooled to 0 °C, quenched with 1N aq. HCl solution, and stirred 35 min at room temperature. The pH was adjusted to a value of 8-9 by addition of 1N aq. NaOH solution. Phases were separated, the aqueous layer was extracted with diethyl ether three times, combined organic layers were washed with water and brine three times, respectivly, and dried over $MgSO_4$. Removal of solvent *in vacuo* and purification of the residue by flash column chromatography using a CH_2Cl_2/Hex (2/8) eluent mixture containing 0.1 vol% triethylamine gave 251 mg of the title compound as a colorless solid (86%). R_f (CH_2Cl_2/Hex, 3/7) = 0.28. ^{1}H-NMR ($CDCl_3$, 400 MHz): δ (ppm) = 7.16 (m, 6H, Ar*H*), 6.92 (s, 3H, Ar*H*), 3.15 (s, broad, 1H, N*H*), 2.14 (s, 12H, C*H*$_3$), 2.07 (s, 3H, NC*H*$_3$). ^{13}C-NMR ($CDCl_3$, 100 MHz): δ (ppm) = 144.82 (C_{Ar}), 140.03 (C_{Ar}), 137.26 (C_{Ar}), 129.63 (C_{Ar}), 128.53 (C_{Ar}), 127.52 (C_{Ar}), 127.32 (C_{Ar}), 119.15 (C_{Ar}), 33.39 (N*C*H$_3$), 20.69 (*C*H$_3$). DEPT135 ($CDCl_3$): δ (ppm) = 129.63 (pos., C_{Ar}), 127.52 (pos., C_{Ar}), 127.32 (pos., C_{Ar}), 119.15 (pos., C_{Ar}), 33.39 (pos., N*C*H$_3$), 20.69 (pos., *C*H$_3$). MS (EI, 65°C): m/z = 315 ($[M]^+$), 300 ($[M - CH_3]^+$), 285 ($[M - 2\ CH_3]^+$), 269 ($[M - 3\ CH_3]^+$), 269 ($[M - 4\ CH_3]^+$), 254 ($[M - 5\ CH_3]^+$), 194.

N,N'-Bis(2,6-dibromophenyl)oxalamide

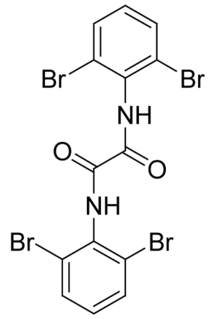

A dry Schlenk-tube was charged with 1.00 g of 2,6-dibromoaniline **14** (3.99 mmol, 2.1 equiv.), 0.79 mL dry triethylamine (5.70 mmol, 3 equiv.), and 5 mL of dry methylene chloride. The tube was cooled to 0 °C and 0.16 mL of oxalyl chloride (1.90 mmol, 1 equiv.) were added dropwise over the course of 10 min. The orange mixture was allowed to warm to room temperature over night. Removal of solvent *in vacuo* and purification of the residue by column chromatography using a CH_2Cl_2/Hex (7/3) eluent mixture gave 0.26 g of pure, colorless product (24%). R_f (CH_2Cl_2/Hex, 8/2) = 0.36. ^{1}H-NMR (DMSO-*d6*, 400 MHz): δ (ppm) = 10.88 (s, 2H, N*H*), 7.77 (d, ^3J = 8.07 Hz, 4H, Ar$H^{3,5}$), 7.25 (t, ^3J = 8.07 Hz, 2H, ArH^4). ^{13}C-NMR (DMSO-*d6*, 100 MHz): δ (ppm) = 158.34 (*C*=O), 135.06 ($C_{Ar}{}^1$), 132.31 ($C_{Ar}{}^4$), 130.73 ($C_{Ar}{}^{3,5}$), 124.02 ($C_{Ar}{}^{2,6}$). DEPT135 (DMSO-*d6*): δ (ppm) = 132.31 (pos., $C_{Ar}{}^4$), 130.73 (pos., $C_{Ar}{}^{3,5}$). MS (EI, 170 °C): m/z = 555 ($[M]^+$), 475, 251, 198, 171, 90, 63. HRMS (ESIpos): *calculated for* $C_{14}H_8N_2O_2Br_4$ + Na: 574.721195, *found*: 574.720684. HPLC (acetonitrile/water = 45/55, 0.8 mL/min, 125 mm Nucleodur 100-5-C18ec, DAD 220 nm): 11.06 min (99% peak area).

N,N'-Bis(2,6-dibromo-4-methylphenyl)ethylenediamine **22**

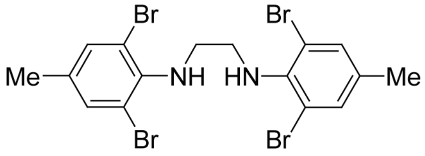

A three-necked flask equipped with an addition funnel and an argon inlet was charged with 6.91 g of *N,N'*-bis(4-methylphenyl)ethylenediamine **25** (28.74 mmol, 1 equiv.) and 100 mL of methylene chloride. The mixture was cooled to -78°C and 5.83 mL of bromine (113.50 mmol, 3.95 equiv.) dissolved in 40 mL of methylene chloride were added dropwise under a steady stream of argon. The mixture was slowly allowed to warm to room temperature and diluted with methylene chloride to a total volume of 600 mL. Under cooling with ice/water 48.00 mL of triethylamine (344.82 mmol, 12 equiv.) were added dropwise. The organic layer was extracted with water, sat. aq. $NaHCO_3$ solution, and brine three times, respectively, dried over $MgSO_4$, and the solvent was removed *in vacuo*. The residue was purified by column chromatography using a CH_2Cl_2/Hex (1/1) eluent mixture containing 1 vol% triethylamine to obtain 2.89 g of the title compound as a brownish oil which solidifies upon standing (18%). GC-MS analysis of other fraction collected identifies them as mixtures of only partially brominated starting material, partly containing tetrabrominated product. The overall yield could be further improved by re-bromination of the combined, partially brominated fractions with an equimolar amount of bromine (based on the GC analysis). Therefore, the partially brominated fractions (m_{tot} = 8.83 g) were re-combined and dissolved in 50 mL of methylene chloride using the same set-up as described above. The mixture was cooled to -78°C and an equimolar amount of bromine (in this case 1.11 mL) in 5 mL of methylene chloride were added slowly under a steady stream of argon. The mixture was stirred at -78°C for 1.5 h and subsequently slowly warmed to room temperature over night. The mixture was poured into ice-cold brine and the pH was adjusted to a value of approx. 8 using aq. NaOH solution. Phases were separated, the aqueous layer was extracted with methylene chloride five times, and combined organic layers were dried over $MgSO_4$. Removal of solvent under reduced pressure and recrystallization of the residue from ethanol gave 7.12 g of pure, tetrabrominated product as a colorless to slightly brown solid (68%, for the rebromination). The overall yield after rebromination was 10.01 g (63% overall). R_f (CH_2Cl_2/Hex, 1/1 + 1 vol% TEA) = 0.32. ^{1}H-NMR (CD_2Cl_2, 400 MHz): δ (ppm) = 7.30 (s, 4H, Ar*H*), 4.04 (s, broad, 2H, N*H*), 3.40 (s, 4H, CH_2), 2.22 (s, 6H, CH_3). ^{13}C-NMR (CD_2Cl_2, 100 MHz): δ (ppm) = 142.31 ($C_{Ar}{}^{1}$), 134.41 ($C_{Ar}{}^{4}$), 133.28 ($C_{Ar}{}^{3,5}$), 117.33 ($C_{Ar}{}^{2,6}$), 48.40 (CH_2), 19.78 (CH_3). DEPT135 (CD_2Cl_2): δ (ppm) = 133.28 (pos., $C_{Ar}{}^{3,5}$), 48.40 (neg., CH_2), 19.78 (pos., CH_3). MS (EI, 135°C): m/z = 556 ($[M]^+$), 475 ($[M - Br]^+$), 279 ($[C_8H_8Br_2N + H]^+$), 197, 131, 90. HRMS (ESIpos): *calculated for* $C_{16}H_{16}N_2Br_4$ + Na: 574.793969, *found*: 574.793427. GC (15m Rtx-1 G/239): 15.14 min (98% peak area).

N,N'-Bis(4-methylphenyl)glyoxal bisimine **24**

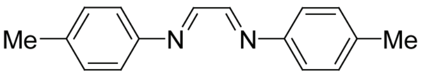

A one-necked flask was charged with 25.62 g of *p*-toluidine **23** (239.07 mmol, 2 equiv.), 13.71 mL of glyoxal (119.54 mmol, 1 equiv., 40 wt% in water), and 110 mL of ethanol. The mixture was stirred at room temperature for 1 h. A yellow solid was isolated by filtration and recrystallized from cyclohexane to give 11.54 g of pure, yellow, finely powdered product (41%). R_f (Hex/EA, 1/1) = 0.64. ^{1}H-NMR (CD_2Cl_2, 400 MHz): δ (ppm) = 8.7 (s, 2H, NC*H*), 7.22 (m, 8H, Ar*H*), 2.37 (s, 6H, CH_3). ^{13}C-NMR (CD_2Cl_2, 100 MHz): δ (ppm) = 159.27 (N*C*H), 147.84 (C_{Ar}), 138.13 (C_{Ar}), 129.99 (C_{Ar}), 121.33 (C_{Ar}), 20.92 (CH_3). DEPT135 (CD_2Cl_2): δ (ppm) = 159.27 (pos., N*C*H), 129.99 (pos., C_{Ar}), 121.33 (pos., C_{Ar}), 20.92 (pos., CH_3). MS (EI, 80 °C): m/z = 235 ($[M]^+$), 221 ($[M - CH_3]^+$), 118 ($[C_8H_8N]^+$), 91 ($[C_7H_7]^+$), 65. HRMS (ESIpos): *calculated for* $C_{16}H_{16}N_2$ + Na: 259.120570, *found*: 259120509. GC (14m Rtx-1 G/130): 18.46 min (99% peak area).

N,N'-Bis(4-methylphenyl)ethylenediamine **25**

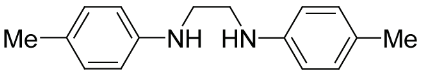

A two-necked flask equipped with a reflux condenser was charged with 1.18 g of *N,N'*-bis(4-methylphenyl)glyoxal bisimine **24** (5.00 mmol, 1 equiv.) and 30 mL of ethanol. The solution was cooled to 0 °C and 0.76 g of sodium borohydride (20.00 mmol, 4 equiv.) were added in small portions. The mixture was heated to reflux under a steady stream of argon for 3 h. Re-cooling to 0 °C was followed by a 1N aq. HCl solution quench and subsequent stirring for 16 h. The pH was checked to make sure the mixture is acidic and phases were separated. The aqueous layer was extracted with diethyl ether three times, combined organic layers were washed with 1N aq. HCl solution and brine three times, respectively, and dried over $MgSO_4$. Removal of solvent under reduced pressure gave 1.19 g of colorless product, which was pure enough for further use (99%). R_f (Hex/EA, 7/3) = 0.44. ^{1}H-NMR ($CDCl_3$, 400 MHz): δ (ppm) = 7.03 (d, ^3J = 8.05 Hz, 4H, Ar$H^{3,5}$), 6.61 (d, ^3J = 8.45 Hz, 4H, Ar$H^{2,6}$), 3.70 (s, broad, 2H, N*H*), 3.38 (s, 4H, CH_2), 2.28 (s, 6H, CH_3). ^{13}C-NMR ($CDCl_3$, 100 MHz): δ (ppm) = 145.88 (C_{Ar}^1), 129.93 ($C_{Ar}^{3,5}$), 127.20 (C_{Ar}^4), 113.40 ($C_{Ar}^{2,6}$), 43.88 (CH_2), 20.52 (CH_3). DEPT135 ($CDCl_3$): δ (ppm) = 129.93 (pos., $C_{Ar}^{3,5}$), 113.40 (pos., $C_{Ar}^{2,6}$), 43.88 (neg., CH_2), 20.52 (pos., CH_3). MS (EI, 80 °C): m/z = 240 ($[M]^+$), 120 ($[C_8H_{10}N]^+$), 106, 91 ($[C_7H_7]^+$), 77, 65. HRMS (ESIpos): *calculated for* $C_{16}H_{20}N_2$ + Na: 263.151863, *found*: 263.151665. GC (13m Rtx-1 G/130): 19.62 min (100% peak area).

N,N'-Bis(2,6-bis(2,6-dimethylphenyl)-4-methylphenyl)ethylenediamine **26**

Synthesis of *N,N'*-bis(2,6-bis(2,6-dimethylphenyl)-4-methylphenyl)ethylenediamine **26** followed a synthetic protocol developed by Walker et. al.[33]

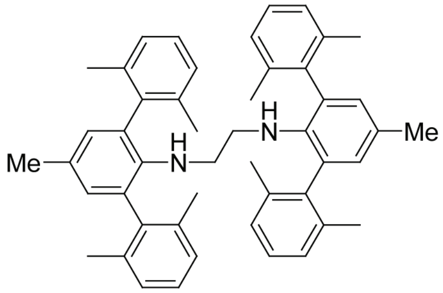

A dry, sealable tube was charged with 217 mg of *N,N'*-bis(2,6-dibromo-4-methylphenyl)ethylenediamine **22** (0.39 mmol, 1 equiv.), 468 mg of 2,6-dimethylphenylboronic acid **15** (3.12 mmol, 8 equiv.), 7 mg of palladium(II)acetate (0.03 mmol, 0.08 equiv.), 26 mg of 2-dicyclohexylphosphino-2′,6′-dimethoxybiphenyl (0.06 mmol, 0.16 equiv.), and 662 mg of dry, finely ground potassium phosphate (3.12 mmol, 8 equiv.). The tube was flushed with argon three times. After adding 10 mL of dry toluene, three freeze-pump-thaw cycles were conducted. The mixture was stirred at 80 °C for 21 h. Dilution with toluene was followed by addition of silica and passing the mixture through a silica plug using ethyl acetate as eluent. The solvent was removed *in vacuo* to give crude product which was further purified by column chromatography using a CH_2Cl_2/Hex (2/8) eluent mixture containing 1 vol% triethylamine to give 163 mg of pure, colorless product (64%). R_f (CH_2Cl_2/Hex, 2/8 + 1 vol% TEA) = 0.24. ^{1}H-NMR (CD_2Cl_2, 400 MHz): δ (ppm) = 7.08 (m, 4H, Ar*H*), 6.99 (m, 8H, Ar*H*), 6.60 (s, 4H, Ar*H*), 2.40 (s, broad, 2H, N*H*), 2.20 (s, 6H, CH_3), 1.88 (s, 24H, CH_3), 1.72 (s, 4H, CH_2). ^{13}C-NMR ($CDCl_3$, 100 MHz): δ (ppm) = 141.38 (C_{Ar}), 139.70 (C_{Ar}), 136.74 (C_{Ar}), 129.85 (C_{Ar}), 129.12 (C_{Ar}), 128.41 (C_{Ar}), 127.38 (C_{Ar}), 127.13 (C_{Ar}), 46.91 (CH_2), 20.25 (CH_3). DEPT135 ($CDCl_3$): δ (ppm) = 129.85 (pos., C_{Ar}), 127.38 (pos., C_{Ar}), 127.13 (pos., C_{Ar}), 46.91 (neg., CH_2), 20.25 (pos., CH_3). MS (ESIpos): m/z = 657.4 ($[M + H]^+$). HRMS (ESIpos): *calculated for* $C_{48}H_{52}N$ + H: 657.420320, *found*:

657.419786. GC (15m Rtx-1 G/239): 21.52 min (100 peak area). X-ray: [$C_{48}H_{52}N_2$], from methylene chloride/methanol, M_r = 656.92, colorless prims, crystal size: 0.359×0.133×0.026 mm^3, a = 8.1329(2) Å, b = 13.5864(3) Å, c = 17.7342(4) Å, α = 94.828(1)°, β = 96.663(1)°, γ = 100.529(1)°, U = 1902.39(8) Å^3, T = 100 K, triclinic, space group P -1, Z = 2, ρ_{calcd} = 1.147 Mg m^{-3}, $F(000)$ = 708, Bruker-AXS X8-Proteum diffractometer, λ(Cu K$_\alpha$) = 1.54178 Å, μ = 0.494 mm^{-1}, 38791 measured and 6521 independent reflections (R_{int} = 0.0537), 5295 with $I > 2\sigma(I)$, $\theta_{\max}$ = 68.20°, apparent $T_{\text{min/max}}$ = 0.778684/1.0, direct methods (*SHELXS-97*) and least-squares refinement (*SHELXL-97*) on F_0^2, programs from G. Sheldrick, University of Göttingen, 1997. 461 parameters, H atoms riding, R_1 = 0.0494 $I > 2\sigma(I)$, wR_2 = 0.1387 (all data), $\Delta\rho_{\text{max/min}}$ = 0.604/-0.603.

N,N'-Bis(2,6-diphenylphenyl)glyoxal bisimine **29**

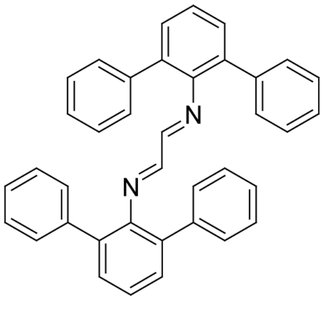

A one-necked flask was charged with 1.08 g of 2,6-diphenylaniline **31** (4.41 mmol, 2 equiv.), 0.25 mL of glyoxal (2.21 mmol, 1 equiv., 40 wt% in water), and 30 mL of ethanol. The mixture was stirred for 4 days, 2 drops of formic acid were added, followed by another 7 days of stirring at room temperature. A yellow solid was isolated by filtration. After drying *in vacuo*, 0.86 g of yellow product could be isolated (76%). R_f (CH_2Cl_2/Hex, 1/1 + 1 vol% TEA) = 0.26. ^{1}H-NMR (CD_2Cl_2, 400 MHz): δ (ppm) = 7.48 (s, 2H, NC*H*), 7.29 (m, 18H, Ar*H*), 7.16 (m, 8H, Ar*H*). ^{13}C-NMR (CD_2Cl_2, 100 MHz): δ (ppm) = 165.25 (*C*=N), 146.95 (C_{Ar}), 139.44 (C_{Ar}), 133.20 (C_{Ar}), 130.19 (C_{Ar}), 129.94 (C_{Ar}), 128.16 (C_{Ar}), 126.93 (C_{Ar}), 125.60 (C_{Ar}). DEPT135

(CD_2Cl_2): δ (ppm) = 165.25 (pos., *C*=N), 130.19 (pos., C_{Ar}), 129.94 (pos., C_{Ar}), 128.16 (pos., C_{Ar}), 126.93 (pos., C_{Ar}), 125.60 (pos., C_{Ar}). MS (EI, 190 °C): m/z = 512 ($[M]^+$), 256 ($[C_{19}H_{14}N]^+$), 218. HRMS (ESIpos): *calculated for* $C_{38}H_{28}N_2$: 512.225246, *found*: 512.225139. GC (15m RTX-1 0.25/0.1df; G/271): 37.03 min (89% peak area, 7% aniline due to partial hydrolysis of product).

2,6-Diphenylaniline **31**

Synthesis of 2,6-diphenylaniline **31** followed a synthetic protocol developed by Walker et. al.[33]

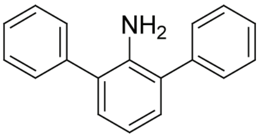

A dry three-necked flask equipped with a reflux condenser and an argon inlet was charged with 4.75 g of 2,6-dibromoaniline **14** (18.92 mmol, 1 equiv.), 6.92 g of phenylboronic acid **32** (56.76 mmol, 3 equiv.), 0.08 g of palladium(II)acetate (0.38 mmol, 0.02 equiv.), 0.31 g of 2-dicyclohexylphosphino-2′,6′-dimethoxybiphenyl (0.76 mmol, 0.04 equiv., S-Phos), and 12.05 g of potassium phosphate (56.76 mmol, 3 equiv.). The flask was flushed with argon three times and 120 mL of dry toluene were added. Degassing by three freeze-pump-thaw cycles was followed by stirring the mixture at 80 °C under a steady stream of argon for 22 h. The mixture was diluted with ethyl acetate and three spoons silica were added. The mixture was filtered and the residue was extensively washed with ethyl acetate. Removal of solvent *in vacuo* and purification of the residue by column chromatography using a CH_2Cl_2/Hex (3/7) eluent mixture gave 4.63 g of pure product as a colorless solid (100%). R_f (CH_2Cl_2/Hex, 3/7) = 0.22. ^{1}H-NMR ($CDCl_3$, 400 MHz): δ (ppm) = 7.54 (m, 4H, Ar*H*), 7.48 (m, 4H, Ar*H*), 7.38 (t, ^3J = 7.36 Hz, 2H, Ar*H*), 7.15 (d, ^3J = 7.53 Hz, 2H, Ar$H^{3,5}$), 6.91 (t, ^3J = 7.52 Hz, 1H, ArH^4), 3.80 (s, broad, 2H, NH_2). ^{13}C-NMR ($CDCl_3$, 100 MHz): δ (ppm) = 140.74 (C_{Ar}), 139.85 (C_{Ar}), 129.89 (C_{Ar}), 129.46 (C_{Ar}), 128.97 (C_{Ar}), 128.16 (C_{Ar}), 127.40

(*C*$_{\text{Ar}}$), 118.36 (*C*$_{\text{Ar}}$). DEPT135 ($CDCl_3$): δ (ppm) = 129.89 (pos., *C*$_{\text{Ar}}$), 129.46 (pos., *C*$_{\text{Ar}}$), 128.97 (pos., *C*$_{\text{Ar}}$), 127.40 (pos., *C*$_{\text{Ar}}$), 118.36 (pos., *C*$_{\text{Ar}}$). MS (EI, 60 °C): m/z = 245 ($[M]^+$). HRMS (ESIpos): *calculated for* $C_{18}H_{15}N$: 245.120452, *found*: 245.120208. GC (15m RTX-1 0.25/0.1df; G/271): 15.08 min (98% peak area).

N,N'-Bis(2,6-diphenyl-4-methylphenyl)ethylenediamine **33**

Synthesis of *N,N'*-bis(2,6-diphenyl-4-methylphenyl)ethylenediamine **33** followed a synthetic protocol developed by Walker et. al.[33]

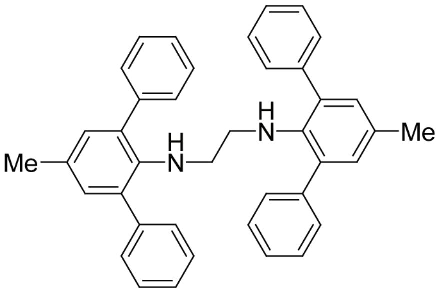

A dry sealable tube was charged with 1.00 g of *N,N'*-bis(2,6-dibromo-4-methylphenyl)-ethylenediamine **22** (1.80 mmol, 1 equiv.), 1.76 g of phenylboronic acid (14.40 mmol, 8 equiv.), 0.03 g of palladium(II)acetate (0.14 mmol, 0.08 equiv.), 0.12 g 2-dicyclohexylphosphino-2′,6′-dimethoxybiphenyl (0.29 mmol, 0.16 equiv., S-Phos), and 3.06 g of potassium phosphate (14.40 mmol, 8 equiv.). The tube was flushed with argon three times and 10 mL of dry toluene were added followed by three freeze-pump-thaw cycles. The mixture was stirred at 80 °C for 16 h. The mixture was filtered and the solid was thoroughly washed with ethyl acetate. The filtrate was passed through a silica plug using ethyl acetate. Purification of the residue obtained after evaporization of the solvent by column chromatography using a CH_2Cl_2/Hex (4/6) eluent mixture containing 0.1 vol% TEA gave 0.24 g of hardly soluble, colorless product (25%). R_f (CH_2Cl_2/Hex + 0.1 vol% TEA) = 0.44. ^{1}H-NMR (CF_3COD, 400 MHz): δ (ppm) = 7.62 (m, 12H, Ar*H*), 7.45 (s, 4H, Ar$H^{3,5}$), 7.16 (m, 8H, Ar*H*), 3.07 (s, 4H, CH_2), 2.73 (s, 6H, CH_3). ^{13}C-NMR (CF_3COD, 100 MHz): δ (ppm) = 145.51 (*C*$_{\text{Ar}}$), 139.77 (*C*$_{\text{Ar}}$), 136.82 (*C*$_{\text{Ar}}$), 135.19 (C_{Ar}), 132.53 (C_{Ar}), 132.41 (C_{Ar}), 130.68 (C_{Ar}), 126.27 (C_{Ar}), 47.62 (CH_2), 21.89 (CH_3). DEPT135 (CF_3COD): δ (ppm) = 135.19 (pos., C_{Ar}), 132.53 (pos., C_{Ar}), 132.41 (pos., C_{Ar}), 130.68 (pos., C_{Ar}), 47.62 (neg., CH_2), 21.89 (pos., CH_3). MS (EI, 190 °C): m/z = 544 ($[M]^+$), 273 ($[C_{20}H_{18}N + H]^+$), 257 ($[C_{20}H_{18}N - CH_3]^+$). HRMS (ESIpos): *calculated for* $C_{40}H_{36}N_2$ + Na: 567.277065, *found*: 567.276836. HPLC (methanol/water = 90/10, 0.8 mL/min, 125 mm Nucleodur 100-5-C18ec, DAD 220 nm): 16.56 min (100% peak area). X-ray: $[C_{40}H_{36}N_2]$, from methylene chloride, M_r = 544.29, a = 8.6802(2) Å, b = 14.0415(4) Å, c = 12.2236(3) Å, β = 104.973(1)°, U = 1439.27 Å^3, space group P 2_1/c.

1,3-Bis(2,6-dibromo-4-methylphenyl)imidazolinium tetrafluoroborate **34**

Synthesis of 1,3-bis(2,6-dibromo-4-methylphenyl)imidazolinium tetrafluoroborate **34** followed a synthetic procedure developed by Khramov et. al.[36]

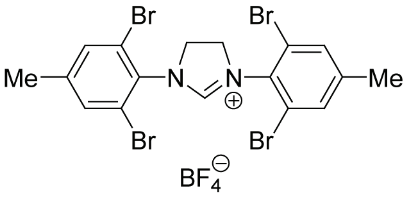

A sealable tube was charged with 224 mg of *N,N'*-bis-(2,6-dibromo-4-methylphenyl)ethylenediamine **22** (0.40 mmol, 1 equiv.), 1.24 mL of triethyl orthoformate, and 0.25 mL of aq HBF_4 solution (~50% in water). The tube was sealed and heated to 140 °C for 16 h. A colorless solid was filtered off and the filtrate was concentrated *in vacuo*. The remaining residue was recollected in ethyl acetate and filtered again to give 116 mg of tan-colored product (44%). R_f (CH_2Cl_2/MeOH, 9.4/0.6) = 0.28. ^{1}H-NMR (CD_3CN, 400 MHz): δ (ppm) = 8.46 (s, 1H, im-H^2), 7.67 (s, 4H, ArH), 4.54 (s, 4H, CH_2), 2.39 (s, 6H, CH_3). ^{13}C-NMR (CD_3CN, 100 MHz): δ (ppm) = 162.24 (im-C^2), 146.39 (C_{Ar}), 134.58 (C_{Ar}), 123.55 (C_{Ar}), 118.34 (C_{Ar}), 52.24 (CH_2), 20.87 (CH_3). DEPT135 (CD_3CN): δ (ppm) = 162.24 (pos., im-C^2), 134.58 (pos., C_{Ar}), 52.24 (neg., CH_2), 20.87 (pos., CH_3). MS (ESIpos): m/z = 566.8 ($[M]^+$). HRMS (ESIpos):

calculated for $C_{17}H_{15}N_2Br_4$: 562.796373, *found*: 562.796640. HPLC (methanol/5 mmol hexansulfonic acid Na-salt = 60/40, 0.8 mL/min, 125 mm Nucleodur 100-5-C18ec, DAD 220 nm): 6.34 min (97% peak area).

4-Iodo-2,6-diphenylaniline **44**

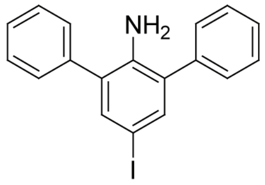

A Schlenk-tube was charged with 4.63 g of 2,6-diphenylaniline **31** (18.85 mmol, 1 equiv.) and 100 mL of glacial acidic acid under an argon atmosphere. At room temperature 2.21 mL of iodinemonochloride (19.32 mmol, 1.03 equiv.) were added over the course of 10 min. Stirring at room temperature was continued for 2 h. The mixture was quenched with sat. aq. $NaHSO_3$ solution and stirred for 1 h. Water and methylene chloride were added and the mixture was cooled to 0 °C. The pH of the biphasic system was adjusted to a value of 8 using solid sodium hydroxide. Layers were separated, the aqueous layer was extracted with methylene chloride five times, and combined organic layers were dried over $MgSO_4$. Removal of solvent under reduced pressure and column chromatography of the residue using a CH_2Cl_2/Hex (2/8) eluent mixture gave 5.61 g of pale-pink, gum-like product (80%). R_f (CH_2Cl_2/Hex, 2/8) = 0.22. ^{1}H-NMR (CD_2Cl_2, 400 MHz): δ (ppm) = 7.44 (m, 8H, Ar*H*), 7.37 (m, 4H, Ar*H*), 3.89 (s, broad, 2H, NH_2). ^{13}C-NMR (CD_2Cl_2, 100 MHz): δ (ppm) =141.09 (C_{Ar}), 138.41 (C_{Ar}), 137.77 (C_{Ar}), 130.17 (C_{Ar}), 129.12 (C_{Ar}), 129.06 (C_{Ar}), 127.78 (C_{Ar}), 78.75 (C_{Ar}). DEPT135 (CD_2Cl_2): δ (ppm) = 137.77 (pos., C_{Ar}), 129.12 (pos., C_{Ar}), 129.06 (pos., C_{Ar}), 127.78 (pos., C_{Ar}). MS (EI, 100 °C): m/z = 371 ($[M]^+$), 243 ($[M - HI]^+$), 215, 122. HRMS (ESIpos): *calculated for* $C_{18}H_{14}NI$: 371.017095, *found*: 371.016851. GC (15m RTX-1 0.25/0.1df; G/271): 20.75 min (97% peak area).

1,3-Dibromo-2-tri-n-butylstannylbenzene **47**

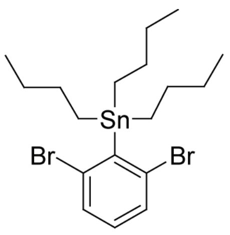

(mixture)

A solution of LDA was prepared as follows. A dry Schlenk-tube was charged with 1.48 mL (10.50 mmol, 1.05 equiv.) and 15 mL of dry THF. Cooling to 0 °C was followed by dropwise addition of 6.56 mL of *n*-butyl lithium (10.50 mmol, 1.05 equiv., 1.6 M in hexanes). Stirring at 0 °C was continued for 4.5 h. Another dry Schlenk-tube was charged with 1.21 mL of 2,6-dibromobenzene (10.00 mmol, 1 equiv.) and 10 mL of dry THF. The mixture was cooled to -78°C and the LDA solution was added over the course of 10 min. The LDA tube was rinsed with 5 mL of dry THF to ensure complete addition. After 5 min stirring at -78°C a colorless solid formed, which was dissolved by addition of additional 20 mL of dry THF. After 30 min overall stirring at -78°C, 2.71 mL of tri-*n*-butylstannylchloride (10.00 mmol, 1 equiv.) were added dropwise at that temperature. The mixture was allowed to slowly warm to room temperature over night. The mixture was diluted with 200 mL of diethyl ether. The organic layer was washed with water three times, dried over $MgSO_4$, and solvent was removed *in vacuo* to obtain 5.64 g of product as a slightly yellow oil. Kugelrohr distillation of product was unsuccessful and the product was used as received. R_f (CH_2Cl_2/Hex, 1/9) = 0.62. ^{1}H-NMR ($CDCl_3$, 400 MHz): δ (ppm) = 7.44 (d, ^3J = 7.86 Hz, 2H, Ar$H^{3,5}$), 6.96 (t, ^3J = 7.78 Hz, 1H, ArH^4), 1.56 (m, 6H, CH_2), 1.35 (m, 6H, CH_2), 1.28 (m, 6H, CH_2), 0.89 (m, 9H, CH_3). ^{13}C-NMR ($CDCl_3$, 100 MHz): δ (ppm) = 149.41 (C_{Ar}), 133.17 (C_{Ar}), 131.30 (C_{Ar}), 130.95 (C_{Ar}), 29.07 (CH_2), 27.44 (CH_2), 15.65 (CH_2), 13.82 (CH_3). DEPT135 ($CDCl_3$): δ (ppm) = 131.30 (pos., C_{Ar}), 130.95 (pos., C_{Ar}), 29.07 (neg., CH_2), 27.44 (neg., CH_2), 15.65 (neg., CH_2), 13.82 (pos., CH_3). MS (EI, 60 °C): m/z = 526 ($[M]^+$), 466 ($[M - C_4H_9]^+$), 410 ($[M - 2\ C_4H_9]^+$), 553 ($[M - 3\ C_4H_9]^+$), 275, 199. HRMS

(ESIpos): no spectra could be obtained. HPLC (methanol, 0.8 mL/min, 125 mm Nucleodur 100-5-C18ec, DAD 220 nm): 4.60 min (94% peak area).

N-(4-Iodo-2,6-diphenylphenyl)-O-ethyl-oxalyl monoamide **48**

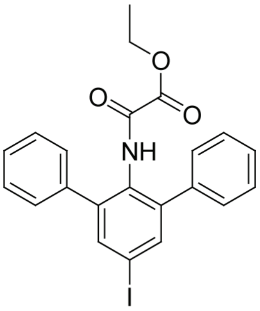

A dry Schlenk-tube was charged with 1.30 g of 4-iodo-2,6-diphenylaniline **44** (3.51 mmol, 1 equiv.), 0.54 mL of dry triethylamine (3.86 mmol, 1.1 equiv.), and 30 mL of dry THF. The mixture was cooled to 0 °C and 0.43 mL of ethyloxalylchloride (3.86 mmol, 1.1 equiv.) were added dropwise. Stirring at 0 °C was continued for 2 h. After addition of 100 mL of methylene chloride, the organic layer was washed with water and brine three times, respectively. The organic layer was dried over $MgSO_4$ and concentrated *in vacuo*. Purification of the residue by column chromatography using a CH_2Cl_2/Hex (7/3) eluent mixture afforded 1.53 g of pure, colorless product (92%). R_f (CH_2Cl_2) = 0.58. ^{1}H-NMR ($CDCl_3$, 400 MHz): δ (ppm) = 8.19 (s, broad, 1H, N*H*), 7.73 (s, 2H, Ar$H^{3,5}$), 7.36 (m, 10H, Ar*H*), 4.18 (q, ^{3}J = 7.14 Hz, 2H, CH_2), 1.24 (t, ^{3}J = 7.15 Hz, 3H, CH_3). ^{13}C-NMR ($CDCl_3$, 100 MHz): δ (ppm) = 160.05 ((*C*=O)OAr), 155.10 ((*C*=O)NAr), 142.51 (C_{Ar}), 138.84 (C_{Ar}), 137.73 (C_{Ar}), 129.82 (C_{Ar}), 128.67 (C_{Ar}), 128.59 (C_{Ar}), 128.19 (C_{Ar}), 93.71 (C_{Ar}^{4}), 63.46 (CH_2), 13.94 (CH_3). DEPT135 ($CDCl_3$): δ (ppm) = 138.84 (pos., C_{Ar}), 128.67 (pos., C_{Ar}), 128.59 (pos., C_{Ar}), 128.19 (pos., C_{Ar}), 63.46 (neg., CH_2), 13.94 (pos., CH_3). MS (EI, 135°C): m/z = 471 ($[M]^+$), 398 ($[M - C_3H_5O_2]^+$), 271 ($[M - C_3H_5O_2 - I]^+$), 243 ($[M - C_4H_5O_3 - I]^+$), 215. HRMS (ESIpos): *calculated for* $C_{22}H_{18}NO_3I$ + Na: 494.022362, *found*: 494.022026. HPLC (methanol/water = 80/20, 0.8 mL/min, 125 mm Nucleodur 100-5-C18ec, DAD 220 nm): 3.69 min (97% peak area).

N-(4-Tri-n-butylstannyl-2,6-diphenylphenyl)-O-ethyl-oxalyl monoamide **50**

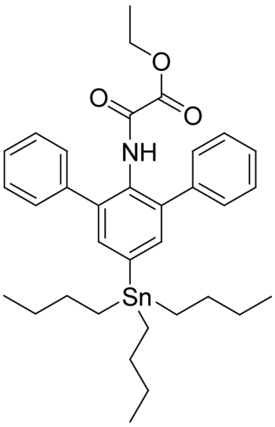

A dry sealable tube was charged with 773 mg of *N*-(4-iodo-2,6-diphenylphenyl)-*O*-ethyl-oxalyl monoamide **48** (1.64 mmol, 1 equiv.), a catalytic amount of $Pd(PPh_3)_4$, and 20 ml of dry toluene. To this mixture were added 1.23 mL of hexa-*n*-butylditin (2.46 mmol, 1.5 equiv.). Three freeze-pump-thaw degassing cycles were followed by 2 days stirring at 120 °C. The now black mixture was quenched using sat. aq. KF solution, stirred for 2 h at room temperature, and filtered through a Celite® pad. The pad was thoroughly rinsed with ethyl acetate. Phases were separated and the aqueous layer was extracted with ethyl acetate five times. Combined organic layers were dried over $MgSO_4$ and solvent was removed *in vacuo*. Column chromatography of the residue using a CH_2Cl_2/Hex (1/1) eluent mixture gave 579 mg of pure, colorless product (56%). R_f (CH_2Cl_2/Hex, 1/1) = 0.2. ^{1}H-NMR ($CDCl_3$, 400 MHz): δ (ppm) = 8.25 (s, broad, 1H, N*H*), 7.46 (s, 2H, Ar$H^{3,5}$), 7.40 (m, 8H, Ar*H*), 7.34 (m, 2H, Ar*H*), 4.19 (q, ^{3}J = 7.14 Hz, 2H, OCH_2), 1.57 (m, 6H, CH_2), 1.35 (sex., ^{3}J = 7.33 Hz, 6H, CH_2), 1.26 (t, ^{3}J = 7.12 Hz, 3H, OCH_2CH_3), 1.09 (t, ^{3}J = 8.16 Hz, 6H, CH_2), 0.90 (t, ^{3}J = 7.30 Hz, 9H, CH_3). ^{13}C-NMR ($CDCl_3$, 100 MHz): δ (ppm) = 160.36 ((*C*=O)OAr), 155.23 ((*C*=O)NAr), 143.16 (C_{Ar}), 139.63 (C_{Ar}), 139.52 (C_{Ar}), 138.00 (C_{Ar}), 129.62 (C_{Ar}), 128.84 (C_{Ar}), 128.51 (C_{Ar}), 127.57 (C_{Ar}), 63.31 (OCH_2), 29.20 (CH_2), 27.49 (CH_2), 13.96 (CH_3), 13.81 (CH_3), 9.89 (CH_2). DEPT135 ($CDCl_3$): δ (ppm) = 138.00 (pos., C_{Ar}), 128.84 (pos., C_{Ar}), 128.51 (pos., C_{Ar}), 127.57 pos., C_{Ar}), 63.31 (neg., OCH_2), 29.20 (neg., CH_2), 27.49 (neg., *C*H$_2$), 13.96 (pos., *C*H$_3$), 13.81 (pos., *C*H$_3$), 9.89 (neg., *C*H$_2$). MS (EI, 160 °C): m/z = 635 ([M]$^+$), 606 ([M - C$_2$H$_5$]$^+$), 578 ([M - C$_4$H$_9$]$^+$), 522 ([M - 2 C$_4$H$_9$]$^+$), 466 ([M - 3 C$_4$H$_9$]$^+$), 390 ([C$_{19}$H$_{13}$NOS]$^+$), 272, 243, 196. HRMS (ESIpos): *calculated for* C$_{34}$H$_{45}$NO$_3$Sn + Na: 658.233229, *found*: 658.233195. HPLC (methanol/water = 90/10, 0.8 mL/min, 125 mm Nucleodur 100-5-C18ec, DAD 220 nm): 9.80 min (99% peak area).

2,6-Dibromoiodobenzene **52**

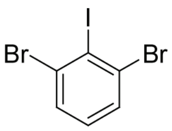

A one-necked flask was charged with 2.51 g of 2,6-dibromoaniline **14** (10.00 mmol, 1 equiv.) and 20 mL conc. sulfuric acid. The mixture was stirred at room temperature until complete dissolution and subsequently cooled to 0 °C. At that temperature 1.52 g of sodium nitrite (22.00 mmol, 2.2 equiv.) were added in portions. Stirring at 0 °C was continued for 3.5 h. During that time the mixture turned brown/yellow. Upon quenching with water and ice, the mixture turned brown/red and was poured into a solution of 9.96 g of potassium iodide (60.00 mmol, 6 equiv.) in 400 mL of water to end up with a total volume of 800 mL. The aqueous layer was extracted with ethyl acetate six times until it was almost colorless. Combined organic layers were washed with sat. aq. NaHSO$_3$ solution five times, the now only slightly yellow organic layers were then washed with water and brine three times, respectively. Drying over MgSO$_4$ and removal of solvent *in vacuo* gave a slightly orange solid as crude product. The residue was recollected in ethanol and a colorless solid was filtered off. Addition of excess water to the ethanol phase and repeated filtration gave additional batches of colorless product. The isolated yield was 1.76 g (49%). R$_f$ (CH$_2$Cl$_2$/Hex) = 0.64. ^{1}H-NMR (CDCl$_3$, 400 MHz): δ (ppm) = 7.55 (d, ^{3}J = 7.95 Hz, 2H, Ar*H*^{3,5}), 7.07 (t, ^{3}J = 8.06 Hz, 1H Ar*H*^{4}). ^{13}C-NMR (CDCl$_3$, 100 MHz): δ (ppm) = 131.47 (*C*$_{Ar}$^{2,6}), 131.24 (*C*$_{Ar}$), 130.48 (*C*$_{Ar}$), 109.51 (*C*$_{Ar}$^{1}). DEPT135 (CDCl$_3$): δ (ppm) = 131.24 (pos., *C*$_{Ar}$), 130.48 (pos.,

C_{Ar}). MS (EI, 30 °C): m/z = 362 ($[M]^+$), 281 ($[M - Br]^+$), 235 ($[M - Br]^+$), 154 ($[M - Br - I]^+$), 127 ($[I]^+$), 75. HRMS (ESIpos): *calculated for* $C_6H_3Br_2I$: 359.764651, *found*: 359.764827. GC (30m RTX-5 id.0.25 df.0.5; G/132): 14.67 min (99% peak area).

(4-Amino-3,5-diphenylphenyl)-4,4,5,5-tetramethyl-1,3,2-dioxaborolane **53**

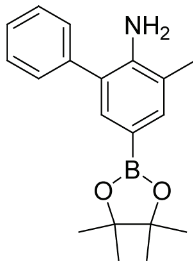

A dry Schlenk-tube was charged with 583 mg of 4-iodo-2,6-diphenylaniline **44** (1.57 mmol, 1 nequiv.), 18 mg palladium(II)acetate (0.08 mmol, 0.05 equiv.), 85 mg bis(2-diphenylphosphinophenyl)ether (0.16 mmol, 0.1 equiv., DPEphos), and 10 mL of dry dioxane. To this mixture 0.87 mL of dry triethylamine (6.28 mmol, 4 equiv.) and 0.68 mL of pinacolborane **54** (4.71 mmol, 3 equiv.) were added. The mixture was flushed with argon five times and subsequently stirred at 100 °C for 19 h. After addition of sat. aq. NH_4Cl solution and methylene chloride phases were separated and aqueous layer was washed with methylene chloride three times. Combined organic layers were dried with $MgSO_4$ and solvent was removed *in vacuo*. Column chromatography using a CH_2Cl_2/Hex (2/8) eluent mixture containing 0.1 vol% triethylamine gave 44 mg of pure, colorless product (8%). Besides 201 mg of the deboronification product 2,6-diphenylaniline were isolated (52%). R_f (CH_2Cl_2/Hex, 2/8 + 0.1 vol% TEA) = 0.1. ^1H-NMR ($CDCl_3$, 400 MHz): δ (ppm) = 7.60 (s, 2H, Ar$H^{3,5}$), 7.52 (m, 4H, Ar*H*), 7.44 (m, 4H, Ar*H*), 7.34 (m, 2H, Ar*H*), 3.70 (s, broad, 2H, NH_2), 1.32 (s, 12H, CH_3). ^{13}C-NMR ($CDCl_3$, 100 MHz): δ (ppm) = 143.46 (C_{Ar}), 139.55 (C_{Ar}), 136.70 (C_{Ar}), 134.89 (C_{Ar}), 129.55 (C_{Ar}), 128.90 (C_{Ar}), 127.46 (C_{Ar}), 127.41 (C_{Ar}), 83.54 ($C(CH_3)_2$), 24.98 (CH_3). DEPT135 ($CDCl_3$): δ (ppm) = 136.70 (pos., C_{Ar}), 129.55 (pos., C_{Ar}), 128.90 (pos., C_{Ar}), 127.41 (pos., C_{Ar}), 24.98 (pos., CH_3). MS (EI, 130 °C): m/z = 371 ($[M]^+$), 298, 272,

252. HRMS (ESIpos): *calculated for* $C_{24}H_{26}NO_2B$ + Na: 394.194879, *found*: 394.194665. GC (28m RTX-1 0.25/0.25df; G/155): 21.71 min (87% peak area, partial decomposition on column).

(4-Ethyloxalylamido-3,5-diphenylphenyl)-4,4,5,5-tetramethyl-1,3,2-dioxaborolane **56**

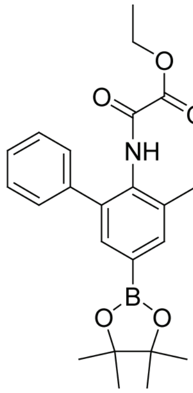

A Schlenk-tube containing 442 mg of potassium phosphate (4.50 mmol, 3 equiv.) was heated to 100 °C *in vacuo* for 30 min. Subsequently, 419 mg of pinacol diborane **55** (1.65 mmol, 1.1 equiv.), 707 mg of *N*-(4-iodo-2,6-diphenylphenyl)-*O*-ethyl-oxalyl-monoamide **48** (1.50 mmol, 1 equiv.), and 12 mg of 1,1'-bis(diphenylphosphino)ferrocenepalladium(II)chloride (0.02 mmol, 0.01 equiv., $PdCl_2(dppf)$ as CH_2Cl_2-complex) were added and vacuum was applied for 5 min. Addition of 12 mL of dry DMSO was followed by three freeze-pump-thaw cycles. The mixture was heated to 80 °C for 17 h. A water-quench was followed by addition of methylene chloride. Phase separation, extraction of the aqueous layer with methylene chloride five times, drying of combined organic layers over $MgSO_4$, and removal of solvent *in vacuo* gave colorless, crude product. Purification by column chromatography using a CH_2Cl_2/Hex gradient (7.5/2.5 to pure CH_2Cl_2) eluent mixture gave 351 mg of pure, colorless product in many fractions (50%). R_f (CH_2Cl_2) = 0.5. ^{1}H-NMR (CD_2Cl_2, 400 MHz): δ (ppm) = 8.33 (s, braod, 1H, N*H*), 7.77 (s, 2H, Ar$H^{3,5}$), 7.37 (m, 10H, Ar*H*), 4.14 (q, $^3J = 7.14$ Hz, 2H, CH_2), 1.32 (s, 12H, CH_3), 1.22 (t, $^3J = 7.16$ Hz, 3H, CH_2CH_3). ^{13}C-NMR (CD_2Cl_2, 100 MHz): δ (ppm) = 160.02 ((*C*=O)OAr), 154.83 ((*C*=O)NAr), 139.64 (C_{Ar}), 139.26 (C_{Ar}), 136.39 (C_{Ar}), 132.31 (C_{Ar}), 128.74 (C_{Ar}), 128.41 (C_{Ar}), 127.59 (C_{Ar}), 84.25 ($C(CH_3)_2$), 63.29 (OCH_2), 24.74 (CH_3), 13.66 (CH_2CH_3). DEPT135 (CD_2Cl_2): δ (ppm) = 136.39 (pos., C_{Ar}), 128.74 (pos., C_{Ar}), 128.41 (pos., C_{Ar}), 127.59 (pos., C_{Ar}), 63.29 (neg., OCH_2), 24.74 (pos., CH_3), 13.66 (pos., CH_2CH_3). MS (EI, 140 °C): m/z = 471 ($[M]^+$), 398 ($[M - C_3H_5O_2]^+$), 298 ($[M - C_6H_{12}BO_2 - C_2H_5O]^+$), 270. HRMS (ESIpos): *calculated for* $C_{28}H_{30}NO_5B + Na$: 494.210919, *found*: 494.210744. HPLC (acetonitrile/water = 60/40, 0.8 mL/min, 125 mm Nucleodur 100-5-C18ec, DAD 220 nm): 12.62 min (100% peak area).

N-(2,6-Diphenylphenyl)oxanilic acid **63**

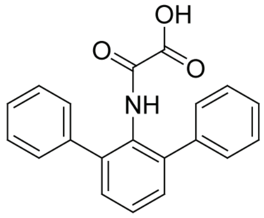

A dry three necked flask equipped with an addition funnel was charged with 24.44 g of 2,6-diphenylaniline **31** (99.64 mmol, 1 equiv.), 15.23 mL of dry triethylamine (109.60 mmol, 1.1 equiv.), and 250 mL of dry THF. The mixture was cooled to 0 °C in an ice/water bath. The addition funnel was charged with a solution of 12.27 mL of ethyl oxalyl chloride (109.60 mmol, 1.1 equiv.) in 20 mL of dry THF. The mixture was added dropwise at 0 °C. Stirring at 0 °C was continued for 1 h during which time a colorless solid formed. After TLC-check, 250 mL of 1N aqueous NaOH solution were added in one portion at 0 °C and the mixture was stirred for 3 h at room temperature. More 1N aqueous NaOH solution was added to drive the reaction to completeness and the mixture was allowed to stir over night at room temperature. After TLC-check, the pH was adjusted to a acidic value using conc. HCl solution and water was added until complete dissolution of all solid material occurred, Phases were separated and the aqueous layer was extracted with methylene chloride three times. Drying combined organic layers over $MgSO_4$ and removal of solvent *in vacuo* afforded 31.7 g of crude product as a brown solid. The material was dissolved in hot toluene and petrolether was added to the hot solution until precipitation occurred. Subsequently, the mixture was cooled to -18 °C over night. Isolation of the colorless solid formed by filtration and washing with cooled petrolether afforded 26.74 g of pure product (85%). R_f (CH_2Cl_2 : petrolether = 1 : 1) = baseline. ^{1}H-NMR ($CDCl_3$, 300 MHz): δ (ppm) = 10.26 (s, broad, 1H, O*H*), 8.68 (s, 1H, N*H*), 7.45 – 7.28 (m, 13H, Ar*H*). ^{13}C-NMR ($CDCl_3$, 75 MHz): δ (ppm) = 160.99 (NHCO*C*OOH), 156.43 (NH*C*OCOOH), 140.51 (C_{Ar}), 139.16 (C_{Ar}), 130.06 (C_{Ar}), 129.81 (C_{Ar}), 128.66 (C_{Ar}), 128.37 (C_{Ar}), 128.25 (C_{Ar}), 127.54 (C_{Ar}). DEPT135 (CDCl3): δ (ppm) = 130.06 (pos., C_{Ar}), 128.66 (pos., C_{Ar}), 128.37 (pos., C_{Ar}), 128.25 (pos., C_{Ar}), 127.54 (pos., C_{Ar}). MS (ESI): *m/z* = 340 ($[M + Na]^+$), 335 ($[M\,H_2O]^+$), 318 ($[M + H]^+$). HRMS (ESI) = 318.1125 (calcd. 318.1124 for $[C_{20}H_{15}NO_3 + H]^+$). HPLC (acetonitrile : water = 60 : 40 to 95 : 5 Grad, Phenyl-Hexyl 3um 2 x 150): 18.36 min (100% peak area).

N-(2,6-Diphenylphenyl)-N'-(2,4,6-trimethylphenyl)oxalamide **64**

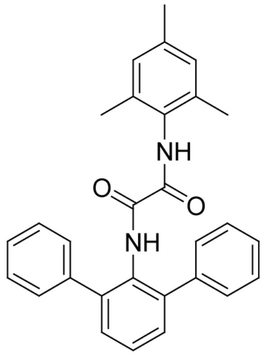

A dry three necked flask equipped with a reflux condenser and an addition funnel was charged with 12.69 g of *N*-(2,6-diphenylphenyl)oxanilic acid **63** (40.00 mmol, 1 equiv.), a drop of dry DMF, and 250 mL of dry methylene chloride. The addition funnel was charged with 8.59 mL of oxalyl chloride (100.00 mmol, 2.5 equiv.) dissolved in 30 mL of dry methylene chloride. The flask was heated to 50 °C and the oxalyl chloride solution was added dropwise. Heating to 50 °C was continued for 3 h. The mixture was allowed to cool to room temperature and the solvent was removed *in vacuo* to obtain crude acid chloride which was dried *in vacuo* for 2.5 h. A dry flask equipped with an addition funnel was charged with 11.27 mL of 2,4,6-trimehtyl aniline (80.00 mmol, 2 equiv.), 13.88 mL of dry triethyl amine (100.00 mmol, 2.5 equiv.), 0.49 g of DMAP (4.00 mmol, 0.1 equiv.), and 150 mL of dry DCM. The addition funnel was charged with a suspension of the crude acid chloride in 200 mL of dry methylene chloride. The suspension was slowly added dropwise at 0 °C. The addition funnel was rinsed with 10 mL of dry methylene chloride and the mixture was allowed to slowly warm to room temperature over night. The mixture was transferred to a separation funnel and washed with 1N aqueous HCl solution and saturated aqueous $NaHCO_3$ solution three times. respectively. The organic layers were dried over $MgSO_4$ and the solvent was removed *in vacuo* to afford colorless crude product which was further purified by column chromatography (gradient CH_2Cl_2 : petrolether = 1 : 1 to 9 : 1). After drying *in vacuo*, 13.58 g of pure, colorless product were obtained (78%). R_f (CH_2Cl_2 : petrolether = 8 : 2) = 0.58. ^{1}H-NMR (DMSO-*d6*, 300 MHz): δ (ppm) = 10.37 (s, 1H, N*H*), 9.81 (s, 1H, N*H*), 7.56 – 7.31 (m, 13H, Ar*H*), 6.83 (s, 2H, Ar*H*), 2.20 (s, 3H, CH_3), 1.89 (s, 6H,CH_3). ^{13}C-NMR (DMSO-*d6*, 75 MHz): δ (ppm) = 159.38 (*C*=O), 158.19 (*C*=O), 141.10 (C_{Ar}), 139.30 (C_{Ar}), 135.89 (C_{Ar}), 134.68 (C_{Ar}), 131.62 (C_{Ar}), 131.50 (C_{Ar}), 129.58 (C_{Ar}), 128.85 (C_{Ar}), 128.44 (C_{Ar}), 128.16 (C_{Ar}), 127.95 (C_{Ar}), 127.21 (C_{Ar}), 20.50 (CH_3), 17.70 (CH_3). DEPT135 (DMSO-*d6*): δ (ppm) = 129.58 (pos., C_{Ar}), 128.85 (pos., C_{Ar}), 128.24 (pos., C_{Ar}), 128.16 (pos., C_{Ar}), 127.95 (pos., C_{Ar}), 127.21 (pos., C_{Ar}), 20.50 (pos., CH_3), 17.19 (pos., CH_3). MS (ESI): *m/z* = 435 ($[M + H]^+$), 452 ($[M + H_2O]^+$), 457 ($[M + Na]^+$), 869 ($[M_2 + H]^+$), 886 ($[M_2 + H_2O]^+$), 892 ($[M_2 + Na]^+$). HRMS (ESI) = 435.2067 (calcd. 435.2067 for $[C_{29}H_{26}N_2O_2 + H]^+$). HPLC (acetonitrile : water = 5 : 95 to 95 : 5 Grad, Luna Phenyl-Hexyl 3um 2 x 150): 23.21 min (97% peak area).

N-(2,6-diphenylphenyl)-N'-(2,4,6-trimethylphenyl)ethylenediamine **65**

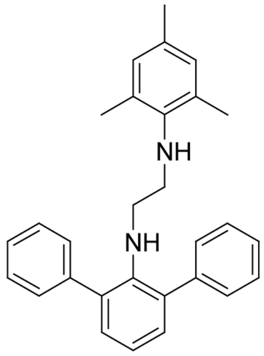

N-(2,6-Diphenylphenyl)-*N'*-(2,4,6-trimethylphenyl)oxalamide **64** (2.39 g, 5.5 mmol) was dissolved in 30 mL of dry THF and diisobutylaluminium hydride (25 wt% in toluene, 50 mL solution, 74.4 mmol) were added dropwise. The mixture was heated to 90 °C for 27 h. After 3 h reaction time, additional 50 mL of diisobutylaluminium hydride (25 wt% in toluene, 50 mL solution, 74.4 mmol) were added maintaining the temperature at 90 °C. The mixture was quenched by the addition of Celite and 1N aq. NaOH-solution until no further gas evolution was detected. The hydrolyzed mixture was filtered and the solid residue was carefully washed with ethyl acetate. The filtrate was concentrated *in vacuo* and the raw product was further purified by column chromatography (silica gel, EA/Hex, 0.5/9.5) afforded 2.00 g of a colorless oil, which turned slightly yellow upon standing (4.95 mmol, 90%). R_f (EA/Hex, 1/9) = 0.36. ^{1}H-NMR ($CDCl_3$, 300 MHz): δ (ppm) = 7.66-7.62 (m, 4H, Ar-*H*), 7.56-7.51 (m, 4H, Ar-*H*), 7.46-7.40 (m, 1H, Ar-*H*), 7.29 (d, ^3J = 7.1 Hz, 2H, Ar-*H*), 7.11 (t, ^3J = 7.1 Hz, 1H, Ar-*H*), 6.84 (s, 2H, Ar-*H*), 3.33 (s, broad, 2*H*, NH), 2.82-2.71 (m, 4H, CH_2), 2.30 (s, 3H, CH_3), 2.09 (s, 6H, CH_3). ^{13}C-NMR ($CDCl_3$, 75 MHz): δ (ppm) = 144.18, 143.14, 140.92, 132.60, 131.41, 130.61, 129.95, 129.36, 129.22, 128.75, 127.20, 120.29. 48.77, 48.50, 20.61, 18.15. DEPT135-NMR ($CDCl_3$): δ (ppm) =130.61 (pos.), 129.36 (pos.), 129.22 (pos.), 128.75 (pos.), 127.20 (pos.), 120.29 (pos.), 48.77 (neg.), 48.50 (neg.), 20.62 (pos.), 18.15 (neg.). MS (ESI pos.): *m/z* = 407 ($[M + H]^+$). HRMS (ESI pos.):

m/z = 407.2479 (calc. 407.2482 for $C_{29}H_{31}N_2$). HPLC (acetonitrile : water = 5 : 95 to 95 : 5 Grad, Luna Phenyl-Hexyl 3um 2 x 150): 23. 58 min (100% peak area).

N-(2,6-diphenylphenyl)-N'-(2,4,6-trimethylphenyl)formamidine **67**

Synthesis of *N*-(2,6-diphenylphenyl)-N'-(2,4,6-trimethylphenyl)formamidine **67** was inspired by a synthetic procedure developed by Kuhn et. al.[27]

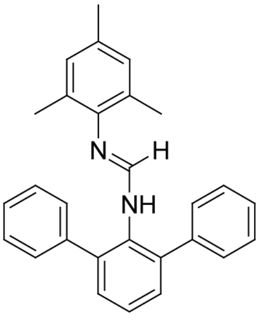

A small flask was charged with 2,6-diphenylaniline **31** (245 mg, 1.0 mmol), triethyl orthoformate (167 µL, 1.0 mmol), and acetic acid (1 drop). The mixture was heated to 140 °C under a steady stream of argon until no further evolution of ethanol was observed (6 h), followed by addition of 2,4,6-trimethylaniline **40** (141 µL, 1.0 mmol). Heating to 140 °C under a steady stream of argon was continued for 12 h until no further condensation of ethanol in the colder parts of the apparatus could be detected. The viscous mixture was triturated with hexanes and a colorless solid was isolated by centrifugation. Recrystallization from cold acetone gave 27 mg of colorless product (0.07 mmol, 7%). ^{1}H-NMR and ^{13}C-NMR proved to be exceedingly complex and are therefore not reported.[27] MS (ESI pos.): *m/z* = 391 ($[M + H]^+$). HRMS (ESI pos.): *m/z* = 391.1870 (calc. 391.2174 for $C_{28}H_{27}N_2$). UPLC (Acquity UPLC column, gradient 20→95% CH_3CN/H_2O): t_R = 3.00 min (98% peak area).

4.10 Literature

(1) Herrmann, W. A. *Angew. Chem., Int. Ed. Engl.* **2002**, *41*, 1290-1309.

(2) Hahn, F. E.; Jahnke, M. C. *Angew. Chem., Int. Ed. Engl.* **2008**, *47*, 3122-3172.

(3) Bourissou, D.; Guerret, O.; Gabbai, F. P.; Bertrand, G. *Chem. Rev.* **2000**, *100*, 39-92.

(4) Wanzlick, H. W. *Angew. Chem., Int. Ed. Engl.* **1962**, *74*, 129-134; Wanzlick, H. W.; Kleiner, H. J. *Angew. Chem., Int. Ed. Engl.* **1961**, *73*, 493; Wanzlick, H. W.; Schikora, E. *Angew. Chem., Int. Ed. Engl.* **1960**, *72*, 494-494.

(5) Winberg, H. E.; Carnahan, J. E.; Coffman, D. D.; Brown, M. *J. Am. Chem. Soc.* **1965**, *87*, 2055-2056; Lemal, D. M.; Lovald, R. A.; Kawano, K. I. *J. Am. Chem. Soc.* **1964**, *86*, 2518-2519.

(6) Alder, R. W.; Blake, M. E.; Chaker, L.; Harvey, J. N.; Paolini, F.; Schutz, J. *Angew. Chem., Int. Ed. Engl.* **2004**, *43*, 5896-5911.

(7) Arduengo, A. J.; Harlow, R. L.; Kline, M. *J. Am. Chem. Soc.* **1991**, *113*, 361-363.

(8) Arduengo, A. J., III *Acc. Chem. Res.* **1999**, *32*, 913-921.

(9) Weskamp, T.; Bohm, V. P. W.; Herrmann, W. A. *J. Organomet. Chem.* **2000**, *600*, 12-22; Crudden, C. M.; Allen, D. P. *Coord. Chem. Rev.* **2004**, *248*, 2247-2273; Glorius, F. A. *Top. Organomet. Chem.* **2007**, *21*, 1-20.

(10) Herrmann, W. A. *Angew. Chem., Int. Ed. Engl.* **2002**, *41*, 1290-1309.

(11) *N-Heterocyclic Carbenes in Synthesis*; Nolan, S. P., Ed.; Wiley-VCH: Weinheim, 2006.

(12) Kantchev, E. A. B.; O'Brien, C. J.; Organ, M. G. *Angew. Chem., Int. Ed. Engl.* **2007**, *46*, 2768-2813.

(13) Trnka, T. M.; Grubbs, R. H. *Acc. Chem. Res.* **2001**, *34*, 18-29; Fürstner, A. *Angew. Chem., Int. Ed. Engl.* **2000**, *39*, 3013-3043; Connon, S. J.; Blechert, S. *Angew. Chem., Int. Ed. Engl.* **2003**, *42*, 1900-1923; Grubbs, R. H. *Tetrahedron* **2004**, *60*, 7117-7140; Clavier, H.; Grela, K.; Kirschning, A.; Mauduit, M.; Nalon, S. P. *Angew. Chem., Int. Ed. Engl.* **2007**, *46*, 6786-6801.

(14) Enders, D.; Balensiefer, T. *Acc. Chem. Res.* **2004**, *37*, 534-541; Enders, D.; Niemeier, O.; Henseler, A. 2007; Vol. 107, p 5606-5655; Marion, N.; Diez-Gonzalez, S.; Nolan, I. P. *Angew. Chem., Int. Ed. Engl.* **2007**, *46*, 2988-3000.

(15) Breslow, R. *J. Am. Chem. Soc.* **1958**, *80*, 3719-3726.

(16) Lai, C. L.; Lee, H. M.; Hu, C. H. *Tetrahedron Lett.* **2005**, *46*, 6265-6270.

(17) Dechy-Cabaret, O.; Martin-Vaca, B.; Bourissou, D. *Chem. Rev.* **2004**, *104*, 6147-6176; Uhrich, K. E.; Cannizzaro, S. M.; Langer, R. S.; Shakesheff, K. M. *Chem. Rev.* **1999**, *99*, 3181-3198.

(18) Coulembier, O.; Degee, P.; Hedrick, J. L.; Dubois, P. *Prog. Polym. Sci.* **2006**, *31*, 723-747; Kamber, N. E.; Jeong, W.; Waymouth, R. M.; Pratt, R. C.; Lohmeijer, B. G. G.; Hedrick, J. L. *Chem. Rev.* **2007**, *107*, 5813-5840.

(19) Nyce, G. W.; Csihony, S.; Waymouth, R. M.; Hedrick, J. L. *Chem. Eur. J.* **2004**, *10*, 4073-4079.

(20) Csihony, S.; Beaudette, T. T.; Sentman, A. C.; Nyce, G. W.; Waymouth, R. M.; Hedrick, J. L. *Adv. Synt. Cataly.* **2004**, *346*, 1081-1086; Sentman, A. C.; Csihony, S.; Waymouth, R. M.; Hedrick, J. L. *J. Org. Chem.* **2005**, *70*, 2391-2393; Csihony, S.; Culkin, D. A.; Sentman, A. C.; Dove, A. P.; Waymouth, R. M.; Hedrick, J. L. *J. Am. Chem. Soc.* **2005**, *127*, 9079-9084; Dove, A. P.; Li, H. B.; Pratt, R. C.; Lohmeijer, B. G. G.; Culkin, D. A.; Waymouth, R. M.; Hedrick, J. L. *Chem. Comm.* **2006**, 2881-2883; Coulembier, O.; Kiesewetter, M. K.; Mason, A.; Dubois, P.; Hedrick, J. L.; Waymouth, R. M. *Angew. Chem., Int. Ed. Engl.* **2007**, *46*, 4719-4721; Culkin, D. A.; Jeong, W. H.; Csihony, S.; Gomez, E. D.; Balsara, N. R.; Hedrick, J. L.; Waymouth, R. M. *Angew. Chem., Int. Ed. Engl.* **2007**, *46*, 2627-2630.

(21) Coulembier, O.; Dove, A. P.; Pratt, R. C.; Sentman, A. C.; Culkin, D. A.; Mespouille, L.; Dubois, P.; Waymouth, R. M.; Hedrick, J. L. *Angew. Chem., Int. Ed. Engl.* **2005**, *44*, 4964-4968; Coulembier, O.; Lohmeijer, B. G. G.; Dove, A. P.; Pratt, R. C.; Mespouille, L.; Culkin, D. A.; Benight, S. J.; Dubois, P.; Waymouth, R. M.; Hedrick, J. L. *Macromolecules* **2006**, *39*, 5617-5628.

(22) Nyce, G. W.; Glauser, T.; Connor, E. F.; Möck, A.; Waymouth, R. M.; Hedrick, J. L. *J. Am. Chem. Soc.* **2003**, *125*, 3046-3056.

(23) Hahn, F. E.; Wittenbecher, L.; Boese, R.; Bläser, D. *Chem. Eur. J.* **1999**, *5*, 1931-1935.

(24) Scholl, M.; Ding, S.; Lee, C. W.; Grubbs, R. H. *Org. Lett.* **1999**, *1*, 953-956.

(25) Blum, A. P.; Ritter, T.; Grubbs, R. H. *Organometallics* **2007**, *26*, 2122-2124.

(26) Vougioukalakis, G. C.; Grubbs, R. H. *Organometallics* **2007**, *26*, 2469-2472; Waltman, A. W.; Grubbs, R. H. *Organometallics* **2004**, *23*, 3105-3107.

(27) Kuhn, K. M.; Grubbs, R. H. *Org. Lett.* **2008**, *10*, 2075-2077.

(28) Yang, J.-S.; Swager, T. M. *J. Am. Chem. Soc.* **1998**, *120*, 5321-5322; Yang, J.-S.; Swager, T. M. *J. Am. Chem. Soc.* **1998**, *120*, 11864-11873.

(29) Williams, V. E.; Swager, T. M. *Macromolecules* **2000**, *33*, 4069-4073.

(30) Zhu, X.-Z.; Chen, C.-F. *J. Org. Chem.* **2005**, *70*, 917-924.

(31) Toda, F.; Tanaka, K.; Tange, H. *J. Chem. Soc., Perkin Trans. 1* **1989**, 1555-6.

(32) Klärner, F.-G.; Panitzky, J.; Bläser, D.; Boese, R. *Tetrahedron* **2001**, *57*, 3673-3687; Fukuda, Y.; Seto, S.; Furuta, H.; Ebisu, H.; Oomori, Y.; Terashima, S. *J. Med. Chem.* **2001**, *44*, 1396-1406.

(33) Walker, S. D.; Barder, T. E.; Martinelli, J. R.; Buchwald, S. L. *Angew. Chem., Int. Ed. Engl.* **2004**, *43*, 1871-1876.

(34) Abrams, M. B.; Scott, B. L.; Baker, R. T. *Organometallics* **2000**, *19*, 4944-4956.

(35) Arduengo, A. J., III; Krafczyk, R.; Schmutzler, R.; Craig, H. A.; Goerlich, J. R.; Marshall, W. J.; Unverzagt, M. *Tetrahedron* **1999**, *55*, 14523-14534.

(36) Khramov, D. M.; Boydston, A. J.; Bielawski, C. W. *Org. Lett.* **2006**, *8*, 1831-1834.

(37) For procedures employing BH_3 as reducing agent, see: Lu, Z.-H.; Bhongle, N.; Su, X.; Ribe, S.; Senanayake, C. H. *Tetrahedron Lett.* **2002**, *43*, 8617-8620.

(38) Ma, D.; Wu, Q. *Tetrahedron Lett.* **2001**, *42*, 5279-5281.

(39) Spivey, A. C.; McKendrick, J.; Srikaran, R.; Helm, B. A. *J. Org. Chem.* **2003**, *68*, 1843-1851.

(40) Lulinski, S.; Serwatowski, J. *J. Org. Chem.* **2003**, *68*, 5384-5387; Negishi, E.; King, A. O.; Okukado, N. *J. Org. Chem.* **1977**, *42*, 1821-1823; Merlic, C. A.; Roberts, W. M. *Tetrahedron Lett.* **1993**, *34*, 7379-7382; Nakamura, Y.; Matsumoto, M.; Hayashida, Y.; Nishimura, J. *Tetrahedron Lett.* **1997**, *38*, 1983-1986.

(41) Espinet, P.; Echavarren, A. M. *Angew. Chem., Int. Ed. Engl.* **2004**, *43*, 4704-4734.

(42) Deng, X.; Liebeskind, L. S. *J. Am. Chem. Soc.* **2001**, *123*, 7703-7704.

(43) Anderson, J. C.; Namli, H.; Roberts, C. A. *Tetrahedron* **1997**, *53*, 15123-15134; Guiles, J. W.; Diana, G. D.; Pevear, D. C. *J. Med. Chem.* **1995**, *38*, 2780-2783.

(44) Mee, S., P. H.; Lee, V.; Baldwin Jack, E. *Angew. Chem., Int. Ed. Engl.* **2004**, *43*, 1132-1136.

(45) Mee, S. P. H.; Lee, V.; Baldwin, J. E. *Chem. Eur. J.* **2005**, *11*, 3294-3308.

(46) Coe, J. W.; Wirtz, M. C.; Bashore, C. G.; Candler, J. *Org. Lett.* **2004**, *6*, 1589-1592.

(47) Miyaura, N.; Suzuki, A. *Chem. Rev.* **1995**, *95*, 2457-2483.

(48) For recent developments see: special issue on cross-coupling edited by S. Buchwald in *Acc. Chem. Res.* **2008**, *41*, Issue 11, p1439-1564.

(49) Broutin, P.-E.; Cerna, I.; Campaniello, M.; Leroux, F.; Colobert, F. *Org. Lett.* **2004**, *6*, 4419-4422.

(50) Quan, M. L.; Lam, P. Y. S.; Han, Q.; Pinto, D. J. P.; He, M. Y.; Li, R.; Ellis, C. D.; Clark, C. G.; Teleha, C. A.; Sun, J.-H.; Alexander, R. S.; Bai, S.; Luettgen, J. M.; Knabb, R. M.; Wong, P. C.; Wexler, R. R. *J. Med. Chem.* **2005**, *48*, 1729-1744.

(51) Modrakowski, C.; Flores, S. C.; Beinhoff, M.; Schlüter, A. D. *Synthesis* **2001**, 2143-2155.

(52) Lee, S. H.; Jang, B.-B.; Kafafi, Z. H. *J. Am. Chem. Soc.* **2005**, *127*, 9071-9078.

5 Outlook

5.1 Photoswitchable Bases

In Chapter 3, efficient photoswitching of basicity was demonstrated and successfully utilized to photocontrol conversion in the Henry reaction, which was chosen as a model system. Further work is directed towards extending the scope of the concept of reversible steric shielding. Obviously, application of the base catalysts described in Chapter 3 to other reaction constitutes an interesting task. Nevertheless, the reactivity of a piperidine base carrying a *tert*-butyl substituent is intrinsically limited due to the steric bulk around the active site and its rather low basicity, making it difficult to access intermediates of outstanding reactivity by deprotonation of relatively acidic substrates. Therefore, a transfer of the concept developed in Chapter 3 to intrinsically more active systems is mandatory, if significant improvements in performance and scope are aspired.

Phosphines are common ligands in organometallic complexes, in general possessing three alkyl- or aryl-substituents. Therefore, a conceptual transfer of the shielding principals described in Chapter 3 is easily possible and leads to the general structure shown in Scheme 1. Photoswitchable phosphine **1** is not only expected to be a valuable organocatalyst for numerous reactions including the polymerization of lactide,[1] but also a valuable ligand for many organometallic complexes catalyzing an immense number of transformations.

Scheme 1: Photoswitchable phosphine **1**.

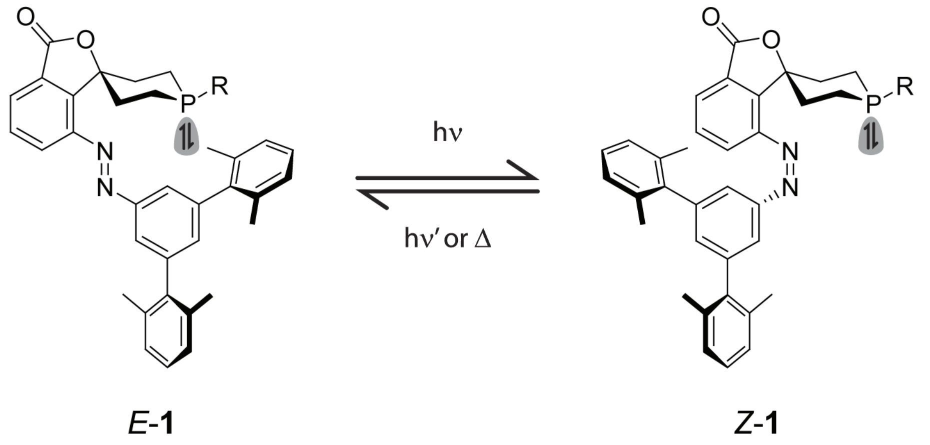

Metathesis catalysts **2** and **3** developed by Grubbs and co-workers constitute an outstanding example for extremely active catalysts (Scheme 2).[2] The ability to catalyze ring-opening metathesis polymerizations (ROMP) of strained, cyclic olefins and the metathesis polymerization of dienes (ADMET polymerization = acyclic diene metathesis polymerization) renders these catalysts extremely interesting for applications in materials chemistry.

Scheme 2: Metathesis catalysts developed by Grubbs and co-workers.

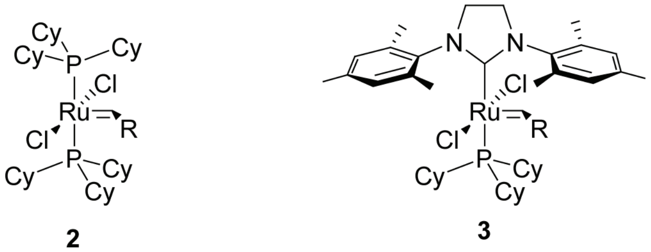

Careful kinetic studies by Grubbs and co-workers revealed a rate-determining dissociation of one phosphine ligand as the initiating step, enabling the resulting 14-electron intermediate to enter the catalytic cycle.[3] Presence of excess phosphine is believed to significantly lower the propagation rate of polymerizations by lowering the number of catalytic turnovers. Considering the concept of reversible steric shielding, *E*-**1** is presumably not able to bind to a vacant coordination site of an active ruthenium species, whereas the lower steric hindrance should allow for coordination of *Z*-**1** (Figure 1). Photochemical conversion of *E*-**1** to *Z*-**1** is therefore expected to attenuate the catalytic performance by enhancing the coordination tendency of the ligand, if *E*-**1** was initially present in large excess. The concept is summarized in Figure 1 for utilization of the more active, second generation Grubbs-catalyst **3**.

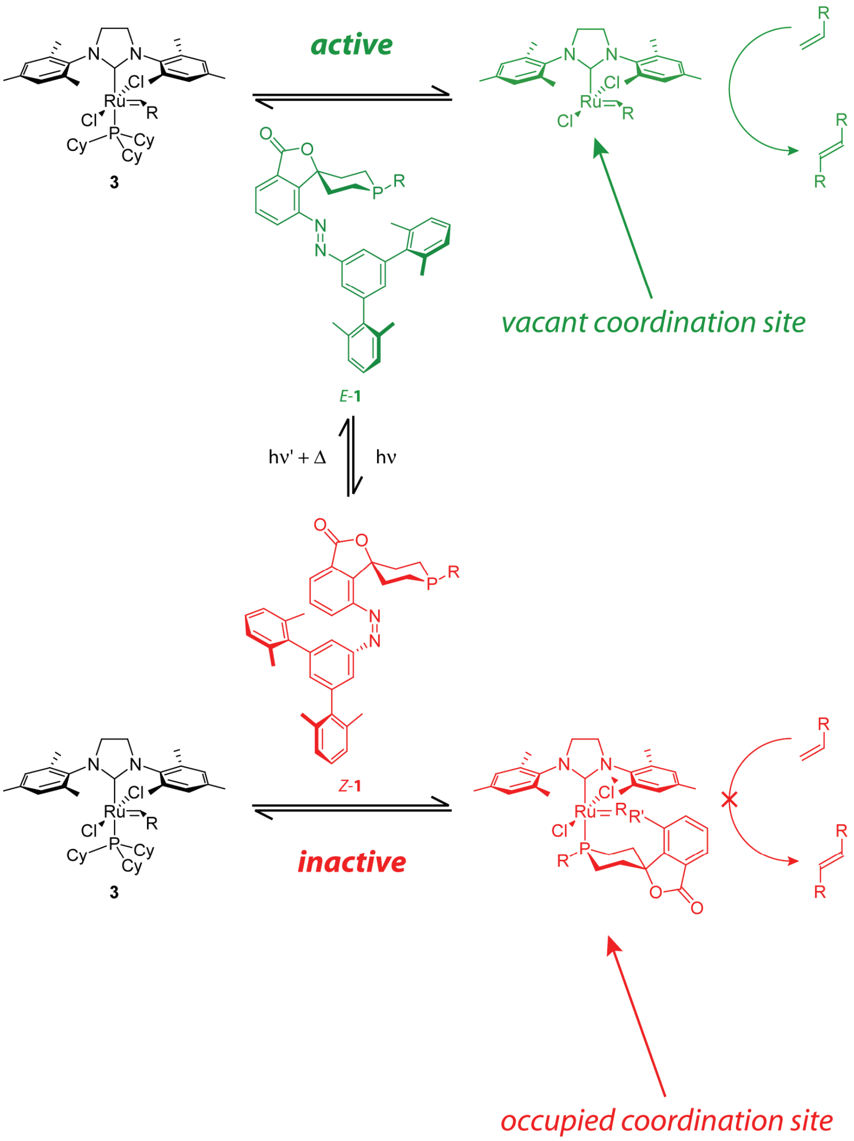
active
3
E-1
vacant coordination site
hν' + Δ
hν
Z-1
3
inactive
occupied coordination site
R
Cl
Ru
Cy
P
N
O

Figure 1: Modulating metathesis activity of a Grubbs-type catalyst by utilization of photoswitchable phosphine **1** (green: ON-state, high reactivity; red: OFF-state, low reactivity).

5.2 Photoswitchable NHC-Ligands

As outlined in Chapter 4, *N*-heterocyclic carbenes are highly promising catalytically active species in their function as either versatile ligands in many organometallic complexes[4,5] or as highly active organocatalysts themselves.[5,6] Performance in catalysis is strongly dependent on steric and electronic factors. For example, carbene **4** exhibits markedly better performance in the ring-opening polymerization (ROP) of lactide compared to carbene **5**, attributable to the lack of electron withdrawing chlorine substituents in **4** (Scheme 3).[7] Photocontrolling the ring-opening polymerization of lactide and related substrates is expected to enable access to highly promising materials for a variety of applications (see Chapter 4).

Scheme 3: Catalysts for the ROP of lactide: *N*,*N'*-dimethylimidazol-2-ylidene **4** and *N*,*N'*-dimethyl-4,5-dichloroimidazol-2-ylidene **5**.

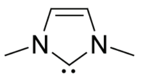

4

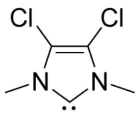

5

Incorporation of the imidazol-2-ylidene into a photochromic diarylethene is expected to allow for a modulation of the electronic situation at the carbene center. Considering the mesomeric structures presented in Figure 2, the ring-opened isomer of carbene **6** does not exhibit the possibility of conjugation of a electron withdrawing substituent in the thiophenes' 5-position with the imidazole-2-ylidene moiety (top left green structure in Figure 2). In contrast, conjugation is possible in the ring-closed isomer of carbene **6**, allowing to formulate several resonance structures, two of which are shown (top right red structures in Figure 2). Obviously, electronic communication between the imidazole-2-ylidene and the electron withdrawing group installed on the thiophene can lead a drop in electron density close to the catalytically active carbene center, as is evident from the positive formal charge placed on the nitrogen atom next to it. From the experimental findings obtained for carbenes **4** and **5** it is becomes evident that a decrease of the carbene's electron density adversely influences the catalytic performance. Therefore, a significant reactivity drop is to be expected upon ring-closure of carbene **6**. Fine tuning of the catalytic performance of carbene **6** should easily be possible by changing the electron withdrawing group and by variation of the substituents R, which allow to dictate the extent of steric bulk around the active site. The concept is not limited to electron withdrawing groups presumably leading to a deactivation of the catalyst, but can be extended to electron donating groups most likely leading to activation. However, considering the high intrinsic reactivity of NHCs towards lactide and related substrates, a photocontrollable activation is of much less interest.

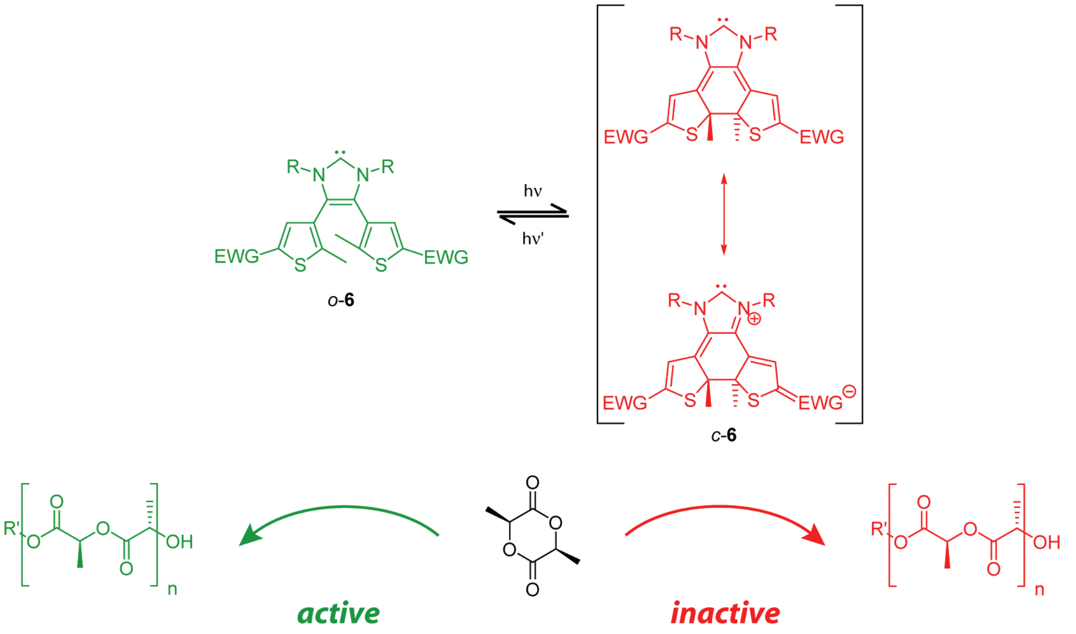

Figure 2: Controlling the ring-opening polymerization of lactide by utilizing photoswitchable *N*-heterocyclic carbene **6** (green: ON-state, high reactivity; red: OFF-state, low reactivity; EWG: electron-withdrawing group).

Ruthenium-based metathesis catalyst **3** presented in Scheme 2 carries a *N*-heterocyclic carbene ligand, which significantly improves the performance compared to catalyst **2**. Potentially, photomodulation of catalytic activity is possible by incorporation of a switchable carbene **6**, if changes in the carbene's electronic situation are transferred to the Ru-center, what is to be expected based on models used to explain the binding mode of NHC ligands. However, this constitutes a formidable task since the transfer of electronic properties from a NHC to a metal center is extremely hard to predict and subtle changes in the coordination sphere of a metal may markedly influence it catalytic activity.

In summery, future work will be directed towards the photocontrol of high-performance catalysts. Control is to be achieved either by extending the concept of reversible steric shielding to organometallic complexes or by altering the electronic properties of *N*-heterocyclic carbenes. Rendering polymerization reactions photocontrollable is of outstanding interest, due to the possibility to access a wide range of applications, ranging from sophisticated surface patterning tasks to the construction of novel polymer architectures for smart materials.

5.3 Literature

(1) Myers, M.; Connor, E. F.; Glauser, T.; Mock, A.; Nyce, G.; Hedrick, J. L. *J. Polym. Sci., Part A: Polym. Chem.* **2002**, *40*, 844-851.

(2) Trnka, T. M.; Grubbs, R. H. *Acc. Chem. Res.* **2001**, *34*, 18-29; Fürstner, A. *Angew. Chem., Int. Ed. Engl.* **2000**, *39*, 3013-3043; Connon, S. J.; Blechert, S. *Angew. Chem., Int. Ed. Engl.* **2003**, *42*, 1900-1923; Grubbs, R. H. *Tetrahedron* **2004**, *60*, 7117-7140; Clavier, H.; Grela, K.; Kirschning, A.; Mauduit, M.; Nalon, S. P. *Angew. Chem., Int. Ed. Engl.* **2007**, *46*, 6786-6801.

(3) Sanford, M. S.; Love, J. A.; Grubbs, R. H. *J. Am. Chem. Soc.* **2001**, *123*, 6543-6554.

(4) Weskamp, T.; Bohm, V. P. W.; Herrmann, W. A. *J. Organomet. Chem.* **2000**, *600*, 12-22; Herrmann, W. A. *Angew. Chem., Int. Ed. Engl.* **2002**, *41*, 1290-1309;

Crudden, C. M.; Allen, D. P. *Coord. Chem. Rev.* **2004**, *248*, 2247-2273; Glorius, F. A. *Top. Organomet. Chem.* **2007**, *21*, 1-20.

(5) *N-Heterocyclic Carbenes in Synthesis*; Nolan, S. P., Ed.; Wiley-VCH: Weinheim, 2006.

(6) Enders, D.; Balensiefer, T. *Acc. Chem. Res.* **2004**, *37*, 534-541; Enders, D.; Niemeier, O.; Henseler *Chem. Rev.* **2007**, *107*, 5606-5655; Marion, N.; Diez-Gonzalez, S.; Nolan, I. P. *Angew. Chem., Int. Ed. Engl.* **2007**, *46*, 2988-3000.

(7) Nyce, G. W.; Glauser, T.; Connor, E. F.; Möck, A.; Waymouth, R. M.; Hedrick, J. L. *J. Am. Chem. Soc.* **2003**, *125*, 3046-3056.

6 Appendix

6.1 Abbreviations

AFM - atomic force microscopy

AIBN - 2,2'-azobisisobutyronitrile

ATR - attenuated total reflexion

BOC - *tert*-butyloxycarbonyl

DIBAL - di-*iso*-butylaluminum hydride

DMAP - 4-dimethylaminopyridine

DMF - *N*,*N*-dimethylformamide

DPEphos - bis(2-diphenylphosphinophenyl)ether

EDC - 1-ethyl-3-(3-dimethylaminopropyl) carbodiimide

edg/EDG - electron donating group

ewg/EWG - electron witdrawing group

HBC - hexabenzocoronene

HOPG - highly oriented pyrolytic graphite

IR - infrared

IRSE - infrared-spectroscopic ellipsometry

LTMP - lithium 2,2,6,6-tetramethylpiperidide

MS - mass spectrometry

NHC - *N*-heterocyclic carbene

PBLG - poly(γ-benzyl-L-glutamate)

PTSA - *para*-toluenesulfonic acid

RDC - residual dipolar coupling

ROMP - ring-opening metathesis polymerization

ROP - ring-opening polymerization

S-Phos - 2-dicyclohexylphosphino-2',6'-dimethoxybiphenyl

STM - scanning tunnel microscopy

THF - tetrahydrofuran

TLC - thin-layer chromatography

VASS - variable angle sample spinning

6.2 Publications

Journals

[1] R. S. Stoll, M. V. Peters, A. Kühn, S. Heiles, R. Goddard, M. Bühl, C. M. Thiele, S. Hecht: "Photoswitchable Catalysts: Correlating Structure and Conformational Dynamics with Reactivity by a Combined Experimental and Computational Approach" *J. Am. Chem. Soc.* **2009**, *131*, 357-367.

[2] R. S. Stoll, M. V. Peters, A. Kühn, S. Hecht: "Photoswitching Basicity" *Angew. Chem.* **2008**, *120*, 6056-6060; *Angew. Chem. Int. Ed.* **2008**, *47*, 5968-5972.

[3] M. V. Peters, R. S. Stoll, R. Goddard, G. Buth, S. Hecht: "On the Illusive Nature of ortho-Formylazobenzenes: Exploiting the Nucleophilicity of the Azo Group for Cyclization to Indazole Derivatives" *J. Org. Chem.* **2006**, *71*, 7840-7845.

[4] R. S. Stoll, N. Severin, J. P. Rabe, S. Hecht: "Synthesis of a Novel Chiral Squaraine Dye and its Unique Aggregation Behavior in Solution and in Self-Assembled Monolayers" *Adv. Mater.* **2006**, *18*, 1271-1275.

Patents

[1] S. Hecht, M. V. Peters, R. S. Stoll: *“Photoschaltbare Katalysatoren”*, German Patent DE 102006057612.8 (5-Dec-2006).

Talks

[1] R. S. Stoll, S. Hecht: "Towards Photocontrolling Catalysis", 10th JCF Symposium, Rostock, Germany, **2008**.

Posters

[1] R. S. Stoll, V. Eberhardt, J. J. Zhu, L. Grubert, N. Severin, J. P. Rabe, S. Hecht: "Structure and Electronic Properties of Squaraine Dyes in Solution and at the Solid-Liquid Interface", DFG Graduate College 1221, Electronic Processes in π-Conjugated Materials, Würzburg, Germany, **2008**.

[2] R. S. Stoll, M. V. Peters, S. Hecht: "Towards Photocontrol of Catalytic Activity", Gordon Research Conference: Polymers East, Mount Holyoke, U.S.A., **2007**.

[3] M. A. Balbo Block, R. S. Stoll, S. Hecht: "Synthesis and Properties of Squaraine-Containing Polymers", Makromolekulares Kolloquium, Freiburg, Germany, **2005**.

Hiermit versichere ich, Ragnar Samson Stoll, geboren am 15.05.1979 in Bad Homburg vor der Höhe, die vorliegende Arbeit selbstständig und nur mit Hilfe der zulässigen und angegebenen Mittel verfasst zu haben.

Ragnar S. Stoll